

# **Chemical and Isotopic Studies of Estuaries and the Ganga Basin Sediments**

**A THESIS**

**Submitted for the Award of Ph. D degree of**

**MOHANLAL SUKHADIA UNIVERSITY**

**In the**

**Faculty of Science**

**By**

**Waliur Rahaman**



**Under the Supervision of**

**Dr. Sunil Kumar Singh**

**ASSOCIATE PROFESSOR**

**Physical Research Laboratory,  
Ahmedabad-380009, India.**

**MOHANLAL SUKHADIA UNIVERSITY  
UDAIPUR**

**2010**

## ***D E C L A R A T I O N***

I, **Mr. Waliur Rahaman**, S/o Mr. Md. Jillar Rahaman, resident of B-4, PDF Qtrs, PRL residences, Navrangpura, Ahmedabad – 380009, hereby declare that the research work incorporated in the present thesis entitled “***Chemical and Isotopic studies of Estuaries and the Ganga Basin Sediments***” is my own work and is original. This work (in part or in full) has not been submitted to any University for the award of a Degree or a Diploma. I have properly acknowledged the material collected from secondary sources wherever required. I solely own the responsibility for the originality of the entire content.

Date:

(Waliur Rahaman)

# *C E R T I F I C A T E*

I feel great pleasure in certifying that the thesis entitled “**Chemical and Isotopic studies of Estuaries and the Ganga Basin Sediments**” by **Waliur Rahaman** under my guidance. He has completed the following requirements as per Ph.D. regulations of the University

- (a) Course work as per the university rules
- (b) Residential requirements of the university
- (c) Presented his work in the departmental committee
- (d) Published/accepted minimum of one research paper in a referred research journal.

I am satisfied with the analysis of data, interpretation of results and conclusions drawn.

I recommend the submission of thesis.

Date:

*Name and designation of supervisor*

**Sunil Kumar Singh,**

**Associate Professor**

*Countersigned by  
Head of the Department*

*Dedicated*

*To*

*Ma, Abba & Reshma*

## Acknowledgements

*This thesis is the destination of five years journey accompanied by sincere guidance, advice, support, wishes and encouragements from many individuals. I am thankful and indebted to all of them. I feel immense pleasure in writing this acknowledgement.*

*First of all, I express my deep sense of gratitude to my thesis guide, Dr. Sunil Kumar Singh. I am extremely privileged to work under his supervision. I am heartily thankful to my supervisor, whose encouragement, guidance and support from the initial to the final level enabled me to develop an understanding of the subject. He taught me right from the fundamentals to the intricacies of geochemistry. He introduced me with the field of mass spectrometry and taught me how to produce good quality data and their interpretations. He gave me freedom to think independently and put my views strongly during any scientific discussions. His friendly nature has always made me comfortable while working in the lab. I have enjoyed working with him.*

*I am highly grateful to Prof. S. Krishnaswami for his suggestions, criticisms and discussion which were always fruitful and improved my scientific knowledge. He always gave me valuable inputs to produce good quality data and their interpretation in the best possible way, preparing manuscripts up to the finest level. I always feel extremely privileged and lucky to be fostered and nurtured by such great, world renowned geochemist. I am indebted to him for his constant encouragement, concern, advice, teaching and care.*

*I sincerely thank Prof. M.M. Sarin for his suggestions and support during all kind of laboratory activities. He has been always enthusiastic to provide me help and advice whenever I needed. I learned lot of instrumental techniques right from operations to circumvent the problems during measurements by ICP-AES, AAS.*

*I thank Prof. J. N. Goswami, the Director, Prof. Utpal Sarkar, Dean and Prof. A.K. Singhvi, former Dean, Physical Research Laboratory, for providing me all kind of necessary facilities and help to carry out my thesis work successfully. I thank all the academic committee members for reviewing my work time to time.*

*I am highly indebted to Dr. Ravi Bhushan (Ravi Da) for providing me help, care and support wherever and whenever I required. I am thankful to Dr. R. Rengarajan and Mr. A.K. Sudheer for helping me in running instruments. Their suggestions and advices were always fruitful. I am extremely thankful to Santoshbhai for his help during experiments and teaching me right from beaker cleaning to TIMS operation. I am highly obliged to Bhavsar Bhai for his enormous help during onboard sampling in estuaries and experiments in lab. I thank my colleagues and friends Gyana, Vineet, Satinder, Jayati, Kirpa, Ashwini Timmy, Prashant and Srinivas who always accompanied me and have been very supportive. Thanks to Sneha for her help in computer related works and dealing with administrative and workshop. My sincere thanks to my seniors of the Chem. Gang Anirban Da, Tarun and Neeraj bhai for their suggestions and encouragements.*

*I am thankful to Dr. Navin Juyal, Dr. J.S Ray, Dr. M.G. Yadava and Mr. A D Shukla for their concern to my work. I benefited a lot by discussing and sharing my ideas and knowledge with them. I was always boosted by their motivation and encouragement.*

*I thank Prof. S.V.S. Murty for providing me instrumentation facility in Planex and Durgaprasad for helping me during measurements.*

*I sincerely thank all the faculties, scientists and staff members of PRL family. My special thanks to Profs. S. K. Bhattacharya, R. Ramesh, Drs. P. Sharma, R.D. Deshpande, Kuljeet Kaur, Vinai K. Rai, Reshmi Das, K. Rao, R.A Jani, D. Panda, Dipbendu Chakravarty, Som K. Sharma and Bhushit for their kind support.*

*I am grateful to the all the staff-members of Library, Computer Centre, Workshop, Administration, Dispensary, Maintenance of PRL for their assistance and cooperation.*

*I would like to thank my collaborators Prof. S.K Tandon of Delhi University, and Prof. Rajiv Sinha of IIT Kanpur for providing core samples. Their suggestions and feedback were helpful in writing the manuscripts.*

*I spend joyful moments at PRL hostel with my close friends. I must thank all of my batch-mates (Alok, Naveen, Sumita, Bhavik, Vishal, Harinder, Manan,*

*Sumanta, Shuchita, Lokesh, Brajesh, Sanjeev, Ram, Rohan and Arvind, my seniors Rohit, Shreyas, Ritesh, Morthekai, Sanat, Uma, Rajesh, Salman Bhai,, Golamnabi bhai, Jayant, Zeen and Mauryaji, and my juniors (Suratna, Rohit, Amjad, Arvind Singh, Naveen Chauhan, Rabiul, Neeraj, Ashish, Tapas, Sunil, Arun, Surichi, Moumita, Arvind Saxena, Chinmay, Iman, Patra, Suman, Ashok, Praveen, Anand, Sandeep, Srikant, Soumya, Subrata, Vimal, Yogita, Zulfikar and Arvind Rajpurohit). I thank all of them for making my stay very pleasant and enjoyable at PRL.*

*I owe my immense respect to Mrs. Renu Singh for her care and affection which makes me feel that I am an integral part of her family. I thank all the family members Mrs Krishnaswami (Nanda), Mrs Sarin, Mrs Bhushan (Sravani Di), Mrs Sudher and Mrs Rengarajan for nice and cheerful company during all the get togethers. My love and affection also remains for Markandeya, Manu and Golu, the youngsters of our family. I thank Mrs. Pauline Josheph for her help, care and support and help.*

*I am deeply grateful to my parents and family for their continuous support, wishes and encouragement. They have always stood by me in strong times and provided me support to complete my thesis. I also thank my in-laws for their sincere care and concern to my work.*

*I would like to thank Swati Dutta (Swati Di) for her help, care and moral support which really matters in my life.*

*Lastly, I offer my regards and extend my sincere thanks to all of those who supported me in any respect during the completion of my PhD thesis.*

## Abstract

This thesis addresses two primary objectives, to determine (i) paleo-erosion distribution over the Himalaya during the past ~100 ka and its relation to climate change and (ii) the factors regulating the abundance and distribution of redox sensitive elements U, Mo and Re and alkaline earth metals Ba, Sr and  $^{87}\text{Sr}/^{86}\text{Sr}$  in selected Indian estuaries and their impact on the oceanic budgets of these elements and isotopes.

Sr-Nd isotopes and major element compositions of a ~50 m long sediment core from the Ganga plain show reduced erosion over the Higher Himalaya and lower intensity of chemical weathering during ~90, ~70, ~40 and ~20 ka coinciding with periods of precipitation minima and glacial maxima. This study underscores the strong coupling between climate and erosion. The  $^{87}\text{Sr}/^{86}\text{Sr}$  of calcretes of various ages from the Ganga plain shows recent abrupt increase in riverine  $^{87}\text{Sr}/^{86}\text{Sr}$  of the Ganga attributed to enhanced weathering in the Lesser Himalaya due to variability of monsoon and/or enhanced agricultural activities and deforestation.

Re is conservative in all the estuaries studied whereas Mo and U behave inconsistently; with significant removal in the Hooghly and the Mandovi estuaries most likely due to their uptake in mangrove swamps. Extrapolation of these results on a global scale indicates that mangrove swamps can act as an important sink of oceanic Mo. This study highlights the significance of anthropogenic Re and Mo supply to oceans; the Re flux from this source seems far in excess of its natural input in some of estuarine/coastal regions. Ba is non-conservative with additional inputs at low to mid-salinites in estuaries; elemental Sr is conservative, however, the distributions of  $^{87}\text{Sr}/^{86}\text{Sr}$  in the estuaries seem to be impacted by supply from additional sources. If Submarine Ground Water Discharge (SGD) is the source of  $^{87}\text{Sr}/^{86}\text{Sr}$ , it offers a good tool to estimate SGD supply to estuaries.

Thus this study have brought out the coupling between erosion and climate in the Himalaya and the role of solute-particle interaction, SGD and uptake in mangroves in regulating the distribution and budget of suit of redox sensitive elements and alkaline earth in estuaries.

**Key-words: Ganga, Himalaya, paleo-erosion, isotope, trace elements, estuary**

# Content

|                  |  | <b>Page</b>  |
|------------------|--|--------------|
|                  | <b>List of Tables</b>  | <b>v</b>     |
|                  | <b>List of Figures</b>   | <b>vii</b>   |
| <b>Chapter 1</b> | <b>Introduction</b>  | <b>1-11</b>  |
| 1.1              | Introduction   | 2            |
| 1.2              | Objectives of the thesis   | 9            |
| 1.3              | Outline of the thesis  | 10           |
| <b>Chapter 2</b> | <b>Materials and Methods</b>                                     | <b>12-56</b> |
| 2.1              | The Ganga Basin  | 13           |
| 2.1.1            | General description of the basin                                 | 13           |
| 2.1.2            | Core Locations in the Ganga plain                                | 15           |
| 2.1.3            | (a) Litho-Stratigraphy and facies of the cores                   | 17           |
|                  | (b) Chronology of the IITK and JP core                           | 20           |
| 2.1.4            | Sub-sampling of the cores for chemical and isotopic studies      | 22           |
| 2.2              | Estuaries and coastal areas of the Arabian Sea and Bay of Bengal | 23           |
| 2.2.1            | Lithology, geohydrology and climate                              | 24           |
| 2.2.2            | Sampling from estuaries and coastal areas                        | 27           |
| 2.3              | Analytical techniques  | 29           |
| 2.3.1            | Water analysis   | 30           |
|                  | (a) Temperature, pH, electrical conductivity and salinity        | 30           |
|                  | (b) Alkalinity and Major Ions                                    | 33           |
|                  | (c) Sr and $^{87}\text{Sr}/^{86}\text{Sr}$ by TIMS               | 33           |
|                  | d) Re, U, Mo and Ba measurements by ICP-MS                       | 35           |
|                  | i) Analysis of dissolved Rhenium                                 | 35           |
|                  | ii) Analysis of dissolved U, Mo and Ba                           | 41           |

|                  |   |               |
|------------------|---|---------------|
| 2.3.2            | Analysis of Sediments   | 47            |
|                  | (a) Major and trace elements  | 47            |
|                  | (b) CaCO <sub>3</sub> and organic carbon  | 49            |
|                  | (c) Sr and Nd isotope measurement in sediments  | 50            |
|                  | (d) Carbon and Oxygen isotopes in carbonate nodules   | 55            |
| <b>Chapter 3</b> | <b>Major &amp; trace elements and Sr &amp; Nd isotope compositions of the Ganga plain sediments: Implication to weathering intensity and erosion distribution over the Himalaya during past ~100 ka</b> | <b>57-79</b>  |
| 3.1              | Introduction  | 58            |
| 3.2              | Results   | 60            |
| 3.3              | Discussion  | 63            |
|                  | 3.3.1 Temporal variation in the paleo-weathering intensity  | 63            |
|                  | 3.3.2 Erosion distribution over the Himalaya  | 69            |
| 3.4              | Conclusions   | 79            |
| <b>Chapter 4</b> | <b>Sr, C and O isotopes in carbonate nodules from the Ganga Plain: Variations in dissolved <sup>87</sup>Sr/<sup>86</sup>Sr of the Ganga water during the past ~100 ka</b>                               | <b>80-102</b> |
| 4.1              | Introduction  | 81            |
| 4.2              | Results   | 83            |
| 4.3              | Discussion  | 87            |
|                  | 4.3.1 Petrography and major element composition   | 87            |
|                  | 4.3.2 How do faithfully these carbonates record riverine Sr isotope signature?  | 88            |
|                  | 4.3.3 Sr isotopic composition in carbonate  | 92            |
|                  | 4.3.4 Carbon and Oxygen isotope composition   | 95            |
|                  | 4.3.5 Recent abrupt rise in <sup>87</sup> Sr/ <sup>86</sup> Sr of the Ganga and its implications  | 100           |
| 4.4              | Conclusions   | 101           |

|                  |  |                |
|------------------|--|----------------|
| <b>Chapter 5</b> | <b>Mo, U and Re in rivers and estuaries of India: Implications to geochemistry of redox sensitive elements and their marine budgets</b>    | <b>103-145</b> |
| 5.1              | Introduction   | 104            |
| 5.2              | Results and Discussion   | 106            |
| 5.2.1            | Dissolved Molybdenum, Uranium and Rhenium in rivers and other samples  | 110            |
|                  | (a) Molybdenum   | 111            |
|                  | (b) Uranium  | 112            |
|                  | (c) Rhenium  | 114            |
| 5.2.2            | Dissolved Mo, U and Re in estuaries  | 115            |
|                  | (a) Molybdenum   | 115            |
|                  | (b) Uranium  | 123            |
|                  | (c) Rhenium  | 124            |
| 5.3              | Particulate Mo, U and Re in estuaries  | 126            |
| 5.4              | Comparative behaviour of U, Mo and Re in estuaries   | 129            |
| 5.5              | Removal of U and Mo in the Hooghly and the Mandovi estuaries   | 131            |
| 5.6              | Mo, U and Re in the Gulf of Cambay   | 133            |
| 5.6.1            | Sources of high Mo and Re to Gulf of Cambay  | 134            |
|                  | (a) Natural supply of Mo and Re  | 134            |
|                  | (b) Anthropogenic supply of Mo and Re  | 135            |
| 5.7              | Riverine fluxes of Mo and Re   | 137            |
| 5.8              | Global oceanic budget of Mo and Re   | 140            |
| 5.9              | Conclusions  | 143            |
| <b>Chapter 6</b> | <b>Ba and Sr in Indian rivers and estuaries: Implications to geochemistry of alkaline earth metals and submarine groundwater discharge</b> | <b>146-173</b> |
| 6.1              | Introduction   | 147            |
| 6.2              | Results and Discussion   | 149            |

|                  |  |                |
|------------------|--|----------------|
| 6.2.1            | Dissolved Sr   | 152            |
| 6.2.2            | Dissolved Ba   | 155            |
| 6.2.3            | Particulate Ba, Sr and major elements in the Narmada estuary   | 158            |
| 6.2.4            | Behaviour of dissolved $^{87}\text{Sr}/^{86}\text{Sr}$ in estuaries  | 159            |
| 6.2.5            | Implication of quasi-conservative behaviour of Sr in estuaries   | 167            |
| 6.2.6            | Dissolved Ba in estuary  | 167            |
| 6.3              | Conclusions  | 172            |
| <b>Chapter 7</b> | <b>Synthesis and future perspective</b>  | <b>174-181</b> |
| 7.1              | Paleo-erosion over the Himalaya  | 175            |
| 7.2              | Reconstruction of dissolved $^{87}\text{Sr}/^{86}\text{Sr}$ of the paleo-Ganga and paleoclimate of the Ganga plain | 176            |
| 7.3              | Study of redox sensitive trace elements (Re, Mo and U) in estuary  | 177            |
| 7.4              | Studies on alkaline earth metals Ba, Sr and $^{87}\text{Sr}/^{86}\text{Sr}$ in estuary                             | 179            |
| 7.5              | Scope of future research   | 180            |
|                  | <b>References</b>  | <b>182-209</b> |
|                  | <b>List of Publications</b>  | <b>210-211</b> |

## List of Tables

| <b>Table</b> | <b>Content</b>   | <b>Page</b> |
|--------------|--|-------------|
| 2.1          | Details of river water, groundwater and mollusk  | 22          |
| 2.2          | Lithological and hydrological details of Rivers  | 25          |
| 2.3          | Sampling location, and Salinity, Conductivity, Temperature<br>Alkalinity and pH in the estuarine waters          | 32          |
| 2.4          | Salinity, Conductivity, Temperature and pH in the<br>miscellaneous samples                                       | 32          |
| 2.5          | Precision of dissolved Sr and $^{87}\text{Sr}/^{86}\text{Sr}$ measurements in estuary<br>samples                 | 35          |
| 2.6          | Details of the two Re spikes   | 37          |
| 2.7          | Calibration of laboratory Re standard against CRPG $^{185}\text{Re}$ spike                                       | 37          |
| 2.8          | Calibration PRL $^{185}\text{Re}$ spike against laboratory standard  | 37          |
| 2.9          | Blank analysis of Re   | 39          |
| 2.10a        | Replicate analysis of dissolved Re in estuary samples  | 40          |
| 2.10b        | Dissolved Re comparison between 0.2 and 0.45 $\mu$ filtered  | 41          |
| 2.10c        | Repeat analysis of Re in particulate phase   | 41          |
| 2.11         | U and Mo in reference materials and in seawater from the<br>Arabian Sea  | 43          |
| 2.12         | Replicate analyses of dissolved U and Mo in estuary samples  | 44          |
| 2.13         | Experiments for Ba measurements by standard addition method  | 46          |
| 2.14         | Elemental analyses in USGS reference material W-1 and G-2  | 47          |
| 2.15         | Replicate analyses of Sr, Nd and their isotope compositions in<br>silicate phase of sediments                    | 53          |
| 2.16         | Replicate analysis of $^{87}\text{Sr}/^{86}\text{Sr}$ in carbonate phase   | 54          |
| 2.17         | Blanks of Sr and Nd  | 54          |
| 2.18a        | Analysis of our laboratory standard Mc. Marbel and Z-Carara<br>carbonates to check accuracy of the measurements. | 55          |

|       |  |         |
|-------|--|---------|
| 2.18b | Replicate analysis of $\delta^{13}\text{C}$ and $\delta^{18}\text{O}$ in carbonate nodules   | 56      |
| 3.1   | Major element composition of bulk sediments of IITK Core   | 60-61   |
| 3.2   | Sr, Nd isotope composition of silicate fraction of sediments of IITK core  | 62-63   |
| 3.3   | Average ( $\pm\sigma$ ) composition of Himalayan Crystallines and the Ganga Sediments  | 65      |
| 3.4   | Comparison of CIA* of different lithologies and sediments from the Ganga system  | 66      |
| 3.5   | $^{87}\text{Sr}/^{86}\text{Sr}$ and $\epsilon_{\text{Nd}}$ of various litho-units of the Ganga System  | 73      |
| 4.1   | Elemental composition, $^{87}\text{Sr}/^{86}\text{Sr}$ , $\delta^{13}\text{C}$ and $\delta^{18}\text{O}$ of carbonate nodules from IITK core | 84      |
| 4.2   | Sr isotope composition of carbonate nodules from Jagdishpur  | 85      |
| 4.3a  | Sr isotope composition of miscellaneous samples from Kanpur  | 86      |
| 4.3b  | Sr isotope composition of miscellaneous samples from Allahabad after the confluence of Yamuna  | 86      |
| 5.1   | Dissolved Mo, U and Re in the Indian Estuaries.  | 108-110 |
| 5.2   | Dissolved Mo, U and Re in miscellaneous samples  | 110     |
| 5.3   | Properties of best fit lines and estimates of U, Mo and Re concentration at 0‰ and 35‰ salinity based on estuarine data                      | 120     |
| 5.4   | Re, Mo, U, organic carbon and Al in suspended and bed/bank sediments of the Narmada and Tapi estuaries.                                      | 127     |
| 5.5   | Compilation of Mo in global rivers along with this study   | 138     |
| 5.6   | Dissolved Re in global rivers measured in this study and available in the literature   | 139-140 |
| 6.1   | Dissolved Ba and Sr concentrations and $^{87}\text{Sr}/^{86}\text{Sr}$ in the Narmada, Tapi, Mandovi and the Hooghly Estuaries               | 150-152 |
| 6.2   | Ba, Sr and major elements abundances in particulate matter from the Narmada estuary during monsoon   | 158     |
| 6.3   | Dissolved and particulate Ba characteristics in estuaries  | 169     |

## List of Figures

| <b>Fig.</b> | <b>Content</b>  | <b>Page</b> |
|-------------|---|-------------|
| 2.1         | Sampling locations.   | 16          |
| 2.2         | Litho-stratigraphy of the IITK core analyzed in this study.   | 18          |
| 2.3         | Lithostratigraphy of JP core.   | 19          |
| 2.4         | Age-depth models of the IITK core.  | 21          |
| 2.5         | Location of the Hooghly, Narmada, Tapi, Mahi, Sabarmati and the Mandovi estuaries.  | 26          |
| 2.6         | The Gulf of Cambay and the estuaries of the Narmada, Tapi, Mahi and the Sabarmati.  | 28          |
| 2.7         | Calibration of three aliquots of known Re metal standard were calibrated using $^{185}\text{Re}$ spike of known concentration from CRPG, CNRS, Nancy, France. | 38          |
| 2.8         | Analysis of three aliquots of the same sample ranging from 20 to 55 g analysed for total Re.  | 39          |
| 2.9         | Standard calibration of Mo and U in the ICP-MS.   | 42          |
| 2.10        | Ba calibration using four standards of known strengths.   | 45          |
| 2.11        | Ba measurement in estuary water samples by standard addition method.  | 46          |
| 2.12        | Comparison of measured and reported elemental concentrations in W-1 and G-2 USGS reference standards.   | 48          |
| 2.13        | Variations of $^{87}\text{Sr}/^{86}\text{Sr}$ in NBS-987 and $^{143}\text{Nd}/^{144}\text{Nd}$ in JNdi-1 with time.   | 52          |
| 3.1         | Scatter plot of $\text{Al}_2\text{O}_3/\text{Na}_2\text{O}$ and CIA* of sediments.  | 67          |
| 3.2         | Temporal variations in chemical indices such as CIA*, $\text{Na}_2\text{O}/\text{Al}_2\text{O}_3$ and $\text{Na}_2\text{O}/\text{TiO}_2$ .                    | 68          |
| 3.3         | Scatter plot of Sr and Nd isotope composition with their concentrations in the sediments.   | 70          |

|          |   |     |
|----------|---|-----|
| 3.4      | Scatter plot of $^{87}\text{Sr}/^{86}\text{Sr}$ and $\epsilon_{\text{Nd}}$ with their Al content and CIA*.  | 71  |
| 3.5      | $^{87}\text{Sr}/^{86}\text{Sr}$ vs $\epsilon_{\text{Nd}}$ of sediments.   | 72  |
| 3.6      | Variation in Sr and Nd isotope composition of the sediments with depth.   | 74  |
| 3.7      | Three-point running average of $^{87}\text{Sr}/^{86}\text{Sr}$ and $\epsilon_{\text{Nd}}$ of the sediments.   | 76  |
| 4.1      | Petrography of some of the carbonate nodules based on Scanning Electron Microscope.   | 90  |
| 4.2 a, b | Scatter plot of Sr/Ca vs Mn and $^{87}\text{Sr}/^{86}\text{Sr}$ vs Mn/Sr of the carbonate nodules.  | 91  |
| 4.3      | $^{87}\text{Sr}/^{86}\text{Sr}$ in carbonate phase of the nodules from the IITK profile.  | 92  |
| 4.4      | Variations in $^{87}\text{Sr}/^{86}\text{Sr}$ of carbonate nodules with depth in JP profile.  | 93  |
| 4.5      | (a) Scatter diagram of $\delta^{13}\text{C}$ and $\delta^{18}\text{O}$ in carbonate nodules from IITK profile. (b) Covariation plot of $\delta^{13}\text{C}$ and $\delta^{18}\text{O}$ of carbonates from different areas of the Ganga plain. | 96  |
| 4.6      | Variations in $^{87}\text{Sr}/^{86}\text{Sr}$ , $\delta^{13}\text{C}$ and $\delta^{18}\text{O}$ with age of the carbonate nodules from IITK profile.  | 99  |
| 5.1      | Alkalinity vs. salinity distribution in estuaries.  | 107 |
| 5.2      | Molybdenum, Uranium and Rhenium vs. salinity plots in the Narmada estuary for monsoon and pre-monsoon seasons.  | 116 |
| 5.3      | Mo, U and Re Vs. salinity in the Tapi estuary.  | 117 |
| 5.4      | Mo, U and Re distribution in the Mandovi estuary.   | 118 |
| 5.5      | Mo, U and Re in the Hooghly estuary.  | 119 |
| 5.6      | Mo/Al, U/Al of suspended load vs. salinity in the Narmada estuary.  | 128 |
| 5.7      | Scatter diagram of Mo, U and Re concentration in suspended matter of the Narmada versus their organic carbon abundance.   | 129 |
| 5.8      | Mo/Re and U/Re vs. salinity distribution.   | 130 |

|     |   |     |
|-----|---|-----|
| 5.9 | Histogram of dissolved Mo concentration of the global rivers based on reported data and from this study.      | 139 |
| 6.1 | Dissolved Sr vs. salinity plots in the Narmada, Tapi and Mandovi estuaries from Arabian Sea.                  | 154 |
| 6.2 | Dissolved Ba-salinity profile in four estuaries.  | 156 |
| 6.3 | Scatter plots of Ca/Al, Sr/Al and Ba/Al of suspended particulate matter with salinity in the Narmada estuary. | 159 |
| 6.4 | Plots of dissolved $^{87}\text{Sr}/^{86}\text{Sr}$ vs. $1/\text{Sr}$ concentration in estuaries.              | 161 |
| 6.5 | Schematic of submarine groundwater discharge in to coastal regions.   | 163 |
| 6.6 | Plot of $^{87}\text{Sr}/^{86}\text{Sr}$ vs. $1/\text{Sr}$ in the Narmada estuary.                             | 164 |
| 6.7 | Effective zero salinity end member concentration of Ba in different estuaries.                                | 170 |

# **CHAPTER-1**

## **Introduction**

## 1.1 Introduction

Weathering and erosion are important earth surface processes that play major role in landscape evolution, global geochemical and sedimentary cycles and influencing earth's climate by maintaining CO<sub>2</sub> level in the atmosphere. Therefore, studying the processes and products of erosion provide better understanding of their impacts on the evolution of the earth. Glaciers, water and wind are the main agents that transfer weathered materials from weathering site such as an orogen to the depositional basin, foreland basin or ultimately to the oceans. Rivers are one of the major pathways through which particulate and dissolved weathering products are transported (Martin and Meybeck, 1979, Stallard 1995; Gaillardet et al., 1995; Canfield 1997; McLennan 1997; Roy et al., 1999; Das and Krishnaswami, 2007). The weathering and erosion processes generally operate at faster rates in young orogenic belts such as the Himalaya (Raymo et al., 1988; Raymo and Rudiman, 1992; Galy et al., 2008). Generally, it is believed that tectonism results in erosion, however, recent studies indicate a two way process where erosion could also cause tectonism and consequently impact on climate. Climate and tectonics are the major factors controlling erosion and play active role in the young orogenic belts. Assessing the role of the Himalaya as one of the most active young orogenic belts influencing global climate, marine chemistry and sedimentary budget has prompted a large number of studies on its rivers and river basins. Despite numerous studies, the coupling between erosion-climate-tectonics and spatial and temporal distribution of erosion over the Himalaya are still a matter of debate.

It has been proposed that increased erosion due to formation of the Himalaya has resulted in the rise in global marine <sup>87</sup>Sr/<sup>86</sup>Sr values since ca. 40 Ma (Richter et al., 1992) as well as Cenozoic global cooling (Raymo and Ruddiman, 1992). Testing these hypotheses requires detailed information on the erosion history of the mountain belt. Raymo et al. (1988) and Raymo and Ruddiman (1992) proposed that enhanced chemical weathering of silicate rocks in the Himalaya due to its rapid uplift during the Cenozoic is responsible for lowering atmospheric CO<sub>2</sub> and thereby global cooling during this period. This hypothesis is supported by the rise of global marine <sup>87</sup>Sr/<sup>86</sup>Sr

during the Cenozoic which has been related to the Himalayan orogeny and enhanced silicate weathering (Richter et al., 1992). It has been also suggested by many workers that the Himalaya plays an important role in the global carbon cycle due to higher silicate weathering over the million year time scales (Raymo et al., 1988; Raymo and Ruddiman, 1992; Molnar and England, 1992; Raymo et al., 1997; Edmond and Huh, 1997; Blum et al., 1998; Krishnaswami et al., 1999; Dalai et al., 2002; Bickle et al., 2003; Singh et al., 2005; Tipper et al., 2006; Hren et al., 2007). However, a recent study (Willenbring and von Blanckenburg, 2010) based on the temporal variation in oceanic  $^9\text{Be}/^{10}\text{Be}$  indicates insignificant change in the continental weathering during last ~15 Ma, contradicting the hypothesis of coupling between the observed Cenozoic cooling with the Himalayan orogeny and associated weathering. Further, few studies describe Himalaya as a source of atmospheric  $\text{CO}_2$  due to metamorphism (for example, Gaillardet and Galy, 2008) and oxidation of fossil organic matter (Dalai et al., 2001). Most of the hypotheses pertaining to tectonic-erosion-climate coupling in the Himalaya are based on contemporary studies. More information of the erosional history of the Himalaya is required to test various hypotheses.

The widespread erosion over the Himalaya produces huge amount of particulate and dissolved materials that are transferred to its foreland basin and to the Bay of Bengal (Sarin et al., 1989; Milliman and Syvitski, 1992; Galy and France-Lanord, 2001; Singh et al., 2008). The Ganga supplies about 500-1000 million tons of sediments and 100 million tons of dissolved load annually to the Bay of Bengal (Sarin et al., 1989; Hay, 1998; Goodbred, 2003). Most of the sediments and the dissolved fluxes are delivered by the Himalayan rivers during the south-west or summer monsoon (Hay, 1998; Goodbred, 2003; Singh et al., 2005) which underscore significant role of precipitation and hence climate on supply of weathering fluxes. Studies carried out in the Nepal Himalaya (Burbank et al., 2003) decouple erosion from precipitation whereas Singh et al. (2008) argue on a strong dependence of erosion on precipitation. Clift et al. (2008) demonstrated the influence of climatic variations on provenance of sediments in the Himalaya over thousand year time scale.

The present study is an attempt to assess the role of climate on influencing erosion over the Himalaya. The spatial and temporal variations in the intensity of monsoon and the extent of glacial cover over the Himalaya can affect the source(s) and intensity of weathering. The record of these variations are likely to be stored in the Ganga Plain sediments are limited though it is one of the largest continental sedimentary repository. These sediments can serve as an excellent archive to investigate the impact of climate (monsoon/glaciation) and/or tectonics on the erosion of the Himalaya over time scales of  $10^4$ - $10^5$  years. These sediments are better suited for studying variations in sediment provenance compared to sediments of the Bay of Bengal, as the latter is a more complex mixture of materials derived from multiple sources and different geological terrains (Colin et al., 1999; Ahmad et al., 2005). Such mixing of sediments can obscure provenance signatures. Further, the sediments of the Ganga Plain are likely to provide better time resolution as they respond faster to the cause of variations in sediment provenances. One of the commonly used approach to track the sediment provinces is through their Sr and Nd isotope signatures, provided the endmember have distinctly different isotope compositions (Colin et al., 1999; Ahmad et al., 2005; Singh et al., 2008). The Sr and Nd isotope composition of the Higher Himalaya (HH) and the Lesser Himalaya (LH), the two major sources of sediments to the Ganga Plain, are quite distinct (Singh et al., 2008) and therefore can serve as potential tracers to track variations in their relative proportion of sediments of the Ganga plain. Sr and Nd isotope composition of the silicate fraction of the sediments of the Bay of Bengal have been used to decipher variations in their provenance with time (France-Lanord et al., 1993; Colin et al., 1999; Ahmad et al., 2005). In this study, for the first time, Sr and Nd isotope composition of silicate fraction of sediments from a core in the Ganga Plain has been used to investigate temporal variations in the provenance of sediments and their causative factors.

Much of the information on weathering and erosion in the Himalaya and its importance in contributing to global geochemical and carbon cycles is based on studies of contemporary reservoirs and processes. There is very little information on

paleo-erosion over the Himalaya which makes it difficult to assess its temporal variation and therefore its potential influence on the global geochemical cycles, evolution of oceanic  $^{87}\text{Sr}/^{86}\text{Sr}$ . Climate variations such as rainfall or glacial-interglacial cycles over different time scale could influence chemical and physical weathering in the Himalaya. Changes in chemical weathering can lead to changes in riverine  $^{87}\text{Sr}/^{86}\text{Sr}$  and variations in atmospheric  $\text{CO}_2$  drawdown (Raymo et al., 1988; Raymo and Rudiman, 1992; Galy et al., 2008). Temporal variations in silicate weathering and hence the dissolved riverine fluxes can challenge the use of contemporary silicate weathering in the Himalaya as an index of weathering during the Cenozoic.

One of the goal of the present study is to assess the variation in paleo-weathering intensity through the study of the weathering products deposited in the Ganga plain, a depositional archive based on the major elements Na, K, Mg, Ca, Al, Fe and Ti composition of the sediments.

The rivers draining the Himalaya have been suggested as key player in contributing to dissolved isotopic and geochemical budgets of the global ocean since the Cenozoic. In addition, there are indications of supply of dissolved material including Sr to the Bay of Bengal by submarine ground water discharge in the Bengal basin, in magnitude comparable to the riverine flux carried by the G-B rivers (Basu et al., 2001). The role of these rivers waters and groundwaters in contributing to the isotopic and geochemical budgets of the global ocean since the Himalayan orogeny has been assessed mainly via studies of their contemporary isotopic and chemical compositions. For example, it is hypothesized that seawater Sr evolution since the Cenozoic is a result of enhanced silicate weathering resulting from rapid uplift of the Himalaya (Richter et al. 1992) with the underlying assumption that Sr isotope composition of the Himalayan silicates undergoing erosion since the Cenozoic has remained invariant which needs to be validated. This was supported by the presence of highly radiogenic  $^{87}\text{Sr}/^{86}\text{Sr}$  with moderately high Sr concentration in the contemporary Ganga-Brahmaputra waters (Krishnaswami et al., 1992; Richter et al., 1992). One of the key requirements to evaluate the role of the Himalayan rivers in

contribution to Sr isotope evolution of Ocean through time is the knowledge of temporal variation in Sr isotope systematics of the G-B system. Further, it is also important to know that role of changing silicate weathering intensity and changing weathering provenances in contributing to Sr isotope composition of rivers and hence it's oceanic evolution. In this connection, some of the earlier studies in the Bay of Bengal clays (Derry and France-Lanord, 1996) and paleosols from Siwaliks (Quade et al., 1997) indicate significant temporal variations in riverine Sr composition on million year time scales which has been attributed to source variation. The alluvial sediments in the Ganga plain, in addition to silicates derived from the Himalaya contain significant amounts of secondary carbonates, locally known as "kankar". These carbonates are precipitated from river and shallow groundwater often near surface of the sediments. These authigenic carbonates have the potential to serve as a repository to retrieve Sr isotope composition of the river/ground water from which they precipitated. Quade et al. (1997) has shown that paleosol carbonates formed by in the Siwalik sediments track the Sr isotope composition of the Ganga water over million year time scale. In addition, oxygen and carbon isotope composition of these secondary carbonates hold clues to the paleoenvironmental conditions, temperature, rainfall and type of vegetation prevailing at the time of their formation. The stable carbon and oxygen isotope composition of calcretes deposited in the Ganga plain though have been used to reconstruct past climatic variations (Alam et al., 1997; Srivastava, 2001; Sinha et al., 2006) there are some concerns about the factors contributing to isotope fractionation (kinetic vs. equilibrium) and therefore the use of these carbonates to retrieve paleoclimate data (Salomons et al., 1978). In this present study attempts have been made to track the temporal evolution of  $^{87}\text{Sr}/^{86}\text{Sr}$  of Ganga water by analyzing carbonate nodules in sediment cores raised from the Ganga plain. In addition to  $^{87}\text{Sr}/^{86}\text{Sr}$ ,  $\delta^{13}\text{C}$  and  $\delta^{18}\text{O}$  have also been measured in the same carbonate nodules to asses their application as paleo-environment and pale-vegetation proxies in the Ganga basin.

The materials transported by rivers enter the ocean through estuaries. Estuary is the mixing zone between river and ocean where geochemical, biological and

sedimentological processes are highly variable both spatially and temporally. The freshwater and saline water mixing within an estuarine system results in strong chemical, physical and biological gradients that can modify the geochemistry of many elements. Processes such as mixing, biological productivity, organic matter-water interaction, changes in Eh-pH and redox condition in the estuaries decide the fate of geochemical behaviour of elements and the ultimate fluxes of elements transported by rivers to the oceans. This makes the study of the geochemical behaviour of elements in estuaries important. Recognizing this, in this thesis the behaviour of alkaline earth metals Ba, Sr and redox sensitive elements Re, Mo and U in selected Indian estuaries have been investigated with a view to learn about the role of anthropogenic inputs and submarine groundwater discharge on their abundances in estuaries and to refine their global marine budget. In this work an effort has been made to elucidate the geochemistry of the redox sensitive elements such as Re, Mo, U and alkaline earth metals Ba, Sr in selected rivers and estuaries and its implications to the global budget of Re and Mo, anthropogenic inputs and submarine ground water discharge.

The behaviour of Re in the ocean is similar to Mo and U, it exhibits covariance with salinity and demonstrates conservative behaviour in oxic waters (Anbar et al., 1992). Re is more sensitive to anoxic conditions compared to U and Mo (Colodner et al., 1993), as a result its concentration in organic rich marine sediments, both modern and ancient, are quite high (Ravizza and Turekian, 1989, Peucker-Ehrenbrink et al., 1995; Singh et al., 1999). Thus, the abundance of Re in sediments and its relation to Mo and U can provide clues to the Eh-pH conditions of the depositional environment (Hodge et al., 1996; Moford et al., 2007; Chappaz et al., 2008). Despite significant similarity in the geochemical nature of Re, U and Mo (Emerson and Hausted, 1991; Colodner et al., 1993b, 1995), it is very difficult to predict their removal rates and relative mobility (Colodner et al., 1995). Variable behaviour of these elements has been reported in the world major river-estuary system such as Amazon, Hooghly, Hudson and Mississippi (Colodner et al., 1993, references there in). For example, U removal has been observed in the Meghna and

the Hooghly estuary (Carroll and Moore, 1993; Somayajulu, 1994), however, it remains conservative in the Narmada estuary (Borole et al., 1982). Further the reasons suggested for U removal in the estuaries do not seem to be conclusive yet. Re shows non-conservative behaviour in the Amazon estuary and conservative in the Mississippi. In this study, behaviour of these three redox sensitive elements has been studied in three estuaries from the Arabian Sea and one from the Bay of Bengal. Studies of these elements were also carried out in the coastal areas of the Gulf of Cambay, salt marsh and effluents from industries located along the coastal areas.

Among the alkaline earth metals, Ba is an important element and its studies have been motivated by its wide application to determine submarine ground water discharge, paleoproductivity, paleoalkalinity and paleocean circulation (Lea and Boyle, 1990, Dymond et al., 1992). In addition, it is also used as an analog to learn about the behaviour of Ra. Existing studies indicate non-conservative behaviour of Ba in river-estuary system (Hanor and Chan, 1977; Edmond et al., 1978; Carroll et al., 1993; Coffey et al., 1997; Li and Chan, 1998; Guay and Fulkner, 1998).

Strontium isotope composition in estuarine environments has been used to study fresh water plume, past changes in salinity and river discharge, particularly when large contrast exists between the Sr concentration and  $^{87}\text{Sr}/^{86}\text{Sr}$  of the riverine and marine end members (Ingram and Sloan, 1992; Bryant et al., 1995; Charette and Sholkovitz, 2006; Wilderund and Andersson, 2006; Huang and You, 2007; Peros et al., 2007). Small variations in  $^{87}\text{Sr}/^{86}\text{Sr}$  in the estuarine region due to varying riverine fluxes and isotope ratio have been successfully used to track changes in paleo-salinity over long time scales. To use Sr isotope composition in the estuary environment as a proxy of paleo-salinity and in the open ocean as proxy of continental weathering, few existing studies on the behaviour of Sr and  $^{87}\text{Sr}/^{86}\text{Sr}$  in the estuarine region demonstrate its variable nature, both conservative and non-conservative in different estuaries (Andersson et al, 1994; Wang et al., 2001; Xu and Marcantano, 2004). Studies of Anderson et al. (1992) and Ingram and Sloan (1992) have reported conservative behaviour in estuaries where its concentration gradient with salinity is determined by the two components mixing between river and sea water. However, in

some of the estuaries, Sr behaves nonconservatively (Wang et al., 2001, Xu and Marcantonio, 2007) which has been attributed to the release of labile Sr from the sediment to the dissolved phase in the lower salinity region (Xu and Marcantonio, 2004). It has also been shown in the Changjiang estuary that strong interaction of sediment and water during high energy condition can release Sr to the water (Wang et al., 2001). Another important source of Sr to the coastal ocean could be through the submarine ground water discharge (SGD; Basu et al., 2001). Therefore, to address some of the important issues related to their sources, transport and behaviour of Ba and Sr and  $^{87}\text{Sr}/^{86}\text{Sr}$  in estuaries which eventually control their final input to the oceans, studies were carried out extensively in Indian estuaries i.e. the Narmada, Tapi and the Mandovi estuaries falling in to the Arabian Sea and the Hooghly in the Bay of Bengal.

## 1.2 Objectives of the thesis

1. To track the temporal variation in the paleo-erosion pattern over the Himalaya and the impact of climate on it using Sr and Nd isotope composition of sediments from a drilled core in the Ganga plain.
2. To decipher paleo-weathering intensity using major element compositions and to understand the geochemistry of major elements and their mobility during chemical weathering.
3. To reconstruct the evolution of the dissolved  $^{87}\text{Sr}/^{86}\text{Sr}$  of the Ganga over the past ~100 ka using  $^{87}\text{Sr}/^{86}\text{Sr}$  of carbonate nodules from Ganga plain sediments and its implications to global sea water budget. Further, to assess the applicability of oxygen and carbon isotopes of these carbonates nodules to constrain the paleo-climate and paleo-vegetation records of the Ganga plain.
4. To determine the geochemical behaviour of the redox sensitive trace elements such as Re, Mo, U in the Indian Estuaries, its implications to global seawater budgets of Re and Mo and impact of anthropogenic inputs.

5. To determine the abundances and the geochemical behaviour of the alkaline earth metals, Ba and Sr in selected Indian rivers and estuaries and to assess the potential of  $^{87}\text{Sr}/^{86}\text{Sr}$  as a proxy for quantifying submarine ground water discharge in estuary.

### 1.3 Outline of the thesis

This thesis has been divided into seven chapters. The contents of each chapter is as follows

*Chapter 1* presents the current knowledge and understanding pertaining to the weathering and erosion in the Himalaya, its coupling with tectonics and climate and ongoing debate on the role of its various controlling factors. Brief introduction to the behaviour of redox sensitive elements Re, U and Mo and alkaline earth metals Sr, Ba in estuaries in the context of current knowledge and understanding is also discussed.

*Chapter 2* describes the general geology, hydrogeology and climatic condition of the Ganga basin and lithostratigraphy of the sediment cores used in this study. Further, this chapter describes the lithology and geohydrology of the selected river and estuaries falling into the Bay of Bengal and the Arabian Sea sampled in this study. The latter part gives a brief description of sampling of water and particulate matter from the rivers and estuaries and the various analytical methods adopted for their chemical and isotope analyses.

*Chapter 3* deals with the erosion distribution over the central Himalaya during past ~100 ka using Sr and Nd proxies in the silicate phase of the bulk sediments and also describes the temporal variation in weathering intensity using major elements in the bulk sediments and its relation with climate.

*Chapter 4* provides the reconstruction of Sr isotope of the Ganga water since past ~100 ka and its implication to sea water Sr evolution and assesses the applicability of stable carbon and oxygen isotopes of the pedogenic carbonates in the Ganga plain to infer about paleoclimate of this region.

*Chapter 5* presents characterization of the sources, behaviour during transportation, fluxes of redox sensitive elements Re, Mo and U. In addition, this chapter highlights the distribution of the redox sensitive elements U, Mo and Re and the processes regulating their concentrations in rivers and estuaries and coastal areas of the Bay of Bengal, the Arabian Sea and the Gulf of Cambay and implications to their oceanic budgets.

*Chapter 6* deals with sources and behaviour during transportation of alkali earth metals Sr and Ba in selected Indian rivers, estuaries and their fluxes to the Bay of Bengal and the Arabian Sea. The potential of using  $^{87}\text{Sr}/^{86}\text{Sr}$  as a proxy for estimating the submarine groundwater discharge is also described in this chapter.

*Chapter 7* synthesises all the results obtained in this thesis and provide the conclusions drawn with brief outlines of the future directions.

## **CHAPTER-2**

### **Materials and Methods**

The primary objectives of this thesis as mentioned in the first chapter are (i) geochemical and isotopic studies of sediments of the Ganga basin to infer about paleo-erosion pattern and paleo-weathering intensity of the Ganga basin and their link to climate change, to learn about temporal variations in climate and dissolved  $^{87}\text{Sr}/^{86}\text{Sr}$  of the Ganga and the implications of the later to global sea water Sr isotope budget, (ii) geochemical behaviour of trace elements in estuaries particularly the redox sensitive elements U, Mo and Re and the alkaline earth metals Ba and Sr to characterize the factors regulating their abundances and distribution in estuaries in terms of their sources, fluxes and biological processes. These studies require detailed sampling of various samples from the Ganga plain and estuaries and their chemical and isotopic analysis. This chapter describes the various methodologies used for sampling and analysis.

## **2.1 The Ganga Basin**

### **2.1.1 General description of the basin**

The Ganga basin is spread over the Himalaya in north to peninsular India in south with the Ganga plain between them. The Ganga is formed at Devprayag by the confluence of the Bhagirathi and the Alaknanda rivers. The Bhagirathi originates from the Gangotri glacier in the Higher Himalaya and the Alaknanda is sourced from Bhagirathi Kharak and Bamak glaciers. Subsequent to its formation, the Ganga drains through the Lesser Himalaya and the Siwalik and descends into the plains. The Ganga basin encompasses the drainage areas of the Ganga main stream and its tributaries the major ones being the Ghaghra, Gandak, and the Kosi from the Himalaya and the Yamuna, draining both the Himalaya and Peninsular India and the Son draining only peninsular India (Fig. 2.1). The Yamuna is the largest tributary of the Ganga predominantly draining through the peninsular India and joins the Ganga main stream at Allahabad. The tributaries of the Yamuna, the Chambal, Sind, Betwa and the Ken drain the Deccan traps and the Vindhyan sedimentary sequences comprising of sandstones, shales and carbonates (Krishnan, 1982) (Fig. 2.1). The

Gomti and the Son are two other tributaries of the Ganga; which have the drainage basin entirely in the Ganga plain/peninsular India. All these tributaries join the main stream Ganga at various locations in the Ganga plain (Fig. 2.1).

The Himalayan sub-basin of the drainage basins of the Ganga and its tributaries consists of four major lithological units, the Tethyan Sedimentary Series (TSS), the Higher Himalaya (HH), the Lesser Himalaya (LH) and the Siwalik (Gansser, 1964; Valdiya, 1980; Sarin et al., 1989; Bickle et al., 2001). The lithology of each of these units over the entire Himalayan range, from east to west, is roughly the same (Gansser, 1964; Le Fort, 1975; Valdiya, 1980). The headwaters of the Alaknanda, Ghaghra, Gandak and the Kosi lie in the Tethyan Sedimentary Series (TSS). The TSS is composed of carbonates and clastic sedimentary rocks (Oliver et al., 2003). The dominant lithologies of the HH are the Higher Himalayan Crystallines (HHC) which consists of granites and gneisses, metamorphosed carbonates and calc-silicates. The HH is separated from the Lesser Himalaya (LH) by the Main Central Thrust (MCT). The lithologies of the LH are meta-sedimentary rocks which include limestones, dolomitic carbonates, shales, slates, quartzites, evaporites and calc-silicates. The LH is divided into two sedimentary sequences, the outer and inner belts, separated by the Lesser Himalayan Crystallines (LHC) consisting of granites and gneisses (Valdiya, 1980). The Siwaliks is the southern most unit of the Himalaya formed by sediments derived from the HH and LH due to the uplift of the Himalaya during Miocene-Pliocene orogeny. The Ganga descends to the plain at Haridwar and traverses through it till drains into the Bay of Bengal. The Ganga receives all its major tributaries mentioned earlier in the Ganga plain. The plain is an alluvial tract formed by materials transported from the Higher and Lesser Himalaya by mountain-fed rivers, the Ganga headwaters, Gandak, Ghaghra and the Kosi all of which carry huge quantity of sediments from the Himalaya and form large depositional areas in the plain (Sinha and Friend, 1994). The sediments of the plain is composed of beds of clay, sand and silt (Sinha et al., 2007). Carbonates, locally known as 'Kankar' formed by precipitation from river and groundwater and saline and alkaline salts formed by

evaporitation are dispersed in the sediments of the Ganga plain (Agarwal, 1992; Srivastava et al., 2001; Pal et al., 2003). These carbonates are generally formed in arid-semiarid regions during summer. Part of the drainage of the Ganga plain is an endoreic system. Because of this endoreic system coupled with semi-arid climatic conditions leads to repeated cycles of drying and wetting of the plain which promotes precipitation of calcite and other saline/alkaline minerals in the plain and in shallow depths in sediments (Srivastava et al., 2001; Pal et al., 2003). These authigenic carbonates are formed by precipitation from soil and groundwater; occurring at different depth horizons of the Ganga plain with more extensive occurrences in the central and the southern parts of the plain. These carbonates are well characterized by earlier workers in widely different parts of the plains on the basis of their petrography, genesis and carbon and oxygen isotopic composition (Salomon et al., 1978; Alam et al., 1997; Srivastava et al., 2001; Sinha et al., 2006). These carbonates though are scattered at different depths in sediments of the Ganga plain, their well-defined horizons are limited to certain depths.

The Ganga plain experiences subtropical and monsoonal climate with average precipitation of  $\sim 800$ - $1000$  mm/year (Singh, 1994). In the central Ganga plain, average minimum and maximum temperatures are  $21^{\circ}\text{C}$  for November to February and  $27^{\circ}\text{C}$  to  $33^{\circ}\text{C}$  for March – June (Sharma et al., 2004). The onset of monsoon is generally in mid-late of June and its retreat begins during October. The south-west monsoon accounts for more than 85% of rainfall in this region. The average annual discharge of the Ganga river at Kanpur before confluence with the Yamuna is  $\sim 900$   $\text{m}^3/\text{s}$  and the bank full discharge is  $8500$   $\text{m}^3/\text{s}$  (Sinha et al., 2007).

### **2.1.2 Core Locations in the Ganga plain**

For studies in paleo-erosion pattern, samples were taken from two cores, a 50-m-long core collected from Indian Institute of Technology, Kanpur campus (IITK) and another 25-m-long core collected from Jagdishpur (JP),  $\sim 25$  km north of Kanpur in the Ganga Plain (Fig. 2.1). These cores were collected by scientists of IITK and the

University of Delhi and provided to us for chemical and isotopic studies. The IITK core represents the southern interfluvial region of the western Ganga plain lying in the southern part of the Himalayan foreland basin and far upstream of the confluence of the Ganga and the Yamuna.

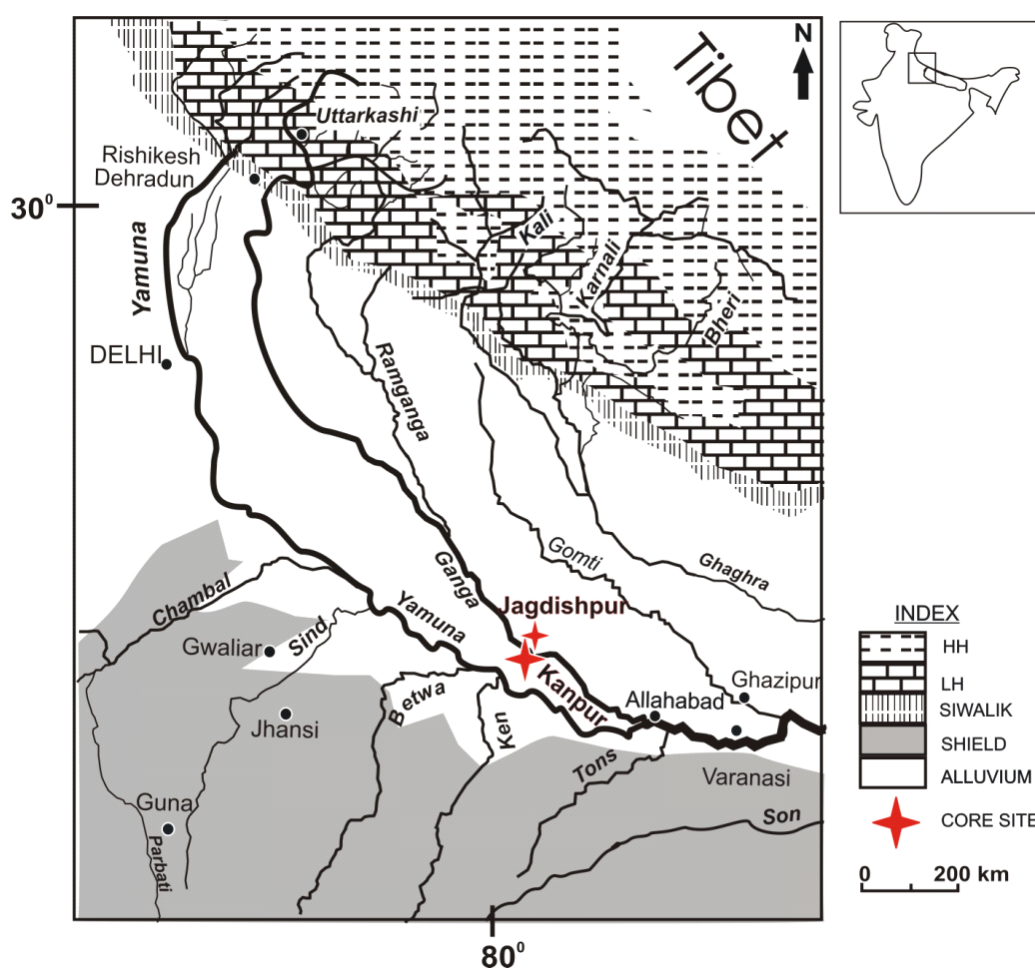


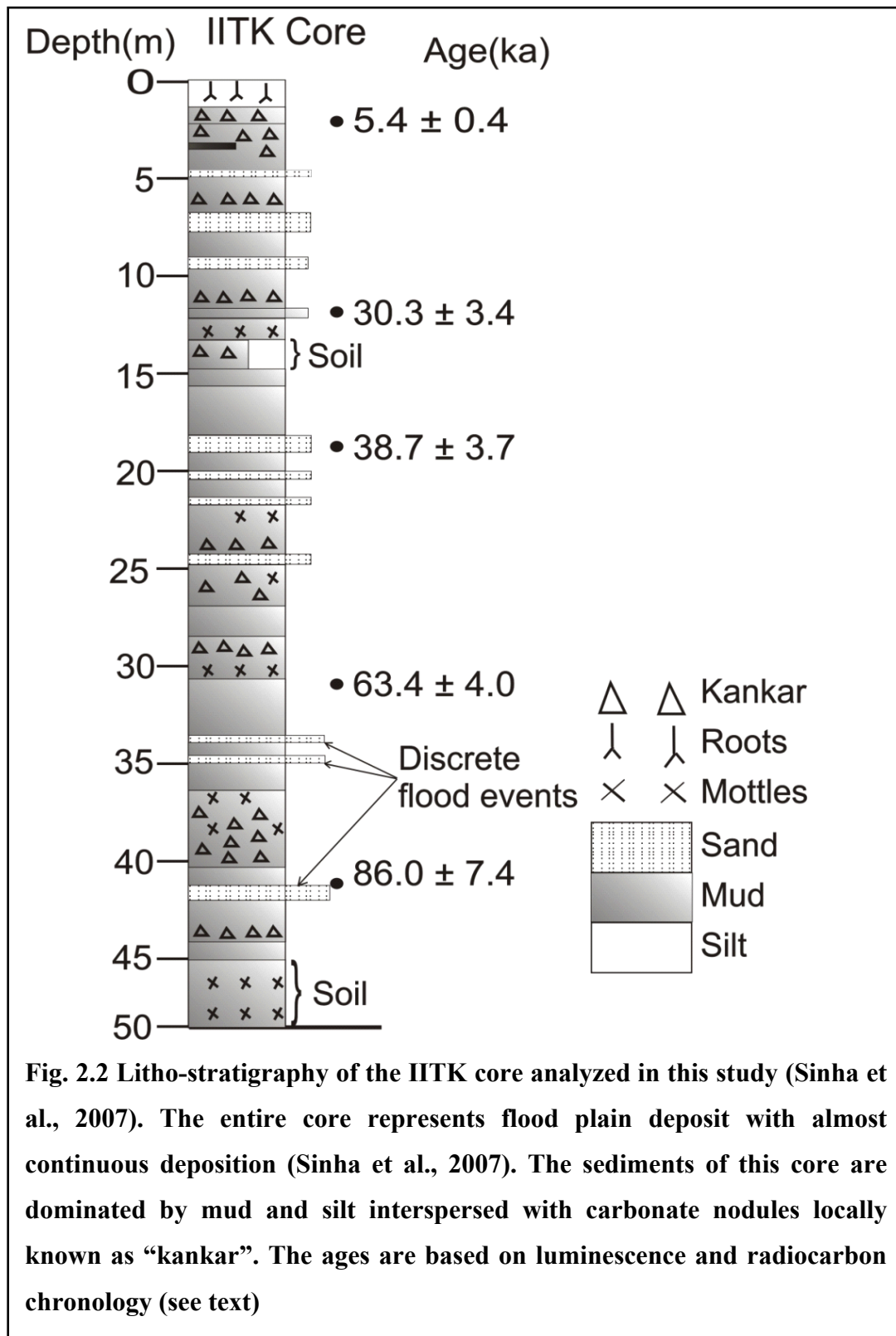
**Fig. 2.1 Sampling locations.** Samples for this study are from depths of a 50-m-long core taken at Indian Institute of Technology Kanpur campus (IITK) and a 25-m-long core from Jagdishpur (JP); ~25 km north of Kanpur core HH—Higher Himalaya; LH—Lesser Himalaya.

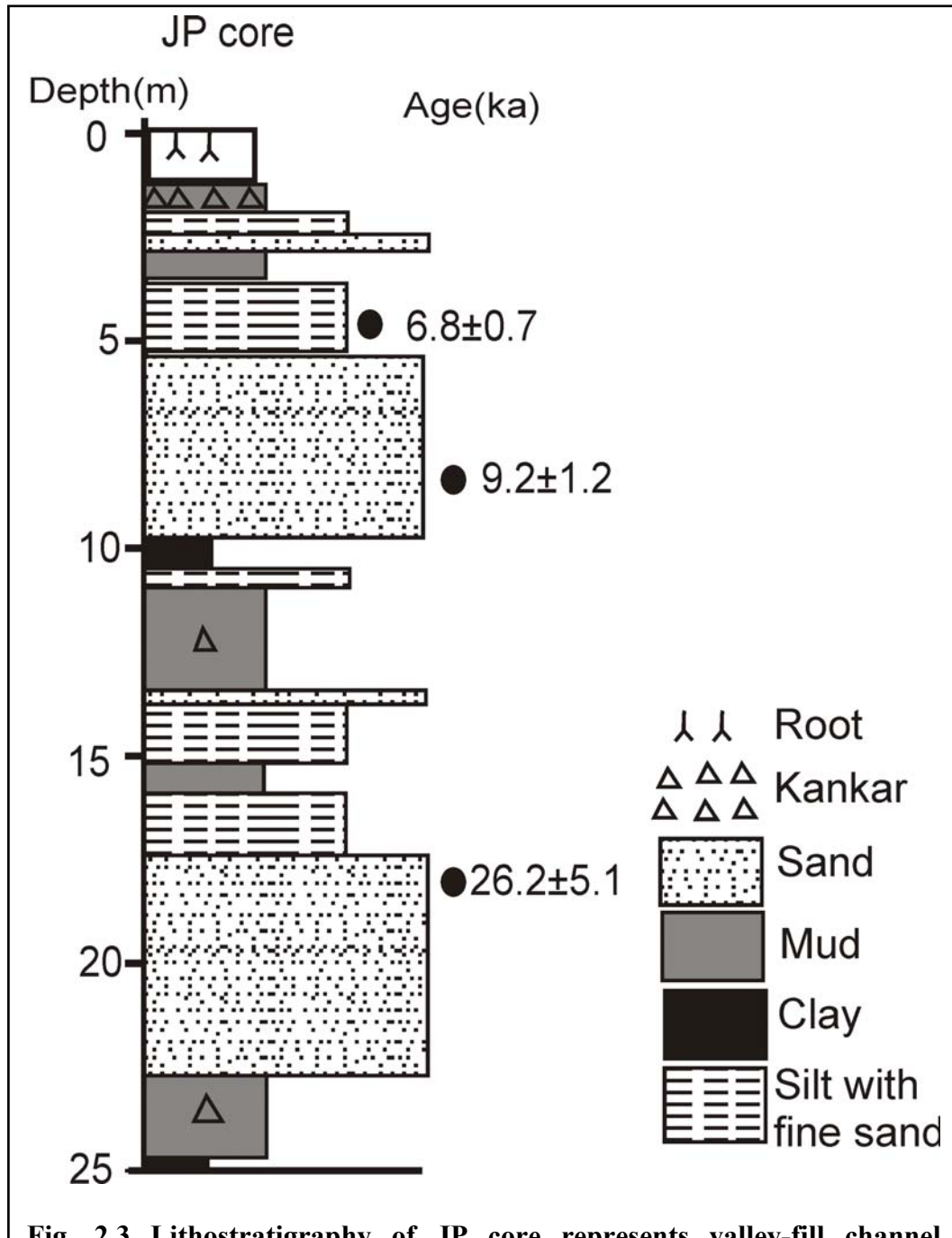
The IITK core, located about 14 km south of the southern bank of the Ganga, represents an interfluvial setting whereas the Jagdishpur core is taken from river channel, ~12 km north of the present location of the Ganga (Fig. 2.1). The Ganga river valley is 20 km wide near Kanpur with surface elevation of 120-130 m above

the mean sea level. Sediments of the core sites are derived from the Himalaya (Singh, 1992, Sinha et al., 2009, Srivastava et al., 2010). The core sites are situated about 80 to 100 km north of the present location of the Yamuna. In the recent past there has been no significant northward movement of the Yamuna from its present position (Singh, 1992; Sinha et al., 2009) and therefore the core site is unlikely to have received sediments from the Yamuna drainage which has contribution from peninsular India (Singh et al., 2008). Mineralogical and micropmorphological studies on the sediments of this core (Srivastava et al., 2010) also confirm their Himalayan sources. Hence the sediments of these two cores collected around Kanpur are derived only from Himalayan sources and any variations in their properties (mineralogical, chemical and isotopic) have to be caused by variations in their supply from different sub-basins of the Himalaya.

### **2.1.3 (a) Litho-Stratigraphy and facies of the cores**

Lithostratigraphy of the IITK and JP cores has been described by Sinha et al. (2007). Their studies show that the entire length of IITK core comprises mostly of silt with few layers of sand and intermittent presence of calcretes located in interfluvial settings. Carbonates though occur dispersed in the Ganga plain (Agarwal et al., 1992), these nodules were abundant only at certain depths and not distributed throughout the core; hence they provide only discontinuous paleo-records. There is no major sand body in the core (Fig. 2.2), since during the last ~100 ka this site has remained in the interfluvial setting. The core does not show any record of major discontinuity. The entire core consists of floodplain facies with continuous over bank muds, interspersed with thin layers of silt (Sinha et al., 2007). The dominant floodplain facies is yellow-brown mud associated with thin silt sheets, the splay deposits. Red-brown mud marks the upper part of each depositional unit. The upper part of the core is interspersed with silt layers. In general, all the individual facies have similar bulk mineralogy (Sinha et al., 2007) with quartz (~65%), mica (20–25%) and feldspar (10–15%).





Texturally, four muddy facies are recognized in this core, with individual facies varying in thickness up to 4 m. Yellow–brown mud, aggradational floodplain sediments, dominates at all locations. Red–brown mud with local silt patches, carbonate nodules and black mottles is the next abundant facies. Hard pale clay, commonly associated with red–brown mud, occurs as rare beds with thickness up to 0.5 m. Carbonate facies consists of layers of carbonate nodules up to 5 cm in diameter, locally termed as ‘kankar’. These layers are associated with other facies. There are minor deposits of discrete flooding events at ~35 m and 42.5 m depths. This core consists of two flood plain accretion units separated by soil layers that represents periods of minimal net sedimentation or minor hiatus at ~15 and ~45 m.

The JP core is taken from river channel in the Ganga valley, ~12 km north of the present location of the Ganga (Sinha et al., 2007, Fig. 2.1). This core consists of valley fill channel deposits and is made of sand, silt and minor abundance of carbonates (Sinha et al., 2007). Four facies were identified in this core viz., (i) fine- to medium-grained channel sand, (ii) concretions and red and brown mottling, (iii) interbedded silt and very fine sand and (iv) yellow–brown floodplain mud with carbonate concretions (Fig. 2.3). Among these, channel facies are prominent as discrete units up to 10 m thick (Fig. 2.3). The units consist mainly of fine to medium sand with layers of carbonate nodules. The bulk mineralogy of the individual facies shows wide range in case of quartz (51-72%) and mica (25-40%) whereas feldspar shows almost uniform abundance ~ (8-9%). Clay minerals abundance shows predominance of illite in fine fraction of both channel and floodplain sediments, with a moderate proportion of kaolinite. The relative abundance of illite and chlorite is highest at the base of the upper cycle, with a sharp rise in the abundance of kaolinite at ~6.5 m relative to illite and chlorite (Sinha et al., 2007).

### **(b) Chronology of the IITK and JP core**

Sinha et al. (2007) reported the chronology of IITK core based on luminescence dating of etched K-feldspars. Four samples of the IITK core from 11.6, 21.5, 31.9 and 41.9 m depths were dated which yielded ages of  $30.3 \pm 3.4$ ,  $38.7 \pm 3.7$ ,

63.4±4.0 and 86.0±7.4 ka respectively. The age of carbonate nodules from 2.3 m depth of this core was determined using  $^{14}\text{C}$  as part of this work. It yielded an age of 5.4±0.4 ka (Rahaman et al., 2009). The radiocarbon age may represent a minimum age for the depositional event as carbonate can precipitate either during or after the sediment deposition. These ages are used to establish an age model for this core which indicates that the sedimentation rate between the depth intervals 2.3 to 11.6 m, 21.5 to 31.9 m and 31.9 to 41.9 m is the same at about 0.41±0.03 m/ka, whereas it is higher, 1.2±0.7 m/ka, between the depths 11.6 to 21.5 m. Age-depth models of the IITK core is given in Fig. 2.4.

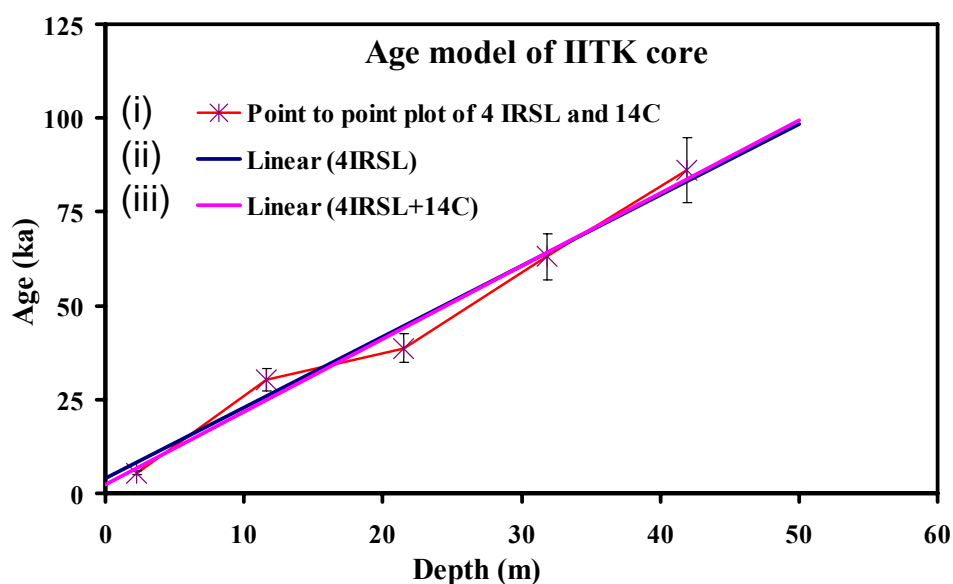


**Fig. 2.4 Age-depth models of the IITK core. Three age models (i), (ii) and (iii) are given here. They all agree within the uncertainty associated with the individual ages.**

Three age models based on (i) point to point fit of four IRSL and one  $^{14}\text{C}$  ages, (ii) linear fit of our IRSL ages and (iii) linear fit of four IRSL and one  $^{14}\text{C}$  age are given (Fig. 2.4). They all well agree within the uncertainty associated with the individual ages. The first age model (Fig. 2.4) based on point to point interpolation of four IRSL ages and one radiocarbon ages has been considered for this study.

The chronology of the JP core was also determined by Sinha et al. (2007) based on luminescence dating of etched K-feldspars. Three feldspar ages of  $6.8 \pm 0.7$  ka,  $9.2 \pm 1.2$  ka and  $26.2 \pm 5.1$  ka are available from this core. The top of the lower sand body has yielded  $26.2 \pm 5.1$  ka. The upper sand body is well constrained with an age of  $9.2 \pm 1.2$  ka for the lower part and  $6.8 \pm 0.7$  ka for the upper part (Fig. 2.3).

#### 2.1.4 Sub-sampling of the cores for chemical and isotopic studies

The sediments were sub-sampled from different depths of the IITK core archived in the core repository at IIT Kanpur. Samples were dried at  $\sim 90^\circ\text{C}$  to remove moisture. The dried sediments were powdered using an agate mortar and pestle and sieved through nylon sieves of  $100\ \mu\text{m}$  size and homogenized thoroughly.

The carbonate nodules of varying sizes, about 0.5 to 5 cm, were hand picked from the various depths of IITK and JP cores. They are white to off-white in colour and irregular in shape, typical of “kankars” found in the Ganga plain (Agarwal, 1992; Srivastava, 2001). These carbonates were generally associated with silty material which was separated physically to some extent before crushing them for chemical analysis.

Considering that the knowledge of isotope composition of contemporary sediments and carbonates may aid in the interpretation of isotope compositions of sediment cores, samples of contemporary river sediments and water from the Ganga at Kanpur and groundwater from the adjacent area were also collected.

**Table 2.1: Details of river water, groundwater and mollusk**

| Sample | Date   | Type        | Latitude           | Longitude          | Location             |
|--------|--------|-------------|--------------------|--------------------|----------------------|
| GP-134 | 3/3/09 | Groundwater | $26^\circ 37.055'$ | $80^\circ 16.766'$ | Ganga valley, Kanpur |
| GP-137 | 3/3/09 | Shells      | $26^\circ 36.648'$ | $80^\circ 16.615'$ | River bank, Kanpur   |
| GP-135 | 3/3/09 | River water | $26^\circ 36.716'$ | $80^\circ 16.598'$ | River bank, Kanpur   |

In addition, a few mollusk shells were also collected from the river channel to compare its isotope composition with that of water.

The second part of this thesis, as mentioned in the earlier chapter, deals with the study of elemental and isotopic distribution in estuaries. In the following, the details of sampling and analysis of estuarine samples are discussed.

## **2.2 Estuaries and coastal areas of the Arabian Sea and Bay of Bengal**

Water and sediments samples were collected from four estuaries; the Hooghly estuary in the Bay of Bengal and from the Narmada, Tapi and the Mandovi estuaries along the western coast of India (Fig. 2.5). The Hooghly estuary was sampled by scientists from Geological Survey of India, Kolkata and samples were provided by them for this study. The Hooghly is one of the distributaries of the Ganga which bifurcates from the mainstream at Farraka and drains into the Bay of Bengal near the Kolkata city (Fig. 2.5). The Ganga drains granite-gneisses and sedimentary rocks of the Himalaya and recent alluvium of the Ganga plain. The west flowing rivers draining into the Arabian Sea flow through the Deccan basalts and the older sedimentary sequence of the Vindhyan and the basement of Dharwar craton (Sastry and Gopinath, 1985; Upadhyay and Gupta, 1995; Alagarsamy, 2006). The hydrological and lithological details of the rivers draining into the estuaries are given in Table 2.2. The west flowing rivers which fall in to the Gulf of Cambay are influenced by industrial activities. Chemical, pharmaceutical, petrochemical and steel industries are situated along the bank of the Narmada, Tapi, Mahi and the Sabarmati rivers, their estuaries and the coast of the Gulf of Cambay. The world's largest ship breaking yard is situated at Alang-Sosia on the west coast of Gulf of Cambay, (Fig. 2.6; GoI Report, 2002). The ship breaking activity generates annually ~7500 million tons of solid waste which include petroleum hydrocarbons and heavy metals (GoI Report, 2002). Other ongoing industrial activities in this area are thermal power plants using coal, lignite or diesel and mining of lignite ([http://ic.gujarat.gov.in/Ind\\_guj/natural\\_resources.html](http://ic.gujarat.gov.in/Ind_guj/natural_resources.html)). In addition, oil and natural gas are also being mined at several locations along the coast of the Gulf of Cambay (GoI Report, 2002), which releases considerable amount of liquid, gaseous and solid wastes to the environment, most of which finally end up in the Gulf. It is estimated

that an annual flux of  $\sim 5000 \times 10^6 \text{ m}^3$  of treated waste water from these industries is discharged directly into the middle of the Gulf (GoI Report, 2002). Therefore, sampling was done strategically along the coastal area of the Gulf of Cambay and industrial effluent which are being directly or indirectly discharged to the river, estuary and coast.

### 2.2.1 Lithology, geohydrology and climate

The Ganga originates in the Himalaya, flows through the Himalaya and the Ganga plain before discharging into the Bay of Bengal. In the Himalaya the prominent lithologies are granite/gneisses, carbonates and shales. Black and gray shales also occur in the Himalaya (Singh et al., 1999; Dalai et al., 2002). The Ganga plain is made of alluvium transported predominantly from the Higher Himalaya (Singh et al., 2008). The peninsular tributaries of the Ganga drain the Vindhyan sedimentary rocks and the Deccan Basalts (Singh et al., 2008). The Hooghly has a very wide mouth and its estuary extends  $\sim 70$  km into the Bay of Bengal because of large fresh water influx. The fresh water discharge varies with season, it is as high as  $3000 \text{ m}^3/\text{s}$  during monsoon (June-September) and  $1000 \text{ m}^3/\text{s}$  during other seasons (November- May) (Sadharam et al., 2005). The water discharge of the Hooghly river is regulated by the Farakka barrage.

The Narmada originates in the Vindhyan mountains in Madhya Pradesh (MP) and the Tapi rises in Betal district of MP (Fig. 2.5). The Narmada drains the Deccan basalts and the Vindhyan made of carbonates, shales and sandstones. Sporadic occurrences of black/gray shales are reported in the Vindhyan (Gupta and Chakrapani, 2007). Tapi drains mostly through the Deccan basalts with part of its downstream drainage in alluvium. Both these rivers discharge into the Gulf of Cambay (Fig. 2.5, 2.6). These rivers receive significant contribution from ground water (Gupta and Chakrapani, 2007) particularly during their lean flow season (November-June). A number of hydrothermal springs have been reported along the Narmada and Tapi lineament (Minissale et al., 2000; Sharma and Subramanian, 2008). The annual rainfall in the Narmada and the Tapi basins is 1250 and 830 mm respectively, of

which 90% is received during the south-west monsoon (Sharma et al., 2007). Both these rivers have dams/reservoirs along their courses (Gupta and Chakrapani, 2007).

**Table 2.2: Lithological and hydrological details of Rivers**

| <b>River</b>       | <b>Major lithologies</b>                                     | <b>Area<br/>(10<sup>6</sup> km<sup>2</sup>)</b> | <b>Discharge<br/>( km<sup>3</sup> yr<sup>-1</sup>)</b> | <b>Runoff<br/>(mm yr<sup>-1</sup>)</b> | <b>Ref.</b> |
|--------------------|--|---|--|--|-------------|
| <b>Hooghly</b>     | Granite-gneisses,<br>Recent alluvium,<br>Carbonates          | 0.750   | 52   | 657                                    | 1           |
| <b>Narmada</b>     | Basalts, Vindhyan<br>sediments, alluvium                     | 0.099   | 47   | 418                                    | 2           |
| <b>Tapi</b>        | Basalts and alluvium   | 0.065   | 19   | 282                                    | 2           |
| <b>Mahi</b>        | Shale-gneisses   | 0.035   | 12   | 339                                    | 2           |
| <b>Sabarmati</b>   | Shale-gneisses   | 0.022   | 4  | 189                                    | 2           |
| <b>Vishwamitri</b> | Trappean, Alluvium   | 0.003   | 1  | 250                                    | 3           |
| <b>Mandovi</b>     | Basalts, granite-<br>gneisses, laterite,<br>coastal alluvium | 0.01  | 16   | 1600                                   | 4           |

**1: Biswas, 1985; 2: Madhavan and Subramanian, 2001; 3: Raj et al., 2004;**

**4: Upadhyay and Gupta, 1995**

The Mandovi originates from the Western Ghats of the Indian peninsula and flows from east to west over a length of 75 km through the rocky terrains of Goa, draining into the Arabian Sea (Upadhyay and Gupta, 1995; Alagarsamy, 2006). This estuary is ~650 kms south of the Gulf of Cambay in the Arabian Sea (Fig. 2.6). The climate of Goa is tropical and the average annual rainfall is 3000 mm, of which about 90% occurs during the southwest monsoon (June-September). A large part of the Mandovi drainage consists of basalts, phyllites, metagreywacke/metabasalts and schists/gneisses which at many locations are capped by laterites (Sastry and Gopinath, 1985). The laterites are abundant in its lower reaches.

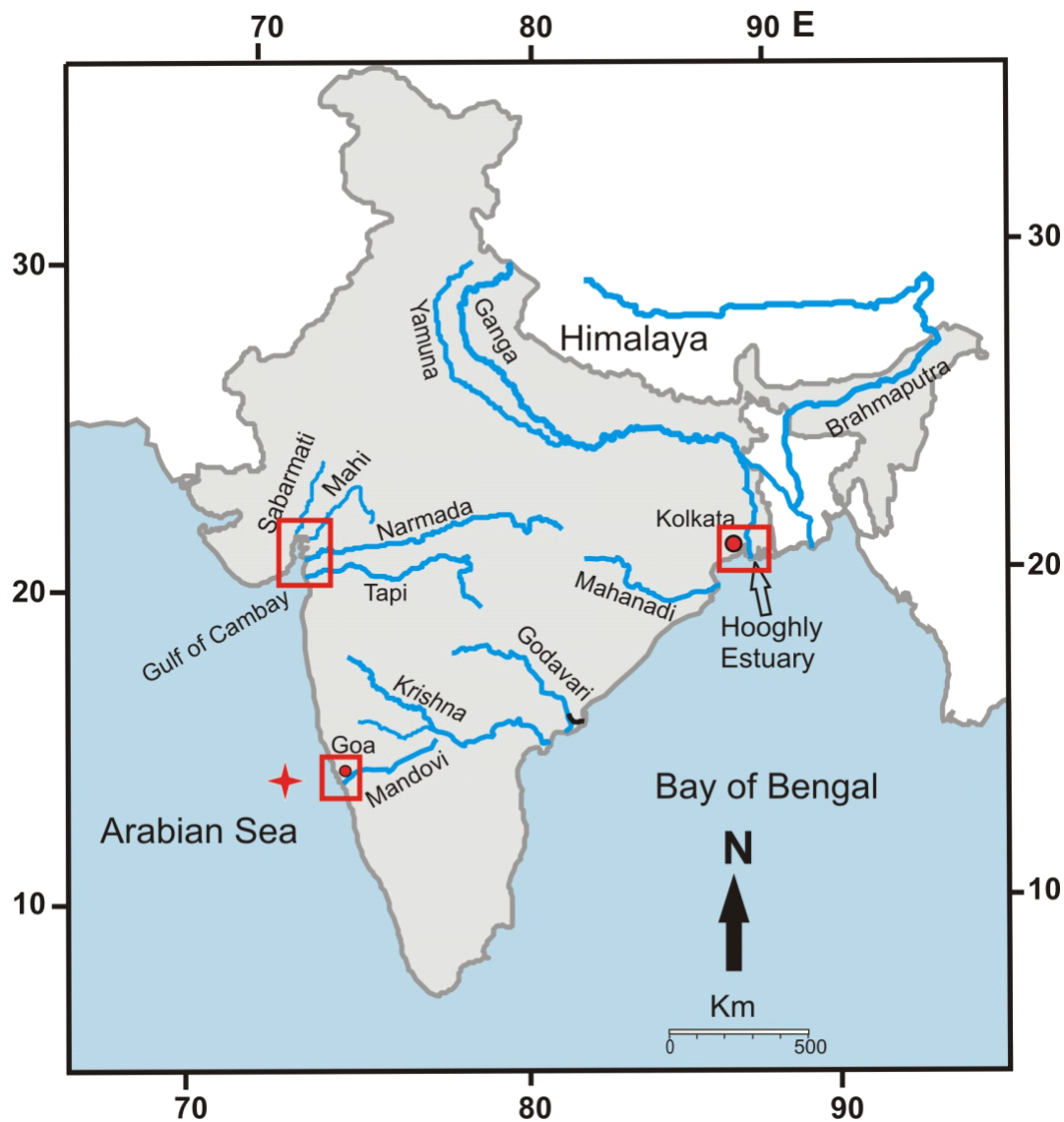


**Fig. 2.5** Location of the Hooghly, Narmada, Tapi, Mahi, Sabarmati and the Mandovi estuaries. Samples for this study were collected from the estuaries of these rivers. In addition, a few samples were also collected from the open Arabian Sea off Goa (★). Rectangles in the figure are the areas of study.

The Narmada, Tapi, Mahi and the Sabarmati rivers drain into the Gulf of Cambay, a semi enclosed basin (Fig. 2.6). It has a positive water balance due to significant fresh water supply from the rivers, particularly from the Narmada and the Tapi. The rivers

supply  $\sim 85 \text{ km}^3$  of fresh water (Table 2.2) and  $74 \times 10^6$  tons of sediments to the Gulf of Cambay annually and the residence time of water in the Gulf varies from 4 to 15 days, increasing northward (GoI Report, 2002). The prevalent tidal oscillations do not flush out the Gulf completely resulting in leftover parcels of water with increasing residence time in the Gulf of Cambay (GSEAP, 2003).

### 2.2.2 Sampling from estuaries and coastal areas

Water and sediment samples were collected from all the four estuaries, the Hooghly, Narmada, Tapi and the Mandovi following the salinity gradient (Fig. 2.5, Table 2.2). In addition, a few samples were also collected from the Mahi estuary (Fig. 2.6). Water and suspended particulate matter samples from the Narmada, Tapi and the Mandovi estuaries were collected during both monsoon and non-monsoon seasons. Generally the sampling was done during one tidal cycle (low tide). Samples from the Hooghly estuary were collected during December 2006, onboard RV Samudra Manthan (Marine Wing, Geological Survey of India). Salinity, dissolved oxygen (DO), conductivity, pH and temperature were measured onboard. In addition to the estuaries, samples were also collected from the rivers upstream, from coastal areas of the Gulf of Cambay and from the open Arabian Sea, offshore Goa coast (Figs. 2.5). The open ocean samples from the Arabian Sea were collected onboard FORV Sagar Sampada (SS 256). Further, a few samples were also collected from the Mahi estuary near its mouth, from the Sabarmati and the Vishwamitri rivers (Fig. 2.6) water off the coast of Bhavnagar, Alang-Sosia and Ghogha and industrial waste water discharging into the Gulf of Cambay.

Water samples were collected in precleaned high density polypropylene bottles. Prior to sampling, the bottles were soaked with 2N HCl for several days and cleaned profusely with MilliQ water. All the water samples for trace elements and Sr isotopes analysis were filtered through nylon filter ( $0.2 \mu\text{m}$ ), acidified to pH  $\sim 2$  using quartz distilled  $\text{HNO}_3$  and stored in the precleaned high density polypropylene bottles.

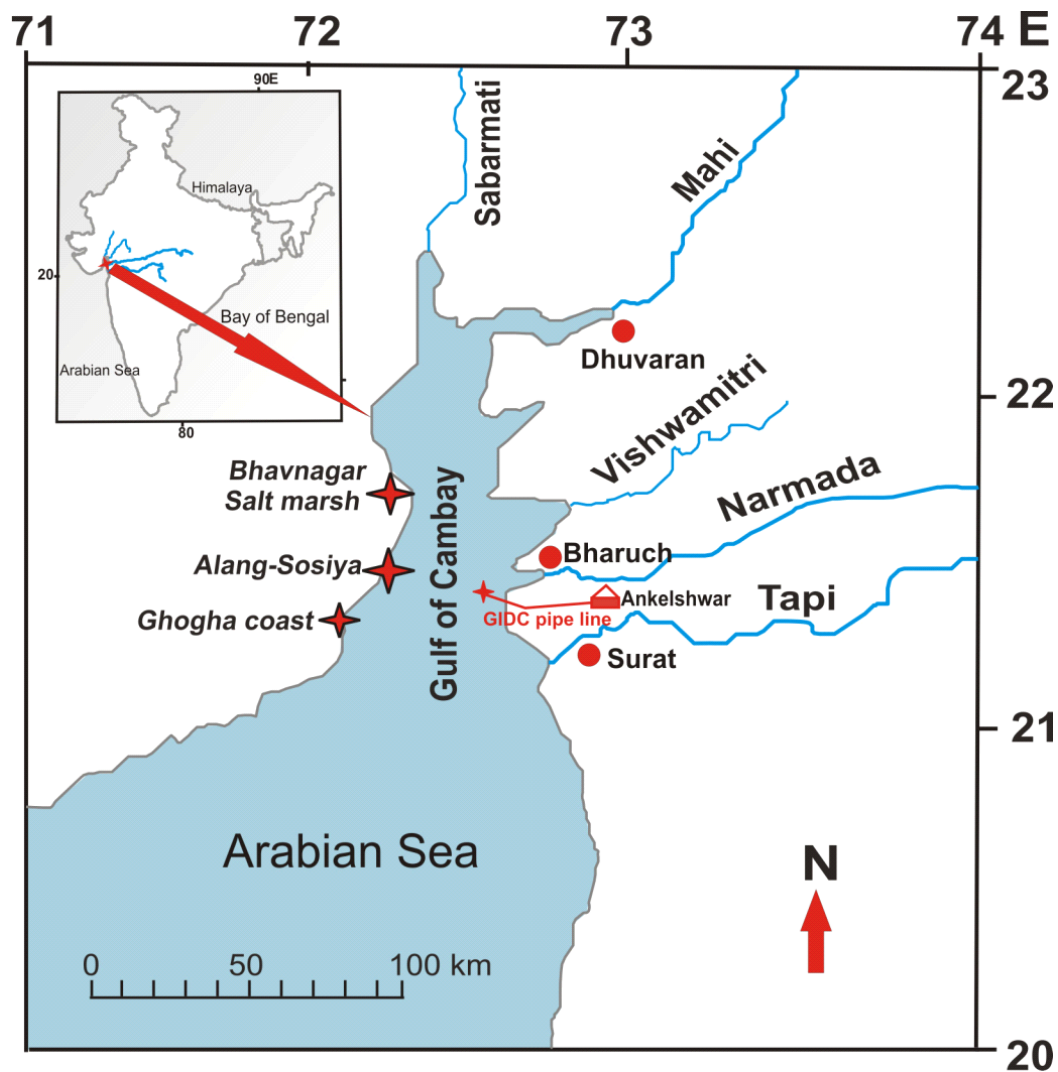


**Fig. 2.6** The Gulf of Cambay and the estuaries of the Narmada, Tapi, Mahi and the Sabarmati. The location of the ship-breaking facility near Alang-Sosia and salt marsh near Bhavnagar are also shown. Two waste water samples from industrial effluent were also collected from GIDC mega pipe line near the Narmada estuary.

A few samples were filtered through Millipore nucleopore filter (0.45  $\mu\text{m}$ ) to check whether the use of 0.2 or 0.45  $\mu\text{m}$  pore size filters make any difference on the dissolved trace elements concentration of these waters. For suspended particulate matter, ~10 liter water samples from different salinities were collected in plastic

carbouys and left undisturbed for two weeks to settle the particulates. The supernatant was decanted and the settled particulate matter was separated. Bed loads and bank sediments were collected from the exposed sand bars and from the banks in selected estuaries.

### 2.3 Analytical techniques

Various analytical techniques were used as shown in the flow chart for the analysis of sediments and water samples collected from the Ganga plain, Indian rivers and estuaries, coastal areas of the Gulf of Cambay and open ocean of the Arabian Sea. Significant efforts were made to establish various analytical techniques and protocol for chemical procedures viz., the extraction and purification of Re from dissolved and particulate phases and their analysis by Inductively Coupled Plasma-Mass Spectrometry (ICP-MS, Quadrupole). Trace element measurement in seawater by ICP-MS is tricky and difficult because of its high matrix and isobaric interference. Therefore, setting up protocol and tuning the newly acquired ICP-MS (Thermo-X Series<sup>II</sup>) at PRL, Ahmedabad for the analysis of trace elements in water having very low concentration (parts per trillion level) was a challenging task. Measurements of trace elements Re, U, Mo and Ba in seawater by ICP-MS was established for the first time in our laboratory during this thesis work. Chemical extraction and purification for the analysis of Re was done following the protocol reported by Trivedi et al. (1999) and Dalai et al. (2001) from this laboratory.

U, Mo and Ba were measured directly by quadrupole ICP-MS (Thermo-X series) following the method published by Rodushkin and Ruth (1997). These chemical procedures and associated mass spectrometric analyses are described in detail in the sub-section below. The elemental abundances in water and sediments were determined following established methods and procedures in this laboratory (Sarin et al., 1989; Dalai, 2001; Das et al., 2005).

### 2.3.1 Water analysis

#### (a) Temperature, pH, electrical conductivity and salinity

Temperature, pH, electrical conductivity (EC) and salinity of river, estuary and seawater samples were measured at site using Multiline kit (Model: Multiline 7000). Data of all these parameters are given in the Table 2.3 and 2.4. The pH calibration was made by freshly prepared buffer solutions of pH 4.0 and 9.2. Salinity and EC were calibrated using 0.01 M KCl solution before making measurements. The precision of pH measurement is better than 0.1 units and EC measurement is better than 10  $\mu\text{S}/\text{cm}$ . The accuracy of the conductivity measurements is better than 1% with ambient temperature ranges from 15-35° C. Temperature of river water was measured by thermometer attached with this multiline kit, with precision better than 0.1 °C. Location of the samples was determined by GPS (Garmin, VISTA Etrex).

**Table 2.3: Sampling location, and Salinity, Conductivity, Temperature Alkalinity and pH in the estuarine waters**

| Sample  | Latitude  | Longitude | Salinity<br>(‰) | Conduc.<br>(mS/cm) | Temp<br>(°C) | Alkalinity<br>( $\mu\text{Eq}/\ell$ ) | pH   |
|---|-----------|-----------|-----------------|--------------------|--------------|---------------------------------------|------|
| <b><u>Narmada (Pre-monsoon, March 2007)</u></b> |           |           |                 |                    |              |                                       |      |
| NE07-20   | 21°41.49' | 73°11.57' | 0               | 0.3                | 27.7         | 2862                                  | 7.99 |
| NE07-21   | 21°50'01' | 73°45.34' | 0               | 0.2                | 27           | 2447                                  | 8.34 |
| NE07-22   | 21°51.81' | 72°41.74' | 0               | 0.3                | 30.1         | 2558                                  | 8.03 |
| NE07-18   | 21°40.51' | 72°57.00' | 0               | 0.6                | 27.9         | 3015                                  | 8.06 |
| NE07-19   | 21°40.63' | 72°57.54' | 0               | 0.6                | 27.7         | 3002                                  | 7.93 |
| NE07-1  | 21°40.81' | 72°54.57' | 4.8             | 8.5                | 25.4         | 2947                                  | 8.08 |
| NE07-2  | 21°41.26' | 72°52.60' | 9.3             | 15.7               | 25.6         | 2962                                  | 7.92 |
| NE07-3  | 21°40.58' | 72°50.39' | 11.8            | 19.7               | 25.8         | 2909                                  | 7.98 |
| NE07-4  | 21°39.20' | 72°47.42' | 15.9            | 26.0               | 26.5         | 2814                                  | 7.93 |
| NE07-5  | 21°38.80' | 72°45.34' | 18.2            | 29.4               | 27.1         | 2807                                  | 7.96 |
| NE07-6  | 21°40.75' | 72°42.05' | 20              | 32.1               | 27.4         | 2754                                  | 8    |
| NE07-7  | 21°40.71' | 72°49.83' | 21.3            | 33.9               | 27           | 2744                                  | 7.95 |
| NE07-8  | 21°39.46' | 72°35.89' | 22.1            | 35.0               | 28.2         | 2776                                  | 8.03 |
| NE07-9  | 21°39.36' | 72°34.51' | 23.9            | 37.7               | 27.7         | 2738                                  | 8.02 |
| NE07-10   | 21°39.62' | 72°33.28' | 25.3            | 39.6               | 27.8         | 2668                                  | 7.98 |
| NE°07-11  | 21°38.73' | 72°33.02' | 25.5            | 39.9               | 28.1         | 2686                                  | 8.11 |

|         |           |           |      |      |      |      |      |
|---------|-----------|-----------|------|------|------|------|------|
| NE07-12 | 21°38.04' | 72°32.70' | 27.2 | 42.2 | 27.1 | 2699 | 7.9  |
| NE07-13 | 21°38.0'  | 72°32.70' | 29   | 44.8 | 26.6 | 2653 | 8.08 |
| NE07-14 | 21°37.94' | 72°32.05' | 30.2 | 46.5 | 26.4 | 2654 | 8.1  |
| NE07-15 | 21°37.94' | 72°32.05' | 31.1 | 47.7 | 26.6 | 2635 | 8.08 |

**Narmada ( Monsoon, July 2007)**

|          |           |           |      |      |      |      |      |
|----------|-----------|-----------|------|------|------|------|------|
| NEM07-14 | -         | -         | 0    | 0.2  | 30.4 | 2009 | 8.49 |
| NEM07-1  | 21°40.59' | 72°55.58' | 0    | 0.3  | 30.3 | 2395 | 8.83 |
| NEM07-2  | 21°39.08' | 72°46.64' | 0    | 0.4  | 30.6 | 2385 | 7.98 |
| NEM07-3  | 21°40.07' | 72°37.12' | 1.3  | 2.8  | 30.6 | 2410 | 8.06 |
| NEM07-4  | 21°39.58' | 72°36.34' | 2.2  | 4.2  | 31.3 | 2405 | 7.99 |
| NEM07-5  | 21°39.42' | 72°35.49' | 3.4  | 6.2  | 30.8 | 2309 | 8    |
| NEM07-6  | 21°39.15' | 72°34.28' | 5.1  | 9.1  | 31.3 | 2270 | 8.03 |
| NEM07-7  | 21°38.55' | 72°33.18' | 6    | 10.5 | 30.5 | 2322 | 8.04 |
| NEM07-8  | 21°38.39' | 72°33.26' | 8    | 13.6 | 30.8 | 2259 | 8    |
| NEM07-9  | 21°39.27' | 72°35.26' | 9.8  | 16.4 | 30.6 | 2219 | 8    |
| NEM07-10 | 21°38.52' | 72°33.2'  | 12.1 | 20.0 | 30.8 | 2222 | 8.03 |
| NEM07-11 | 21°38.81' | 72°33.94' | 14.1 | 23.1 | 30.8 | 2180 | 8.03 |
| NEM07-12 | 21°38.05' | 72°33.19' | 15.5 | 25.3 | 30   | 2155 | 8.02 |
| NEM07-13 | 21°38.55' | 72°32.93' | 17.2 | 28.0 | 32.3 | 2146 | 8.25 |

**Narmada Second Channel (Monsoon, July 2008)**

|           |   |   |      |      |      |   |      |
|-----------|---|---|------|------|------|---|------|
| KOH-08-1  | - | - | 1.1  | 2.4  | 30.3 | - | 8.11 |
| KOH-08-2  | - | - | 1.8  | 3.5  | 30.1 | - | 8.16 |
| KOH-08-3  | - | - | 7.2  | 12.4 | 29.8 | - | 8    |
| KOH-08-4  | - | - | 17.7 | 28.6 | 30   | - | 8.05 |
| KOH-08-5  | - | - | 19.9 | 31.6 | 30   | - | 8.08 |
| KOH-08-6  | - | - | 25   | 39.0 | 30.5 | - | 8.04 |
| KOH-08-7  | - | - | 28.1 | 43.4 | 29.5 | - | 8.04 |
| KOH-08-8  | - | - | 29.3 | 45.1 | 30.3 | - | 8.03 |
| KOH-08-9  | - | - | 30.5 | 46.5 | 30.5 | - | 7.98 |
| KOH-08-10 | - | - | 30.7 | 46.9 | 30.7 | - | 8.04 |

**Tapi (Monsoon, July2007)**

|         |           |           |      |      |      |      |      |
|---------|-----------|-----------|------|------|------|------|------|
| TPM07-1 | 21°10.56' | 72°46.74' | 0    | 0.6  | 30.6 | 2848 | 7.57 |
| TPM07-2 | 21°8.9'   | 72°45.8'  | 1.1  | 2.4  | 30.5 | 2942 | 7.66 |
| TPM07-3 | 21°8.52'  | 72°43.61' | 2.1  | 4.1  | 30.6 | 2937 | 7.73 |
| TPM07-4 | 21°8.86'  | 72°42.26' | 3.9  | 7.1  | 30.5 | 3008 | 7.8  |
| TPM07-5 | 21°9.15'  | 72°4.73'  | 4.9  | 8.6  | 30.2 | 3085 | 7.74 |
| TPM07-6 | 21°9.3'   | 72°40.19' | 5.8  | 10.0 | 30.3 | 3030 | 7.84 |
| TPM07-7 | 21°7.97'  | 72°39.58' | 7.8  | 13.4 | 29.9 | 2941 | 7.9  |
| TPM07-8 | 21°7.05'  | 72°39.74' | 9.8  | 16.4 | 29.6 | 2809 | 7.92 |
| TPM07-9 | 21°5.79'  | 72°39.98' | 11.5 | 19.1 | 29.6 | 2700 | 7.35 |

|  |           |                   |      |      |      |      |      |
|--|-----------|-------------------|------|------|------|------|------|
| TPM07-10                                     | 21°4.97'  | 72°40.64'         | 13.1 | 21.6 | 29.6 | 2710 | 8.02 |
| TPM07-11                                     | 21°4.41'  | 72°40.71'         | 14.9 | 24.3 | 29.6 | 2685 | 8.01 |
| TPM07-12                                     | 21°3.6'   | 72°40.68'         | 17.4 | 28.1 | 29.8 | 2715 | 7.99 |
| TPM07-13                                     | 21°3.16'  | 72°40.35'         | 20.3 | 32.2 | 29.7 | 2530 | 8.02 |
| <b>Mandovi (Post-Monsoon, October 2007)</b>  |           |                   |      |      |      |      |      |
| MD07-1                                       | 15°32.56' | 73°57.69'         | 0    | 0.5  | 27.8 | 384  | 6.61 |
| MD07-2                                       | 15°32.39' | 73°55.95'         | 2.7  | 5.1  | 27.8 | 515  | 6.95 |
| MD07-3                                       | 15°31.55' | 73°55.60'         | 6    | 10.4 | 28.2 | 672  | 6.9  |
| MD07-4                                       | 15°31.33' | 73°55.38'         | 13.5 | 22.3 | 28   | 1113 | 7.43 |
| MD07-5                                       | 15°30.33' | 73°54.82'         | 16.1 | 26.2 | 28.9 | 1363 | 7.53 |
| MD07-6                                       | 15°30.27' | 73°54.16'         | 19.7 | 31.5 | 29   | 1512 | 7.72 |
| MD07-7                                       | 15°30.11' | 73°52.88'         | 26.9 | 41.7 | 28.9 | 1902 | 7.92 |
| MD07-8                                       | 15°30.34' | 73°50.63'         | 31.3 | 48.0 | 29   | 2131 | 7.98 |
| MD07-9                                       | 15°29.29' | 73°48.40'         | 33.7 | 51.1 | 28.5 | 2233 | 8    |
| MD07-10                                      | 15°29.07' | 73°41.09'         | 33.6 | 51.0 | 28.9 | 2236 | 8.18 |
| <b>Hooghly (Post-monsoon, December 2006)</b> |           |                   |      |      |      |      |      |
| W -1   | 22.01°    | 88.19°            | 0.5  | 1.4  | -    | -    | -    |
| W-2  | 21.9°     | 88.09°            | 2.6  | 5.0  | -    | -    | -    |
| W-3  | 21.77°    | 88.02°            | 7.7  | 13.3 | -    | -    | -    |
| W-4  | 21.65°    | 88.02°            | 11.8 | 19.7 | -    | -    | -    |
| W-5  | 21.58°    | 88.08°            | 14.7 | 24.3 | -    | -    | -    |
| W-6  | 21.49°    | 88.13°            | 16.7 | 27.3 | -    | -    | -    |
| W-7  | 21.33°    | 88.19°            | 20.5 | 32.9 | -    | -    | -    |
| W-8  | 21.06°    | 88.2 <sup>0</sup> | 22.5 | 35.9 | -    | -    | -    |
| W-9  | 20.69°    | 88.21°            | 30   | 46.4 | -    | -    | -    |
| W-10   | 20.0°     | 88.2°             | 32   | 49.1 | -    | -    | -    |

**Table 2.4: Salinity, Conductivity, Temperature and pH in the miscellaneous samples**

| Sample    | Sample type / River / Place | Salinity (%) | Conductivity (mS/cm) | Temp (°C) | pH   |
|-----------|-----------------------------|--------------|----------------------|-----------|------|
| KOH-08-11 | Pipe-line waste water       | 10.8         | 18.2                 | 28.3      | 7.73 |
| KOH-08-12 | Pipe-line waste water       | 11.6         | 19.2                 | 28.9      | 7.6  |
| KOH-08-13 | Vishwamitri river           | 0.1          | 0.7                  | 30.6      | 7.9  |
| KOH-08-14 | Mahi estuary                | 27           | 41.8                 | 31.9      | 7.93 |
| KOH-08-15 | Mahi estuary                | 25.6         | 40                   | 28.9      | 8.4  |
| KOH-08-16 | Mahi river                  | 0            | 0.5                  | 29.1      | 8.57 |
| KOH-08-17 | Sabarmati river             | 1.2          | 2.6                  | 32.5      | 7.92 |
| KOH-08-18 | Salt marsh, Bhavnagar       | 120          | 161                  | 35.1      | 7.11 |
| KOH-08-19 | Ghogha coast                | 32.4         | 49.2                 | 29.8      | 7.79 |

|           |                     |      |      |      |      |
|-----------|---------------------|------|------|------|------|
| KOH-08-20 | Ghogha coast        | 32.5 | 49.5 | 29.6 | 7.95 |
| GA07-1    | Arabian Sea off Goa | -    | -    | -    | -    |
| GA07-2    | Arabian Sea off Goa | -    | -    | -    | -    |
| GA07-3    | Arabian Sea off Goa | -    | -    | -    | -    |
| GA07-4    | Arabian Sea off Goa | -    | -    | -    | -    |
| GA07-5    | Arabian Sea off Goa | -    | -    | -    | -    |

- Not analysed

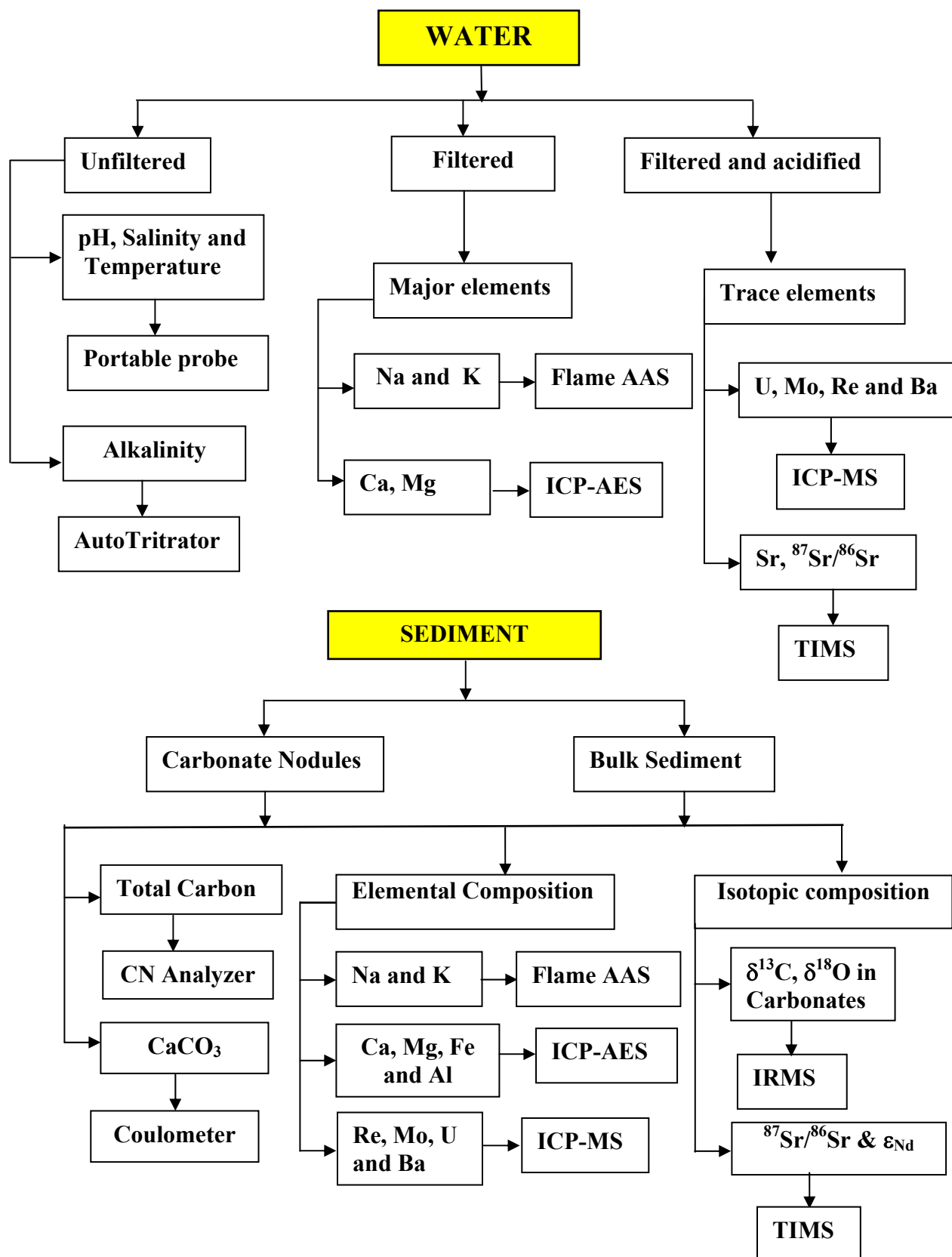
### (b) Alkalinity and Major Ions

Alkalinity was measured on unfiltered water samples kept in air-tight cleaned bottles and collected as a separate aliquot during sampling. This measurement was carried out in the laboratory within 2-3 days of sampling. Alkalinity was measured by acid titration with known strength (~0.01M) of diluted HCl using auto-titrator (Metrohm 702 SM Titrino) following end point titration method. There are two fixed end points at pH values of 8.3 and 4.3 at which  $\text{CO}_3^{2-}$  and total carbonate species ( $\text{HCO}_3^-$  and  $\text{CO}_3^{2-}$ ) respectively get completely neutralized. Major elements, Ca & Mg, were measured by ICP-AES (Jobin Yvon, Model 38S) and K & Na were measured by Flame AAS (Perkin Elmer Model 4000) in filtered and un-acidified samples. The concentrations of major elements were measured by standard calibration method using elemental standards procured from Merck<sup>®</sup> Company. The precision of the measurements is better than 5% (Rai, 2008).

### (c) Sr and $^{87}\text{Sr}/^{86}\text{Sr}$ by TIMS

Sr concentration and isotope composition in water samples were measured in filtered, acidified samples using thermal ionization mass spectrometry (TIMS). Sr concentration was determined by isotope dilution. The amount of water samples taken for Sr isotope analysis was decided based on their Sr concentration; about 2-10  $\mu\text{g}$  of total Sr is analyzed for Sr isotope measurements. Sr was separated using Eichrom<sup>®</sup> Sr specific resin (50-100 $\mu\text{m}$ ; Horwitz, et al., 1992; Pin and Bassin, 1992; Pin et al., 1994; Rai, 2008).

# ANALYSIS SCHEME



The procedure for the extraction of Sr from water samples and the measurement of its isotopic compositions adopted in this study is similar to that followed in Rai and Singh (2007). The Sr isotope measurements were carried out on ISOPROBE-T Thermal Ionization Mass Spectrometer (TIMS) in multi collector static mode. The pure Sr fraction was loaded with dissolved TaO activator on degassed high purity Re filament. Several repeat measurements were made to check the reproducibility, the results of which are listed in Table 2.5. Several procedural blanks were measured during the course of these analyses. The total procedural blank for Sr was ~ 500 pg which is three orders of magnitude lower than that of Sr processed from the samples, and therefore blank correction was not done.

**Table 2.5: Precision of dissolved Sr and  $^{87}\text{Sr}/^{86}\text{Sr}$  measurements in estuary samples**

| <b>Sample</b>   | <b>[Sr] <math>\mu\text{mol/kg}</math></b> | <b><math>\Delta_{\text{Sr}}(\%)</math></b> | <b><math>^{87}\text{Sr}/^{86}\text{Sr}</math></b> | <b><math>\Delta_{87\text{Sr}/86\text{Sr}}(\text{ppm})</math></b> |
|-----------------|---|--|---|--|
| NE07-1          | 12.3                                      |  | 0.709390  |  |
| NE07-1R         | 12.2                                      | 0.8  | 0.709400  | 14.1   |
| NEM07-10        | 37.4                                      |  | 0.709182  |  |
| NEM07-10R       | 37.1                                      | 0.8  | 0.709184  | 2.8  |
| TPM-10          | 29.9                                      |  | 0.709154  |  |
| TPM-10R         | 33.4                                      | 10.5                                       | 0.709153  | 1.4  |
| MD07-8          | 77.7                                      |  | 0.709168  |  |
| MD07-8R(1)      | 77.3                                      | 0.5  | 0.709160  | 11.3   |
| MD07-8R(2)      | 76.9                                      | 0.5  | 0.709164  | 5.6  |
| MD07-8R(3)      | 77.3                                      | 0.5  | 0.709160  | 5.6  |
| <b>Average*</b> |   | <b>0.6<math>\pm</math>0.1</b>              |   | <b>7.9<math>\pm</math>4.1</b>                                    |

\* Excluding the TPM-10 pair

#### **d) Re, U, Mo and Ba measurements by ICP-MS**

##### **i) Analysis of dissolved Rhenium**

Dissolved Re was measured by isotope dilution technique using ICP-MS (Quadrupole). For Re measurements, ~25-50 g of water (sample size depending on salinity) was taken in precleaned PFA beaker and spiked with a known weight of

$^{185}\text{Re}$  tracer and stored at least for 24 hours for sample and spike equilibration. The samples were dried at 80 °C and digested with few drops of quartz distilled  $\text{HNO}_3$ . Finally Re was purified and preconcentrated using anion exchange resin (Biorad AG1X8) in nitric acid medium (Trivedi et al., 1999; Dalai et al., 2002). The preconcentrated and pure Re was dissolved in 3 ml 0.5N  $\text{HNO}_3$ . The Re concentration in these solutions were determined by measuring their  $^{185}\text{Re}/^{187}\text{Re}$  using ICP-MS (Thermo X-series II). Instrumental mass fractionation correction was done by frequently measuring Re standard of natural composition. The counts for the measured isotopes were always more than ~10000 cps. The background counts were ~5 cps which increased with time but always remained insignificant with respect to sample counts. The background counts were measured after five samples and corrected from the sample signals.  $^{185}\text{Re}$  spike used in this study was in use earlier in the laboratory (Singh, 1999). The concentration of  $^{185}\text{Re}$  tracer was calibrated with a standard prepared in the laboratory using pure Re metal. Several sets of the standards were equilibrated with  $^{185}\text{Re}$  tracer and their isotopic composition was measured using ICP-MS (Fig. 2.7). The precision of the measurements was always better than  $\pm 1\%$ . Further, the concentration of this laboratory standard was calibrated using another  $^{185}\text{Re}$  tracer procured from CRPG, CNRS, Nancy, France. Details of the experiments for the calibration of standard and spike are given below.

### **Calibration of $^{185}\text{Re}$ spike and standard:**

#### **Re standard preparation:**

Re standard was prepared by dissolving a precisely known weight of Re metal (99.98% purity mass spectrometric Re Filament procured from H. Cross, USA) in 8 N nitric acid. The nitric acid solution was diluted to known weight using 2N  $\text{HNO}_3$  and stored in precleaned PFE bottle.

#### **Details of $^{185}\text{Re}$ spikes**

$^{185}\text{Re}$  spike used in this study (Singh, 1999) is calibrated with respect to the Re standard prepared above which in turn was calibrated against  $^{185}\text{Re}$  spike procured from CRPG, Nancy. The details of the two calibrations are given in Table 2.7 & 2.8.

**Table 2.6: Details of the two Re spikes**

| Spike | Abundances (%)    |                   | Atomic Wt(g)      |                   | Atomic wt of Re(g) | Con.<br>ng/g |
|-------|-------------------|-------------------|-------------------|-------------------|--------------------|--------------|
|       | <sup>185</sup> Re | <sup>187</sup> Re | <sup>185</sup> Re | <sup>187</sup> Re |                    |              |
| CRPG  | 97.40             | 2.60              | 184.95            | 186.96            | 185.005024         | 41.26        |
| PRL   | 94.5              | 5.5               | 184.95            | 186.96            | 185.063105         | ?            |

**Calibration of metal standard against CRPG <sup>185</sup>Re spike**

Three aliquots of Re standard were taken and calibrated with respect to the CRPG <sup>185</sup>Re spike. Re concentration of the metal standard is calculated for the individual aliquot. The average concentration of the laboratory Re standard is determined to be 1141.5±1.3 pg/g (Table 2.6).

**Table 2.7: Calibration of laboratory Re standard against CRPG <sup>185</sup>Re spike**

| Sample | <sup>185</sup> Re/ <sup>187</sup> Re | Wt. of | Wt. of   | Total Re       | Con of Re         |
|--------|--------------------------------------|--------|----------|----------------|-------------------|
|        |                                      | Spike  | Standard |                | standard          |
|        |                                      | g      | g        | pg             | pg/g              |
| EXP-1  | 33715                                | 0.211  | 2.07427  | 2364.0         | 1139.7            |
| EXP-2  | 33961                                | 0.201  | 2.10439  | 2404.6         | 1142.6            |
| EXP-3  | 36273                                | 0.211  | 2.29201  | 2617.6         | 1142.1            |
|        |                                      |        |          | <b>Average</b> | <b>1141.5±1.3</b> |

**Calibration of PRL spike against Re standard****Table 2.8: Calibration PRL <sup>185</sup>Re spike against laboratory standard**

| Spike | Wt. of  | Wt of standard | Total Re    | Conc. of PRL Spike |
|-------|---------|----------------|-------------|--------------------|
|       | Spike   |                |             |                    |
|       |         | g              | pg          | pg/g               |
| PRL-1 | 1.06993 | 1.05909        | 1209        | 5186               |
| PRL-2 | 1.10178 | 1.00751        | 1150        | 5153               |
| PRL-3 | 1.07154 | 1.15183        | 1315        | 5054               |
|       |         |                | <b>Mean</b> | <b>5131±56</b>     |

The calibration carried out with three separate aliquots provided average concentration of PRL <sup>185</sup>Re as 5131±56 pg/g, which has been used in this study.

Calibration experiment shows that good co-rrrelation ( $R^2 \sim 1$ ) exist between the weight of the standard taken for the analysis and total Re analysed in the standard solution (Fig. 2.7).

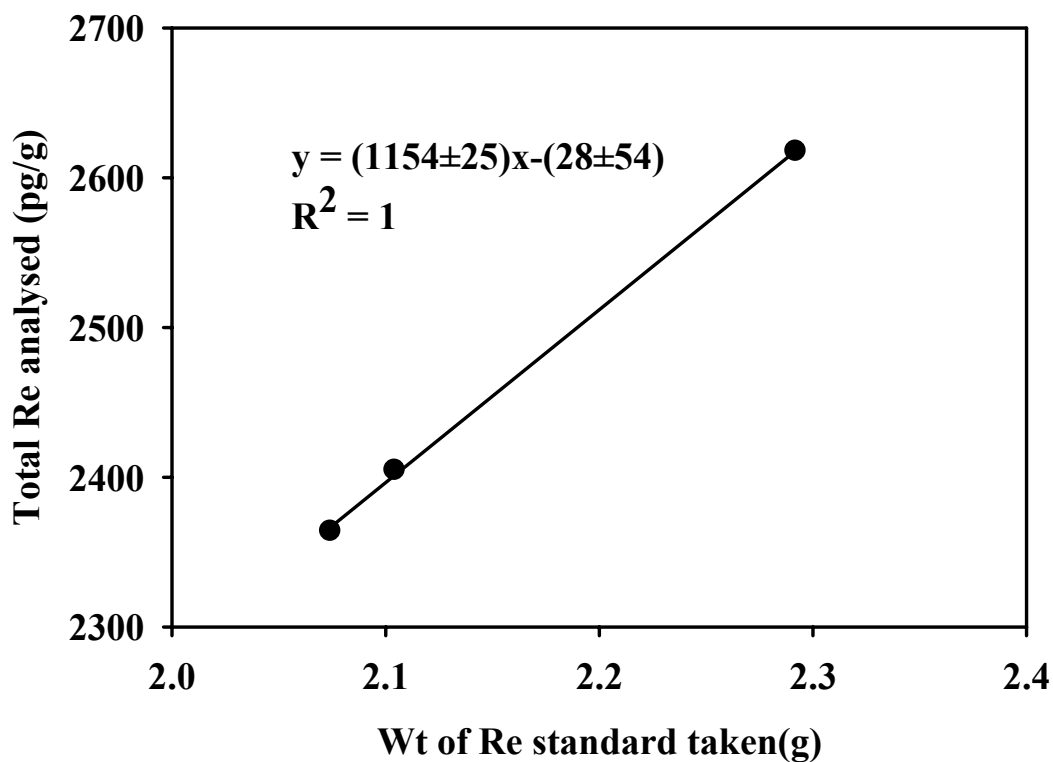


**Fig. 2.7** Three aliquots of known Re metal standards were calibrated using  $^{185}\text{Re}$  spike of known concentration from CRPG, CNRS, Nancy, France. The results showed weight of the Re standard used for analysis and the total Re as determined for the calibration are correlated with correlation coefficient  $R^2 \sim 1$ .

Several blanks of individual reagents and total procedural blank were measured for Re. Details of the individual blank analysis are given in the Table 2.9. The procedural blank was also ascertained using the standard addition method. Three aliquots of the same sample, weighing between 20 to 55 g were equilibrated with  $^{185}\text{Re}$  tracer and Re in these aliquots were measured following the same chemical separation protocols with the same quantity of reagents used for sample analysis. Total Re content and

weight of the different aliquots are plotted in Fig. 2.8, the intercept of the best fit line on the axis represents total procedural blank. This is determined to be  $\sim 2.6$  pg (Fig. 2.8). The reported concentrations of the samples are not corrected for the blank as total blank is much lower compared to the total amount of Re analyzed in samples.

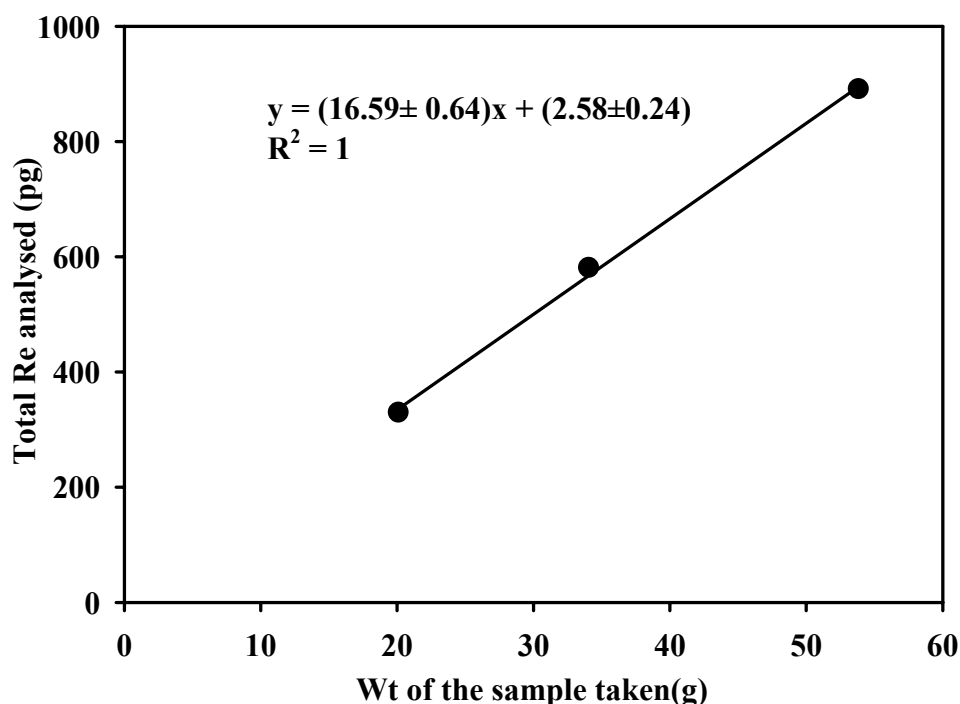


**Fig. 2.8** Three aliquots of the same sample ranging from 20 to 55 g analysed for total Re. The intercept of the straight line in the Y-axis represents amount of total procedural blank, which is  $\sim 2.6$  pg.

**Table 2.9: Blank analysis of Re**

| Blank  | $^{185}\text{Re}$<br>ICP-MS counts | $^{187}\text{Re}$<br>ICP-MS counts | Spike<br>Wt (g) | Total blank<br>[Re] pg | Sample<br>Wt (g) | Blank Con.<br>[Re] pg/g |
|--|------------------------------------|------------------------------------|-----------------|------------------------|------------------|-------------------------|
| <b><i>Reagents blank</i></b>                       |                                    |                                    |                 |                        |                  |                         |
| HNO <sub>3</sub> -1                                | 3316                               | 205                                | 0.02950         | 0.6                    | 2.06             | 0.30                    |
| HNO <sub>3</sub> -2                                | 2335                               | 147                                | 0.08400         | 2.7                    | 2.66             | 1.02                    |
| HNO <sub>3</sub> -3                                | 688                                | 48                                 | 0.06940         | 5.7                    | 2.77             | 2.07                    |
| MQ water   | 1443                               | 94                                 | 0.01680         | 0.8                    | 101.84           | 0.01                    |
| <b><i>Total procedural blank for sediments</i></b> |                                    |                                    |                 |                        |                  |                         |

|  |      |     |         |     |      |      |
|--|------|-----|---------|-----|------|------|
| BLK- 1   | 4669 | 436 | 0.02067 | 5.6 | 1.00 | 5.61 |
| BLK- 2   | 3483 | 248 | 0.02187 | 2.0 | 1.00 | 1.96 |
| <b><i>Total procedural blank for water</i></b> |      |     |         |     |      |      |
| BLANK-1  | 432  | 26  | 0.03568 | 0.7 | 1.00 | 0.72 |
| BLANK-2  | 2587 | 179 | 0.02721 | 2.2 | 1.00 | 2.23 |
| BLANK-3  | 1786 | 113 | 0.03733 | 1.5 | 1.00 | 1.54 |

Analytical precision of Re measurement determined using the replicate analysis of water samples (Table 2.10a & b; N=11 pairs) is given in terms of coefficient of variations, CV as

$$CV(\%) = \left( \frac{1}{2n} \sum \left( \frac{d_i}{x_i} \right)^2 \right)^{\frac{1}{2}} \times 100 \dots\dots\dots (i)$$

where  $d_i$  is difference between the duplicates with mean  $x_i$  and  $n$  is the total set of duplicates. The coefficient of variation calculated based on 10 sets of replicates is  $\pm 2\%$ . The precision of measurements in samples of higher salinity is generally better than those with lower salinities due to the higher concentration of Re in the former.

**Table 2.10a: Replicate analysis of dissolved Re in estuary samples**

| <b>Sample</b>   | <b>Sample [Re] pmol/kg</b> | <b>Replicate</b> | <b>Difference %</b> |
|---|----------------------------|------------------|---------------------|
| <b><i>Re in dissolved phase (0.2 <math>\mu</math> filtered)</i></b> |                            |                  |                     |
| <b>NE07-8</b>   | 76.8                       | 77.6             | 1.0                 |
| <b>NE07-9</b>   | 82.2                       | 82.0             | 0.2                 |
| <b>NE07-10</b>  | 88.7                       | 90.0             | 1.4                 |
| <b>NE07-16</b>  | 52.0                       | 51.0             | 2.0                 |
| <b>MD07-5</b>   | 19.1                       | 18.9             | 1.1                 |
| <b>MD07-10</b>  | 39.3                       | 38.0             | 3.4                 |
| <b>W-10</b>   | 37.2                       | 37.5             | 0.8                 |
| <b>GA 07-5</b>  | 40.9                       | 40.8             | 0.2                 |
| <b>TPM07-7</b>  | 24.9                       | 23.7             | 5.1                 |
| <b>NEM07-7</b>  | 39.6                       | 39.3             | 0.8                 |

The Re concentrations of the replicate analyses are indistinguishable within analytical uncertainties from each other. For some samples, Re concentrations were measured in

the two aliquots, one filtered through 0.2  $\mu\text{m}$  and the other through 0.45  $\mu\text{m}$  size nucleopore filters to check any measurable variation of Re concentration in them. The data sets of two measurements are indistinguishable (Table 2.10b).

**Table 2.10b: Dissolved Re comparison between 0.2 and 0.45 $\mu$  filtered**

| Sample    | [Re] pmol/kg in filtered through |                    | Difference (%) |
|-----------|----------------------------------|--------------------|----------------|
|           | 0.2 $\mu\text{m}$                | 0.45 $\mu\text{m}$ |                |
| TPM 07-4  | 12.8                             | 13.6               | 5.9            |
| TPM 07-14 | 4.1                              | 4.1                | 0.0            |
| NEM 07-7  | 39.6                             | 39.3               | 0.8            |

**Table 2.10c: Repeat analysis of Re in particulate phase**

| Sample      | Sample Replicate |      | Difference % |
|-------------|------------------|------|--------------|
|             | [Re] pmol/kg     |      |              |
| NESS-10     | 232              | 215  | 7.9          |
| TPM(BS)-12  | 2871             | 2845 | 0.9          |
| NEM(SUS)-6  | 211              | 213  | 0.9          |
| NEM(SUS)-13 | 205              | 216  | 5.1          |

## ii) Analysis of dissolved U, Mo and Ba

U, Mo and Ba were measured in the water samples directly by quadrupole ICP-MS (Thermo-X series) following the procedure published by Rodushkin and Ruth, 1997. Samples were diluted suitably using 2%  $\text{HNO}_3$  to maintain low and similar matrix in all the samples of different salinities. Dilutions for the individual sample were done in such way that (i) matrix was at same level for all samples, (ii) the matrix was low enough to minimize the matrix effect and (iii) counts were at least three orders of magnitude higher than the detection limit. Samples collected from the sea water side, were diluted 30 times before measurements whereas the river water samples were measured directly. Abundances of Mo, U and Ba were determined by measuring  $^{98}\text{Mo}$ ,  $^{238}\text{U}$  and  $^{137}\text{Ba}$  isotopes. However, signals of other isotopes of these

elements such as  $^{95}\text{Mo}$ ,  $^{235}\text{U}$ ,  $^{134}\text{Ba}$ ,  $^{135}\text{Ba}$ ,  $^{136}\text{Ba}$  and  $^{138}\text{Ba}$  were also monitored during analysis.

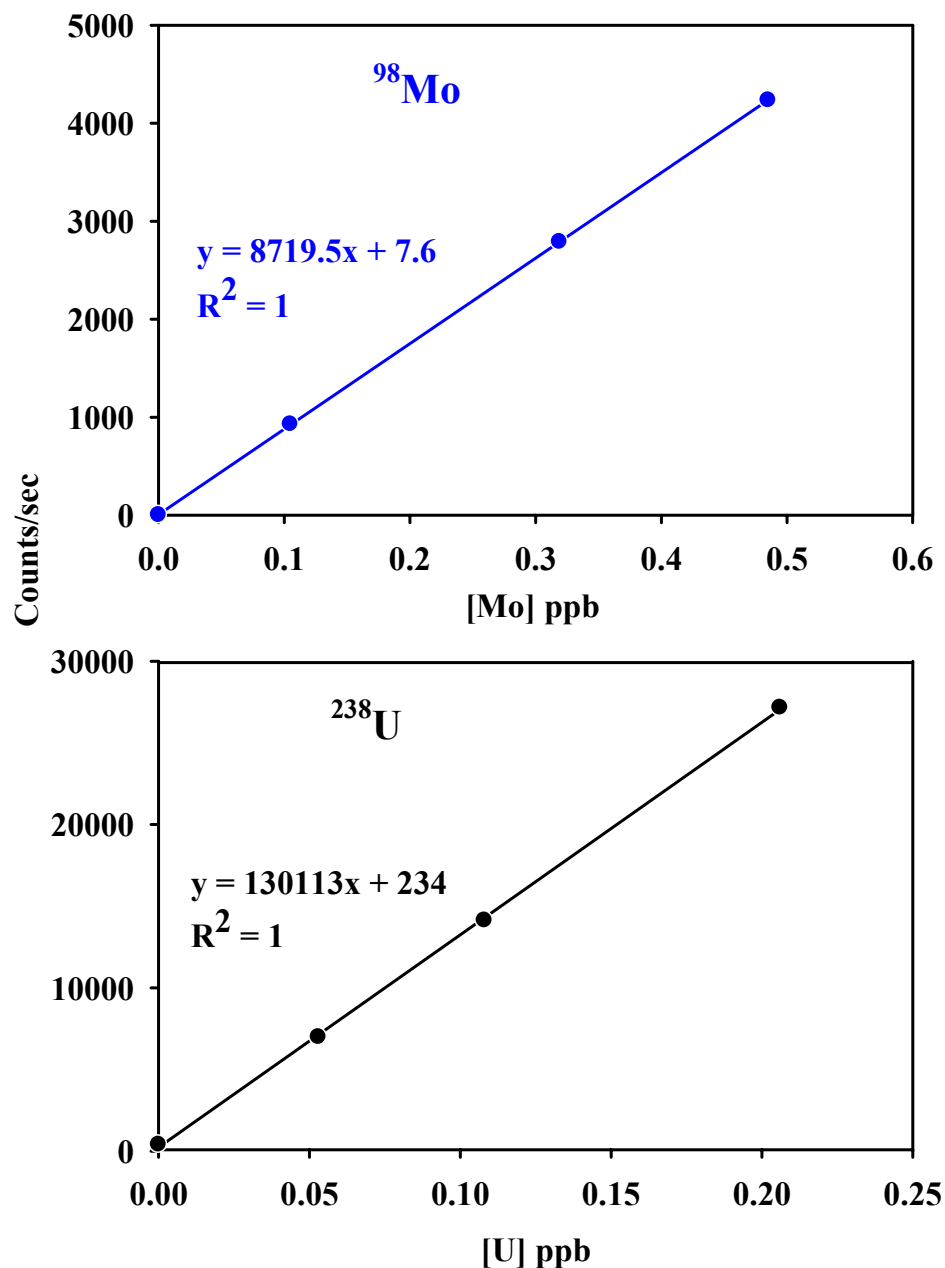


**Fig. 2.9** Standard calibration of Mo and U. The ICP-MS counts of  $^{98}\text{Mo}$  and  $^{238}\text{U}$  isotopes show very good correlation with the absolute concentrations of the standard used for analysis.

Table 2.11: U and Mo in reference materials and in seawater from the Arabian Sea

| Sample                            | Measured    |          |             |           | Reported |         |           |            |
|-----------------------------------|-------------|----------|-------------|-----------|----------|---------|-----------|------------|
|                                   | U           |          | Mo          |           | U        |         | Mo        |            |
|                                   | ppb         | pmol/kg  | ppb         | pmol/kg   | ppb      | nmol/kg | ppb       | nmol/kg    |
| <b>SLEW-3</b><br><b>For n=12</b>  | 1.40 ± 0.03 | 5.9±0.1  | 4.02 ± 0.02 | 41.9±0.2  | 1.8*     | 7.6*    | 5.1*      | 53.2*      |
| <b>NASS-5</b><br><b>For n=15</b>  | 2.60 ± 0.10 | 10.9±0.4 | 8.6 ± 0.3   | 89.6±3.1  | 2.6*     | 10.9*   | 9.6 ± 1.0 | 100.1±10.4 |
| <b>Seawater</b><br><b>For n=5</b> | 3.03 ± 0.05 | 12.7±0.2 | 9.7 ± 0.1   | 101.1±1.0 |          |         |           |            |

These are “information only” values. SLEW-3 and NASS-5 are reference materials from the National Research Council, Canada.

It has been reported that measurement of  $^{95}\text{Mo}$  can be subject to interference from  $\text{BrO}$  (Rodushkin and Ruth, 1997). Further, Mo has significant memory effect during analysis through retention in the sample introducing system (tubings and nebuliser). To avoid this, the system needs to be flushed after each measurement. In this work, the sample introducing system was flushed at least for 60 sec to minimize the memory effect. Precision and accuracy of all measurements were checked by analyzing replicate samples and reference standards (NASS-5 and SLEW-1) procured from the National Research Council, Canada. Certified and measured data of the reference materials are given in the Table 2.11. To determine the precision of U and Mo measurements, several replicates were also measured the results of which are given in the Table 2.12.

**Table 2.12: Replicate analyses of dissolved U and Mo in estuary samples**

| Sample  | Salinity | [Mo]            | [U]             |
|---------|----------|-----------------|-----------------|
|         | ‰        | nmol/kg         |                 |
| NE-5    | 18.2     | $54.0 \pm 0.6$  | $7.8 \pm 0.03$  |
| NE-5R   |          | $54.3 \pm 1.1$  | $7.8 \pm 0.1$   |
| NE-10   | 25.3     | $75.0 \pm 0.7$  | $10.3 \pm 0.04$ |
| NE-10R  |          | $71.8 \pm 1.1$  | $10.2 \pm 0.1$  |
| NEM-5   | 3.4      | $16.2 \pm 0.3$  | $2.7 \pm 0.02$  |
| NEM-5R  |          | $17.1 \pm 0.4$  | $2.8 \pm 0.03$  |
| NEM-14  | 0        | $2.9 \pm 0.05$  | $1.2 \pm 0.01$  |
| NEM-14R |          | $2.9 \pm 0.1$   | $1.2 \pm 0.01$  |
| MD-5    | 16.1     | $47.1 \pm 0.7$  | $4.6 \pm 0.1$   |
| MD-5R   |          | $50.0 \pm 0.6$  | $4.7 \pm 0.1$   |
| TPM-12  | 17.4     | $61.2 \pm 1.1$  | $6.8 \pm 0.1$   |
| TPM-12R |          | $59.5 \pm 1.2$  | $6.8 \pm 0.1$   |
| W-5     | 14.7     | $50.0 \pm 0.7$  | $8.4 \pm 0.1$   |
| W-5R    |          | $49.1 \pm 1.3$  | $8.3 \pm 0.04$  |
| KOH-15  | 25.6     | $132.2 \pm 1.9$ | $15.2 \pm 0.1$  |
| KOH-15R |          | $135.0 \pm 1.7$ | $15.3 \pm 0.1$  |

The precessions of the measurements were 5% and 7% for U and Mo respectively based on the replicate analyses. For blank analysis, same matrix (2 %  $\text{HNO}_3$ ) which was used for the dilution of the estuary and sea water samples was run several times. The blank concentration is below the detection limit of the instrument.

Ba was determined in the river, estuary and seawater samples directly using ICP-MS. The instrument was calibrated using standards of various concentrations (Fig. 2.10). The samples were diluted with MQ water and HNO<sub>3</sub> to make the salinities ~1 ‰ and acid strength ~0.4 N HNO<sub>3</sub>.

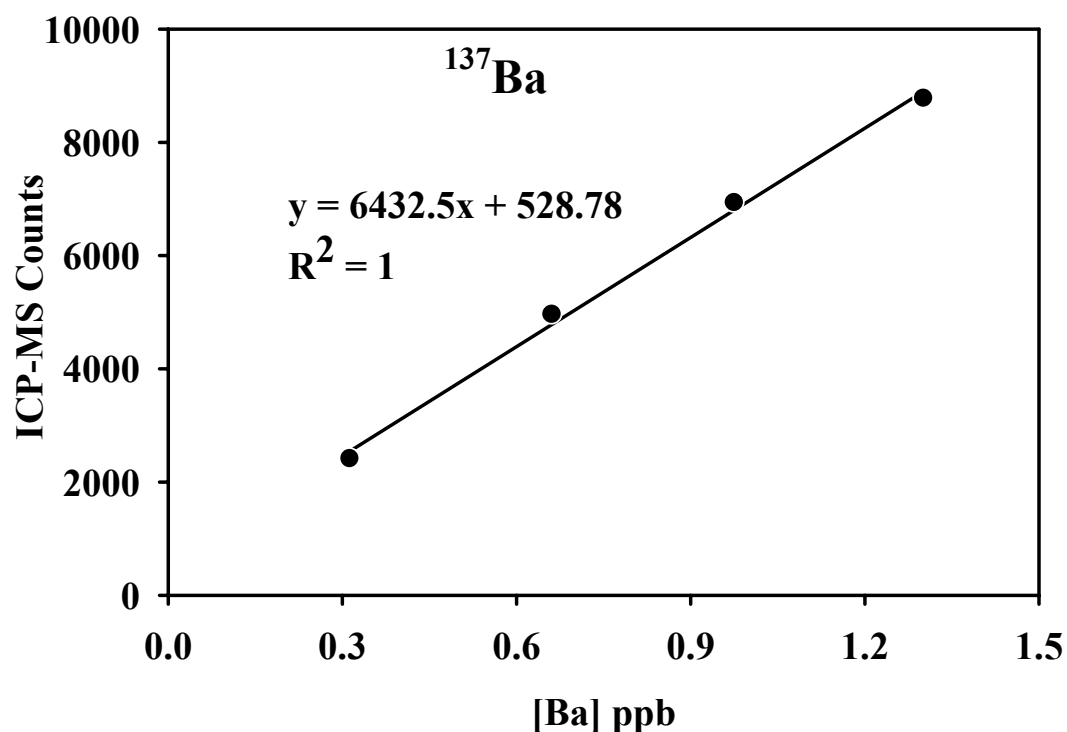


**Fig. 2.10 Ba calibration using four standards of known strengths. The Ba concentration and ICP-MS counts show very good correlation with correlation coefficient ( $R^2$ ) ~1.**

To check the interference and matrix effect, three seawater samples were analyzed by the standard addition method (Table 2.13, Fig. 2.11). Each sample was diluted about thirty times and divided into four aliquots. Different amount of Ba standard was added to each aliquot. One aliquot of each sample was measured directly without adding Ba standard.

Table 2.13: Experiments for Ba measurements by standard addition method

| Experiments | Ba (ng) added to samples | [Ba] ppb |  | Differences (%) |     |
|-------------|--------------------------|----------|--|-----------------|-----|
|             |                          | Measured | [Ba] ppb in samples<br>Standard addition<br>Direct |                 |     |
| EX-1        | (A)                      | 2.94     | 0.32   | 4.8             | 2.9 |
|             | (B)                      | 6.19     | 0.49   |                 |     |
|             | (C)                      | 8.54     | 0.64   |                 |     |
| EX-2        | (A)                      | 3.08     | 0.69   | 15.5            | 1.2 |
|             | (B)                      | 6.19     | 0.85   |                 |     |
|             | (C)                      | 9.58     | 1.05   |                 |     |
| EX-3        | (A)                      | 3.16     | 0.53   | 10.2            | 4.7 |
|             | (B)                      | 6.00     | 0.69   |                 |     |
|             | (C)                      | 9.07     | 0.88   |                 |     |

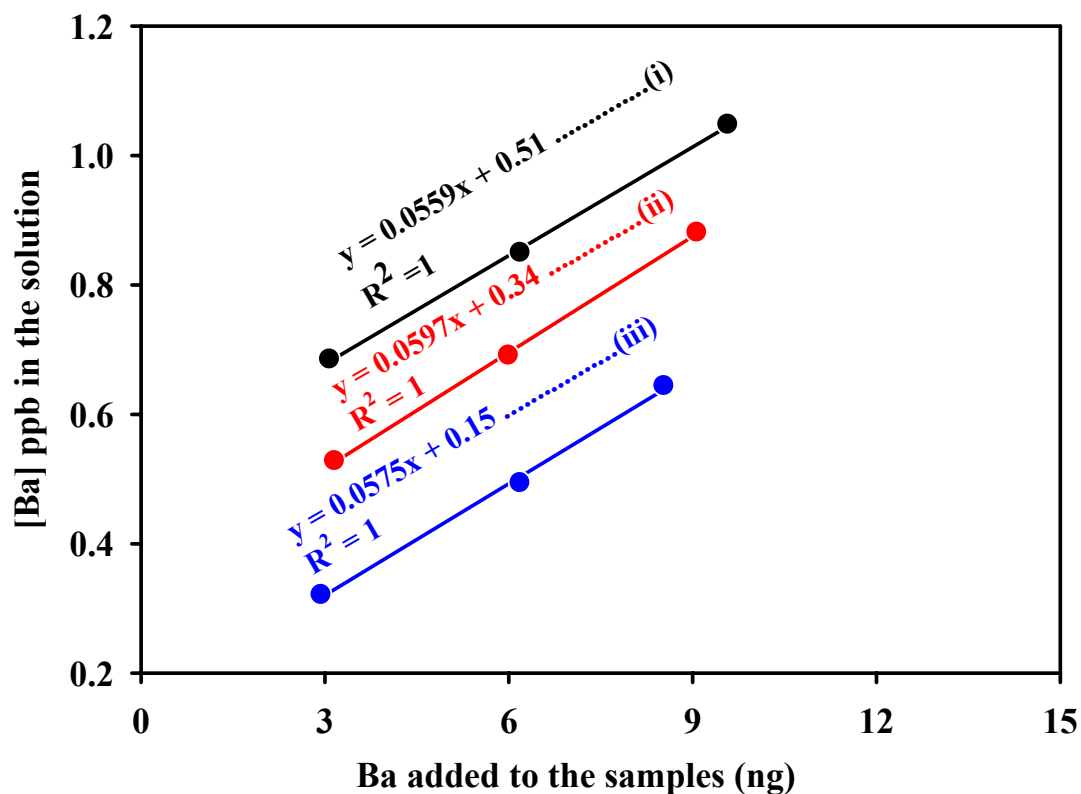


Fig. 2.11 Ba measurement in estuary water samples by standard addition method. The estimated Ba concentration based on standard addition method and direct measurements are the same within errors (Table 2.12)

The measured concentrations versus amount of Ba added to the three aliquots of each sample show very good correlation,  $R^2 \sim 1$  for all samples (Fig. 2.11). The Y-axis intercepts of the lines represents the Ba concentration in the sample solution. The Ba measurements by standard addition method and direct analysis agree within  $\pm 5\%$  within the analytical precision (Table 2.13). Ba concentrations measured in seawater samples collected from seawater off the Goa coast is  $35 \pm 3$  nmol/kg, close to the global average open ocean value  $\sim 40$  nM (Shaw et al., 1998).

### 2.3.2 Analysis of Sediments

#### (a) Major and trace elements

About 0.5g of ashed sediment samples were brought to solution by repeated digestion with HF, HCl and HNO<sub>3</sub>. Along with samples, a few duplicate samples were also digested to check analytical precision. USGS reference standard materials W-1 and G-2 were analyzed following the same analytical procedure to ascertain the accuracy of measurements (Table 2.14).

**Table 2.14: Elemental analyses in USGS reference material W-1 and G-2**

| Element                            | Technique | Measured<br>(Wt %) | SD            | Reported<br>(Wt %) | SD   |
|------------------------------------|-----------|--------------------|---------------|--------------------|------|
| <b>USGS reference material W-1</b> |           |                    | <b>(N= 3)</b> |                    |      |
| <b>Ca</b>                          | ICP-AES   | 7.94               | 0.18          | 7.86               | 0.09 |
| <b>Mg</b>                          | ICP-AES   | 3.92               | 0.35          | 3.99               | 0.08 |
| <b>Na</b>                          | AAS       | 1.68               | 0.08          | 1.60               | 0.04 |
| <b>K</b>                           | AAS       | 0.61               | 0.03          | 0.53               | 0.02 |
| <b>Fe</b>                          | ICP-AES   | 8.11               | 0.17          | 7.71               | 0.16 |
| <b>Al</b>                          | ICP-AES   | 7.75               | 0.39          | 7.88               | 0.14 |
| <b>USGS reference material G-2</b> |           |                    | <b>(N=4)</b>  |                    |      |
| <b>Ca</b>                          | ICP-AES   | 1.40               | 0.03          | 1.40               | 0.30 |
| <b>Mg</b>                          | ICP-AES   | 0.47               | 0.07          | 0.45               | 0.08 |
| <b>Na</b>                          | AAS       | 3.01               | 0.15          | 3.03               | 0.17 |
| <b>K</b>                           | AAS       | 3.62               | 0.18          | 3.72               | 0.13 |
| <b>Fe</b>                          | ICP-AES   | 1.94               | 0.10          | 2.07               | 0.13 |
| <b>Al</b>                          | ICP-AES   | 8.01               | 0.07          | 8.15               | 0.03 |

N=Number of analysis

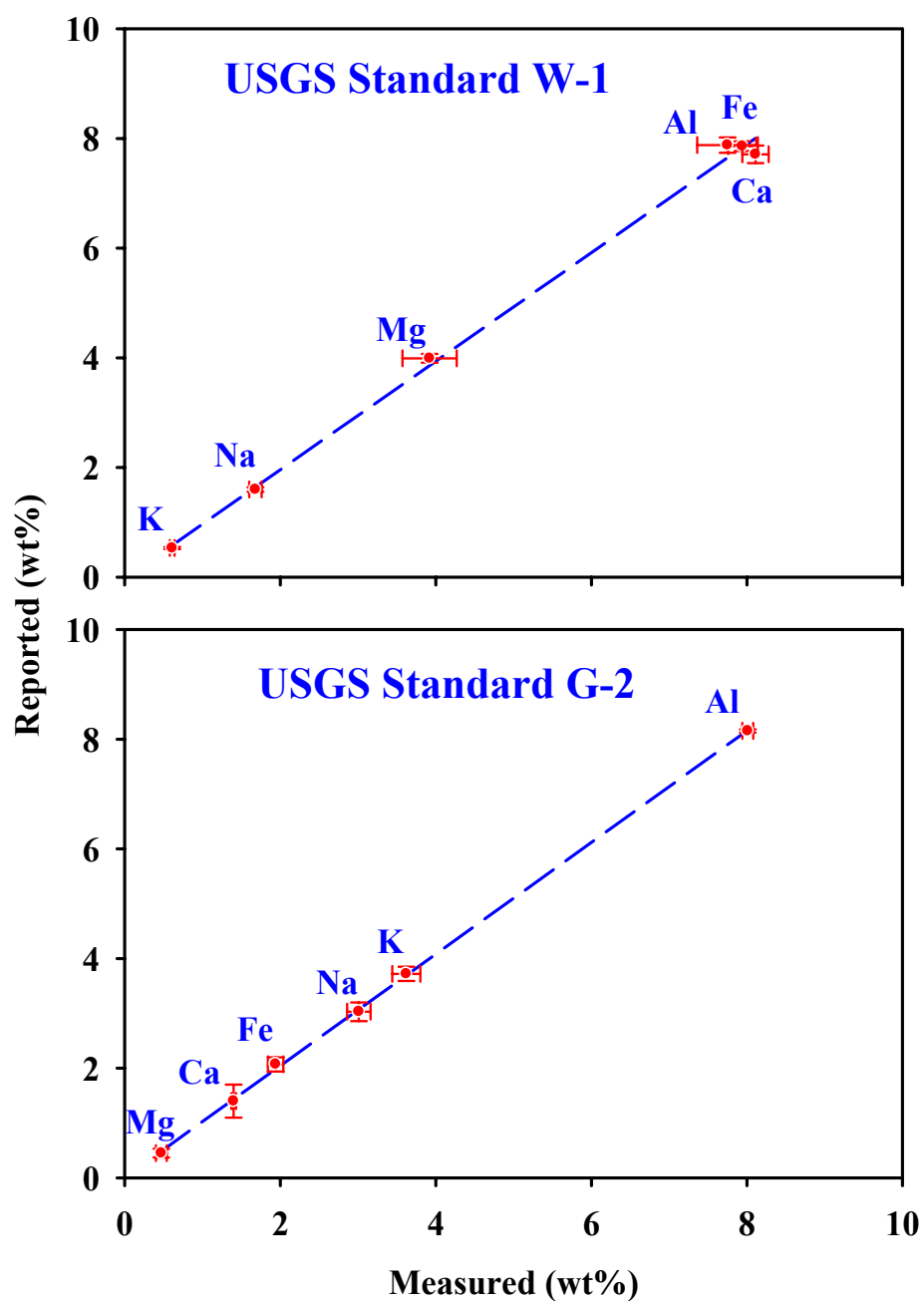


**Fig. 2.12 Comparison of measured and reported elemental concentrations in W-1 and G-2 USGS reference standards.**

Ca, Mg, Al, Fe, Sr, Ba, Co, Cu, Ni, V and Zn were measured by ICP-AES whereas Na and K were measured by flame AAS. Procedural blanks were negligible. Precision and accuracy were determined based on several repeats and W-1 and G-2

measurements. The measured and reported elemental concentrations in W-1 and G-2 USGS reference standards show very good agreement within the analytical uncertainty (Fig. 2.12).

The trace elements Re, U, Mo and Ba were measured primarily in suspended sediments from the Narmada and the Tapi estuaries collected during monsoon and pre-monsoon samples. A few samples of bank sediments were also analysed for Re from the Narmada and Tapi estuary. Re was measured by isotope dilution technique using ICP-MS whereas U, Mo and Ba were measured directly in acid solution of the sample after suitable dilution. For Re, prior to acid digestion, sediments were combusted at 450° C for 7 to 8 hours to remove the organic matter (Jaffe et al., 2002; Singh et al., 1999). ~0.5gm of organic matter free sample was digested along with <sup>185</sup>Re spike using HF-HNO<sub>3</sub>-HCl at 120° C to bring the sediment to solution. Re was purified from solution and preconcentrated using column chromatography adopted for water analysis and measured using ICP-MS. The Re blank contribution from individual reagent and total procedural blank were analysed. Total procedural blank, ~3 pg, measured in this study is negligible with respect to the total amount of Re analysed and hence blank correction was not made. The average precession of the Re measurement in sediments, based on several repeat analysis, is ±4% (Fig. 2.10c).

U, Mo and Ba were measured by ICP-MS following the similar procedure adopted for the measurement of these elements in water samples discussed detail in above sections. About 0.1gm organic matter free combusted sediment was taken and was brought to solution by treating with HF-HNO<sub>3</sub>-HCl repeatedly at 120° C. Digested samples were diluted up to 2500 times using 2% HNO<sub>3</sub> and elements measured using ICP-MS.

#### **(b) CaCO<sub>3</sub> and organic carbon**

Inorganic carbon measurements were made by the coulometric titration method using UIC Coulometer Model 5012 (UIC Inc., Illinois, USA). For this, about 100 mg of dry sample powder was treated with 40% H<sub>3</sub>PO<sub>4</sub> at 85° C for 10 minutes in an extraction cell. The quantity of liberated CO<sub>2</sub> was measured in the coulometer

titration cell, after purifying through a column of silica gel and anhydrous  $\text{MgClO}_4$ . A three-point calibration was drawn using standard solution of  $\text{Na}_2\text{CO}_3$  over a wide range of concentration. The samples were measured within the range of standards. The precision of measurement based on replicate analyses and standard solutions of  $\text{Na}_2\text{CO}_3$  was better than  $\pm 2.5\%$ .

Total carbon was measured in carbonates and bulk sediments samples using FISIONS NA1500 CN elemental analyzer (Fisons Inc., Italy; Sarin et al., 1997). About 10-20 mg of dried sediment sample was packed in aluminum cups and was combusted completely at  $\sim 1080^\circ\text{C}$  in presence of high purity oxygen flow for total carbon and nitrogen measurements. A three-point calibration was made using international standards, low organic carbon soil standard and high organic carbon sediment standards having carbon abundance  $1.65 \pm 0.02\%$  and  $6.72 \pm 0.17\%$  respectively procured from Elemental Microanalysis Limited, UK. It was cross checked by running another standard, the Deer River Shale containing 2.53% carbon as the reference material (Krom and Berner, 1982; Sarin et al., 1997; Bhushan et al., 2001). Organic carbon was calculated for each sample by subtracting inorganic carbon from their corresponding total carbon (Bhushan et al., 2001). The analytical precision for total carbon measurements is better than  $\pm 4\%$ .

### **(c) Sr and Nd isotope measurement in sediments**

Initial sample preparations for Sr isotope measurements in carbonate and silicate phases of sediments are common. Sr and Nd isotope measurements were made on the silicate fraction of sediments after decarbonating the bulk sample by leaching with 0.6 N HCl at  $80^\circ\text{C}$  for  $\sim 30$  minutes with intermittent ultrasonic treatment. The slurry was centrifuged, washed and decarbonated samples were ashed at  $\sim 600^\circ\text{C}$  to oxidize organic matter.  $\sim 100$  mg of carbonate and organic matter free sediments were digested with HF- $\text{HNO}_3$  acids in the presence of  $^{84}\text{Sr}$  and  $^{150}\text{Nd}$  spikes. Finally they were taken in 2N HCl and Sr and Nd were separated from the solution following reported ion exchange procedures (Alibert et al., 1983; Galy, 1999; Rai and Singh, 2007; Singh et al., 2008). The purified Nd was loaded with  $\text{H}_3\text{PO}_4$  on

degassed and oxidized high purity Ta filaments on the outer Tantalum filament of the triple filament assembly whereas the pure Sr fraction was loaded on the Ta single filament. Sr isotope measurements were carried out in carbonate phase of the carbonate nodules. Considering that the carbonate nodules contain silicate phases embedded in them, it is important that procedure used for measuring  $^{87}\text{Sr}/^{86}\text{Sr}$  in carbonate phase do not leach Sr from silicates. Considering this, the samples were leached with dilute acetic acid, which is known to dissolve only the carbonate phase without attacking the silicates (Asahara et al., 1995; Hart et al., 2004). Further, the leaching was done for short time and at room temperature. Approximately 0.5 g of dried powdered samples were treated with 5% acetic acid (Suprapure, Merck) at room temperature for ~15 minutes. The slurry was centrifuged and the leachates were decanted into another clean vial. Pure Sr was separated from the leachates by ion exchange procedure (Rai and Singh, 2007; Singh et al., 2008).

Sr and Nd concentrations and their  $^{87}\text{Sr}/^{86}\text{Sr}$  and  $^{143}\text{Nd}/^{144}\text{Nd}$  were measured on Isoprobe-T Thermal Ionization Mass Spectrometer in static multi-collection mode. Mass fractionation corrections for Sr and Nd were made by normalizing  $^{86}\text{Sr}/^{88}\text{Sr}$  to 0.1194 and  $^{146}\text{Nd}/^{144}\text{Nd}$  to 0.7219. During the course of analyses, NBS 987 Sr and JNdi-1 Nd standards were repeatedly measured, these yielded values of  $0.710227 \pm 0.000014$  ( $1\sigma$ ,  $n = 110$ ) for  $^{86}\text{Sr}/^{88}\text{Sr}$  and  $0.512107 \pm 0.000008$  ( $1\sigma$ ,  $n = 35$ ) for  $^{143}\text{Nd}/^{144}\text{Nd}$ , well within their recommended values. Variations  $^{87}\text{Sr}/^{86}\text{Sr}$  of NBS 987 and  $^{143}\text{Nd}/^{144}\text{Nd}$  of JNdi-1 standards are plotted with time which shows instrument behaviour during course of this study (Fig. 2.13).

Several replicate analyses of Sr in carbonates and Sr and Nd in silicates were carried out (Table 2.15 and 2.16) to estimate the over all reproducibility of these measurements. Carbonate nodules from three depths of the JP core were analysed for their  $^{87}\text{Sr}/^{86}\text{Sr}$  in duplicate using separate nodules from each depth to assess heterogeneity in their  $^{87}\text{Sr}/^{86}\text{Sr}$  composition. Based on this exercise the variation in Sr isotope composition in duplicates from the same depth horizon is determined to be in the range of 40 to 1180 ppm (Table 2.16); though all but one sample fall in the range, 0 to 190 ppm.

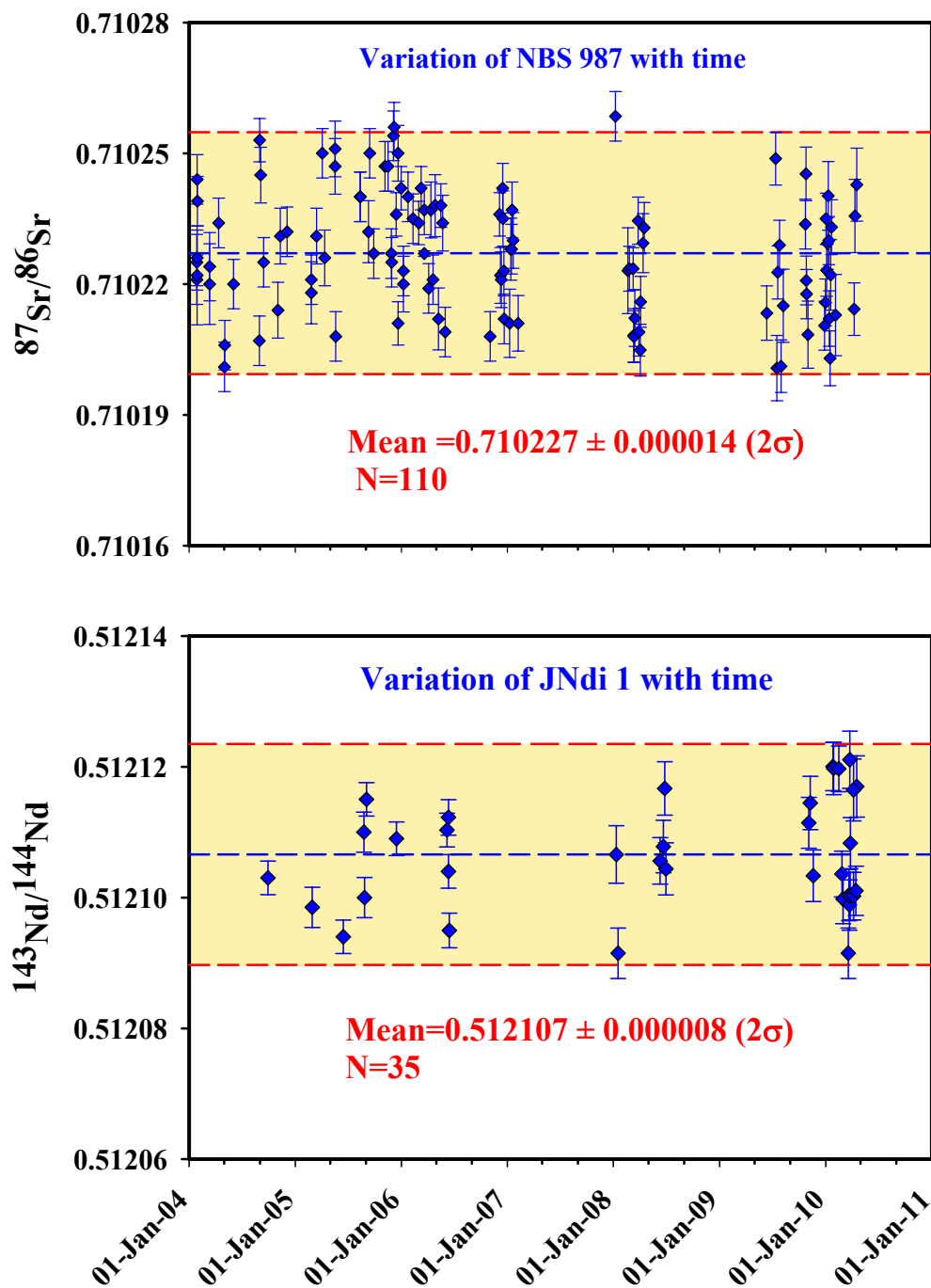


Fig. 2.13 Variations of  $^{87}\text{Sr}/^{86}\text{Sr}$  in NBS-987 and  $^{143}\text{Nd}/^{144}\text{Nd}$  in JNdi-1 with time. Shaded band represents mean $\pm$ SD( $2\sigma$ ) of the data points. All the data points falling in shaded band and agree well within uncertainties with the reported values. Shaded bands represent two times SD.

**Table 2.15: Replicate analyses of Sr, Nd and their isotope compositions in silicate phase of sediments**

| <b>Sample</b>      | <b><math>^{87}\text{Sr}/^{86}\text{Sr}</math></b> | <b>[Sr] <math>\mu\text{g/g}</math></b> | <b><math>^{143}\text{Nd}/^{144}\text{Nd}</math></b> | <b><math>\epsilon_{\text{Nd}}</math></b> | <b>[Nd] <math>\mu\text{g/g}</math></b> |
|--------------------|---|--|---|--|--|
| <b>IITK-0.06</b>   | 0.74825   | 93                                     |   |  |  |
| <b>IITK-0.06R</b>  | 0.74846   | 94                                     | -   | -  | -                                      |
| <b>IITK-3.68</b>   | 0.76078   | 79                                     | -   | -  | -                                      |
| <b>IITK-3.68R</b>  | 0.76161   | 86                                     | -   | -  | -                                      |
| <b>IITK-7.08</b>   | 0.73516   | 123                                    | -   | -  | -                                      |
| <b>IITK-7.08R</b>  | 0.73515   | 117                                    | -   | -  | -                                      |
| <b>IITK-7.67</b>   | 0.74073   | 117                                    | -   | -  | -                                      |
| <b>IITK-7.67R</b>  | 0.74085   | 112                                    | -   | -  | -                                      |
| <b>IITK-11.14</b>  | 0.75148   | 114                                    | -   | -  | -                                      |
| <b>IITK-11.14R</b> | 0.75179   | 109                                    | -   | -  | -                                      |
| <b>IITK-24.72</b>  | 0.73389   | 122                                    | -   | -  | -                                      |
| <b>IITK-24.72R</b> | 0.73376   | 123                                    | -   | -  | -                                      |
| <b>IITK-29.80</b>  | 0.74574   | 78                                     | -   | -  | -                                      |
| <b>IITK-29.80R</b> | 0.74589   | 77                                     | -   | -  | -                                      |
| <b>IITK-37.1</b>   | 0.73677   | 112                                    | 0.511919  | -14.0                                    | 28.2                                   |
| <b>IITK-37.1R</b>  | 0.73682   | 110                                    | 0.511939  | -13.6                                    | 29.3                                   |
| <b>IITK45.4</b>    | 0.74002   | 91                                     | 0.511879  | -14.8                                    | 22.0                                   |
| <b>IITK45.4R</b>   | 0.73994   | 93                                     | 0.511871  | -15.0                                    | 23.1                                   |
| <b>IITK51.0</b>    | 0.74042   | 97                                     | 0.511813  | -16.1                                    | 21.2                                   |
| <b>IITK51.0R</b>   | 0.74057   | 104                                    | 0.511846  | -15.5                                    | 24.2                                   |
| <b>GP-60</b>       | 0.76124   | 93                                     | 0.511774  | -16.8                                    | 23.1                                   |
| <b>GP-60R</b>      | 0.76098   | 103                                    | 0.511787  | -16.6                                    | 23.7                                   |
| <b>GP-161</b>      | 0.77388   | 83                                     | 0.511755  | -17.2                                    | 26.0                                   |
| <b>GP-161R</b>     | 0.77412   | 89                                     | 0.511750  | -17.3                                    | 24.4                                   |

The average uncertainty based on repeat measurements of the samples from the same horizons is larger than analytical precision and can be explained in terms of sample heterogeneity (Table 2.16, 2.17).

**Table 2.16: Replicate analysis of  $^{87}\text{Sr}/^{86}\text{Sr}$  in carbonate phase**

| Sample   | $^{87}\text{Sr}/^{86}\text{Sr}$ | Replicate | Difference(ppm) |
|--|---------------------------------|-----------|-----------------|
| <i><u>Replicate of the same aliquot of powdered samples</u></i>                              |                                 |           |                 |
| IITK Carb-4.05   | 0.71683                         | 0.71687   | 56              |
| IITK Carb-11.7   | 0.71714                         | 0.71717   | 42              |
| IITK Carb-13.12  | 0.71590                         | 0.71590   | 0               |
| IITK Carb-16.23  | 0.71721                         | 0.71721   | 0               |
| IITK Carb-23.85  | 0.71722                         | 0.71726   | 56              |
| IITK Carb-39.02  | 0.71745                         | 0.71748   | 42              |
| IITK Carb-40.0   | 0.71715                         | 0.71718   | 42              |
| IITK Carb-44.82  | 0.71761                         | 0.71758   | 42              |
| IITK Carb-48.40  | 0.71833                         | 0.71826   | 97              |
| <i><u>Replicate analysis of separately hand picked carbonate nodules from same depth</u></i> |                                 |           |                 |
| P-2.25   | 0.73651                         | 0.73665   | 190             |
| JP-21.20   | 0.72064                         | 0.72149   | 1178            |
| JP-24.65   | 0.71685                         | 0.71688   | 42              |

**Table 17: Blanks of Sr and Nd**

| Blank                       | $^{143}\text{Nd}/^{144}\text{Nd}$ | $^{87}\text{Sr}/^{86}\text{Sr}$ | [Nd] [Sr] |     |
|-----------------------------|-----------------------------------|---------------------------------|-----------|-----|
|                             |                                   |                                 | ng        |     |
| <i><u>For Silicate</u></i>  |                                   |                                 |           |     |
| BLK-1                       | 0.513093                          | 0.73279                         | 1.4       | 2.9 |
| BLK-2                       | 0.504967                          | 0.70794                         | 0.2       | 3.1 |
| BLK-3                       | 0.504461                          | -                               | 1.7       | -   |
| BLK-4                       | 0.503817                          | 0.71868                         | 0.6       | 1.0 |
| BLK-5                       | 0.506462                          | 0.72122                         | 0.6       | 1.0 |
| <i><u>For Carbonate</u></i> |                                   |                                 |           |     |
| BLK-1                       |                                   | 0.71128                         |           | 3.8 |
| BLK-2                       |                                   | 0.71197                         |           | 6.8 |
| <i><u>For Water</u></i>     |                                   |                                 |           |     |
| BLK-1                       |                                   | 0.71165                         |           | 0.7 |
| BLK-2                       |                                   | 0.71410                         |           | 0.5 |

Several total procedural blanks of Sr and Nd were processed along with the samples (Table 2.17). These blanks are several orders of magnitude lower than typical total Sr and Nd loads analysed and hence no corrections for blanks were made.

#### (d) Carbon and Oxygen isotopes in carbonate nodules

Carbon and oxygen isotope measurements were performed on the powdered carbonate nodules. These measurements were carried out following the protocol adopted by Sanyal (2004). A few milligrams of powdered samples were reacted with 100% of orthophosphoric acid at 25° C under vacuum in water bath and the liberated CO<sub>2</sub> was purified cryogenically and analyzed by GEO20-20 dual inlet mass spectrometer. Samples were analyzed along with Internal Laboratory standards, Z-Carrara ( $\delta^{13}\text{C} = 2.3 \pm 0.1\text{‰}$  and  $\delta^{18}\text{O} = -1.3 \pm 0.1\text{‰}$ ) and Mc. Marble ( $\delta^{13}\text{C} = 3.76 \pm 0.12\text{‰}$  and  $\delta^{18}\text{O} = -10.62 \pm 0.15\text{‰}$ ). Isotopic ratios of carbon and oxygen are presented in the usual  $\delta$  notation with respect to international standard V-PDB and V-SMOW respectively. The accuracy and precision of the measurement is better than  $\pm 0.2\text{‰}$  ( $2\sigma$ ) based on the several samples and standard measurements (Table 2.18a, 2.18b).

**Table 2.18a: Analysis of our laboratory standard Mc. Marbel and Z-Carara carbonates to check accuracy of the measurements.**

| Standard | Measured |                                 | Reported                        |                                 |                                 |
|----------|----------|---------------------------------|---------------------------------|---------------------------------|---------------------------------|
|          | ID       | $\delta^{13}\text{C}(\text{‰})$ | $\delta^{18}\text{O}(\text{‰})$ | $\delta^{13}\text{C}(\text{‰})$ | $\delta^{18}\text{O}(\text{‰})$ |
| Mc Mar-1 |          | 3.85±0.05                       | 10.98±0.03                      | 3.76±0.12                       | 10.62±0.15                      |
| Mc Mar-2 |          | 4.17±0.09                       | 10.51±0.09                      | 3.76±0.12                       | 10.62±0.15                      |
| Mc Mar-3 |          | 3.93±0.03                       | 10.85±0.05                      | 3.76±0.12                       | 10.62±0.15                      |
| Mc Mar-4 |          | 3.93±0.02                       | 10.80±0.04                      | 3.76±0.12                       | 10.62±0.15                      |
| Z-Car-1  |          | 2.31±0.01                       | -1.55±0.05                      | 2.30                            | -1.30                           |
| Z-Car-2  |          | 2.32±0.05                       | -1.80±0.07                      | 2.30                            | -1.30                           |

**Table 2.18b: Replicate analysis of  $\delta^{13}\text{C}$  and  $\delta^{18}\text{O}$  in carbonate nodules**

| <b>Sample ID</b>    | <b><math>\delta^{13}\text{C}</math></b> | <b><math>\delta^{18}\text{O}</math></b> |
|---------------------|---|---|
|                     | <b>(‰)</b>                              |   |
| <b>IITK-6.8</b>     | -6.82±0.03                              | -8.32±0.09                              |
| <b>IITK-6.8R</b>    | -6.85±0.03                              | -8.10±0.05                              |
| <b>IITK-14.46</b>   | 1.46±0.02                               | -5.52±0.03                              |
| <b>IITK-14.46R</b>  | 1.74±0.05                               | -5.04±0.04                              |
| <b>IITK-43.73R</b>  | -1.41±0.03                              | -7.15±0.33                              |
| <b>IITK-43.73R</b>  | -1.44±0.02                              | -7.01±0.13                              |
| <b>IITK-48.31</b>   | -0.80±0.05                              | -7.64±0.08                              |
| <b>IITK-48.31R1</b> | -0.81±0.03                              | -7.73±0.17                              |
| <b>IITK-48.31R2</b> | -0.79±0.03                              | -7.88±0.06                              |

## **CHAPTER-3**

**Major & trace elements and Sr & Nd isotope compositions of the Ganga plain sediments: Implication to weathering intensity and erosion distribution over the Himalaya during past ~100 ka**

### 3.1 Introduction

The Himalaya, a young orogenic belt, is undergoing widespread erosion resulting in the transfer of large amount of particulate and dissolved materials to its foreland basin and to the Bay of Bengal (Sarin et al., 1989; Milliman and Syvitski, 1992; Hay, 1998; Goodbred and Kuehl., 2000; Galy and France-Lanord, 2001; Singh et al., 2005; 2008). The Ganga supplies about 500-1000 million tons of sediments annually to the Bay of Bengal (Hay, 1998; Galy and France-Lanord, 2001; Goodbred, 2003). These sediments are derived both from the Higher and Lesser Himalaya, the former dominating the contemporary supply (Campbell et al., 2005; Foster et al., 2007; Singh et al., 2008). Most of these sediments are delivered during the south-west or summer monsoon (Goodbred, 2003) underscoring the significant role played by precipitation and hence climate on sediment supply. Therefore, spatial and temporal variations in the intensity of monsoon and the extent of glacial cover over the Himalaya can affect the source of sediments to the Ganga and its delivery (Goodbred, 2003). Studies of Bookhagen et al. (2005a), Clift et al. (2008) and Srivastava et al. (2008) demonstrated the influence of climatic variations on provenance of sediments in the Himalaya. However, such studies on the Ganga plain sediments are limited though it is one of the largest continental sedimentary repositories that can serve as an excellent archive to investigate the impact of climate (monsoon/glaciations) and/or tectonics on the erosion of the Himalaya over the time scales of  $10^4$ - $10^5$  years. The sediments of the Ganga plain are more suited for studying variations in sediment provenance compared to sediments of the Bay of Bengal, as the later is a more complex mixture of materials derived from multiple sources and different geological terrains (Colin et al., 1999; Ahmad et al., 2005; Liu et al., 2005). Such mixing of sediments can fudge provenance signatures. Further, the sediments of the Ganga plain are likely to provide better time resolution information as they may respond faster to the cause of variations in sediment provenances (Goodbred, 2003). Sr and Nd isotope composition of the Higher Himalaya (HH) and the Lesser Himalaya (LH), the two major sources of sediments to the Ganga plain, are quite distinct (Singh et al., 2008) and therefore can be used as tracers to track variations in relative proportion of

sediments derived from each of them. Sr and Nd isotope composition of the silicate fraction of the sediments of the Bay of Bengal have been used to study temporal variations in their provenance (France-Lanord et al., 1993; Colin et al., 1999; Ahmad et al., 2005; Liu et al., 2005). In this study, for the first time, Sr and Nd isotope composition of silicate fraction of sediments from a core in the Ganga plain has been used to investigate temporal variations in the provenance of sediments and their causative factors.

In addition to large sediment flux, the Ganga supply enormous amount of dissolved flux to the Bay of Bengal indicating significantly high chemical erosion over the Himalaya. Higher chemical weathering particularly the silicate weathering, resulting from rapid uplift of the Himalaya, has been suggested as one of important factors influencing the global temperature during the Cenozoic (Raymo et al., 1988; Raymo and Ruddiman, 1992; Galy et al., 2008). Available studies do suggest that the Himalaya plays an important role in the global carbon cycle due to higher silicate weathering and it controls global geochemical and carbon cycles over million year time scales (Raymo and Ruddiman, 1992. Ruddiman, 1997). CO<sub>2</sub> drawdown due to enhanced silicate weathering associated with the Himalaya-Tibetan orogenic belt has been linked to the late Cenozoic cooling (Raymo and Ruddiman, 1992). Contemporary silicate weathering and associated CO<sub>2</sub> consumption over the Himalaya is indeed higher compared to its global average and many other river drainages (Krishnaswami et al, 1999; Gaillardet et al., 1999; Singh et al. 2005). However, very little is known about the temporal variation in the intensity of paleo-weathering over the Himalaya. Few studies carried on the sediments of the Bay of Bengal (France Lanord et al., 1993; Colin et al., 1999) hint towards temporal variation in the weathering intensity. This study assesses the temporal variation in the weathering intensity over the Himalaya using the major element composition of the sediments of a core taken from the Ganga plain at Kanpur. As the core location receives sediments only from the Himalaya, any temporal variability observed in their chemical composition could be attributed to that of the change in the weathering intensity over the Himalaya. Further the role of various factors, such as climate,

rainfall, temperature, tectonics etc. in controlling the weathering intensity will be evaluated.

### 3.2 Results

Major and trace elements were measured in the bulk sediments of the IITK core to determine the degree of chemical weathering intensity and their behaviour during chemical weathering and transport. The data of major elements Na, K, Ca, Mg, Al, Fe, Ti, and organic and inorganic carbon are presented in Table 3.1. Mean and standard deviations of these data are also reported in Table 3.1. All major elements except CaO show variability of 12-29% from their mean. CaO in these sediments show large variability, ~95% from the mean. Higher variability in the CaO is controlled by the presence of detrital and authigenic carbonates as these measurements are based on bulk analysis.

**Table 3.1: Major element composition of bulk sediments of IITK Core**

| Sample    | Na <sub>2</sub> O | K <sub>2</sub> O | MgO | CaO  | Al <sub>2</sub> O <sub>3</sub> | FeO | TiO <sub>2</sub> | IC  | OC  |
|-----------|-------------------|------------------|-----|------|--------------------------------|-----|------------------|-----|-----|
| Wt (%)    |                   |                  |     |      |                                |     |                  |     |     |
| IITK0.06  | 1.4               | 5.6              | 1.5 | 1.0  | 12.7                           | 3.8 | 0.7              | 0.0 | 0.6 |
| IITK0.5   | 1.3               | 5.7              | 1.6 | 0.9  | 13.6                           | 4.3 | 0.6              | 0.0 | 0.3 |
| IITK1.4   | 1.2               | 5.8              | 1.8 | 1.0  | 15.1                           | 5.3 | 0.7              | 0.0 | 0.2 |
| IITK2.25  | 1.1               | 6.5              | 2.4 | 3.6  | 15.2                           | 5.9 | 0.8              | 0.6 | 0.2 |
| IITK3.05  | 1.4               | 6.2              | 2.5 | 2.7  | 14.6                           | 2.5 | 0.8              | 0.3 | 0.1 |
| IITK3.68  | 1.5               | 7.0              | 3.0 | 3.0  | 15.3                           | 1.0 | 0.8              | 0.4 | 0.2 |
| IITK5.33  | 1.5               | 6.9              | 3.1 | 4.1  | 14.4                           | 5.3 | 0.6              | 0.8 | 0.2 |
| IITK6.55  | 1.2               | 7.9              | 3.5 | 5.6  | 15.4                           | 6.1 | 0.8              | 1.2 | 0.5 |
| IITK7.08  | 1.6               | 4.6              | 2.2 | 6.8  | 10.9                           | 1.7 | 0.7              | 1.3 | 0.3 |
| IITK7.67  | 1.6               | 4.8              | 2.2 | 7.9  | 10.9                           | 3.8 | 0.7              | 1.6 | 0.2 |
| IITK9.06  | 1.7               | 5.0              | 2.1 | 5.3  | 11.0                           | 3.4 | 0.6              | 1.0 | 0.2 |
| IITK10.3  | 1.1               | 4.8              | 2.4 | 14.1 | 10.4                           | 3.6 | 0.5              | 2.8 | 0.7 |
| IITK11.14 | 1.7               | 4.8              | 2.3 | 4.4  | 10.8                           | 3.4 | 0.6              | 0.8 | 0.2 |
| IITK11.88 | 1.6               | 6.1              | 2.7 | 4.9  | 13.0                           | 4.4 | 0.6              | 0.9 | 0.2 |
| IITK12.98 | 1.5               | 5.8              | 2.1 | 3.6  | 13.1                           | 4.5 | 0.7              | 0.5 | 0.2 |
| IITK14.46 | 1.0               | 5.3              | 3.9 | 15.0 | 11.3                           | 4.3 | 0.6              | 3.5 | 0.4 |
| IITK15.79 | 1.6               | 5.3              | 2.8 | 8.1  | 11.1                           | 3.6 | 0.0              | 1.8 | 0.2 |
| IITK17.37 | 1.9               | 4.2              | 1.4 | 3.1  | 9.7                            | 2.6 | 0.6              | 0.4 | 0.1 |
| IITK20.46 | 1.7               | 4.8              | 2.1 | 3.9  | 11.6                           | 4.1 | 0.7              | 0.6 | 0.2 |
| IITK21.10 | 1.4               | 5.7              | 2.4 | 8.7  | 12.5                           | 4.6 | 0.6              | -   | -   |

|                   |            |            |            |            |             |            |            |            |            |
|-------------------|------------|------------|------------|------------|-------------|------------|------------|------------|------------|
| <b>IITK24.72</b>  | 1.6        | 5.3        | 1.9        | 1.8        | 12.6        | 4.3        | 0.7        | 0.1        | 0.1        |
| <b>IITK25.72</b>  | 1.1        | 5.2        | 1.7        | 2.4        | 12.3        | 4.5        | 0.8        | 0.3        | 0.1        |
| <b>IITK28.46</b>  | 1.1        | 5.0        | 1.5        | 1.1        | 12.1        | 4.4        | -          | 0.0        | 0.0        |
| <b>IITK28.92</b>  | 1.1        | 5.0        | 1.6        | 1.0        | 12.5        | 4.8        | 0.7        | 0.0        | 0.1        |
| <b>IITK29.80</b>  | 1.3        | 5.1        | 1.6        | 1.0        | 12.9        | 4.6        | 0.7        | 0.0        | 0.1        |
| <b>IITK30.42</b>  | 1.0        | 5.2        | 1.4        | 0.7        | 11.5        | 4.2        | 0.7        | 0.0        | 0.0        |
| <b>IITK-31.52</b> | 1.1        | 5.1        | 1.4        | 0.9        | 11.0        | 5.1        | 0.7        | 0.0        | -          |
| <b>IITK-32.5</b>  | 0.9        | 4.2        | 1.8        | 16.3       | 10.3        | 3.3        | 0.5        | 4.1        | 0.2        |
| <b>IITK-34.09</b> | 1.8        | 5.2        | 1.6        | 1.2        | 11.2        | 3.7        | 0.7        | 0.0        | 0.0        |
| <b>IITK-34.7</b>  | 1.8        | 5.0        | 1.7        | 1.0        | 11.6        | 3.9        | 0.7        | 0.0        | 0.0        |
| <b>IITK-35.16</b> | 1.9        | 5.3        | 1.4        | 1.2        | 11.1        | 3.5        | 0.6        | 0.0        | 0.2        |
| <b>IITK-37.97</b> | 1.5        | 4.5        | 1.6        | 1.2        | 10.9        | 3.9        | 1.3        | 0.0        | 0.1        |
| <b>IITK-38.55</b> | 1.1        | 5.4        | 1.9        | 1.4        | 11.9        | 4.7        | 0.9        | 0.1        | 0.3        |
| <b>IITK-38.85</b> | 1.0        | 4.3        | 2.0        | 2.5        | 11.7        | 4.3        | 0.9        | 0.4        | 0.1        |
| <b>IITK-41.23</b> | 1.1        | 4.5        | 1.8        | 13.4       | 10.4        | 3.4        | 0.6        | 0.5        | -          |
| <b>IITK-41.78</b> | 1.5        | 5.2        | 1.7        | 2.5        | 11.2        | 3.9        | 0.7        | 0.3        | 0.1        |
| <b>IITK-43.72</b> | 1.4        | 5.3        | 2.2        | 3.1        | 12.4        | 4.6        | 0.7        | 0.5        | 0.1        |
| <b>IITK-45.4</b>  | 1.2        | 4.7        | 1.6        | 3.0        | 11.4        | 3.9        | 0.7        | 0.5        | 0.1        |
| <b>IITK-46.0</b>  | 1.0        | 5.1        | 1.5        | 1.3        | 11.9        | 4.1        | 0.8        | 0.1        | 0.1        |
| <b>IITK-46.42</b> | 1.5        | 5.2        | 2.0        | 2.8        | 12.7        | 4.6        | 0.8        | 0.3        | 0.1        |
| <b>IITK-47.1</b>  | 0.9        | 5.3        | 2.0        | 1.1        | 13.5        | 5.0        | 0.7        | 0.1        | 0.1        |
| <b>IITK-51.0</b>  | 0.9        | 5.8        | 2.6        | 6.2        | 13.8        | 5.5        | 0.8        | 1.1        | 0.2        |
| <b>Mean(n=42)</b> | <b>1.3</b> | <b>5.3</b> | <b>2.1</b> | <b>4.2</b> | <b>12.2</b> | <b>4.1</b> | <b>0.7</b> | <b>0.7</b> | <b>0.2</b> |
| <b>SD</b>         | <b>0.3</b> | <b>0.7</b> | <b>0.6</b> | <b>4.0</b> | <b>1.5</b>  | <b>1.0</b> | <b>0.2</b> | <b>0.9</b> | <b>0.1</b> |

**IC: inorganic carbon and OC: organic carbon, SD: Standard deviation,**

**n: number of samples.**

Sr, Nd concentrations in sediments and their isotope compositions of IITK core are given in Table 3.2. Unlike major elements, Sr and Nd concentrations and their isotope compositions are measured in silicate phase of the sediments as discussed in chapter 2. Table 3.2 contains data of sediment samples in addition to those reported in Rahaman et al., (2009). Subsequent to study of Rahaman et al. (2009), more sediment samples from various depth of the IITK core were analysed to increase the temporal resolution. Sr and Nd concentration varies from 49 to 225 and from 18 to 42  $\mu\text{g/g}$  respectively, similar to their sources, the Higher Himalaya (HH) and the Lesser Himalaya (LH). Sr and Nd isotope composition range from 0.72701 to 0.76708 and from -17.7 to -13.5 respectively. The  $^{87}\text{Sr}/^{86}\text{Sr}$  and  $\epsilon_{\text{Nd}}$  of these sediments

fall between the range defined by the lithologies of the Higher and the Lesser Himalaya. The spread in Sr and Nd isotope composition with depth in the IITK core is much larger compared to those in the Bay of Bengal sediments (Colin et al., 1999; Ahmad et al., 2005; Liu et al., 2005) as the signals in the later are attenuated due to sediment supply from multiple sources. The large spread in  $^{87}\text{Sr}/^{86}\text{Sr}$  and  $\epsilon_{\text{Nd}}$  in the IITK core enables to discern the provenance variations better.

**Table 3.2: Sr, Nd isotope composition of silicate fraction of sediments of IITK core**

| Depth<br>(m) | $^{87}\text{Sr}/^{86}\text{Sr}$ | [Sr]<br>$\mu\text{g/g}$ | $^{143}\text{Nd}/^{144}\text{Nd}$ | $\epsilon_{\text{Nd}}$ | [Nd]<br>$\mu\text{g/g}$ |
|--------------|---------------------------------|-------------------------|-----------------------------------|------------------------|-------------------------|
| IITK0.06     | 0.74846                         | 94                      | 0.511756                          | -17.2                  | 26                      |
| IITK0.5      | 0.74756                         | 88                      | 0.511842                          | -15.5                  | 24                      |
| IITK1.4      | 0.74548                         | 84                      | 0.511902                          | -14.4                  | 19                      |
| IITK-2.55    | 0.75069                         | 72                      | 0.511859                          | -15.2                  | 22                      |
| IITK3.05     | 0.74196                         | 98                      | 0.511871                          | -15.0                  | 22                      |
| IITK-3.68    | 0.76161                         | 86                      | 0.511842                          | -15.5                  | 18                      |
| IITK-4.03    | 0.75235                         | 92                      | 0.511820                          | -16.0                  | 26                      |
| IITK-4.75    | 0.76535                         | 74                      | 0.511794                          | -16.5                  | 19                      |
| IITK-5.33    | 0.76027                         | 80                      | 0.511786                          | -16.6                  | 21                      |
| IITK-5.87    | 0.75701                         | 103                     | 0.511812                          | -16.1                  | 22                      |
| IITK6.55     | 0.76510                         | 77                      | 0.511786                          | -16.6                  | 23                      |
| IITK-7.08    | 0.73515                         | 117                     | 0.511875                          | -14.9                  | 24                      |
| IITK-7.67    | 0.74085                         | 112                     | 0.511880                          | -14.8                  | 26                      |
| IITK-8.10    | 0.75096                         | 121                     | 0.511732                          | -17.7                  | 23                      |
| IITK9.06     | 0.75008                         | 49                      | 0.511816                          | -16.0                  | 23                      |
| IITK-9.7     | 0.73299                         | 124                     | 0.511944                          | -13.5                  | 29                      |
| IITK-10.30   | 0.75096                         | 97                      | 0.511825                          | -15.9                  | 23                      |
| IITK-11.14   | 0.75148                         | 114                     | 0.511811                          | -16.1                  | 32                      |
| IITK11.88    | 0.75624                         | 100                     | 0.511812                          | -16.1                  | 22                      |
| IITK14.46    | 0.72701                         | 225                     | 0.511846                          | -15.5                  | 18                      |
| IITK15.79    | 0.74732                         | 122                     | 0.511805                          | -16.3                  | 26                      |
| IITK17.37    | 0.75214                         | 122                     | 0.511791                          | -16.5                  | 42                      |
| IITK20.46    | 0.73447                         | 141                     | 0.511857                          | -15.2                  | 26                      |
| IITK21.10    | 0.73998                         | 101                     | 0.511857                          | -15.2                  | 23                      |
| IITK24.72    | 0.73376                         | 123                     | 0.511908                          | -14.2                  | 27                      |

|                   |         |     |          |       |    |
|-------------------|---------|-----|----------|-------|----|
| <b>IITK25.72</b>  | 0.73580 | 80  | 0.511902 | -14.4 | 22 |
| <b>IITK28.46</b>  | 0.74044 | 88  | 0.511868 | -15.0 | 31 |
| <b>IITK29.8</b>   | 0.74589 | 77  | 0.511865 | -15.1 | 22 |
| <b>IITK31.52</b>  | 0.74504 | 88  | 0.511866 | -15.1 | 27 |
| <b>IITK34.09</b>  | 0.76708 | 126 | 0.511862 | -15.1 | 28 |
| <b>IITK-34.7</b>  | 0.75854 | 94  | 0.51184  | -15.6 | 22 |
| <b>IITK35.16</b>  | 0.75804 | 97  | 0.511822 | -15.9 | 25 |
| <b>IITK-36.0</b>  | 0.75847 | 58  | 0.511836 | -15.6 | 18 |
| <b>IITK-36.53</b> | 0.73266 | 133 | 0.511919 | -14.0 | 28 |
| <b>IITK-37.1</b>  | 0.73677 | 112 | 0.511919 | -14.0 | 28 |
| <b>IITK38.55</b>  | 0.73824 | 106 | 0.511858 | -15.2 | 31 |
| <b>IITK41.23</b>  | 0.74583 | 105 | 0.511821 | -15.9 | 21 |
| <b>IITK43.72</b>  | 0.73625 | 128 | 0.511863 | -15.1 | 29 |
| <b>IITK45.4</b>   | 0.74002 | 91  | 0.511871 | -14.8 | 22 |
| <b>IITK46.0</b>   | 0.73646 | 109 | 0.511847 | -15.4 | 28 |
| <b>IITK47.1</b>   | 0.73687 | 107 | 0.511857 | -15.2 | 26 |
| <b>IITK51.0</b>   | 0.74042 | 97  | 0.511813 | -16.1 | 21 |

### 3.3 Discussion

#### 3.3.1 Temporal variation in the paleo-weathering intensity

During chemical weathering mobile elements will be depleted in the sediments whereas relatively immobile elements could be enriched due to mass loss of the sediments. To assess the depletion/enrichment of the elements in the sediment, chemical compositions of these sediments are compared with respect to that of their source rocks. Chemical composition of the source rocks is given in Table 3.3 based on the compilation of France-Lanord and Derry (1997) and Rai (2008). Al or Ti normalized concentration of major elements of the sediments are compared with those of their source rocks to assess their mobility. Among the large ion lithophile elements Na has more tendency to leach out from the source rocks during the chemical weathering. Therefore, (Na, Ca, K/Al) is expected to deplete in the sediments with respect to the source rocks. Data indicate that Ca, Mg, Fe and Ti are enriched whereas K and Na are depleted in the sediment with respect to source rock. Ca and Mg are enriched in the IITK core sediments due to presence of detrital and pedogenic carbonates whereas Ti is enriched due to its refractory nature. As Na and K

are mobile elements, they are depleted in the sediments due to chemical weathering. In order to understand the temporal variability in the intensity of chemical weathering in the Ganga plain sediments during past ~100 ka, an attempt has been made to quantify Chemical Index of Alteration (CIA) of the sediments of IITK core. CIA has been used to measure chemical weathering intensity (Nesbitt and Young, 1985) and is defined as  $100 \times (\text{Al}_2\text{O}_3) / (\text{Al}_2\text{O}_3 + \text{CaO}^* + \text{K}_2\text{O} + \text{Na}_2\text{O})$  where concentration of all the elements are in mol percentage and  $\text{CaO}^*$  is CaO from the silicates. CIA reflect removal of labile cations ( $\text{Ca}^{2+}$ ,  $\text{Na}^+$ ,  $\text{K}^+$ ) relative to stable residual constituents ( $\text{Al}^{3+}$ ,  $\text{Ti}^{4+}$ ) during weathering. CIA provides a measure of the proportion of secondary aluminous clay minerals to primary silicate minerals (Nesbitt and Young, 1982; Fedo et al., 1995). However, Ca in silicate phase is required to precisely estimate CIA which is difficult in this study as carbonates are often associated with these sediments making decoupling of Ca between silicate and carbonate component difficult. To avoid this uncertainty, CIA is used after slight modifications. This modified CIA\* was first introduced by Colin et al. (1999) to determine chemical weathering intensity in the Bay of Bengal sediments. The modified CIA\* defined as  $100 \times (\text{Al}_2\text{O}_3) / (\text{Al}_2\text{O}_3 + \text{K}_2\text{O} + \text{Na}_2\text{O})$ . CIA\* of the HH, LH source rocks and of contemporary sediments are given in Table 3.4. Contemporary bank sediments have CIA\* similar to that of source rocks, indicating very little chemical weathering whereas suspended load and finer fraction show the impact of weathering. The cross plot between CIA\* and  $\text{Al}_2\text{O}_3/\text{Na}_2\text{O}$  shows the degree of chemical weathering intensity of the IITK core sediments. The CIA\* of majority of IITK core sediments are slightly higher than that of the source rocks, the HH and the LH, indicating low to moderate intensity of chemical weathering. The average CIA\* of the LH and HH rocks ranges from 60 to 70 as they were formed by recycled crust. Based on the CIA\* scale, the sediments of the IITK profile have suffered low to moderate degree of chemical weathering (Fig. 3.1).  $\text{Al}_2\text{O}_3$  and  $\text{TiO}_2$  are the resistant minerals which are enriched in the residual phase after weathering. Therefore, it is expected that  $\text{Na}_2\text{O}/\text{Al}_2\text{O}_3$  and  $\text{Na}_2\text{O}/\text{TiO}_2$  will vary synchronously following intensity of weathering.

**Table 3.3: Average ( $\pm\sigma$ ) composition of Himalayan Crystallines and the Ganga Sediments**

| Samples Rocks                                 | Al            | Fe            | Ca            | Mg             | K             | Na            | Ti            |
|---|---------------|---------------|---------------|----------------|---------------|---------------|---------------|
|   | ( $\%$ )      |               |               |                |               |               |               |
| Higher Himalayan Crystallines<br>(HHC) n = 99 | 6.9 $\pm$ 1.4 | 3.0 $\pm$ 0.9 | 0.8 $\pm$ 0.4 | 1.1 $\pm$ 0.6  | 2.5 $\pm$ 0.5 | 1.7 $\pm$ 0.4 |               |
| Lesser Himalayan<br>Meta Sediments n=77       | 7.3 $\pm$ 1.8 | 4.2 $\pm$ 3.0 | 1.0 $\pm$ 0.7 | 1.15 $\pm$ 0.9 | 4.7 $\pm$ 2.1 | 2.0 $\pm$ 1.4 | 0.3 $\pm$ 0.1 |
| HHC n = 56                                    | 7.3 $\pm$ 1.4 | 2.5 $\pm$ 2.1 | 0.9 $\pm$ 0.6 | 0.5 $\pm$ 0.6  | 3.6 $\pm$ 1.0 | 2.4 $\pm$ 0.9 | 0.2 $\pm$ 0.1 |
| LHC (Compiled) n = 108                        | 7.2 $\pm$ 0.9 | 2.8 $\pm$ 1.4 | 1.1 $\pm$ 0.7 | 0.9 $\pm$ 0.7  | 4.0 $\pm$ 1.1 | 2.1 $\pm$ 0.9 | 0.2 $\pm$ 0.2 |
| IITK Core bulk sediments n=42                 | 6.5 $\pm$ 0.8 | 3.2 $\pm$ 0.8 | 3.1 $\pm$ 3.0 | 1.2 $\pm$ 0.3  | 2.2 $\pm$ 0.3 | 1.0 $\pm$ 0.2 | 0.4 $\pm$ 0.1 |

**Source: Rai, 2008 and reference there in. Chemical compositions of IITK core sediments of this study were measured in bulk samples.**

**Table 3.4: Comparison of CIA\* of different lithologies and sediments from the Ganga system**

| <b>Region/ Basin</b>         | <b>(n)</b> | <b>Sample</b>       | <b>CIA Range</b> | <b>CIA Mean</b> | <b>CIA* Mean</b> | <b>Data source</b>  |
|------------------------------|------------|---------------------|------------------|-----------------|------------------|---|
| Higher Himalayan Crystalline | 99         | Total               |                  | 59              | 65               | Lanord and Derry, 1997  |
| Lesser Himalaya              | 75         | Meta Sediments      | 24-73            | 53±8            | 58±9             | Kashyap 1972; Mishra, 1973; Rawat 1984                              |
| Lesser Himalaya              | 108        | Granites/ Gneisses  | 21-70            | 52±7            | 58±7             | Rao,1983 ; Bhattacharya et al., 1984 ; Nautiyal, 1990 ; Gupta, 1994 |
| Higher Himalaya              | 56         | Granites/ Gneisses  | 29-83            | 53±7            | 58±6             | Rao, 1983 ; Bruno et al., 1990 ; Choudhuri 1991 ; Chamyal, 1996     |
| Ganga sediments              | 28         | Bank sediments      | 31-64            | 52±6            | 63±2             | Rai, 2008   |
| Ganga sediments              | 8          | Suspended sediments | 61-68            | 65±2            | 73±2             | Rai, 2008   |
| Ganga sediments              | 3          | <4 µm sediments     | 73-76            | 75±2            | 81±3             | Rai, 2008   |
| IITK Core sediments          |            | Bulk sediments      |                  |                 | 70±3             | This study  |

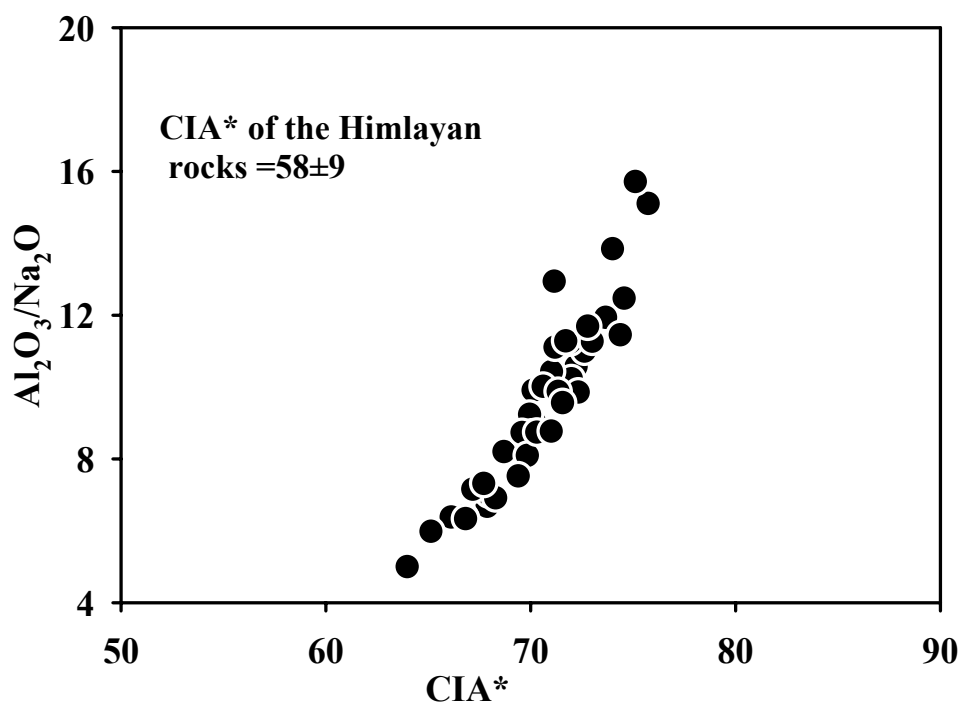


**Fig. 3.1** scatter plot of  $\text{Al}_2\text{O}_3/\text{Na}_2\text{O}$  and  $\text{CIA}^*$  shows linear trend.

Higher values of chemical indices,  $\text{Na}_2\text{O}/\text{Al}_2\text{O}_3$  and  $\text{Na}_2\text{O}/\text{TiO}_2$  represent the lower degree of chemical weathering and vice versa. In contrast, the higher value of  $\text{CIA}^*$  represents the higher degree of chemical weathering and follows inverse relationship with the  $\text{Na}_2\text{O}/\text{Al}_2\text{O}_3$  and  $\text{Na}_2\text{O}/\text{TiO}_2$ . The  $\text{CIA}^*$  value of the IITK core sediments range between 64 to 76 with average value  $70\pm 3$  which is marginally above the range defined by crystalline from the Himalaya,  $58\pm 6$  and 65 reported for HHC (Table 3.4). The average  $\text{CIA}^*$  value of the IITK core sediments  $70\pm 3$  is close to the contemporary suspended sediments (Table 3.4) which have been subjected to moderate chemical weathering (Rai, 2008). Fig. 3.2 shows the variations in  $\text{CIA}^*$ ,  $\text{Na}_2\text{O}/\text{Al}_2\text{O}_3$  and  $\text{Na}_2\text{O}/\text{TiO}_2$  with depth. All of them show considerable variation indicating variation in intensity of chemical weathering with time. Variation in  $\text{CIA}^*$  show opposite trend to that of  $\text{Na}_2\text{O}/\text{Al}_2\text{O}_3$  and  $\text{Na}_2\text{O}/\text{TiO}_2$ .  $\text{CIA}^*$ ,  $\text{Na}_2\text{O}/\text{Al}_2\text{O}_3$  and  $\text{Na}_2\text{O}/\text{TiO}_2$  all show four prominent excursions at  $\sim 90$  ka,  $\sim 70$  ka,  $\sim 40$  ka and  $\sim 20$  ka.

At these ages, the sediments has lower CIA\* coinciding with higher values of the  $\text{Na}_2\text{O}/\text{Al}_2\text{O}_3$  and  $\text{Na}_2\text{O}/\text{TiO}_2$  which represent lesser extent of chemical weathering. These four periods are known to have lower precipitation and lower solar insolation (Prell and Kutzbuch, 1987). Further, the ages ~20 and 70 ka are known glacial periods. These chemical indices indicate that intensity of chemical weathering of the

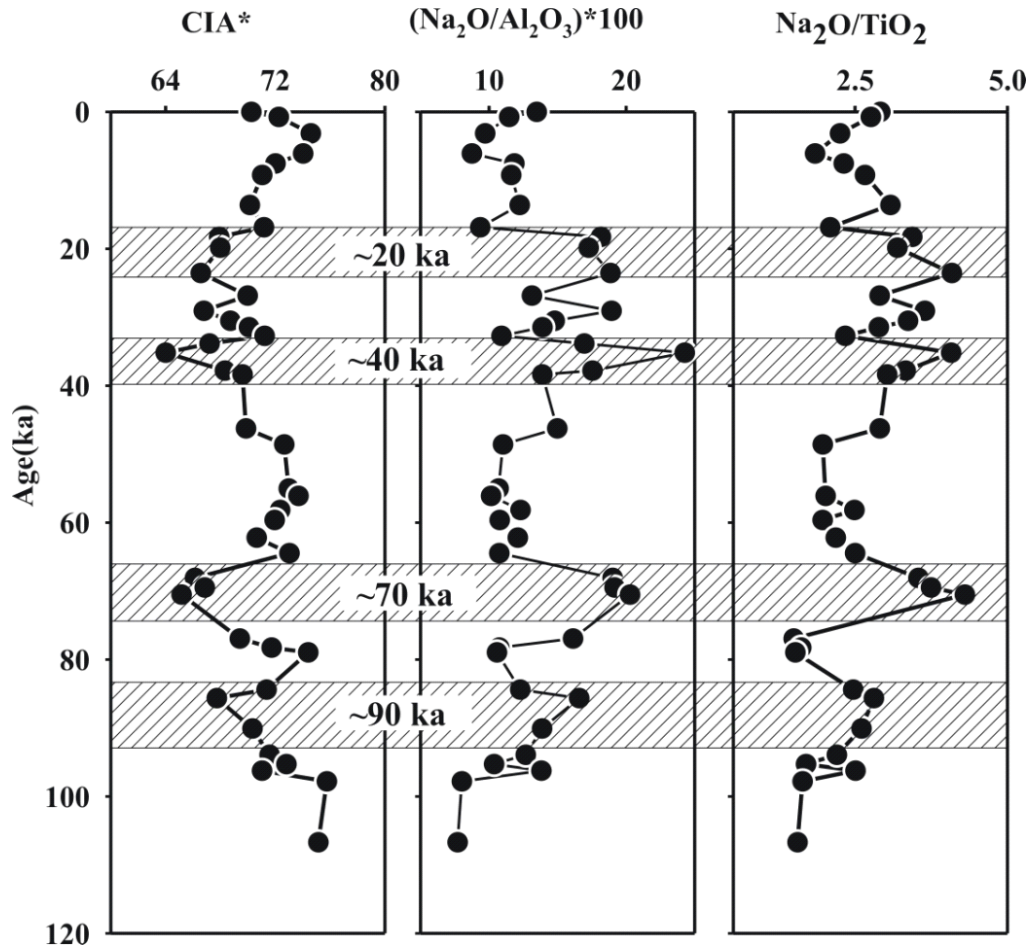


**Fig. 3.2** Chemical indices such as CIA\*,  $\text{Na}_2\text{O}/\text{Al}_2\text{O}_3$  and  $\text{Na}_2\text{O}/\text{TiO}_2$  are the parameters of measuring the degree of chemical weathering intensity. Intensity of chemical weathering of the sediments deposited during ~90, ~70, ~40 and ~20 were lower which coincide with the periods of lower precipitation and glacial maxima (Prell and Kutzbuch, 1987).

sediment deposited during ~90, ~70, ~40 and ~20 ka were lower due to the lower

temperature and lower precipitation during these periods. This observation suggests that chemical weathering over the Himalaya has varied during last 100 ka and temperature and precipitation seem to control weathering intensity. Lowering of continental weathering during glacial period is reported using the marine Os isotope composition (Oxburgh, 1998; Dalai et al., 2005; Oxburgh et al., 2007). This observation that intensity of chemical weathering over the Himalaya has varied with time would have significant impact on the global geochemical budget and carbon cycle. The Himalaya being one of the major contributors to the global geochemical budget, any variation in its intensity of chemical weathering will influence the supply of elements to the ocean influencing their budgets. For example, variation in intensity of chemical weathering over the Himalaya would supply variable flux of dissolved Os to the ocean which will modulate the  $^{187}\text{Os}/^{186}\text{Os}$  of the seawater with time.

### **3.3.2 Erosion distribution over the Himalaya**

Tectonics and climate are two major factors controlling the erosion in the Himalaya. However, at shorter time scale, impact of tectonics might be negligible on the erosion variability if any. Climate has changed significantly over the time period considered in this study and can affect the erosion pattern over the Himalaya. Any variability in the erosion pattern over Himalaya, will be the best recorded in the Ganga plain, particularly at the core site as it receives sediments only from the Himalaya, i.e. the Higher and the Lesser Himalaya. Based on the compiled data from the literature, it is clearly observed that major elements abundances of the sediments are similar to their ranges of the Higher and the Lesser Himalayan rocks (Table 3.4). Therefore, it is very difficult to apportion the sources of these sediments based on their major element composition. The HH and the LH both have their characteristic Sr and Nd isotope composition. Therefore, Sr and Nd isotope composition of the sediments deposited at the core site of this study can be used to track any variability in the erosion pattern over HH and LH as their isotope compositions are quite distinct provided that the sediments deposited in the plain preserve the isotope characteristics of their sources. Several studies have been carried out using Sr and Nd isotope

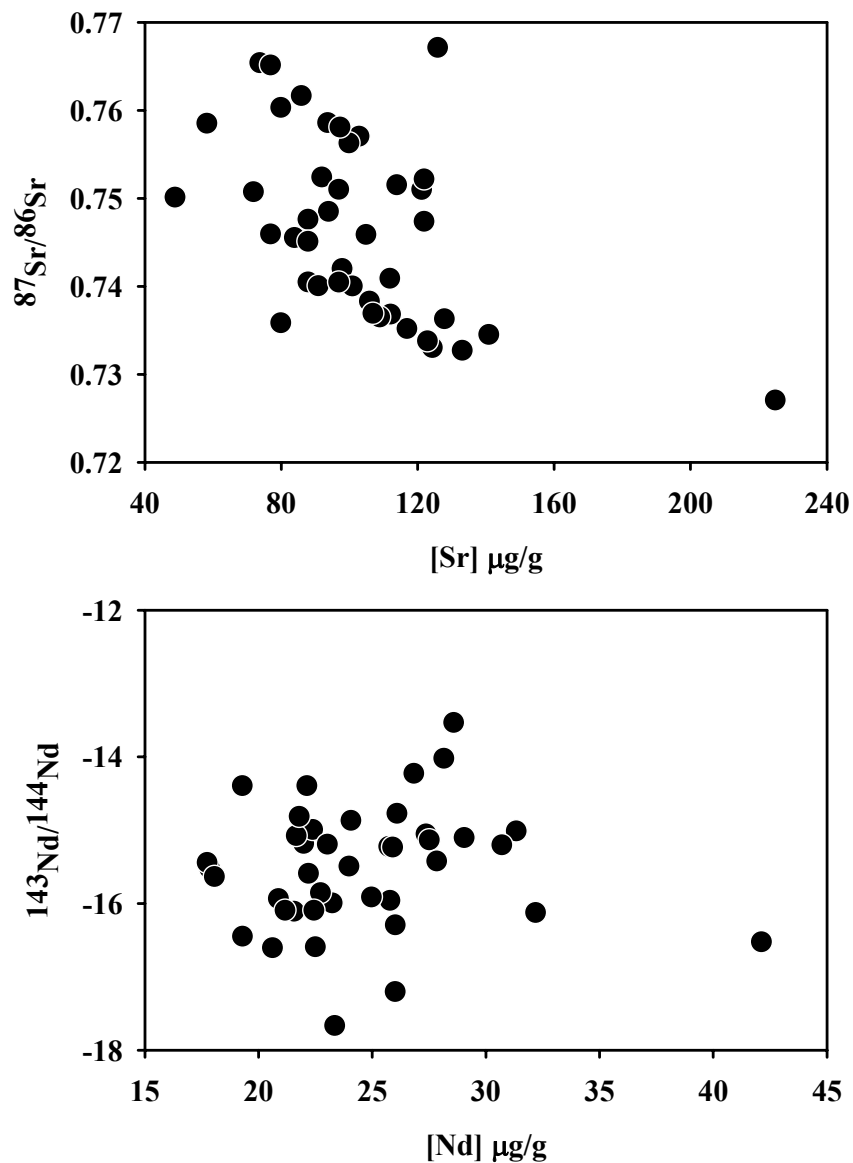


**Fig. 3.3** Scatter plot of Sr and Nd isotope composition with their concentrations in the sediments. Absence of any correlation among them rules out possibility of alteration of their isotope composition due to size sorting or weathering and hence they represent their source composition.

composition of the contemporary sediments (Singh and France-Lanord, 2002; Singh et al., 2008) and sediments deposited in the Bay of Bengal and in the Indus delta (Colin et al., 1999; Ahmad et al., 2005; Clift et al., 2008) to track their sources. It has

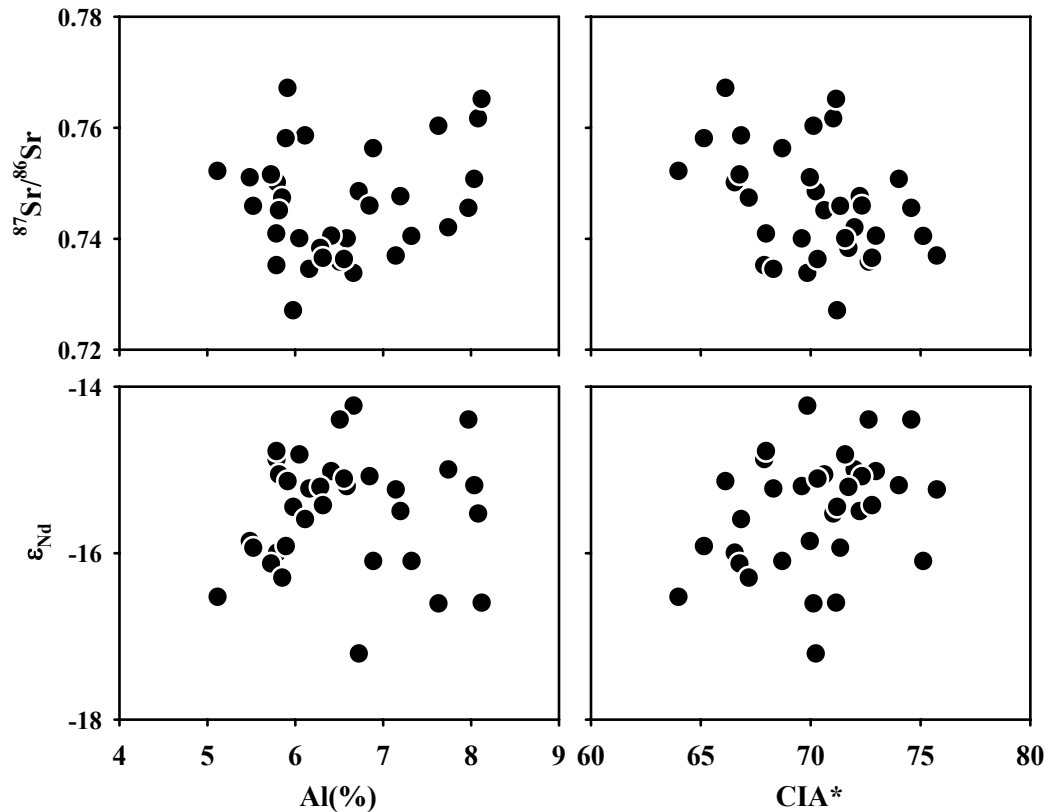


**Fig. 3.4 Scatter plot of  $^{87}\text{Sr}/^{86}\text{Sr}$  and  $\epsilon_{\text{Nd}}$  with their Al content and CIA\*. Sr and Nd isotope compositions of the sediments are not correlated with their Al abundance and CIA\*, indicating very little impact of transport and weathering on the isotope composition of the sediments, if any.**

been shown (Singh et al., 2008) that the isotopic composition of the contemporary sediments of the Ganga in the plain represents their sources and weathering and transport do not alter their isotopic signature. Similar to the coarser fraction, even the finer size fraction of the sediments represents their source isotope composition ruling out any impact of weathering and transport on their isotope composition (Galy and France-Lanord, 2001; Singh and France-Lanord et al., 2002; Singh et al., 2008). However concentrations of Sr and Nd shows variability arising due to size sorting and chemical weathering and it is difficult to use the concentration alone to track their sources. As discussed earlier the sediments analysed in this study are mostly flood

plain deposits and in general they are dominated by mud and silt. Both Sr and Nd isotope composition of these sediments do not show any correlation with their respective concentrations (Fig. 3.3) or with Al content of these sediments and CIA\* (Fig. 3.4), indicating very little affect of alteration on these sediments by weathering and transport processes. Despite variation in the intensity of weathering, as discussed above, these sediments preserved their source signature.

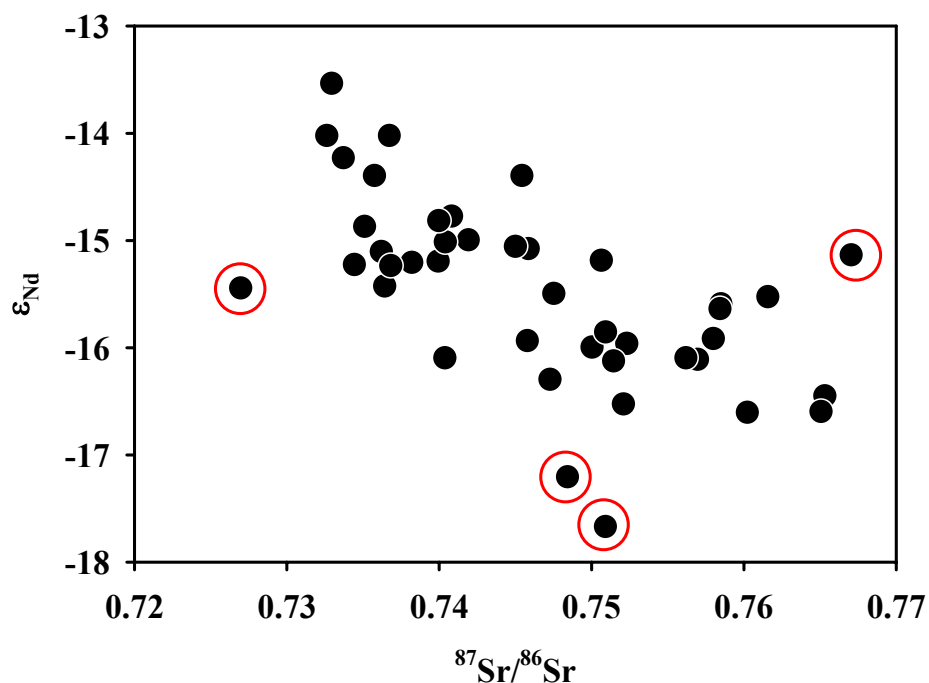


**Fig. 3.5  $^{87}\text{Sr}/^{86}\text{Sr}$  vs  $\epsilon_{\text{Nd}}$ . Sr and Nd isotopes of these sediments are result of the mixing between the sediments derived from the Higher and Lesser Himalaya. Four anomalous samples (encircled in red) could be due to the large variability in the sources or related to the discrete flood events as discussed in the text.**

Further, in the scatter plot of  $^{87}\text{Sr}/^{86}\text{Sr}$  versus  $\epsilon_{\text{Nd}}$  (Fig. 3.5), they show a trend similar to those observed for contemporary sediments (Singh et al., 2008) and can be explained by mixing between the sediments derived from the Higher and Lesser Himalaya. The  $\epsilon_{\text{Nd}}$  of these sediments decreases with increasing  $^{87}\text{Sr}/^{86}\text{Sr}$ , indicating

varying proportion of the sediments from HH and LH. The observed scatter in the plot is due to the scatter in the source rocks of HH and LH (Table 3.5). In Fig. 3.5, four samples in red circle seem to show anomalous behaviour. These samples were collected from the depths of 0.06, 8.1, 14.46 and 34.09 m and they fall out of the general inverse trend defined by  $\epsilon_{Nd}$  and  $^{87}Sr/^{86}Sr$  (Fig. 3.5). There could be several reasons for anomalous features of these samples. It could be either due to the source variability with higher proportion from the Tethyan Sedimentary Sequence of HH or due to flooding effect. The anomalous sample from depth 34.09 m has higher  $^{87}Sr/^{86}Sr$ , 0.76708 but not so lower  $\epsilon_{Nd}$  (-15.1). This sample has low CIA\*, 66 and high  $Na_2O/Al_2O_3$ , 16 indicating less chemical weathering. This sample was collected from a section of the core with discrete flood deposit (Fig. 2.2) and may represent the sediments derived from a small basin characterized by Sr and Nd isotope composition similar to those observed for this sample. Sample from depth 14.46 has the lowest  $^{87}Sr/^{86}Sr$ , 0.72701 with  $\epsilon_{Nd}$ , -15.5.  $^{87}Sr/^{86}Sr$  of these two samples (depths 14.46 and 34.09 m) show two extreme values even though they have similar  $\epsilon_{Nd}$ , reasons for which are not very clear at this moment. These four samples are not included in the further discussions, however the interpretation of this study remains the same even if these anomalous samples are included.

**Table 3.5:  $^{87}Sr/^{86}Sr$  and  $\epsilon_{Nd}$  of various litho-units of the Ganga System**

| Lithology                     | $^{87}Sr/^{86}Sr$ |                   | $\epsilon_{Nd}$ |                 |
|-------------------------------|-------------------|-------------------|-----------------|-----------------|
|                               | Range             | Typical           | Range           | Typical         |
| <b><u>Higher Himalaya</u></b> |                   |                   |                 |                 |
| TSS                           | 0.71-0.73         | $0.727 \pm 0.012$ | -15 – -12       | -13             |
| HHC                           | 0.73-0.79         | $0.76 \pm 0.03$   | -16.4 – -13.6   | $-15 \pm 1.4$   |
| <b><u>Lesser Himalaya</u></b> |                   |                   |                 |                 |
| LH                            | 0.72-0.94         | $0.85 \pm 0.09$   | -25.3 – -23.5   | $-24.4 \pm 0.9$ |
| <b><u>Siwaliks</u></b>        | 0.72-0.76         | $0.738 \pm 0.018$ | -19 – -15       | $-17.2 \pm 1.2$ |

Singh et al., 2008 and references therein; TSS: Tethyan Sedimentary Sequence; HHC: Higher Himalaya Crystallines; LH: Lesser Himalaya

Variations in the concentrations of Sr and Nd in these sediments could be partly due to source variability and, in part, could arise due to size sorting/quartz dilution. Further, available results on Sr and Nd concentrations of rocks of HH and LH display similar range and therefore cannot be used for tracking their varying contributions.

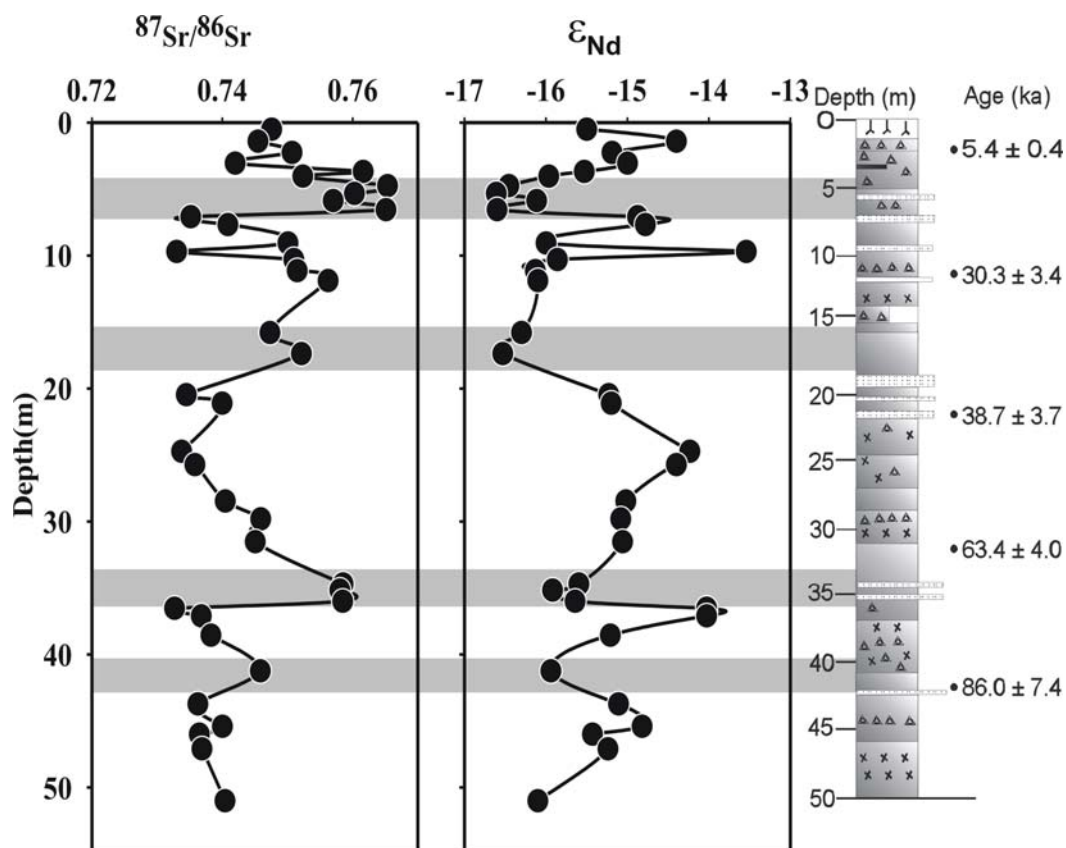


**Fig. 3.6** Variation in Sr and Nd isotope composition of the sediments with depth. Besides minor fluctuations, four larger excursions in the Sr and Nd isotope compositions are observed.  $^{87}\text{Sr}/^{86}\text{Sr}$  and  $\epsilon_{\text{Nd}}$  show opposite variations and could result due to variations in sediment proportions from the two major sources of sediments at this location, i.e., the Higher and Lesser Himalaya. Core litho-stratigraphy is also shown.

The variations in the  $^{87}\text{Sr}/^{86}\text{Sr}$  and  $\epsilon_{\text{Nd}}$  in the IITK core (Table 3.2, Fig. 3.6) can be interpreted in terms of variations in the mixing proportions of HH and LH as their

silicates have distinct Sr and Nd isotope compositions (Table 3.5; Singh et al., 2008) which are preserved in the sediments (Figs. 3.6 and 3.7). The Higher Himalayan rocks are characterized by radiogenic Nd and lower  $^{87}\text{Sr}/^{86}\text{Sr}$  whereas those of the Lesser Himalaya have more radiogenic Sr and less radiogenic Nd (Table 3.5; Singh et al., 2008). The core site of this study receives sediments brought by the Ganga or ancestor of the Ganga. These sediments are sourced from the Higher and Lesser Himalaya. Studies on the contemporary sediments indicate that ~70% of the sediments in the Ganga are derived from the Higher Himalaya (Singh et al., 2008; Campbell et al., 2005). The Higher Himalaya has remained the main source of sediment to the Bay of Bengal since the Miocene (France-Lanord et al., 1993). The magnitude of these variations (Table 3.2, Fig. 3.6) is much larger than the average uncertainty estimated based on replicate measurements and therefore has to be attributed to source variations. The Sr and Nd concentrations and their isotope composition in these sediments are within the range of source rocks in HH and LH (Table 3.5; Singh et al., 2008). The  $^{87}\text{Sr}/^{86}\text{Sr}$  of the sediments shows peaks at depths ~6.6, ~17.4, ~34 and ~41 m with concomitant decrease in  $\epsilon_{\text{Nd}}$  (Fig. 3.6). Three-point running average of  $^{87}\text{Sr}/^{86}\text{Sr}$  and  $\epsilon_{\text{Nd}}$  of the sediments shows four pronounced excursions at ~20, ~40, ~70 and ~90 ka with higher  $^{87}\text{Sr}/^{86}\text{Sr}$  and lower  $\epsilon_{\text{Nd}}$  (Fig. 3.7). This can be explained in terms of decrease in the relative proportion of sediments from HH which has lower  $^{87}\text{Sr}/^{86}\text{Sr}$  and enriched  $\epsilon_{\text{Nd}}$ . These excursions show increase in  $^{87}\text{Sr}/^{86}\text{Sr}$  coincides with decrease in  $\epsilon_{\text{Nd}}$ . Such an opposite trend is expected for a two end member mixing between HH and LH lithologies as HH is less radiogenic in Sr with higher  $\epsilon_{\text{Nd}}$ , whereas LH is more radiogenic in  $^{87}\text{Sr}/^{86}\text{Sr}$  and lower in  $\epsilon_{\text{Nd}}$ .

The excursions in Sr and Nd isotope composition of sediments in the Ganga plain correlate well with the climatic records of this region (Van Campo et al., 1982; Prell and Kutzbuch, 1987; Fleitmann et al., 2003; Goodbred., 2003). The timings of  $^{87}\text{Sr}/^{86}\text{Sr}$  peaks and  $\epsilon_{\text{Nd}}$  excursions in the core (Fig. 3.7) coincide with periods of lower precipitation and lower solar insolation at ~20, ~40, ~70 and ~90 ka

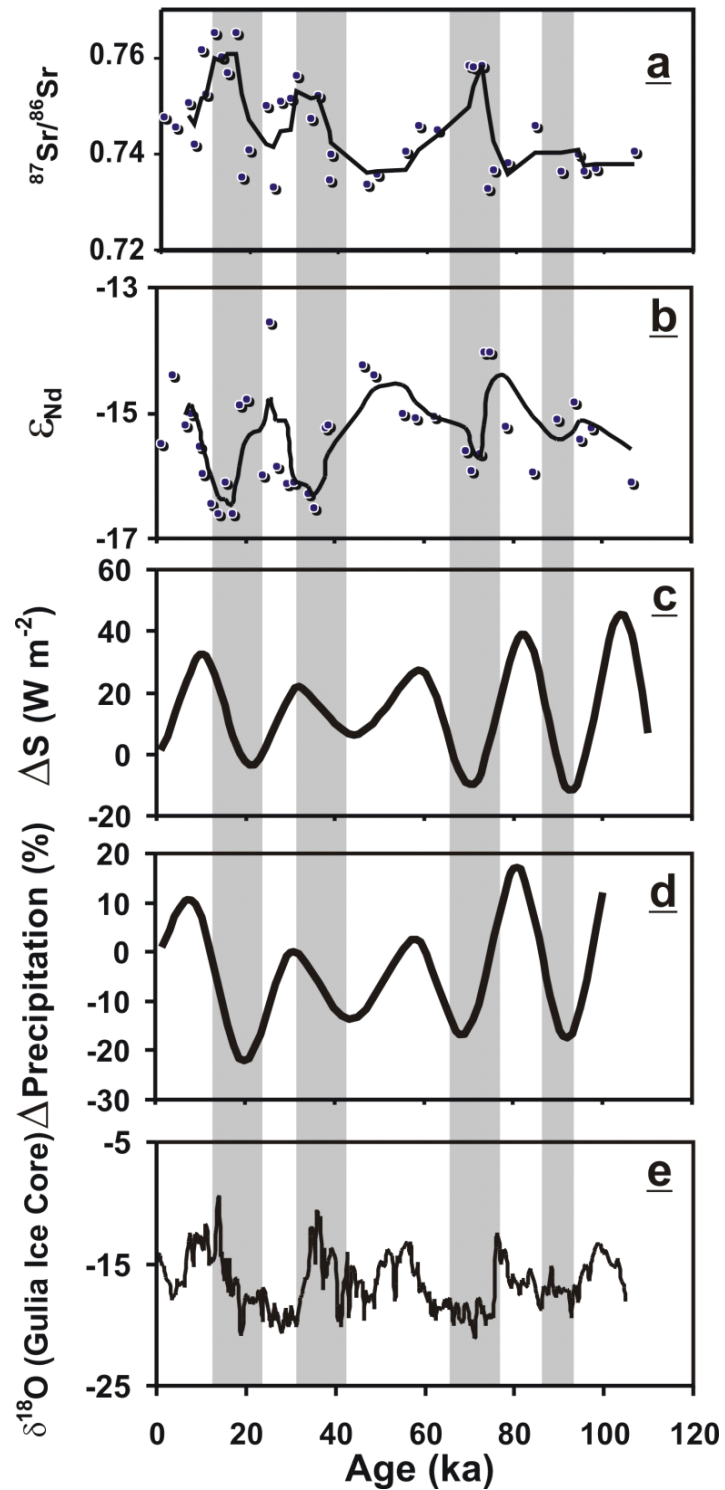


**Fig. 3.7** Three-point running average of  $^{87}\text{Sr}/^{86}\text{Sr}$  and  $\epsilon_{\text{Nd}}$  of the sediments (a and b). The four major excursions during ~90, ~70, ~40 and ~20 ka in  $^{87}\text{Sr}/^{86}\text{Sr}$  and  $\epsilon_{\text{Nd}}$  coincide with the available climatic records.

(Van Campo et al., 1982; Prell and Kutzbach., 1987; Clemens et al., 1996; Clemens and Prell, 2007) and also with lower  $\delta^{18}\text{O}$  values in Tibetan ice cores (Thompson et al., 1997). Small degree of mismatch between the timings of Sr, Nd isotope excursion and available climatic records could be due to uncertainty in the ages of the sediments resulting due to interpolation of ages between the control points. It has been shown that the glacial cover over the Higher Himalaya advanced at  $\sim 70$  and  $\sim 20$  ka (Owen et al., 2002) coinciding with the insolation minima. The  $^{87}\text{Sr}/^{86}\text{Sr}$  and  $\epsilon_{\text{Nd}}$  data of the IITK core suggest that relative proportion of sediments derived from HH was decreased during the precipitation minima and the glacial maxima. Such decrease in sediment delivery from HH can occur if its aerial coverage is diminished by snow/ice and/or if precipitation decreases. Recent studies of Singh et al. (2008) have shown that contemporary erosion rates over HH and LH have a strong dependence on the rainfall which has two spatial maxima, one at LH and another at the rising limb of HH causing intense erosion in HH (Bookhagen et al., 2006). It has already been demonstrated that intense monsoonal precipitation penetrates deeper in the valleys in HH causing higher erosion in the region (Bookhagen et al., 2005b). The interpretation of this study is similar to that of Bookhagen et al. (2005a) who reported higher erosion in the interior (HH) of the NW Himalaya caused by intense monsoon phases during late Pleistocene and Holocene. The report of Clift et al. (2008) based on the sediments of the Indus delta that erosion of LH has increased during Holocene due to increase in monsoon precipitation differs from that of this study probably due to the fact that the sediments from the Indus delta are complex mixture of sediments derived from multiple sources, such as Trans-Himalaya, Karakoram, Nanga-Parbat, HH and LH whereas sediments of this core are derived only from two sources, HH and LH and their isotope composition can directly be used to track the variation in sediment supply from HH and LH. Further, during lower insolation period, HH had larger ice-cover (Owen et al., 2002) which reduces the available area in HH for erosion thereby decreasing the sediment yield contrary to the report of Pelletier (2008 and references therein) indicating higher erosion during glacial expansion. Thus, lower precipitation coupled with a greater aerial extent of glaciations in HH appears to be responsible for

decreasing erosion rates in HH and enhancing the relative contribution of sediments from LH substantially during ~20, ~40, ~70 ka and ~90 ka. All these independent records show in-phase variation suggesting a common causative factor - variation in solar insolation. This study indicates that the variation in solar insolation indirectly controls the erosion rate in the Himalaya by varying precipitation and glacial cover. Besides variation in the erosion rates of HH and LH, the enhanced dust deposition during LGM (Harrison et al., 2001) can also change the  $^{87}\text{Sr}/^{86}\text{Sr}$  and  $\epsilon_{\text{Nd}}$  of sediments at the core site, however available data on mineral aerosols over the Ganga plain and their potential sources, the Thar Desert and the Tethyan Sedimentary Series (Tripathi et al., 2004; Yadav and Rajamani, 2004), indicate that they would tend to decrease  $^{87}\text{Sr}/^{86}\text{Sr}$  and increase  $\epsilon_{\text{Nd}}$ , contrary to the results of the IITK core during ~20, ~40, ~70 and ~90 ka and can be ruled out as a major factor contributing to sedimentary deposits in the Ganga plain. The observed variation in the Sr and Nd isotope composition and hence that in sediment sources can also result from tectonic processes which has significant control on erosion rates and patterns over the Himalaya (Burbank, 2003). The Himalayan Frontal Fault (HFF) has been active in recent times and is reported to be producing significant amount of sediment from the Siwalik (Lave and Avouac, 2001). However, the Siwalik contribution to the contemporary sediment budget of the Ganga has been reported to be insignificant (Campbell, 2005; Singh et al., 2008). The Siwalik sediments, exposed in the Ganga drainage are derived from HH and LH. Their  $^{87}\text{Sr}/^{86}\text{Sr}$  and  $\epsilon_{\text{Nd}}$  (Table 3.6; Najman et al., 2000) are similar to those of the contemporary sediments of the Ganga (Tripathy et al., 2004; Singh et al., 2008). Therefore, any variation in the sediment supply from the Siwalik would not change Sr and Nd isotope composition of the foreland sediments. Thus, variation in tectonic activity along the HFF is unlikely to produce the observed isotope signatures in the IITK core. Beside HFF, the Main Central Thrust and/or Main Boundary Thrust also get activated often (Wobus et al., 2005) and can change the erosion pattern but they are controlled by climate change (Wobus et al., 2005). Further, as the temporal variations in Sr and Nd isotope composition of the IITK core coincides with the reported climatic variations; it seems unlikely that

tectonic activity would have played a significant role in contributing to the observed variations in isotopic composition, unless tectonics and climate are coupled.

### 3.4 Conclusions

Major elements analysed from a 50-m long sediment core samples in the Ganga plain show significant temporal variations. Major element compositions show depletion/enrichment of various elements in sediments with respect to their source rock compositions indicating variation in intensity of chemical weathering. Four major excursions in the indices of intensity of chemical weathering are observed at ~20, ~40, ~70 and ~90 ka showing lower chemical weathering intensity during these time periods. The timing of the lower intensity in the chemical weathering coincides with that of the lower precipitation and lower temperature. This suggests that the lesser extent of chemical weathering was resulted from lower temperature coupled with low precipitation during those periods.

There is no correlation exist between the chemical parameters such as CIA\* and Sr, Nd isotope compositions which clearly indicate that Sr and Nd isotope have potential to use them as a proxy for provenance studies. Sr and Nd isotope compositions of sediments core exhibit significant temporal variation which correlate significantly with available paleo-climatic records of precipitation and glaciations. Reduced monsoon intensity during ~20, ~40, ~70 and ~90 ka and higher glacial cover during ~ 20, and ~70 ka over HH reduced erosion over HH which in turn enhanced the relative proportion of LH sediments to the Ganga plain causing higher  $^{87}\text{Sr}/^{86}\text{Sr}$  and depleted  $\epsilon_{\text{Nd}}$  in the Ganga plain sediments. This study underscores the significant influence of climate, particularly precipitation, on the Himalayan erosion over millennium time scale as suggested earlier (Goodbred, 2003; Clift et al., 2008) and thereby highlights the climatic control on the regional tectonics by isostatic rebound. However, it is at variance with the report (Burbank et al., 2003) that erosion is decoupled with precipitation in the Himalaya. This study also illustrates that there is almost no time lag between the transfer of signal from source to sink (Clift et al., 2008) unlike the report by Granet et al. (2007) that it is of the order of about 100 ka.

## **CHAPTER-4**

**Sr, C and O isotopes in carbonate nodules from the  
Ganga Plain: Variations in dissolved  $^{87}\text{Sr}/^{86}\text{Sr}$  of the  
Ganga water during the past ~100 ka**

#### 4.1 Introduction

The Himalaya is undergoing rapid erosion under the influence of active tectonics and monsoonal climate; therefore, the interplay among tectonics-erosion-climate continues to be a topic of debate among geochemists (Molnar and England, 1992; Raymo and Ruddiman, 1992; Edmond, 1992; Burbank, et al., 2003; Wobus et al., 2005). Long term erosional pattern on million year time scales are controlled by tectonics (Burbank et al., 2003), whereas, climate modifies some of these processes on a shorter (kilo year) time scale (Goodbred et al., 2003; Bookhagen et al., 2005b; Clift et al., 2008, Rahaman et al. 2009). Recent studies of the Ganga-Brahmaputra drainages suggest that the contemporary chemical and physical erosion of their catchments in the Himalaya are quite high; they together supply one to two billion tons of particulate matter and ~100 million tons of dissolved material to the Bay of Bengal annually (Sarin et al., 1989; Hay, 1998; Galy and France-Lanord., 2001; Singh et al., 2005). In addition, there are indications of supply of dissolved material including Sr to the Bay of Bengal by submarine ground water discharge in magnitude comparable to the riverine flux carried by the G-B rivers (Basu et al., 2001).

The role of these rivers and groundwaters in contributing to the isotopic and geochemical budgets of the global ocean, since the Himalayan orogeny, has been assessed mainly via studies of their contemporary isotopic and chemical compositions. For example, the present day Ganga-Brahmaputra waters are characterized by high  $^{87}\text{Sr}/^{86}\text{Sr}$  and moderately high Sr concentration which has led to the suggestion that the G-B rivers play a key role in the Sr isotope evolution of seawater during the Cenozoic (Veizer, 1989; Krishnaswami et al., 1992; Edmond, 1992; Richter et al., 1992; Raymo and Ruddiman, 1992). The steady increase in marine  $^{87}\text{Sr}/^{86}\text{Sr}$  since the Cenozoic led to the further hypothesis that seawater Sr evolution during this period was a result of enhanced silicate weathering resulting from rapid uplift of the Himalaya (Raymo and Ruddiman, 1992; Richter et al. 1992). This hypothesis relies on the assumption that the Sr isotope composition of the Himalayan rivers and hence the silicates undergoing erosion has remained invariant since the Cenozoic, an assumption that remains to be validated. Studies on clays of the Bay of Bengal (Derry

and France-Lanord, 1996) and paleosols from the Siwaliks (Quade et al., 1997), however seem to indicate that the Sr isotope composition of the G-B rivers may have varied over million year time scale, challenging the validity of the above assumption.

In this study an effort has been made to retrieve  $^{87}\text{Sr}/^{86}\text{Sr}$  of the Ganga by analyzing secondary carbonates, locally known as “kankar” contained in the alluvial sediments of the Ganga plain (Quade et al., 1997). These carbonates are precipitated from both river and groundwater/soil moisture and formed along with sediments in the plain. They contain several tens to hundreds of ppm Sr in them and therefore serve as a repository of Sr isotope composition of river/ground water from which they are formed. Prior to this work, a few studies have been there on  $^{87}\text{Sr}/^{86}\text{Sr}$  in carbonates. Quade et al. (1997) tracked the Sr isotope composition of the Ganga over million year time scale using paleosol carbonates in the Siwaliks. Yang et al. (2000) brought out coupling between the chemical weathering and East Asian monsoon based from calcretes of Chinese loess. Hart et al. (2004) investigated the lake-level history of the Bonneville paleo lake system based on  $^{87}\text{Sr}/^{86}\text{Sr}$  of lacustrine carbonates.

The oxygen and carbon isotope composition of these secondary carbonates also hold clues to the paleoenvironmental conditions, temperature, rainfall and type of vegetation prevailing at the time of their formation (Sinha et al., 2006). Fresh water carbonates including the “kankars” from the Ganga plain have been studied to infer the paleo-environmental conditions during their formation (Srivastava, 2001; Sharma et al., 2004; Sinha et al., 2006). In one such study, the  $\delta^{13}\text{C}$  and  $\delta^{18}\text{O}$  of the mollusk shells from the Ganga system were analysed to evaluate their potential as paleo-climatic indicators (Gajurel et al., 2006).

The aim of this work is to track the temporal evolution of  $^{87}\text{Sr}/^{86}\text{Sr}$  of Ganga water by analyzing carbonate nodules in sediment cores raised from the Ganga plain. In addition to  $^{87}\text{Sr}/^{86}\text{Sr}$ , their  $\delta^{13}\text{C}$  and  $\delta^{18}\text{O}$  were also measured to assess their application as paleo-environmental and paleo-vegetation proxies in the Ganga basin.

## 4.2 Results

In this work, a total of twenty six carbonate samples from the IITK core and eight samples from the JP core have been analysed for their Sr isotope composition. In addition, the IITK carbonates were also analysed for their major element composition, inorganic carbon,  $\delta^{13}\text{C}$  and  $\delta^{18}\text{O}$ . The carbonate content of the IITK samples based on their inorganic carbon abundance, ranges from 28 to 72 wt%; with two samples having very low abundance,  $\sim 1\%$  of  $\text{CaCO}_3$ . The Ca, Mg, Sr and Mn abundances given in Table 4.1 are based on the analysis of the acetic acid leaches and reported with respect to total sediment weight. Sr concentrations in these samples vary from 94 to 551  $\mu\text{g/g}$  (Table 4.1) and seem to depend on their carbonate content. These carbonates have minor amounts of Mg, 0.1 to 0.8% (Table 4.1). The Mg may be associated with magnesium carbonates reported to be precipitated with calcium carbonate in the Gangetic Plain (Agarwal, 1992). The  $^{87}\text{Sr}/^{86}\text{Sr}$  of the IITK carbonate nodules ranges from 0.7142 to 0.7189, with the lowest value at a depth of 10.3 m (Table 4.1). In the JP core,  $^{87}\text{Sr}/^{86}\text{Sr}$  is more radiogenic and ranges from 0.7142 to 0.7367 (Table 4.2). The most radiogenic Sr in the JP core is near its surface, at 2.25 m depth. The  $^{87}\text{Sr}/^{86}\text{Sr}$  of this sample is close to that of present day Ganga river water at Kanpur (Table 4.3a). Carbonate nodules from three depths of the JP core were analysed for their  $^{87}\text{Sr}/^{86}\text{Sr}$  in duplicate using separate nodules from each depth to assess heterogeneity in their  $^{87}\text{Sr}/^{86}\text{Sr}$  composition. It is observed from this exercise that the variation in Sr isotope composition from the same depth horizon due to sample heterogeneity is within the range of 40 to 1180 ppm (Table 4.2). Based on this exercise, a maximum uncertainty of 1000 ppm on  $^{87}\text{Sr}/^{86}\text{Sr}$  of the carbonates is assigned. The  $\delta^{13}\text{C}$  and  $\delta^{18}\text{O}$ , analyzed only in the IITK carbonate samples, vary from -6.8 to 1.6 ‰ and -8.3 to -5.4 ‰ respectively. The variability of  $\delta^{13}\text{C}$  in the carbonate nodules is higher than that of  $\delta^{18}\text{O}$  (Table 4.1).

**Table 4.1: Elemental composition,  $^{87}\text{Sr}/^{86}\text{Sr}$ ,  $\delta^{13}\text{C}$  and  $\delta^{18}\text{O}$  of carbonate nodules from IITK core**

| Depth (m) | $\text{C}_{\text{inorg}}$ | Ca   | Mg  | Mn                   | Sr  | $^{87}\text{Sr}/^{86}\text{Sr}$ | $\delta^{13}\text{C}$ | $\delta^{18}\text{O}$ |
|-----------|---------------------------|------|-----|----------------------|-----|---------------------------------|-----------------------|-----------------------|
|           | wt %                      |      |     | $\mu\text{g g}^{-1}$ |     |                                 | (‰)                   |                       |
| 1.25      | 0.04                      | -    | -   | -                    | -   | 0.71888                         | -                     | -                     |
| 1.85      | 6.6                       | 10.8 | 0.3 | 238                  | 215 | 0.71559                         | -3.1                  | -7.7                  |
| 2.50      | 6.7                       | 10.3 | 0.3 | 207                  | 222 | 0.71606                         | -0.2                  | -6.3                  |
| 2.85      | -                         | -    | -   | -                    | -   | 0.71666                         | -                     | -                     |
| 2.85-R    | -                         | -    | -   | -                    | -   | 0.71676                         | -                     | -                     |
| 3.15      | 6.4                       | 9.8  | 0.3 | 292                  | 232 | 0.71666                         | -3.6                  | -7.1                  |
| 4.03      | 6.6                       | 10.3 | 0.3 | 184                  | 156 | 0.71683                         | -3.1                  | -6.8                  |
| 4.03-R    | -                         | -    | -   | -                    | -   | 0.71687                         | -                     | -                     |
| 6.80      | -                         | 9.7  | 0.3 | 157                  | 173 | 0.71700                         | -6.8                  | -8.3                  |
| 6.80R     | -                         | -    | -   | -                    | -   | -                               | -6.8                  | -8.1                  |
| 10.30     | 6.6                       | 10.9 | 0.4 | 541                  | 245 | 0.71418                         | 0.9                   | -5.4                  |
| 11.70     | 7.3                       | 12.1 | 0.3 | 261                  | 187 | 0.71714                         | -3.0                  | -6.7                  |
| 11.70-R   | -                         | -    | -   | -                    | -   | 0.71717                         | -                     | -                     |
| 13.12     | 6.0                       | 8.8  | 0.4 | 734                  | 551 | 0.71590                         | -2.4                  | -5.9                  |
| 13.12-R   | -                         | -    | -   | -                    | -   | 0.71590                         | -                     | -                     |
| 13.54     | 6.1                       | 9.9  | 0.3 | 764                  | 172 | 0.71534                         | 1.1                   | -5.8                  |
| 14.16     | 6.5                       | 24.7 | 0.6 | 1426                 | 488 | 0.71530                         | 1.6                   | -5.8                  |
| 14.46     | 8.1                       | 11.5 | 0.8 | 1003                 | 479 | 0.71588                         | 1.5                   | -5.5                  |
| 16.23     | 6.9                       | 12.0 | 0.3 | 257                  | 217 | 0.71721                         | -3.4                  | -6.8                  |
| 16.23-R   | -                         | -    | -   | -                    | -   | 0.71721                         | -                     | -                     |
| 23.85     | 6.6                       | 11.2 | 0.3 | 314                  | 218 | 0.71722                         | -5.5                  | -7.7                  |
| 23.85-R   | -                         | -    | -   | -                    | -   | 0.71726                         | -                     | -                     |
| 28.40     | 0.1                       | -    | -   | -                    | -   | 0.71751                         | -                     | -                     |
| 39.02     | 7.6                       | 10.5 | 0.2 | 135                  | 189 | 0.71745                         | -0.4                  | -6.8                  |
| 39.02-R   | -                         | -    | -   | -                    | -   | 0.71748                         | -                     | -                     |
| 39.60     | 8.0                       | 11.9 | 0.2 | 82                   | 250 | -                               | -                     | -                     |
| 40.00     | 6.2                       | 8.7  | 0.2 | 106                  | 265 | 0.71715                         | -0.2                  | -6.7                  |
| 40.00-R   | -                         | -    | -   | -                    | -   | 0.71718                         | -                     | -                     |
| 40.40     | 7.4                       | 8.6  | 0.2 | 106                  | 201 | 0.71674                         | -0.8                  | -6.8                  |
| 43.18     | 6.0                       | 10.9 | 0.3 | 250                  | 233 | 0.71725                         | -                     | -                     |
| 43.72     | 4.9                       | 7.5  | 0.2 | 61                   | 168 | 0.71690                         | -1.5                  | -7.2                  |
| 44.42     | 3.4                       | 6.3  | 0.2 | 58                   | 167 | 0.71744                         | -2.9                  | -7.0                  |
| 44.82     | 4.5                       | 6.6  | 0.1 | 247                  | 94  | 0.71761                         | -3.8                  | -7.5                  |
| 44.82-R   | -                         | -    | -   | -                    | -   | 0.71758                         | -                     | -                     |
| 48.31     | 8.6                       | 12.3 | 0.3 | 120                  | 269 | 0.71835                         | -0.8                  | -7.6                  |
| 48.31-R   | -                         | -    | -   | -                    | -   | -                               | -0.8                  | -7.7                  |
| 48.40     | 8.1                       | 10.9 | 0.3 | 120                  | 240 | 0.71833                         | -0.8                  | -7.8                  |
| 48.40-R   | -                         | -    | -   | -                    | -   | 0.71831                         | -                     | -                     |

**R: replicate analysis of the same aliquot.**

**Table 4.2: Sr isotope composition of carbonate nodules from Jagdishpur**

| <b>Sample ID</b>   | <b>Depth(m)</b> | <b><math>^{87}\text{Sr}/^{86}\text{Sr}</math></b> | <b><math>\Delta</math>(ppm)</b> |
|--------------------|-----------------|---|---------------------------------|
| <b>JP-2.25(A)</b>  | 2.25            | 0.73651   | 190                             |
| <b>JP-2.25(B)</b>  | 2.25            | 0.73665   |                                 |
| <b>JP-2.80</b>     | 2.8             | 0.73514   |                                 |
| <b>JP-9.4</b>      | 9.4             | 0.71416   |                                 |
| <b>JP-13.0</b>     | 13.0            | 0.71961   |                                 |
| <b>JP-21.20(A)</b> | 21.2            | 0.72064   | 1180                            |
| <b>JP-21.20(B)</b> | 21.2            | 0.72149   |                                 |
| <b>JP-23.75</b>    | 23.75           | 0.71521   |                                 |
| <b>JP-24.45</b>    | 24.45           | 0.71858   |                                 |
| <b>JP-24.65(A)</b> | 24.65           | 0.71685   | 40                              |
| <b>JP-24.65(B)</b> | 24.65           | 0.71688   |                                 |

**(A) and (B) of the same samples represent replicate analysis on separately hand picked nodules of carbonates.  $\Delta$  is the difference in the  $^{87}\text{Sr}/^{86}\text{Sr}$  of the replicates.**

**Table 4.3a: Sr isotope composition of miscellaneous samples from Kanpur**

| Sample ID   | Date      | Type        | Latitude   | Longitude  | Location             | $^{87}\text{Sr}/^{86}\text{Sr}$ | Uncertainty | Ref.       |
|-------------|-----------|-------------|------------|------------|----------------------|---------------------------------|-------------|------------|
| GP-134      | 3.03.2009 | Groundwater | 26°37.055' | 80°16.766' | Ganga valley, Kanpur | 0.72934                         | 0.00001     | This study |
| GP-134R     | 3.03.2009 | Groundwater | 26°37.055' | 80°16.766' | Ganga valley, Kanpur | 0.72930                         | 0.00001     | This study |
| GP-137      | 3.03.2009 | Shells      | 26°36.648' | 80°16.615' | River bank, Kanpur   | 0.72936                         | 0.00001     | This study |
| GP-135      | 3.03.2009 | River water | 26°36.716' | 80°16.598' | River bank, Kanpur   | 0.73240                         | 0.00001     | This study |
| RW7 (3/82)  | 03.1982   | River water |            |            | Kanpur               | 0.7312                          |             | 1          |
| RW7 (11/83) | 11.1983   | River water |            |            | Kanpur               | 0.7373                          |             | 1          |

1-Palmer and Edmond, 1992

**Table 4.3b: Sr isotope composition of miscellaneous samples from Allahabad after the confluence of Yamuna**

| Sample ID | Date     | Location  | Type         | $^{87}\text{Sr}/^{86}\text{Sr}$ | Reference            |
|-----------|----------|-----------|--------------|---------------------------------|----------------------|
| RW        | 07.02.06 | Allahabad | River water  | 0.71699                         | Rai et al., in prep. |
| GW-1      | 07.02.06 | Allahabad | Ground Water | 0.71761                         | Rai et al., in prep. |
| GW-2      | 07.02.06 | Allahabad | Ground Water | 0.71760                         | Rai et al., in prep. |
| KANKAR-1  | 07.02.06 | Allahabad | Kankar       | 0.71761                         | Rai et al., in prep. |
| KANKAR-2  | 07.02.06 | Allahabad | Kankar       | 0.71536                         | Rai et al., in prep. |

### 4.3 Discussion

Carbonate nodules analyzed in this study to infer about the paleoenvironment and to reconstruct the  $^{87}\text{Sr}/^{86}\text{Sr}$  of the paleo water of the Ganga are sensitive to later diagenesis processes. Their pristine signature can be altered by the later processes acting on them. To ensure what is being measured is the pristine signature, it is required to make sure that these carbonates are not affected by later diagenesis. Therefore, we have attempted petrographic and geochemical approach to test whether they are pristine or not.

#### 4.3.1 Petrography and major element composition

Thin sections of carbonate nodules indicate the dominance of micrites with microspar. The matrix is commonly characterized by a gremulose (mottled) texture, created by complex and highly irregular variability in crystal sizes. Fine grained, dark micrites are abundant and compacted (Fig. 4.1). All the nodules in the SEM study exhibit  $\alpha$ -type fabric (Wright and Tucker., 1991). SEM photomicrographs of these carbonate nodules (Fig. 4.1) do not indicate any significant effect of later diagenesis, however, petrographic and textural studies of the carbonate nodules are not always of help to identify the diagenesis and alteration effects (Leier et al., 2009). It has also been shown that isotope redistribution in carbonates may not always be associated with change in their petrographic characteristics (Denison et al., 1994). Therefore, a combined photographic, trace element and stable isotope study was carried out to identify possible diagenesis and alteration effects in the carbonates.

The use of  $\delta^{13}\text{C}$  and  $\delta^{18}\text{O}$  to infer about the paleoenvironment, paleovegetation and  $^{87}\text{Sr}/^{86}\text{Sr}$  to reconstruct the Sr isotope evolution of the paleo Ganga waters require that these carbonates have not been affected by later diagenesis. The relative abundances of Ca, Sr, Fe and Mn of the marine carbonates have been used to study their later diagenesis. Repetitive dissolution and precipitation decreases Sr/Ca of the carbonates due to low partition coefficient of Sr in carbonates (Banner and Hanson, 1990). The decrease in Sr/Ca is associated with increase in Mn concentration (Veizer, 1983). Fig. 4.2a shows the variations in Sr/Ca versus Mn, the

scatter in data suggest that Sr/Ca of these carbonates is independent of Mn, indicating very little alteration, if any, by later diagenesis. Similarly,  $^{87}\text{Sr}/^{86}\text{Sr}$  of these carbonates are in general independent of their Mn/Sr (Fig. 4.2b) indicating preservation of original isotope signatures in them. All these lines of evidences suggest very little alteration, if any, of these carbonates. The extent of such alteration is inadequate to modify their  $^{87}\text{Sr}/^{86}\text{Sr}$  significantly, and therefore the  $^{87}\text{Sr}/^{86}\text{Sr}$  measured in them is taken to represent that of the water from which they precipitated.

#### 4.3.2 How faithfully do these carbonates record riverine Sr isotope signature?

The use of calcretes (kankars) to retrieve  $^{87}\text{Sr}/^{86}\text{Sr}$  of river water requires that they (i) faithfully record  $^{87}\text{Sr}/^{86}\text{Sr}$  signatures of rivers and (ii) retain these signatures through time. To confirm that these carbonates indeed record the  $^{87}\text{Sr}/^{86}\text{Sr}$  of the paleowater, samples of contemporary river water, groundwater, shells from surface sediments collected around Kanpur were analysed for their Sr isotope composition. The results are listed in Table 3a.  $^{87}\text{Sr}/^{86}\text{Sr}$  of river water, 0.73240 is slightly more radiogenic compared to the ground water, 0.72934 and adjacent shells, 0.72936. Both groundwater and shells average the  $^{87}\text{Sr}/^{86}\text{Sr}$  of several years whereas the river water data is a snapshot sample. Thus, difference between these two sets is most likely a result of averaging effects. Further, available data on  $^{87}\text{Sr}/^{86}\text{Sr}$  of river water from the Himalaya show seasonal variations (Bickle et al., 2003; Rai and Singh 2007); which constrains the use of a single season measurement as the average value for the year. In addition,  $^{87}\text{Sr}/^{86}\text{Sr}$  of river water and kankar of the Ganga at Allahabad (after its confluence with Yamuna) and adjacent groundwaters overlap with values of  $\sim 0.715$  (Table 4.3b, Rai, 2008). The data of this study and those from Allahabad thus indicate that the shells and carbonates of the Ganga plain incorporate Sr with isotope composition within the range of river and ground waters (Table 4.3a, b), satisfying the first requirement. The second requirement pertains to that preservation of Sr ratio with time. In this study, attempts were made to evaluate by measuring Sr isotope composition in separate aliquots of carbonate nodules taken from the same depth with the premise that the extent of alterations of different nodules may be different,

thereby impacting their Sr isotope ratios differently. The result of this exercise shows that  $^{87}\text{Sr}/^{86}\text{Sr}$  of separate nodules from same depth is less than 1180 ppm (Table 4.2), providing an upper limit on the extent of variability.

In addition to diagenesis, contamination of calcretes/kankars with clays and detrital carbonate derived from the Himalaya can also lead to difference in  $^{87}\text{Sr}/^{86}\text{Sr}$  compared to that of the river/ground water from which they form. Efforts were made to minimize the impact of such contamination by selecting larger carbonates/nodules for analysis. Most of the calcretes used in this study are of a few cm in size. Further, the presence of ~5% detrital carbonates with  $^{87}\text{Sr}/^{86}\text{Sr} \sim 0.72$  (typical Himalayan carbonates, Singh et al., 1998) in these calcretes, can alter their  $^{87}\text{Sr}/^{86}\text{Sr}$  only at 1-10 ppm level, much lower than the variability observed in  $^{87}\text{Sr}/^{86}\text{Sr}$  of the calcretes of various depths in this study. Hence it can be concluded that the detrital carbonates from the Himalaya have very little effect on the Sr isotope composition of the calcretes used in this study. In addition, significant co-variation of  $\delta^{13}\text{C}$  and  $\delta^{18}\text{O}$  of these carbonates which are not evident in detrital carbonates (Singh et al., 1998) rules out any significant contamination by them.

Another potential source of alteration of these calcretes is rain water interaction. However, it can be shown that with an average ~16 nM of Sr with  $^{87}\text{Sr}/^{86}\text{Sr} \sim 0.714$  (Galy et al., 1999) in rains, the exchange of Sr in the secondary carbonates to alter  $^{87}\text{Sr}/^{86}\text{Sr}$  to any significant extent is very unlikely. The various evidences discussed above indicate that the Sr in the carbonate nodules are of authigenic origin that they retain isotopic and chemical signatures of the waters from which they were precipitated.

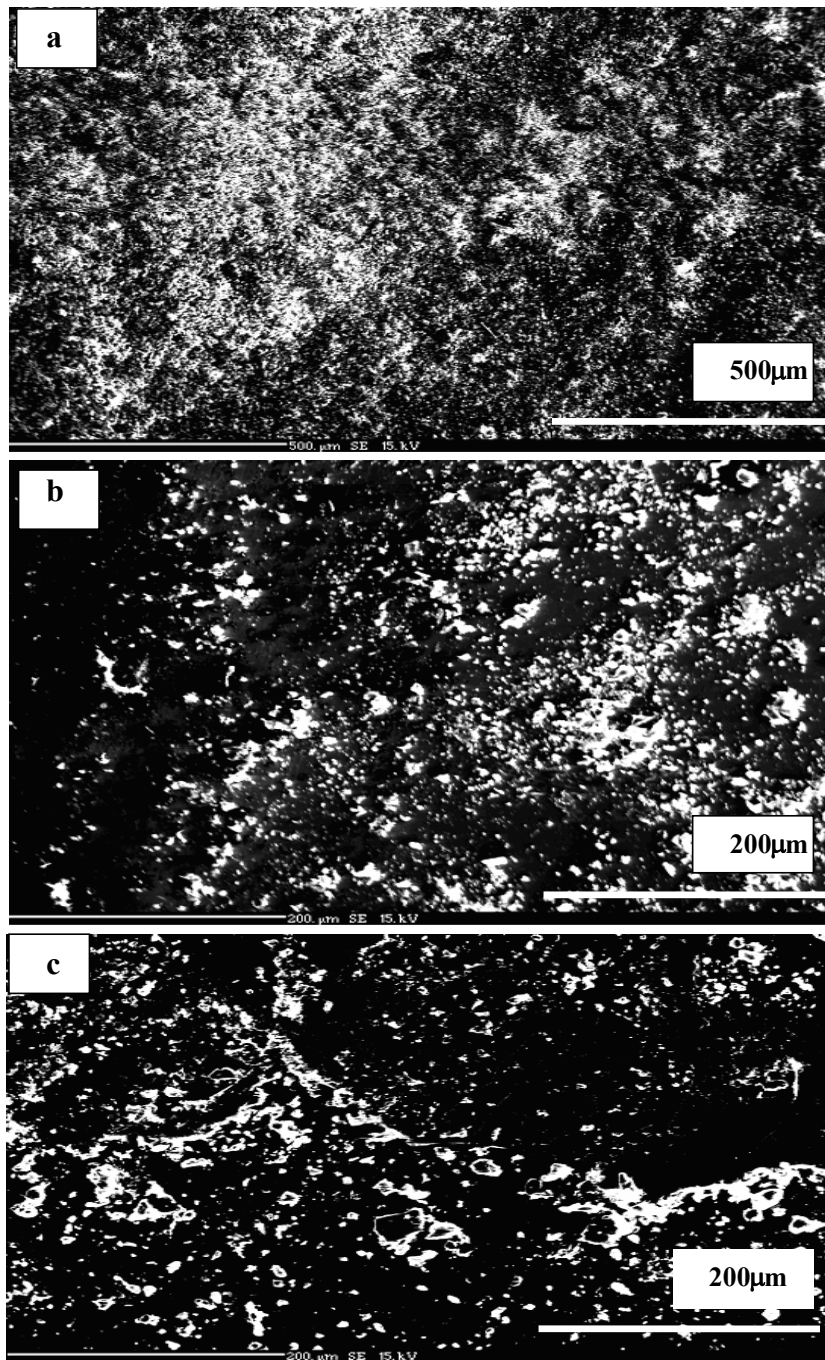


**Fig. 4.1** Petrography of some of the carbonate nodules based on Scanning Electron Microscope. a) Dense occurrence of micrite crystal with matrix of quartz. b, c) Abundance of anhedral to subhedral calcite crystals of micrite and microspar with the ground mass of quartz.

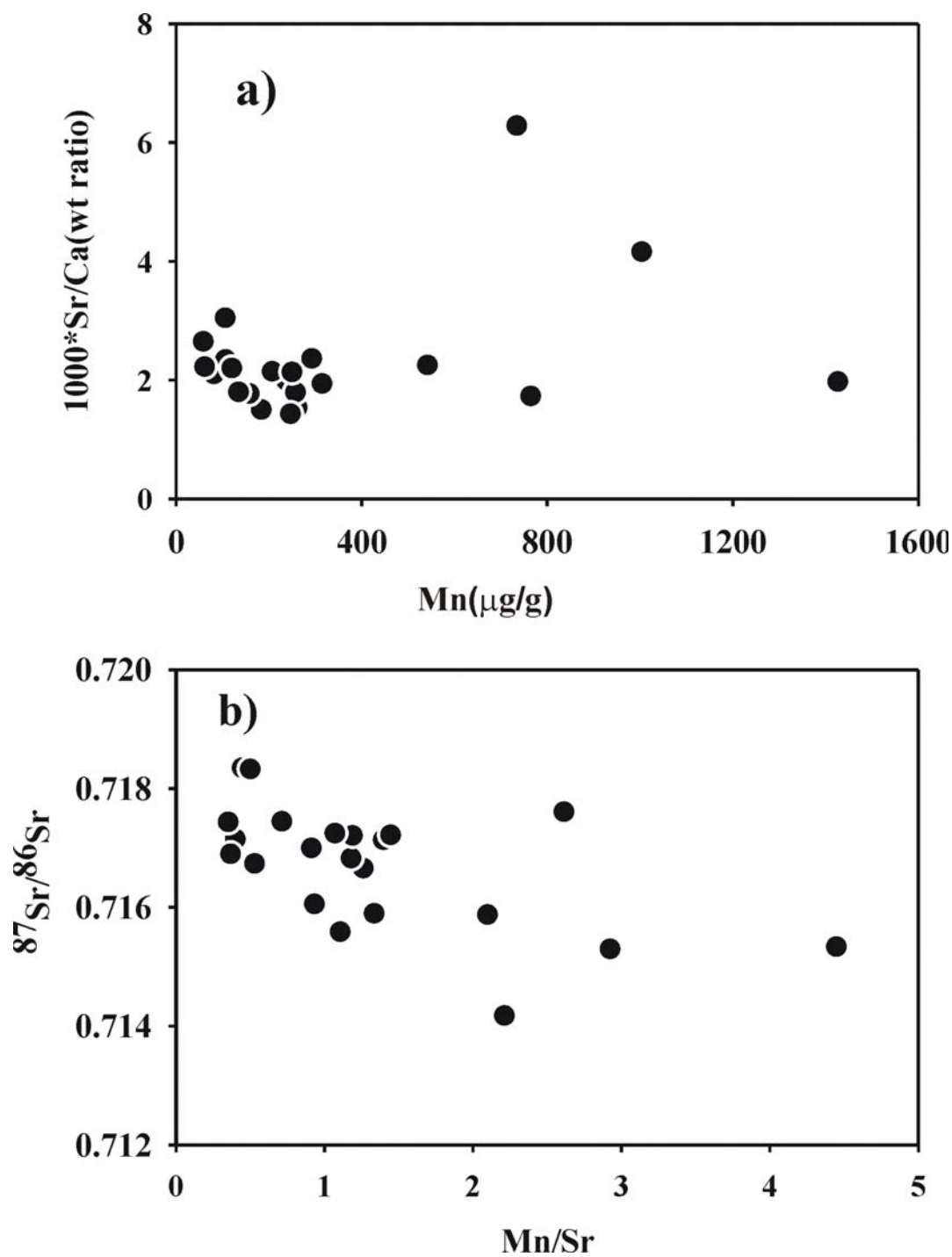
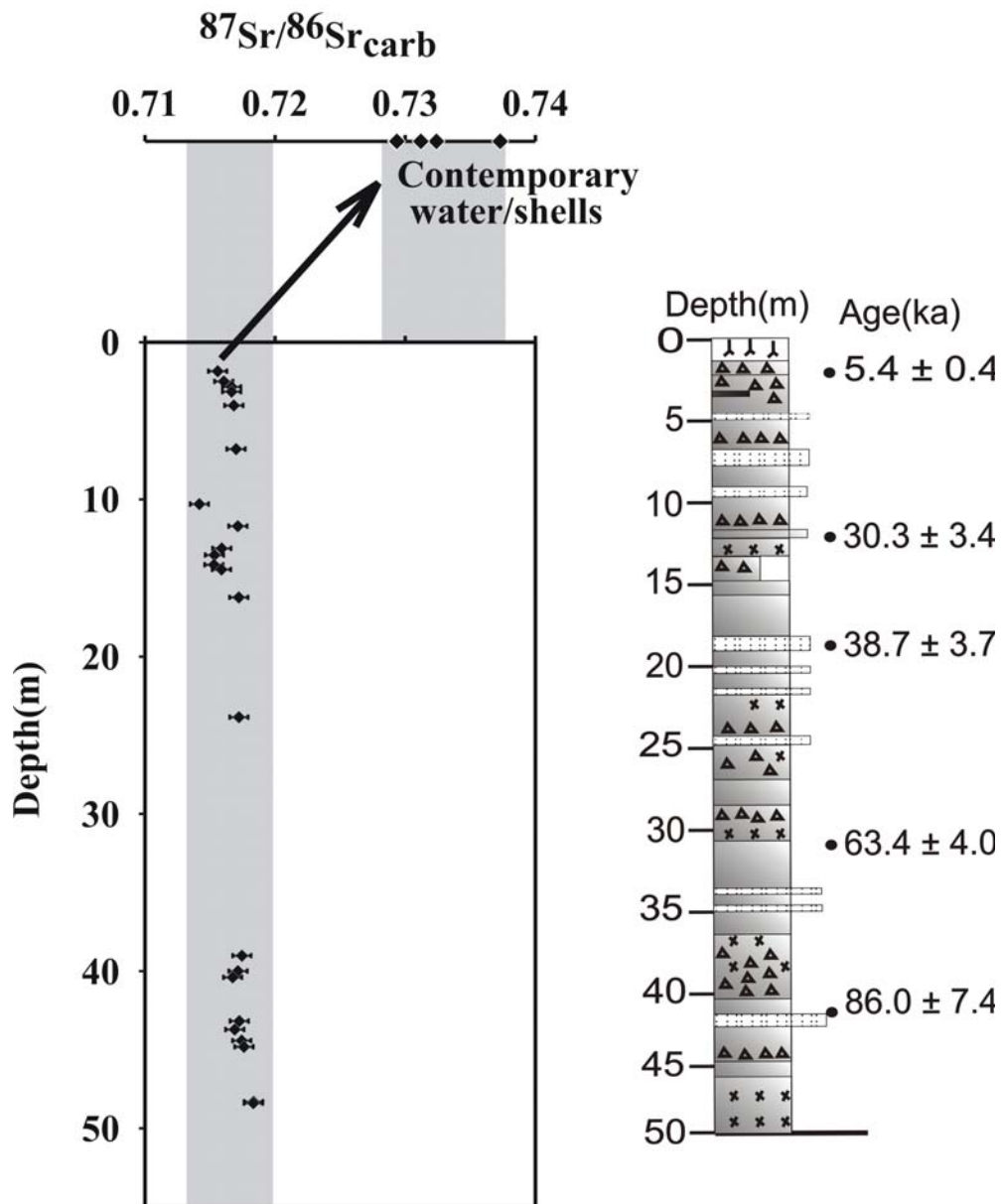


Fig. 4.2 a, b Scatter plot of Sr/Ca vs Mn and  $^{87}\text{Sr}/^{86}\text{Sr}$  vs Mn/Sr of the carbonate nodules. Sr/Ca of these nodules is independent of their Mn content indicating their pristine signature.  $^{87}\text{Sr}/^{86}\text{Sr}$  vs. Mn/Sr plot does not show any significant correlation.

### 4.3.3 Sr isotopic composition in carbonate

The Sr isotope data of pedogenic calcretes in the IITK and the JP cores are presented in Figs. 4.3 and 4.4.



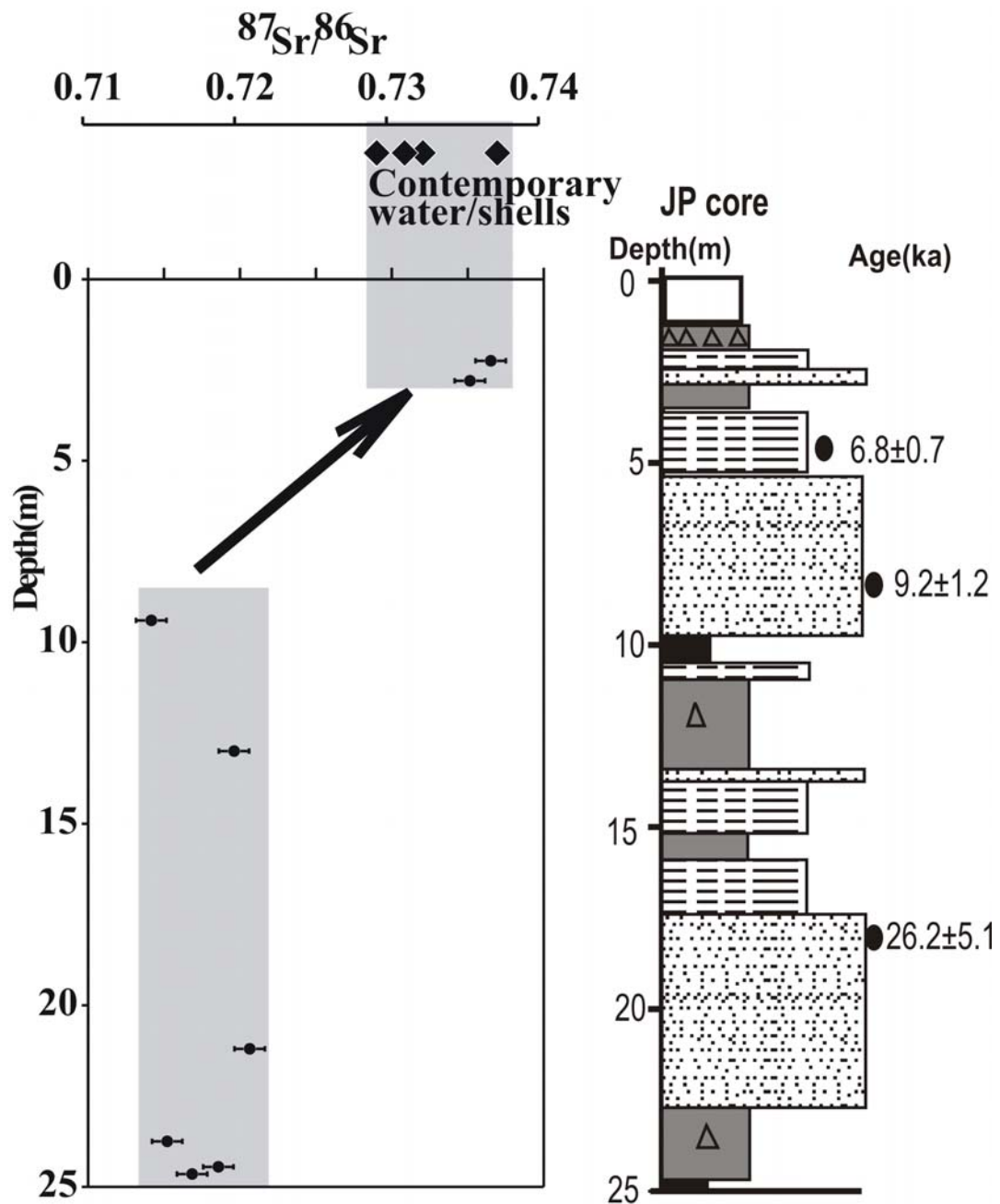


Fig. 4.4: Variations in  $^{87}\text{Sr}/^{86}\text{Sr}$  of carbonate nodules with depth in JP profile. Lithostratigraphy and chronology (Sinha et al., 2007) of the core is also presented. The  $^{87}\text{Sr}/^{86}\text{Sr}$  carbonates shows sudden rise near the surface at ~2.5 m depth in JP.

The data from the carbonates show that except for two points at the top of the JP core which have highly radiogenic  $^{87}\text{Sr}/^{86}\text{Sr} \sim 0.736$ , the  $^{87}\text{Sr}/^{86}\text{Sr}$  with depths in both the cores varies within a small range  $\sim 0.71416$  to  $0.72149$ . The magnitude of the abrupt increase in  $^{87}\text{Sr}/^{86}\text{Sr}$  of the JP core near surface carbonates is far more than that can be due to analytical uncertainties and sample heterogeneity. These surface samples of the JP core have  $^{87}\text{Sr}/^{86}\text{Sr}$  within the range of contemporary river and ground water at Kanpur (Table 4.3a, Palmer and Edmond, 1992). Therefore, the increase in  $^{87}\text{Sr}/^{86}\text{Sr}$  of these recent carbonates occurring near the surface can be interpreted in terms of temporal variation in the riverine Sr isotope composition over kilo year time scales, with significantly more radiogenic ratio during the recent past compared to older samples up to  $\sim 100$  ka. It is difficult to assign a precise time frame to the surface sections of the JP core and hence to the abrupt rise in their  $^{87}\text{Sr}/^{86}\text{Sr}$ . The increase in  $^{87}\text{Sr}/^{86}\text{Sr}$  of contemporary water and the pedogenic carbonates of the Ganga compared to the past  $\sim 100$  ka is supported by increase in  $^{87}\text{Sr}/^{86}\text{Sr}$  of silicate part of contemporary sediments.  $^{87}\text{Sr}/^{86}\text{Sr}$  of silicate component of contemporary sediments of the Ganga at Kanpur (Singh et al., 2008) is the highest ever since last  $\sim 100$  ka (chapter 3). During the past  $\sim 100$  ka of sedimentary history, the  $^{87}\text{Sr}/^{86}\text{Sr}$  of silicates of the sediments of the Ganga has never gone beyond  $0.767$  (most of the time it has remained between  $0.73$  and  $0.76$ ), whereas present value is the highest ever,  $\sim 0.78$ .

The dissolved Sr of the Ganga at Kanpur is controlled mainly by the three main tectonic units of the Himalaya; (i) Lesser Himalayan carbonates dominated by low  $^{87}\text{Sr}/^{86}\text{Sr}$  with scattered occurrences of metamorphosed carbonates with more radiogenic Sr, (ii) Higher and Lesser Himalayan crystallines with high  $^{87}\text{Sr}/^{86}\text{Sr}$  and (iii) Tethyan sedimentary sequences (TSS) with low  $^{87}\text{Sr}/^{86}\text{Sr}$ . The dissolved Sr of the Ganga at study area is a mixture of contribution from radiogenic silicates and unradiogenic carbonates with the latter dominating in the Sr budget (Krishnaswami et al., 1992; Singh et al., 1998; Galy et al., 1998; Krishnaswami et al., 1999; English et al., 2000; Bickle et al., 2003; Oliver et al., 2003, Tipper et al., 2006). Among these three tectonic units, the Lesser Himalaya contributes  $38 \pm 8\%$  of contemporary dissolved Sr budget of the Ganga (Bickle et al., 2003). It has also been inferred that

the radiogenic meta-carbonates could be important in supplying radiogenic Sr on a local scale, however, their contribution on a basin wide scale is expected to be only minor owing to their limited exposure in the basin (Singh et al., 1998; Galy et al., 1999, English et al., 2000). The variations in  $^{87}\text{Sr}/^{86}\text{Sr}$  of carbonates from the deeper section of both the IITK and JP cores is only minor, making it difficult to infer about the temporal variations of relative contributions of Sr from different sources. The data also seems to indicate that the profile of Sr isotope composition of the carbonates does not follow that of this silicate; however the comparison is not detail as carbonates are present at selected depths.

One of the key observations of this study is that all the measured  $^{87}\text{Sr}/^{86}\text{Sr}$  in the carbonates of the IITK core and the deeper samples of the JP core (Tables 4.1, 4.2) are significantly less radiogenic than the present day Ganga water at Kanpur, 0.7324 and 0.7312 (Table 4.3a of this study and Palmer and Edmond, 1992) and the two near surface samples of the JP core.

#### **4.3.4 Carbon and Oxygen isotope composition**

Stable carbon and oxygen isotope composition of calcretes deposited in the Ganga plain and the Thar have been used to reconstruct past climate (Alam et al., 1997; Andrews et al., 1998; Srivastava, 2001; Sinha et al., 2006) with the premise that the carbonate nodules have been formed in isotope equilibrium with soil water. Salomons et al. (1978), however, based on studies of calcretes from the Indian subcontinent observed that the calcretes formed far from isotope equilibrium from rain water and hence are not suitable for paleo-climate reconstruction. The carbonate nodules collected from IITK core in this study were analysed for their carbon and oxygen isotope composition with the aim of reconstructing the past climate and vegetation pattern that prevailed during their formation. There is large spatial variability in climatic pattern and hydrological system in the Ganga plain, from foothills of the Himalaya to Bangladesh (Singh et al., 2008).

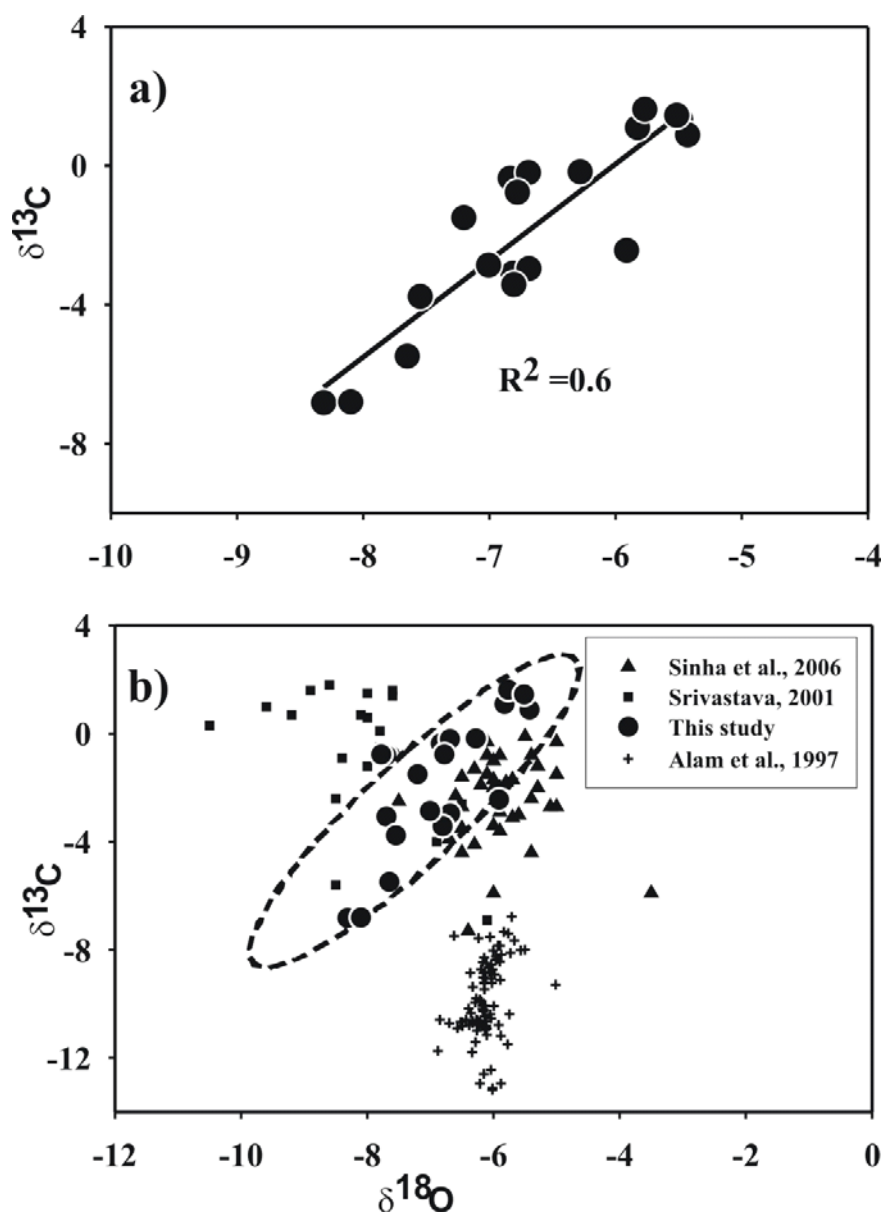


**Fig. 4.5 (a) Scatter diagram of  $\delta^{13}\text{C}$  and  $\delta^{18}\text{O}$  in carbonate nodules from IITK profile. Data show significant correlation ( $r=0.72$ ,  $n=21$ ,  $p<0.01$ ). (b) Covariation plot of  $\delta^{13}\text{C}$  and  $\delta^{18}\text{O}$  of carbonates from different areas of the Ganga plain are presented which are available in the literature and compared with this study.**

The location of this study lies in semiarid region where temperature exceeds  $45^\circ\text{C}$  with scanty precipitation during summer (Sinha et al., 2007). Under this condition,

evaporation is more extensive and calcite super-saturation and its precipitation are common phenomena (Jacobson et al., 2002). The sources of dissolved inorganic carbon of the Ganga are chemical weathering of silicate and carbonate rocks with soil CO<sub>2</sub>. It is estimated that 50% of the total alkalinity budget of the Himalayan rivers is from the dissolution of carbonate rocks of the Himalaya (Galy et al., 1998). The  $\delta^{13}\text{C}$  and  $\delta^{18}\text{O}$  values of the Precambrian Himalayan carbonates are  $0.7\pm 1.2\text{‰}$  and  $-9.1\pm 2.9\text{‰}$  respectively (Singh et al., 2006). The  $\delta^{13}\text{C}$  of reservoir from which carbonate precipitate is controlled by the carbon isotope composition of DIC which includes the signature of the isotopic composition of the local soil CO<sub>2</sub> derived from the vegetation in the basin (Cerling, 1984). The vegetation could be various mixing proportions of C<sub>3</sub> and/or C<sub>4</sub> type depending on the climatic as well as paleohydrologic conditions. The  $\delta^{13}\text{C}$  values of C<sub>3</sub> plants range from  $-20\text{‰}$  to  $-35\text{‰}$  with an average of  $-27\text{‰}$  (Ehleringer, 1989) and that of C<sub>4</sub> type vegetation ranges from  $-6\text{‰}$  to  $-19\text{‰}$  with an average of  $-13\text{‰}$  (Smith and Epstein, 1971).

Carbonate nodules collected from the sediment core at the IIT Kanpur show a range of variability of  $\sim 3\text{‰}$  in their  $\delta^{18}\text{O}$  (Table 1). For paleoclimatic interpretation of the  $\delta^{18}\text{O}$ , it is required that the carbonate nodules are formed in isotope equilibrium with soil water. Sinha et al. (2006) demonstrated that the pedogenic carbonates precipitated in areas around Kanpur is in isotopic equilibrium with soil water. The calculated  $\delta^{18}\text{O}$  value of pedogenic carbonates, assuming the  $\delta^{18}\text{O}$  value of soil water to be  $-5.4\text{‰}$ , same as the shallow ground water value near Kanpur (Krishnamurthy and Bhattacharya, 1991) and mean annual temperature of  $25^\circ\text{C}$  (Singh, 1994) is  $-7.3\text{‰}$ . This is very close to the average  $\delta^{18}\text{O}$  value  $-7\text{‰}$  obtained for the carbonate samples from the Ganga valley near Kanpur (Sinha et al., 2006).  $\delta^{18}\text{O}$  measured in carbonate nodules in this study range between  $-8.3$  and  $-5.4\text{‰}$ , similar to the range observed by Sinha et al. (2006) and hence these carbonate can be considered to be formed in equilibrium making them suitable to retrieve paleoclimatic reconstruction. The  $\delta^{18}\text{O}$  of carbonates indicate significant positive correlation with  $\delta^{13}\text{C}$  ( $r=0.72$ ,  $n=21$ ,  $p<0.01$ ; Fig. 4.5a). It is tempting to interpret this correlation as combination of evaporation influencing the oxygen isotope composition and varying vegetation type

controlling the carbon isotope composition. For example, the enriched O and C isotope values for calcretes observed in this study could arise due to higher evaporation and increase in proportion of C<sub>4</sub> vegetation during the glacial periods (Andrews et al., 1998). However, the positive correlation between  $\delta^{18}\text{O}$  and  $\delta^{13}\text{C}$  of calcretes has often been suggested due to kinetic fractionation during their deposition (Hendy et al. 1971; Mickler et al., 2006). In such cases, the C and O isotope composition of carbonates are not suitable to extract information about paleoclimate and paleovegetation (Hendy, 1971). However, it is puzzling to note that some of the earlier results on carbonates from nearby localities of Kanpur (Srivastava, 2001; Sinha et al., 2006) and from Bangladesh (Alam et al., 1997) do not seem to show effects of kinetic fractionation (Fig. 4.5b). Some of the earlier studies (e.g., Andrews et al., 1998) have interpreted the observed C and O isotope compositions of calcretes of western India in terms of variations in climate and vegetation even, as discussed above, despite significant positive correlation between  $\delta^{13}\text{C}$  and  $\delta^{18}\text{O}$ . Considering these conflicting interpretations, more study is needed to explain the differences observed for mode of precipitation, i.e. equilibrium (Srivastava, 2001., Sinha et al., 2006) and kinetic as in this study and that of Salomon et al. (1978).

The  $\delta^{18}\text{O}$  and  $\delta^{13}\text{C}$  variations are expected to be the direct consequences of climatic changes whereas the Sr isotope composition variation is caused by the variation in the proportion of its sources which in turn seems to be controlled by climate. It is noteworthy to observe that  $\delta^{13}\text{C}$  of calcretes in the IITK profile vary synchronously with  $\delta^{18}\text{O}$  and both correlate negatively with their  $^{87}\text{Sr}/^{86}\text{Sr}$ ; i.e., the peaks of the  $\delta^{13}\text{C}$  and  $\delta^{18}\text{O}$  coincide with the dips of the  $^{87}\text{Sr}/^{86}\text{Sr}$  (Fig. 4.6). In general,  $^{87}\text{Sr}/^{86}\text{Sr}$  in calcretes of IITK core show a uniform composition of  $\sim 0.717$  throughout the profile except it decreases at  $\sim 33$  ka and  $\sim 27$  ka and  $\sim 4$  ka. As mentioned earlier, occurrences of calcretes in the core is irregular and at many depths it was unavailable. The calcretes were not present in the depth 6.8-10.3 m and 24-39 m representing the 17.5 to 26.8 and 40 to 80 ka overlapping with MIS 2 and MIS 4 stages. The available records of IITK core indicate a decrease to 0.7142 from the

uniform  $^{87}\text{Sr}/^{86}\text{Sr}$  of 0.717 at  $\sim 27$  ka and further at  $\sim 4$  ka. The carbon and oxygen isotope compositions of these calcretes vary synchronously with their ages (Fig. 4.6).

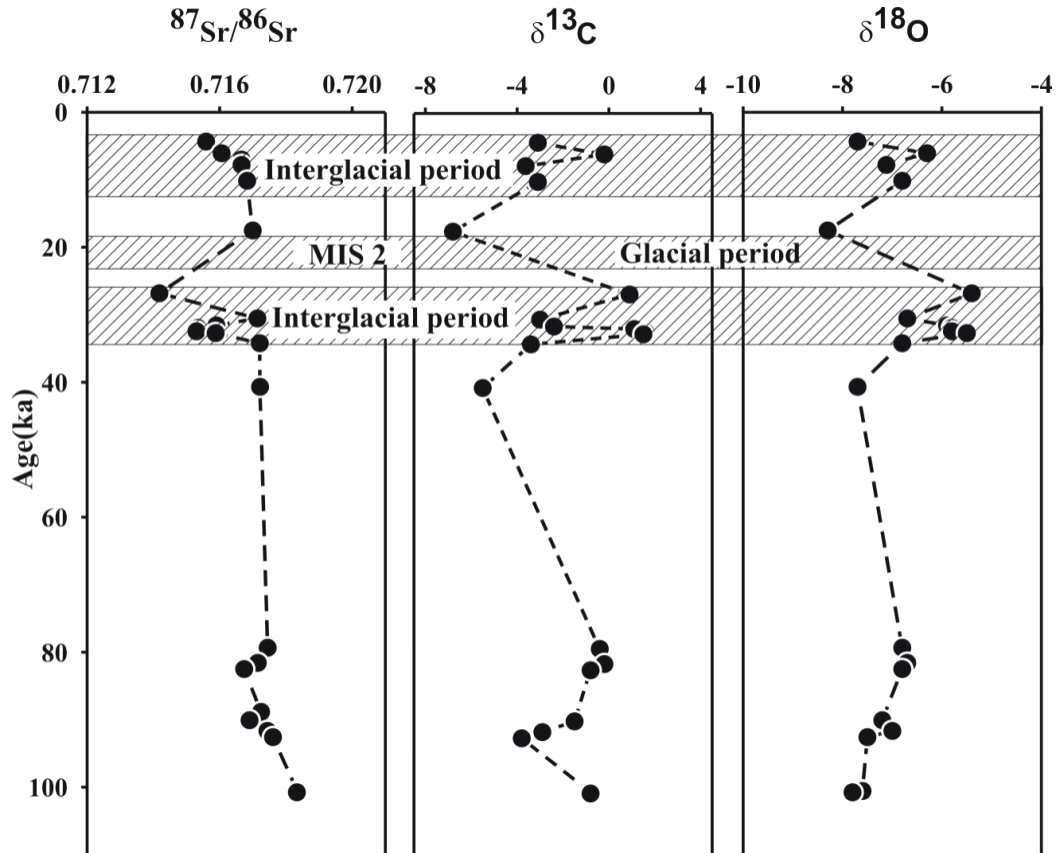


**Fig. 4.6: Variations in  $^{87}\text{Sr}/^{86}\text{Sr}$ ,  $\delta^{13}\text{C}$  and  $\delta^{18}\text{O}$  with age of the carbonate nodules from IITK profile. The average  $^{87}\text{Sr}/^{86}\text{Sr}$  of the calcretes from IITK core is  $\sim 0.717$ . In general, the decrease of  $^{87}\text{Sr}/^{86}\text{Sr}$  coincides with the increase of  $\delta^{18}\text{O}$  and  $\delta^{13}\text{C}$  and vice versa.**

The most depleted value of  $\delta^{18}\text{O}$  ( $-8.3\text{‰}$ ) and  $\delta^{13}\text{C}$  ( $-6.8\text{‰}$ ) are observed at 6.8 m depth corresponding to  $\sim 17.5$  ka of depositional age. Its  $\delta^{18}\text{O}$  is  $\sim 1\text{‰}$  depleted compared to that of contemporary rain water near the core location (Sinha et al., 2006). This depletion with respect to rain water could be difficult to explain in terms of kinetic effect if the rain water isotope composition has remained the same in past as its contemporary value. The kinetic effect due to intense evaporation could explain the enrichment with respect to the rainwater. Possible explanation for the depletion in

$\delta^{18}\text{O}$  at  $\sim 17.5$  ka could be either due to the increased supply of snowmelt from the Himalaya and/or increase in rainfall during the declining phase of LGM. The increase in melt water component could also explain the depletion in  $\delta^{13}\text{C}$  and increase in  $^{87}\text{Sr}/^{86}\text{Sr}$  due to silicate weathering (Das et al., 2005) resulting from exposure of fresh and fine silicate materials from the glacial moraines during the immediate demise of the LGM phase (Vance et al., 2009). Silicate weathering derived  $\text{HCO}_3^-$  has more depleted  $\delta^{13}\text{C}$  than the carbonates. Decrease in  $^{87}\text{Sr}/^{86}\text{Sr}$  and corresponding increase in  $\delta^{18}\text{O}$  and  $\delta^{13}\text{C}$  at some depths (Fig. 4.6) could result from the enhanced monsoon causing increase in carbonate weathering.

#### **4.3.5 Recent abrupt rise in $^{87}\text{Sr}/^{86}\text{Sr}$ of the Ganga and its implications**

The inference that  $^{87}\text{Sr}/^{86}\text{Sr}$  of the contemporary Ganga is significantly more radiogenic than that during past  $\sim 100$  ka is intriguing. Some of the earlier studies had reported change in  $^{87}\text{Sr}/^{86}\text{Sr}$  on million year times scales (Harris, 1995, Derry and France-Lanord., 1996., Quade et al., 1997). The observation of sudden rise in  $^{87}\text{Sr}/^{86}\text{Sr}$  in paleosol carbonates from the Siwalik during late Miocene was explained in terms of exhumation and weathering of high  $^{87}\text{Sr}/^{86}\text{Sr}$  metalimestones in the central Himalaya (Quade et al., 1997). Subsequent studies of English et al. (2000) also arrived at a similar conclusion based on  $^{87}\text{Sr}/^{86}\text{Sr}$  in the Himalayan paleosols during the late Miocene and Pliocene. A plausible explanation for the recent sudden increase in  $^{87}\text{Sr}/^{86}\text{Sr}$  is relatively enhanced contribution of radiogenic Sr from silicates, calc-silicates and metacarbonates of the Lesser Himalaya. These lithologies of the Lesser Himalaya are more radiogenic in Sr, enhanced weathering of which could contribute the excess  $^{87}\text{Sr}$  in the contemporary Ganga. The reason for enhanced weathering of the Lesser Himalayan lithologies with more radiogenic Sr during last few ka is not reported. Available information does not indicate any tectonic model which can be correlated with the sudden increase in  $^{87}\text{Sr}/^{86}\text{Sr}$ . Climate variations during recent times could cause such variability in  $^{87}\text{Sr}/^{86}\text{Sr}$ . Alternatively, anthropogenic activities such as expansion of cultivated land and deforestation in the Lesser Himalaya since the onset of human occupation could be one of the plausible mechanisms to enhance

more erosion over the Lesser Himalaya. More work needs to be done to understand the causes of the recent increase in  $^{87}\text{Sr}/^{86}\text{Sr}$  of the Ganga water. The results of this study show recent abrupt increase in  $^{87}\text{Sr}/^{86}\text{Sr}$  of the Ganga water from  $\sim 0.718$  to  $\sim 0.735$  which had remained within a narrow range of  $\sim 0.713$  to  $0.718$  during past  $\sim 100$  ka. If this observation is representative of the entire Ganga basin, it would suggest that the present day  $^{87}\text{Sr}/^{86}\text{Sr}$  of the Ganga water is not the representative value since the Cenozoic, as has been assumed to evaluate the impact of the Himalayan orogeny on the Sr isotope evolution of seawater. If the significantly higher  $^{87}\text{Sr}/^{86}\text{Sr}$  of contemporary water of the Ganga is only due to some recent activity, the earlier estimates of the contribution of the Ganga to the Sr evolution budget of the seawater could be an overestimate.

Stable carbon and oxygen data of these carbonates are strongly correlated, indicating kinetic fractionation during their formation in the Ganga plain. This observation raised issues regarding the use of these carbonates for the reconstruction of paleoclimate and paleovegetation.

#### 4.4 Conclusions

$^{87}\text{Sr}/^{86}\text{Sr}$ ,  $\delta^{18}\text{O}$  and  $\delta^{13}\text{C}$  of the carbonate nodules analysed from cores in the Ganga plain show significant temporal variations. Chemical compositions coupled with petrography of these carbonates indicate minor extent of later diagenesis effect and thereby indicating the preservation of their pristine chemical and isotopic signature. It is clearly observed that  $\delta^{18}\text{O}$  and  $\delta^{13}\text{C}$  show significant co-variations which could indicate climatic variation, as a decrease in temperature and humidity (for example, during glacial periods) enhances evaporation causing enrichment in  $\delta^{18}\text{O}$ . This will be associated with increase in the proportion of  $\text{C}_4$  plants increasing the  $\delta^{13}\text{C}$ . However, this interpretation needs more work as positive correlation between O and C isotopes is generally considered to be the result of kinetic fractionation and carbonates precipitation takes place out of equilibrium and hence they can not be used as a proxy for paleoclimatic indicator. The  $^{87}\text{Sr}/^{86}\text{Sr}$  of the calcretes is primarily controlled by its composition in the river and ground water from

which they precipitate. This study shows that the Sr isotope composition of the Ganga water was low during last ~100 ka compared to contemporary water. Ganga water became more radiogenic in Sr in recent past. This abrupt increase in  $^{87}\text{Sr}/^{86}\text{Sr}$  of the Ganga water could be a result of enhanced weathering of the Lesser Himalaya containing lithologies with higher  $^{87}\text{Sr}/^{86}\text{Sr}$ . Recent enhanced weathering in the LH could result either from climatic change or from human occupation and associated activities over the mountains. This study indicates, in view of recent increase observed in  $^{87}\text{Sr}/^{86}\text{Sr}$  of water of the Ganga at Kanpur, the need of constructing temporal variation in  $^{87}\text{Sr}/^{86}\text{Sr}$  of the paleo Ganga at its out flow to assess its impact on oceanic  $^{87}\text{Sr}/^{86}\text{Sr}$  evolution.

## **CHAPTER-5**

**Mo, U and Re in rivers and estuaries of India:  
Implications to geochemistry of redox sensitive  
elements and their marine budgets**

## 5.1 Introduction

Estuary is the mixing zone between river and ocean where geochemical, biological and sedimentological processes are highly variable both spatially and temporally. These processes determine the riverine contribution of elements to the oceans. The study of the behaviour of various elements in the estuary therefore becomes important not only to understand their geochemistry but also to evaluate their marine budgets. Among the various groups of elements that are being investigated, one is the redox sensitive group of elements that include U, Mo and Re. This group of elements finds applications in studies of marine paleoenvironmental conditions because of their property to be sequestered with the organic rich marine sediments (Ravizza et al., 1991, Colodner et al., 1992, Morford and Emerson 1999, Jaffe et al., 2000). The dominant source of all these elements to the ocean is river input (Martin and Meybeck, 1979). In rivers, these elements are derived from chemical weathering of various lithologies, an important one being organic rich sediments, black shales (Colodner et al., 1993, Jaffe et al., 2000, Singh et al., 2003). Recent studies, however, have shown that anthropogenic sources can also be significant to their riverine budgets in some rivers (Colodner et al., 1993, 1995, Pucker-Ehrenbrink et al., 2006, Rahaman and Singh, 2010). The behaviour of these elements in estuaries is complex and its understanding is essential to estimate their continental fluxes to the oceans.

Trace elements and their isotopes serve as proxies to study several biogeochemical processes especially in the marine environment. The trace elements those find applications in such studies are Re, Mo and U due to their redox sensitive behaviour in aquatic systems. In sea water, U, Mo and Re occur as stable oxyanions,  $\text{UO}_2(\text{CO}_3)_3^{4-}$ ,  $(\text{MoO}_4)^{2-}$  and stable perrhenate oxyanion  $\text{ReO}_4^-$  and their geochemistry are similar to each other (Colodner et al., 1993, 1995). In the ocean the behaviour of Re, Mo and U are analogous; they exhibit covariance with salinity and demonstrate generally conservative behaviour in oxic waters (Anbar et al., 1992). In anoxic/reducing waters, Re probably exists as more reactive  $\text{Re}(\text{OH})_4$  (Xiong, 2003) and gets sequestered to sediments whereas  $\text{UO}_2(\text{CO}_3)_3^{4-}$ ,  $(\text{MoO}_4)^{2-}$  oxyanions can be effected in both oxic and anoxic conditions and can be removed from water column in both oxic and reducing conditions. All

these elements have long residence time in the oceans, orders of magnitude higher than ocean mixing times. Residence time of U, Mo and Re in the oceans are within the similar ranges  $\sim 250,000$ - $500,000$ ,  $780,000$  and  $\sim 750,000$  yr respectively (Turekian and Chan., 1971, Bertine and Turekian, 1997, Colodner et al., 1993). As a result, these elements have uniform concentration in the ocean. U behaves conservatively in the ocean, with very uniform dissolved concentration of  $13.6$  nM (Ku et al, 1977). Despite its biological involvement, Mo is the most abundant transition element in the sea and its average dissolved concentration is  $110 \pm 10$  nM (Morris, 1975; Collier, 1985; Quiby-Hunt and Turekian, 1983). It displays conservative behaviour in ocean water column though it plays an important role in nitrogen metabolism of planktonic organisms (Dewllig et al., 2007). Analogous to U and Mo, Re also shows conservative behaviour with uniform concentration  $\sim 40$  pmol/kg in the vertical profile in the open ocean.

Available studies (Emerson and Hausted, 1991; Colodner et al., 1993, 1995) indicate overall similarity among their geochemistry, however, their behaviour may differ locally, depending on the regional environmental chemistry. For example both U and Re exhibit conservative and non-conservative behaviour in estuaries (McKee, 2008 and reference there in; Colodner et al., 1993; Rahaman and Singh, 2010). Studies of Mo in estuaries are sparse (Colodner et al., 1993, Dalai et al., 2005, Audry et al., 2007; Archer and Vance, 2008, Scheiderich et al., 2010). The major sink for these elements is removal to particulate phases in reducing conditions (Colodner et al., 1995), however their sensitivity to redox condition which determines their removal from dissolved phase to solid phase is different, with rhenium being the most sensitive (Colodner et al., 1993, Morford and Emerson, 1999). The association of these elements with reducing conditions makes their concentrations high, both in modern and ancient organic rich marine sediments, (Ravizza et al., 1991; Peucker-Ehrenbrink et al., 1995, Morford and Emerson 1999, Singh et al., 1999; McManus et al., 2006). Thus, their abundances in sediments and their inter-relation can provide clues to the Eh-pH conditions of the depositional environment (Hodge et al., 1996; Morford et al., 2007; Chappaz et al., 2008).

This study focuses on the distribution of the redox sensitive elements U, Mo and Re and the processes regulating their concentrations in rivers and estuaries draining into the Bay of Bengal, the Arabian Sea and the Gulf of Cambay and compare among each other in the same rivers/estuaries (Rahaman and Singh, 2010; Rahaman et al., 2010). Such a study, in addition to characterizing their behaviour in estuaries will also provide data to constrain their inputs to the open ocean and therefore their marine budgets, particularly for Mo and Re. Available data suggest that present input of Mo and Re to the global ocean is significantly higher compared to its known sinks (Morford and Emerson 1999, MacManus et al., 2006). Attempts are being made to constrain their oceanic budgets to utilize them as proxies to study various oceanic processes (Vance et al. 2009).

Re and Mo measurements have been carried out for the first time in Indian estuaries as part of this study whereas in some of these estuaries particularly in the Narmada, Tapi, and the Hooghly U measurements have been reported earlier (Borole et al., 1982, Somayajulu, 1994). In this study, however, U has been measured along with Mo and Re to assess their relative behaviour and temporal variations (Colodner et al., 1995). In addition, dissolved Mo, U, and Re concentration in coastal waters, salt marshes and effluent discharges have been measured to better understand their geochemistry and their influence on their abundance in coastal waters of the Arabian Sea and the Bay of Bengal.

## **5.2 Results and Discussion**

The dissolved Mo, U and Re concentrations measured in the estuaries along with salinity, pH, alkalinity and temperature are given in Tables 2.2 and 5.1. In the Narmada estuary, the pH remains nearly constant at ~8 from fresh water to sea water (Table 2.2), unlike in the Tapi and the Mandovi estuaries which show significant variations between 7.5 to 8.0 and 6.6 to 8.2 respectively. Alkalinity lies between 2000 and 3000  $\mu\text{eq/l}$  in all the estuaries except in the Mandovi where it varies from 384 to 2236  $\mu\text{eq/l}$  (Table 2.2).

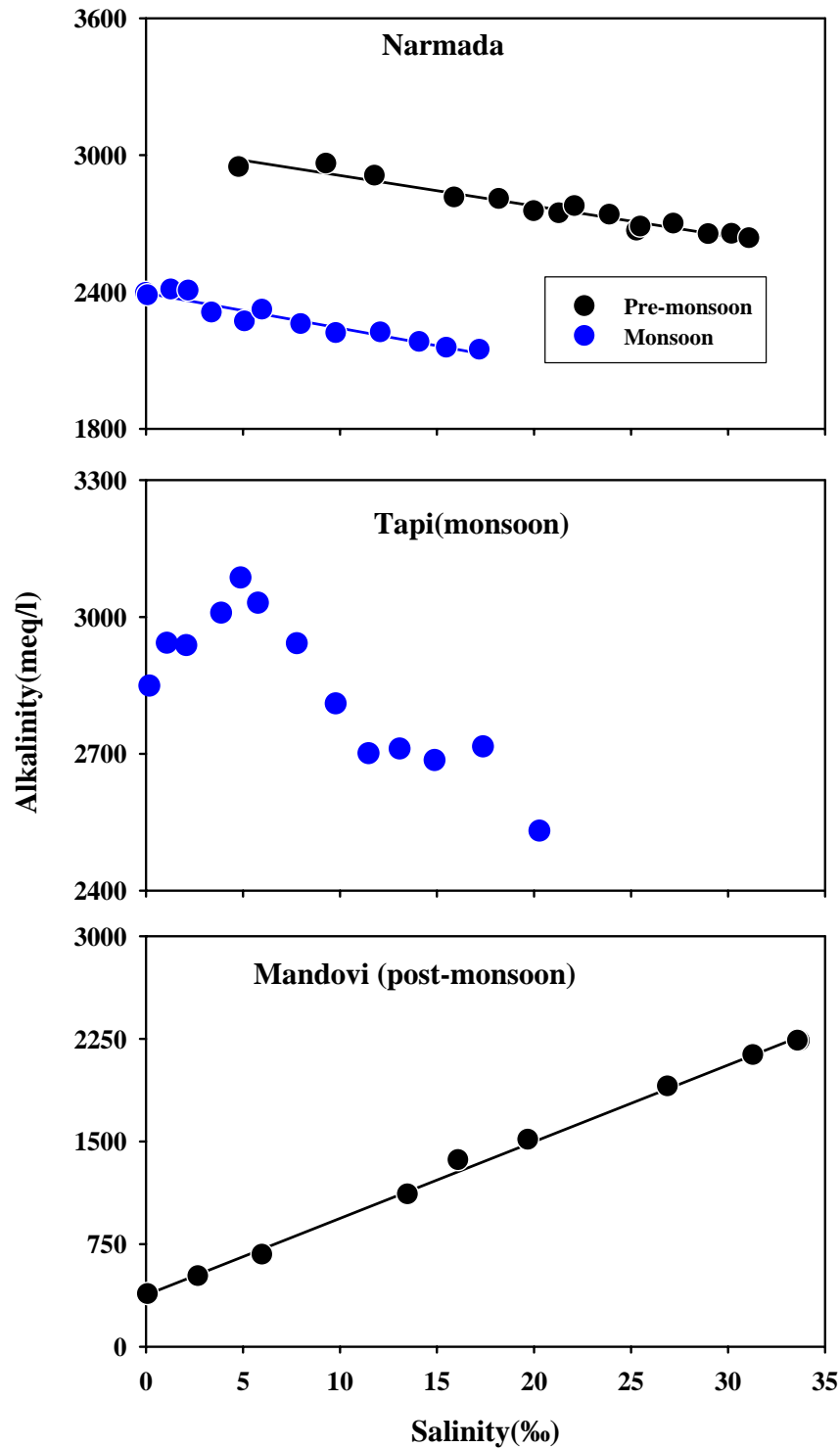


**Fig. 5.1 Alkalinity vs. salinity distribution in estuaries. All estuaries except the Tapi show conservative mixing. There is systematic gain in alkalinity in the lower salinity (5-13‰) of the Tapi estuary. The location of this hump coincides with the location of a steel plant.**

Lower pH and alkalinity in the Mandovi river indicates the dominance of rainwater and lower water rock interaction. Alkalinity shows systematic gain around 4-11 ‰ salinity range in the Tapi estuary.

**Table 5.1: Dissolved Mo, U and Re in the Indian Estuaries.**

| Sample  | Latitude  | Longitude | Salinity | [Mo]    | [U]  | [Re]    |
|---|-----------|-----------|----------|---------|------|---------|
|   |           |           | (‰)      | nmol/kg |      | pmol/kg |
| <b><u>Narmada (Pre-monsoon, March 2007)</u></b> |           |           |          |         |      |         |
| NE07-20   | 21°49.49' | 73°11.57' | 0        | -       | -    | 13.1    |
| NE07-21   | 21°50.01' | 73°45.34' | 0        | 2.3     | 1.4  | 13.9    |
| NE07-22   | 21°51.81' | 72°41.74' | 0        | 2.6     | 1.4  | 14.7    |
| NE07-18   | 21°40.51' | 72°57.00' | 0.2      | -       | -    | 14.8    |
| NE07-19   | 21°40.63' | 72°57.54' | 0.2      | -       | -    | 15.1    |
| NE07-1  | 21°40.81' | 72°54.57' | 4.8      | 20.9    | 3.7  | 27.4    |
| NE07-2  | 21°41.26' | 72°52.60' | 9.3      | 36.9    | 5.7  | 43.6    |
| NE07-3  | 21°40.58' | 72°50.39' | 11.8     | 40.0    | 6.2  | 47.8    |
| NE07-4  | 21°39.20' | 72°47.42' | 15.9     | 50.1    | 7.3  | 60.5    |
| NE07-5  | 21°38.80' | 72°45.34' | 18.2     | 54.0    | 7.8  | 64.7    |
| NE07-6  | 21°40.75' | 72°42.05' | 20       | 60.7    | 8.5  | 71.1    |
| NE07-7  | 21°40.71' | 72°49.83' | 21.3     | 62.7    | 8.7  | 75      |
| NE07-8  | 21°39.46' | 72°35.89' | 22.1     | 66.9    | 9.3  | 76.8    |
| NE07-9  | 21°39.36' | 72°34.51' | 23.9     | 70.2    | 9.8  | 82.3    |
| NE07-10   | 21°39.62' | 72°33.28' | 25.3     | 75.0    | 10.3 | 88.8    |
| NE07-11   | 21°38.73' | 72°33.02' | 25.5     | 73.6    | 10.1 | 85.2    |
| NE07-12   | 21°38.04' | 72°32.70' | 27.2     | 78.3    | 10.8 | 89.7    |
| NE07-13   | 21°38.0'  | 72°32.7'  | 29       | 82.9    | 11.3 | 94      |
| NE07-14   | 21°37.94' | 72°32.05' | 30.2     | 86.6    | 11.7 | 98.2    |
| NE07-15   | 21°37.94' | 72°32.05' | 31.1     | 89.6    | 12.0 | 103     |
| <b><u>Narmada ( Monsoon, July 2007)</u></b>     |           |           |          |         |      |         |
| NEM07-14  | -         | -         | 0        | 2.9     | 1.2  | 8.5     |
| NEM07-1   | 21°40.59' | 72°55.58' | 0        | 4.3     | 1.5  | 10      |
| NEM07-2   | 21°39.08' | 72°46.64' | 0.1      | 8.7     | 1.9  | 11.1    |
| NEM07-3   | 21°40.07' | 72°37.12' | 1.3      | 10.7    | 2.0  | 16.8    |
| NEM07-4   | 21°39.58' | 72°36.34' | 2.2      | 12.9    | 2.2  | 20.8    |
| NEM07-5   | 21°39.42' | 72°35.49' | 3.4      | 16.2    | 2.7  | 26.7    |
| NEM07-6   | 21°39.15' | 72°34.28' | 5.1      | 21.6    | 3.3  | 37.4    |
| NEM07-7   | 21°38.55' | 72°33.18' | 6        | 23.7    | 3.5  | 39.6    |
| NEM07-8   | 21°38.39' | 72°33.26' | 8        | 28.9    | 4.0  | 48.3    |
| NEM07-9   | 21°39.27' | 72°35.26' | 9.8      | 34.2    | 4.7  | 59.9    |
| NEM07-10  | 21°38.52' | 72°33.2'  | 12.1     | 46.9    | 5.9  | 84.6    |
| NEM07-11  | 21°38.81' | 72°33.94' | 14.1     | 51.2    | 6.1  | 80      |

|          |           |           |      |      |     |      |
|----------|-----------|-----------|------|------|-----|------|
| NEM07-12 | 21°38.05' | 72°33.19' | 15.5 | 49.6 | 6.3 | 87.6 |
| NEM07-13 | 21°38.55' | 72°32.93' | 17.2 | 53.8 | 7.0 | 97.4 |

**Narmada Second Channel (Monsoon, July 2008)**

|           |   |   |      |   |   |     |
|-----------|---|---|------|---|---|-----|
| KOH-08-1  | - | - | 1.1  | - | - | 21  |
| KOH-08-2  | - | - | 1.8  | - | - | 24  |
| KOH-08-3  | - | - | 7.2  | - | - | 46  |
| KOH-08-4  | - | - | 17.7 | - | - | 94  |
| KOH-08-5  | - | - | 19.9 | - | - | 102 |
| KOH-08-6  | - | - | 25   | - | - | 121 |
| KOH-08-7  | - | - | 28.1 | - | - | 136 |
| KOH-08-8  | - | - | 29.3 | - | - | 144 |
| KOH-08-9  | - | - | 30.5 | - | - | 145 |
| KOH-08-10 | - | - | 30.7 | - | - | 153 |

**Tapi (Monsoon, July 2007)**

|          |           |           |       |      |     |      |
|----------|-----------|-----------|-------|------|-----|------|
| TPM07-14 | -         | -         | 0     | 3.6  | 0.9 | 4.1  |
| TPM07-1  | 21°10.56' | 72°46.74' | 0-0.2 | 6.1  | 1.4 | 7.6  |
| TPM07-2  | 21°8.9'   | 72°45.8'  | 1.1   | 9.6  | 1.8 | 7.4  |
| TPM07-3  | 21°8.52'  | 72°43.61' | 2.1   | 12.4 | 2.0 | 8.8  |
| TPM07-4  | 21°8.86'  | 72°42.26' | 3.9   | 20.3 | 2.6 | 12.8 |
| TPM07-5  | 21°9.15'  | 72°4.73'  | 4.9   | 25.1 | 3.1 | 17.1 |
| TPM07-6  | 21°9.3'   | 72°40.19' | 5.8   | 31.8 | 3.4 | 19.1 |
| TPM07-7  | 21°7.97'  | 72°39.58' | 7.8   | 37.9 | 4.1 | 25   |
| TPM07-8  | 21°7.05'  | 72°39.74' | 9.8   | 42.4 | 4.6 | 27.5 |
| TPM07-9  | 21°5.79'  | 72°39.98' | 11.5  | 44.0 | 5.1 | 32.3 |
| TPM07-10 | 21°4.97'  | 72°40.64' | 13.1  | 47.2 | 5.4 | 34.6 |
| TPM07-11 | 21°4.41'  | 72°40.71' | 14.9  | 54.3 | 6.1 | 39.6 |
| TPM07-12 | 21°36'    | 72°40.68' | 17.4  | 61.2 | 6.8 | 45.3 |
| TPM07-13 | 21°316'   | 72°40.35' | 20.3  | 70.5 | 7.7 | 51.3 |

**Mandovi (Post-Monsoon, October 2007)**

|         |           |           |       |       |      |      |
|---------|-----------|-----------|-------|-------|------|------|
| MD07-1  | 15°32.56' | 73°57.69' | 0-0.1 | 1.0   | 0.02 | 1.4  |
| MD07-2  | 15°32.39' | 73°55.95' | 2.7   | 7.4   | 0.1  | 4.3  |
| MD07-3  | 15°31.55' | 73°55.60' | 6     | 7.3   | 0.7  | 7.5  |
| MD07-4  | 15°31.33' | 73°55.38' | 13.5  | 42.0  | 4.2  | 16.1 |
| MD07-5  | 15°30.33' | 73°54.82' | 16.1  | 47.1  | 4.6  | 19.1 |
| MD07-6  | 15°30.27' | 73°54.16' | 19.7  | 58.0  | 6.2  | 23.2 |
| MD07-7  | 15°30.11' | 73°52.88' | 26.9  | 84.0  | 9.3  | 30.8 |
| MD07-8  | 15°30.34' | 73°50.63' | 31.3  | 100.0 | 11.2 | 36.9 |
| MD07-9  | 15°29.29' | 73°48.40' | 33.7  | 109.0 | 12.1 | 39.1 |
| MD07-10 | 15°29.07' | 73°41.09' | 33.6  | 109.1 | 11.9 | 39.3 |

**Hooghly (Post-monsoon, December 2006)**

|     |        |        |     |      |     |     |
|-----|--------|--------|-----|------|-----|-----|
| W-1 | 22.01° | 88.19° | 0.5 | 13.8 | 8.0 | 6.6 |
| W-2 | 21.9°  | 88.09° | 2.6 | 20.3 | 7.2 | 7.8 |

|      |        |        |      |       |      |      |
|------|--------|--------|------|-------|------|------|
| W-3  | 21.77° | 88.02° | 7.7  | 24.4  | 6.8  | 12.6 |
| W-4  | 21.65° | 88.02° | 11.8 | 25.8  | 8.1  | 16.4 |
| W-5  | 21.58° | 88.08° | 14.7 | 50.0  | 8.4  | 19.4 |
| W-6  | 21.49° | 88.13° | 16.7 | 58.1  | 8.9  | 21.3 |
| W-7  | 21.33° | 88.19° | 20.5 | 63.6  | 9.9  | 25.2 |
| W-8  | 21.06° | 88.2°  | 22.5 | 76.0  | 10.5 | 27.5 |
| W-9  | 20.69° | 88.21° | 30   | 102.4 | 12.2 | 35.1 |
| W-10 | 20.0°  | 88.2°  | 32   | 112.3 | 13.0 | 37.2 |

**Table 5.2: Dissolved Mo, U and Re in miscellaneous samples**

| Sample                                   | Type/River/Place      | Salinity | [Mo] | [U]     | [Re]    |
|--|-----------------------|----------|------|---------|---------|
|  |                       |          | %    | nmol/kg | pmol/kg |
| <b><u>River waters</u></b>               |                       |          |      |         |         |
| KOH-08-13                                | Vishwamitri           | 0.1      | 23   | 5.3     | 18      |
| KOH-08-17                                | Sabarmati             | 1.2      | 48   | 19.0    | 37      |
| KOH-08-16                                | Mahi                  | 0        | 90   | 7.9     | 41      |
| <b><u>Estuary and coastal waters</u></b> |                       |          |      |         |         |
| KOH-08-14                                | Mahi                  | 27       | 118  | 12.2    | 208     |
| KOH-08-15                                | Mahi                  | 25.6     | 132  | 15.2    | 118     |
| KOH-08-19                                | Ghogha                | 32.4     | 110  | 12.5    | 171     |
| KOH-08-20                                | Ghogha                | 32.5     | 111  | 12.7    | 129     |
| <b><u>Salt marsh water</u></b>           |                       |          |      |         |         |
| KOH-08-18                                | Near Bhavnagar        | 120      | 655  | 27.9    | 695     |
| <b><u>Open ocean water</u></b>           |                       |          |      |         |         |
| GA 07-1                                  | Open Ocean near Goa   | -        | 99   | 12.4    | -       |
| GA 07-2                                  | Open Ocean near Goa   | -        | 101  | 12.6    | -       |
| GA 07-3                                  | Open Ocean near Goa   | -        | 101  | 12.8    | 41      |
| GA 07-4                                  | Open Ocean near Goa   | -        | 100  | 12.9    | 40.4    |
| GA 07-5                                  | Open Ocean near Goa   | -        | 103  | 13.0    | 40.9    |
| <b><u>Waste waters</u></b>               |                       |          |      |         |         |
| KOH-08-11                                | Pipe-line waste water | 10.8     | 569  | 2.8     | 178     |
| KOH-08-12                                | Pipe-line waste water | 11.6     | 828  | 1.4     | 175     |

### 5.2.1 Dissolved Molybdenum, Uranium and Rhenium in rivers and other samples

The concentrations of dissolved Mo, U and Re were analysed in rivers, salt marsh and in the open oceans to evaluate their (i) sources in the river water, (ii) fate in salt marsh and (iii) distribution in open ocean.

**(a) Molybdenum**

Mo in river water end members of the estuaries (the Narmada, Tapi, Mandovi and the Hooghly) ranges from 1.0 to 14 nmol/kg with the Mandovi and the Hooghly end members having the lowest and the highest concentrations respectively (Table 5.1). Mo in the Narmada, Tapi and the Mandovi rivers can be accounted from weathering of lithologies exposed in their drainage basins. Basalts, the major lithology of the Narmada and the Tapi basins and laterites of the Mandovi contain ~1 ppm Mo, similar to average crustal abundance (Manheim and Landergren, 1978). Therefore, release of Mo from a few hundred milligrams of these rocks can sustain its measured concentration. Mo concentration for the Hooghly river is not measured, however, considering that the sample with 0.5 ‰ salinity has 14 nmol/kg, it is expected that the Hooghly river water would have Mo concentration ~14 nmol/kg. Concentration of ~14 nmol/kg is difficult to be explained in term of silicate/carbonate weathering in the Ganga basin. Dissolved load in the Ganga can support only 15% of dissolved Mo of the Ganga from the weathering of silicate/carbonate rocks having average Mo abundance ~1 ppm (Manheim and Landergren, 1978). Therefore, the source of Mo in this water has to be the lithologies rich in Mo, such as organic rich sediments e.g. the black shales containing 10-1000 ppm of Mo (Yamaguchi, 2002) which is several magnitudes higher than the average continental crust. Further, it has been suggested that the high concentration of both Re and U in the Himalayan rivers comes from weathering of black shales (Dalai et al., 2002; Singh et al., 2003).

In contrast to the above rivers, the Mahi and the Sabarmati rivers have very high Mo, 90 and 48 nmol/kg respectively. The sources for such high Mo is unlikely to be of various lithologies present in their basins; the high Mo in them seems to be supplied by anthropogenic sources. The drainage basins of the Mahi and the Sabarmati are heavily industrialized and these industries could be an important source of dissolved Mo to these rivers. Mo is used in pharmaceutical and steel industries as catalyst and hardening agent respectively and effluent discharges from these industries can be a source of Mo to rivers. This hypothesis draws support from the observation that the industrial effluents with salinity of

10.8 to 11.6‰ analyzed in this study contain very high concentration of Mo (560 and 820 nmol/kg; Table 5.2).

Water samples from a salt marsh at the western coast of the Gulf of Cambay near Bhavnagar with salinity of 120 ‰ have very high Mo concentration, 655 nmol/kg compared to ~111 nmol/kg (Table 5.2) for seawater (32.5 ‰) from these regions (near the Ghogha coast). Mo/salinity ratio in the seawater near the Ghogha coast is 3.4 whereas for the salt marsh sample it is 6.0. The Mo in the salt marsh basin is “in excess” of what would have been expected if seawater with salinity of 32.5 ‰ and Mo of 111 nmol/kg is concentrated to 120‰ salinity. The amount of “excess” Mo in salt marsh water is ~ 75%, indicating this salt marsh as a source of Mo to the overlying water unlike to that reported by Roychoudhury (2006) that Mo gets sequestered from the water to particulate phase under reducing condition via sulfate reduction (Helz et al., 1996) in Sapelo Island salt marsh, USA.

Five seawater samples from the Arabian Sea off Goa have dissolved Mo  $101 \pm 1$  nmol/kg (Table 5.2), within the range reported for seawater  $110 \pm 10$  nmol/l (Morris, 1975; Collier, 1985; Quiby-Hunt and Turekian, 1983).

### ***(b) Uranium***

Uranium concentrations in rivers analysed in this study varies from a very low value of 0.02 nmol/kg in the Mandovi to 19 nmol/kg in the Sabarmati river and seem to follow the weathering intensity in the basin and the lithology. The Narmada and the Tapi rivers have U in the range of 1 to 3 nmol/kg, in the range of the global average riverine U concentration ~1.3 nmol/kg (Palmer and Edmond, 1993). U in the Narmada and the Tapi measured in this study overlaps with those reported by Borole et al. (1977, 1982). It is suggested (Borole et al., 1982) that weathering of basalts and alluviums in the basin can sustain the dissolved U in these rivers. U content of the Sabarmati is higher than that reported for its upper reaches (3.4 to 15.8 nM; Borole et al., 1979) underscoring the importance of temporal and spatial variability. High U in the Sabarmati can result from the uraniferous granites present in the Aravalli mountains, the source region of the Sabarmati river and/ or ground water contribution to the river which

have U content as high as 91 nmol/l (Hussain et al., 1980). The impact of anthropogenic activity in contributing to the higher U seems unlikely though this basin supports large agricultural activities and is significantly industrialized as U concentration in the industrial effluents is only 1.4-2.8 nmol/kg (Table 5.2).

In the Mandovi river, U concentration is among the lowest of the world rivers (Palmer and Edmond, 1993; Windom et al., 2000) similar to that observed for Mo and Re. The low U in the Mandovi River associated with lower alkalinity and TDS (Table 2.2) is due to dominance of laterites in the basin and high rainfall. Singh et al (2003) suggested that the high U in the Ganga source water can be derived from weathering of black shales and /or uraniferous granite of the Himalaya. These sources may also be important to account for high concentration of U in the Hooghly as it is one of the tributaries of the Ganga.

Beside rivers and estuaries, a few additional samples collected from the Ghogha coast, salt marsh, open Arabian Sea off the Mandovi estuary and industrial effluents near the Narmada and the Tapi estuaries were also measured for U to decipher the role of natural and anthropogenic inputs via river and estuary and directly to the sea. Seawater from the Gulf of Cambay, collected off the Ghogha coast, has U ~12.6 nmol/kg (Table 5.2), similar to those reported for U in the open Arabian Sea  $13.44 \pm 0.84$  nmol/kg (Rengarajan et al., 2003) and to those measured in this study in five samples off Goa coast 12.4 to 13.0 nmol/kg (Table 5.2). U concentration in the industrial effluent waste waters does not show any enrichment, it is only 1.4 and 2.8 nmol/kg, similar to their range in the Narmada and the Tapi rivers (Borole et al., 1982). In the salt marsh sample (salinity 120‰), dissolved U is only 27.9 nmol/kg U (Table 5.2) much lower than that expected for this salinity if U behaves conservatively with concentration of 12.6 nmol/kg in nearby seawater at salinity 32 ‰. U content in this salt marsh sample shows ~35% depletion with respect to the seawater near Ghogha coast and considering the evaporation enrichment, which is consistent with earlier observation in the Delaware Bay salt marsh (Maeda and Windom, 1982; Church et al.1996).

**(c) Rhenium**

Re concentration of rivers analysed in this study, ~1 and 41 pmol/kg, is within the wide range reported for global rivers, ~1 to ~240 pmol/kg (Table 5.2, 5.6). Re concentration in all the rivers measured in this study, except the Mandovi, are higher than that estimated for average global river water, 2.1 pmol/kg (Colodner et al., 1993). Re was not measured in the Hooghly river, however, the intercept of the salinity versus Re concentration plot of this estuary yield a riverine Re concentration of 5.2 pmol/kg, similar to the values reported for the headwaters of the Ganga at Rishikesh, 5.3 pmol/kg, (Dalai et al., 2002) but lower than that reported for the Ganga at Arichaghat, 9.1 pmol/kg (Colodner et al., 1993). Re in the Narmada and the Tapi rivers are in the range of 4.1 to ~15 pmol/kg (Table 5.1). Temporal variation in dissolved Re in the Narmada river indicates the impact of dilution during monsoon. The major lithology of these river basins is Deccan basalts, which is known to be quite low in Re (Allegre et al., 1999, Wimpenny et al., 2007). Therefore, moderately high Re in these rivers has to be from other sources, one likely candidate being weathering of organic matter rich shales present in the Vindhya through which these rivers flow. The high Re in the Mahi, Vishwamitri and the Sabarmati rivers, 18-41 pmol/kg (Table 5.2) is unlikely to be sourced from the Aravalli granites (equivalent to the Lesser Himalayan Granites having Re concentration ~26 pg/g; Dalai et al., 2001), major lithology of the basin, and the alluvial tracts through which they flow, as they are expected to be low in Re. This brings out the potential role of minor lithologies in these basins rich in Re and anthropogenic sources in contributing to their high Re. The low Re in the Mandovi river is consistent with the lithology of its basin which is dominated by laterites.

Re concentrations in the open ocean end member of the Mahi estuary and in the Ghogha coast samples (Fig. 2.5) are high and range from 129 to 208 pmol/kg (Table 5.2). Similarly, Re is also quite high, 175 and 178 pmol/kg, in the industrial waste waters. The highest Re concentration, 695 pmol/kg, was measured in the sample collected from a salt marsh near Bhavnagar. Three open ocean surface water samples collected off the Goa coast have Re concentration in

range of 40.4 to 41.0 pmol/kg, nearly identical to those reported for the open Pacific ocean (Anbar et al., 1992).

Unlike Mo and U, Re display conservative behaviour in the salt marsh, i.e., its enrichment in the marsh is commensurate with increase in salinity (Table 5.2). The available results of Mo, Re and U in the salt marsh sample analyzed in this study show very contrasting behavior; gain and loss of Mo and U respectively with Re behaving conservatively. More systematic study of these elements is required in this salt marsh to understand their behaviour properly.

### **5.2.2 Dissolved Mo, U and Re in estuaries**

Dissolved Mo, U and Re concentration in the estuaries of the Hooghly in the Bay of Bengal and the Mahi, Narmada, Tapi and the Mandovi estuaries in the Arabian Sea are analysed in this study (Table 5.1). Behaviour of Mo, U and Re in the four estuaries analysed in this study are highly variable. Mo and Re were analysed for the first time in the Indian estuaries.

#### **(a) *Molybdenum***

Available results on Mo in estuaries show both conservative and non-conservative behaviour, for example; in the Southampton estuary (Head and Burton, 1970) removal of Mo was observed during spring season which was attributed to its biological utilization and/or sequestration by organic matter. Similarly, loss of Mo was reported from the coastal waters of Wadden Sea (Dellwig et al., 2007) which was ascribed to its incorporation into sediment aggregates formed in the oxygen depleted zone. In contrast, in the Chao Phraya estuary (Dalai et al., 2005) and near shore surface sea waters of the North Wales (Jones, 1974) show addition of Mo in mid salinity waters resulting either from its desorption from particulate material (Jones, 1974) or to its supply due to interaction of bottom reducing sediments with overlying oxic water (Dalai et al., 2005). Oxygen from bottom oxic water penetrates the sediments causing release of Mo and other redox sensitive trace elements (U and Re) to the pore water and subsequently to the bottom water (Morford et al., 2007).

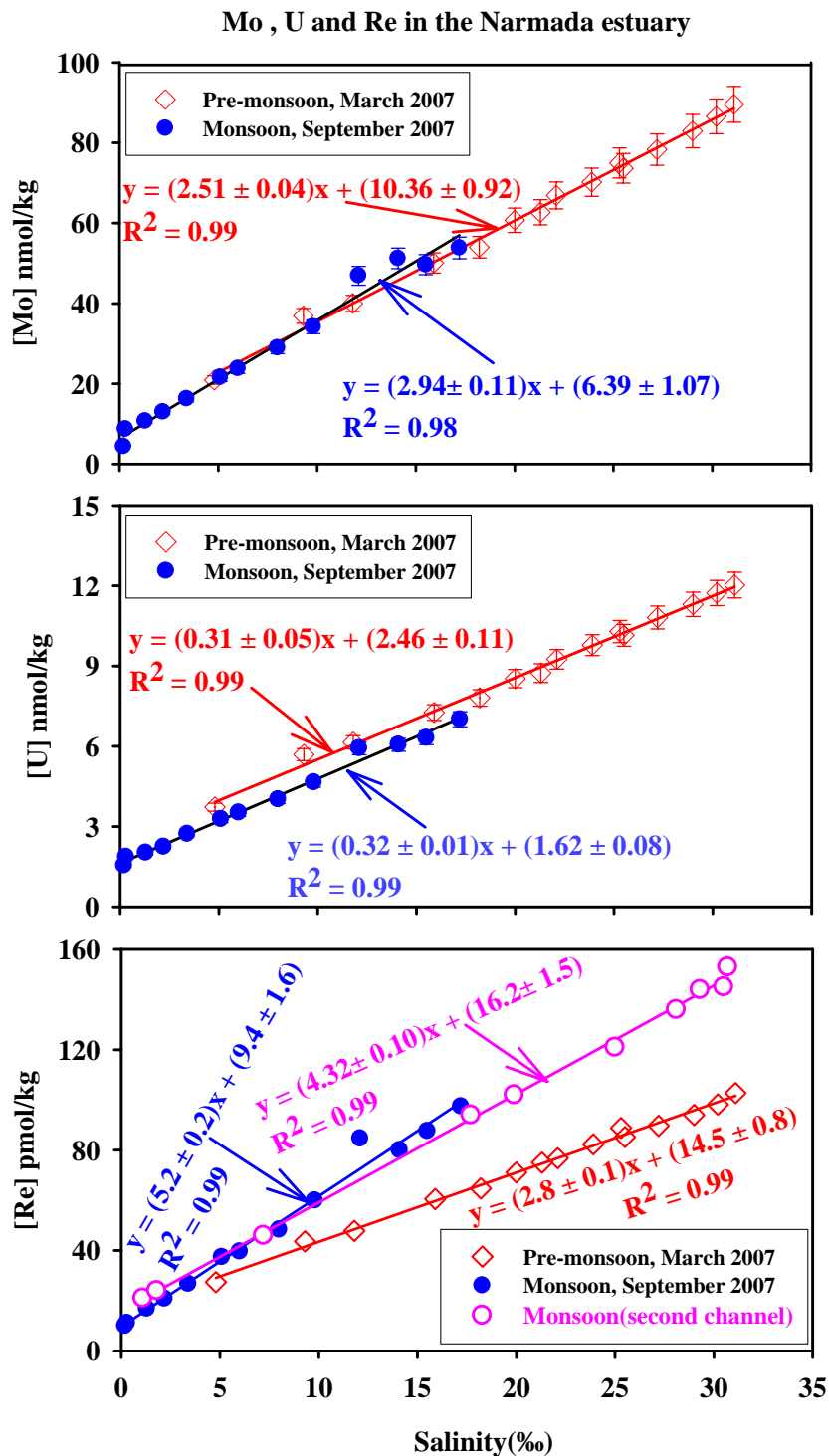


**Fig: 5.2 Molybdenum, Uranium and Rhenium vs. salinity plots in the Narmada estuary for monsoon and pre-monsoon seasons. Both Mo and U show conservative behaviour in this estuary. Seawater endmembers concentrations of U and Mo in this estuary obtained from the best fit lines of the data are nearly the same as those reported and measured in the Arabian Sea.**

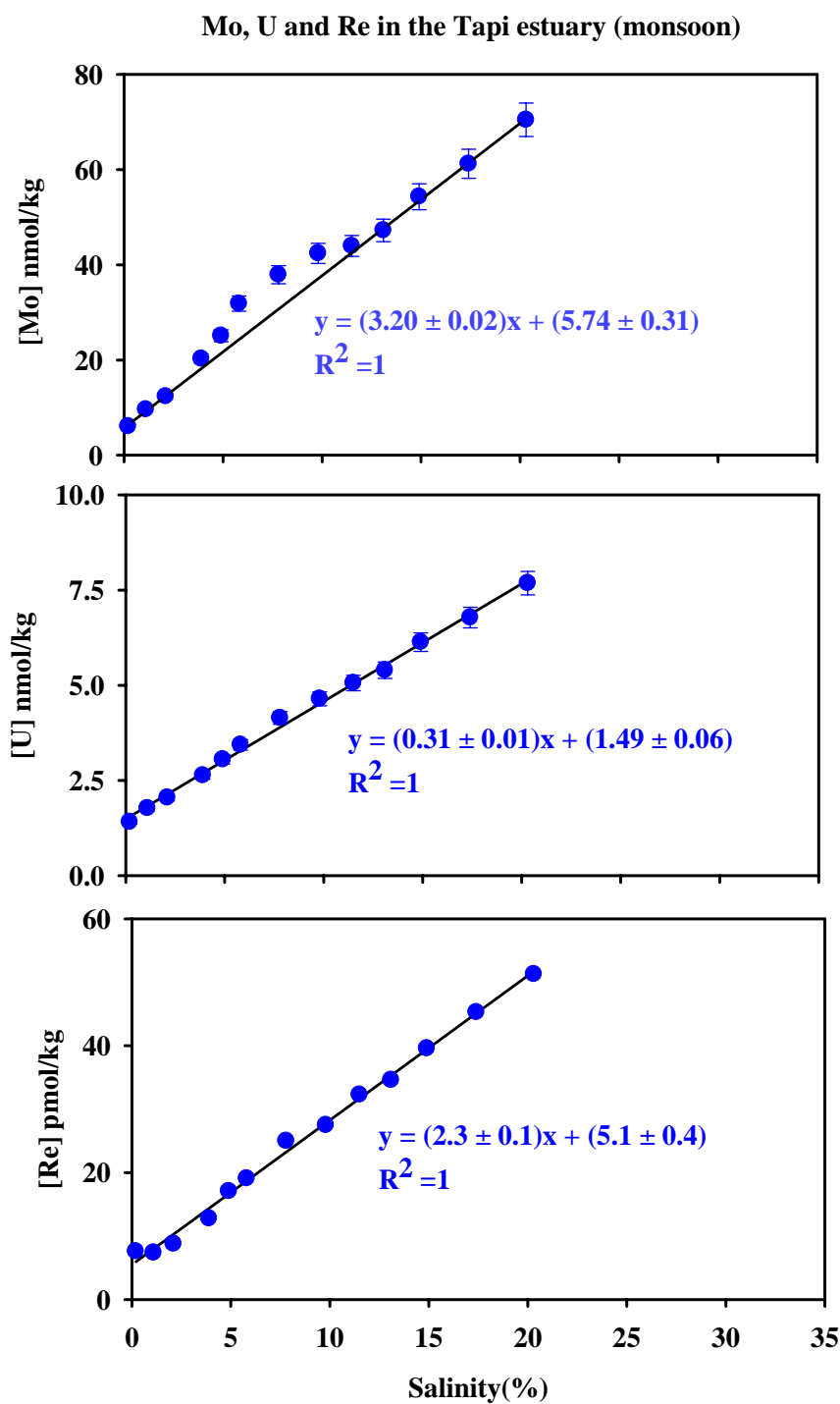


**Fig. 5.3 Mo, U and Re Vs. salinity in the Tapi estuary. Mo shows a gain in the salinity range of ~4 to 12 ‰ in this estuary. Effluent discharge from a steel plant situated in the vicinity of this estuary seems to be the source for Mo “bulge”. The best fit line is based on data in the 0.0-1.1 and 13.1-20.3 ‰ (i.e. excluding the bulge). U and Re shows conservative behaviour in this estuary.**

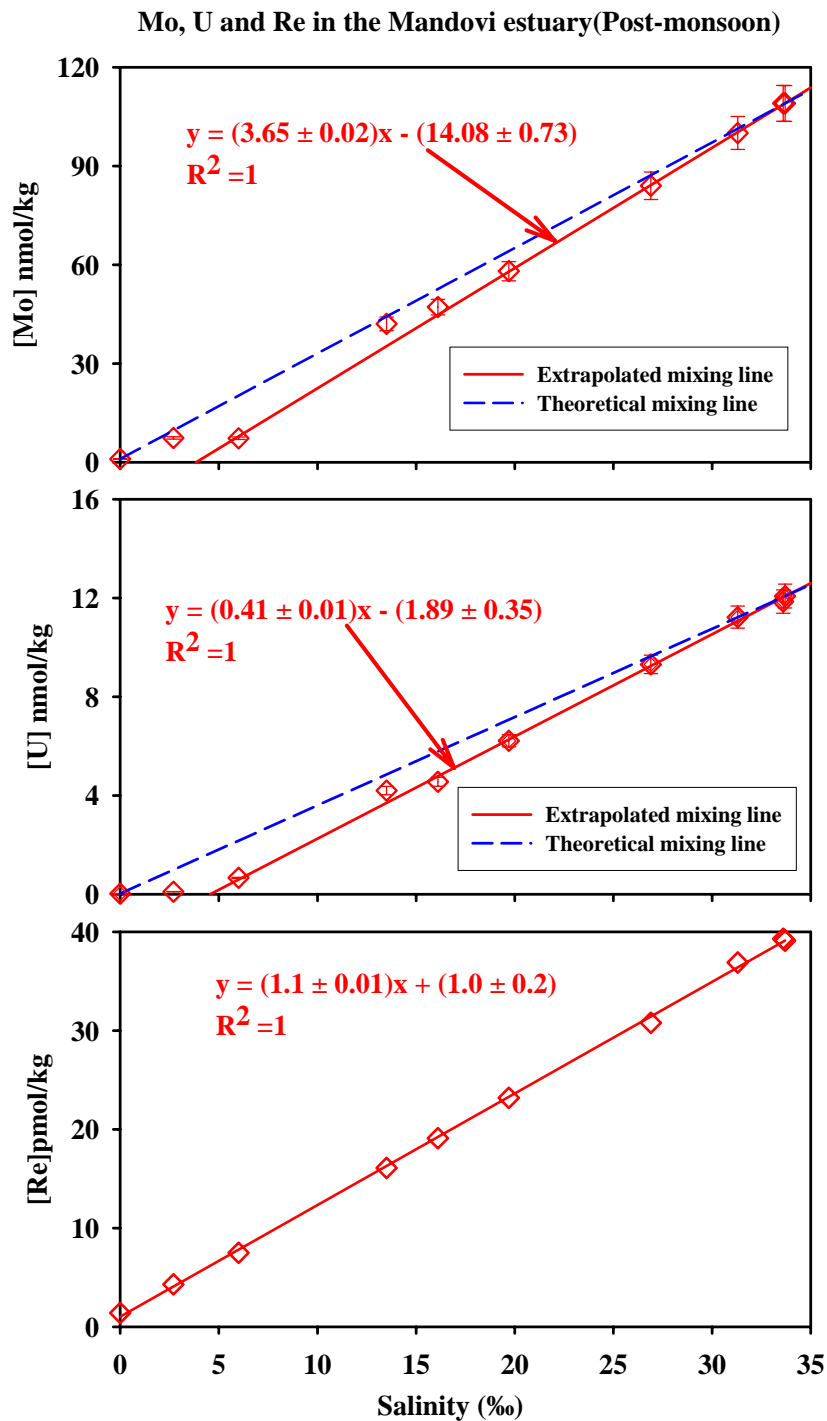


**Fig. 5.4** Mo, U and Re distribution in the Mandovi estuary. Theoretical mixing line is drawn by joining the river and sea water end member assuming conservative mixing and the ‘extrapolated mixing line’ drawn by extrapolating of the linear segment of the higher salinity data points to river end members. Both these elements show removal in the lower salinity range. The equations of the extrapolated mixing lines of Mo and U are based on five data points from 19.7 - 33.7‰.

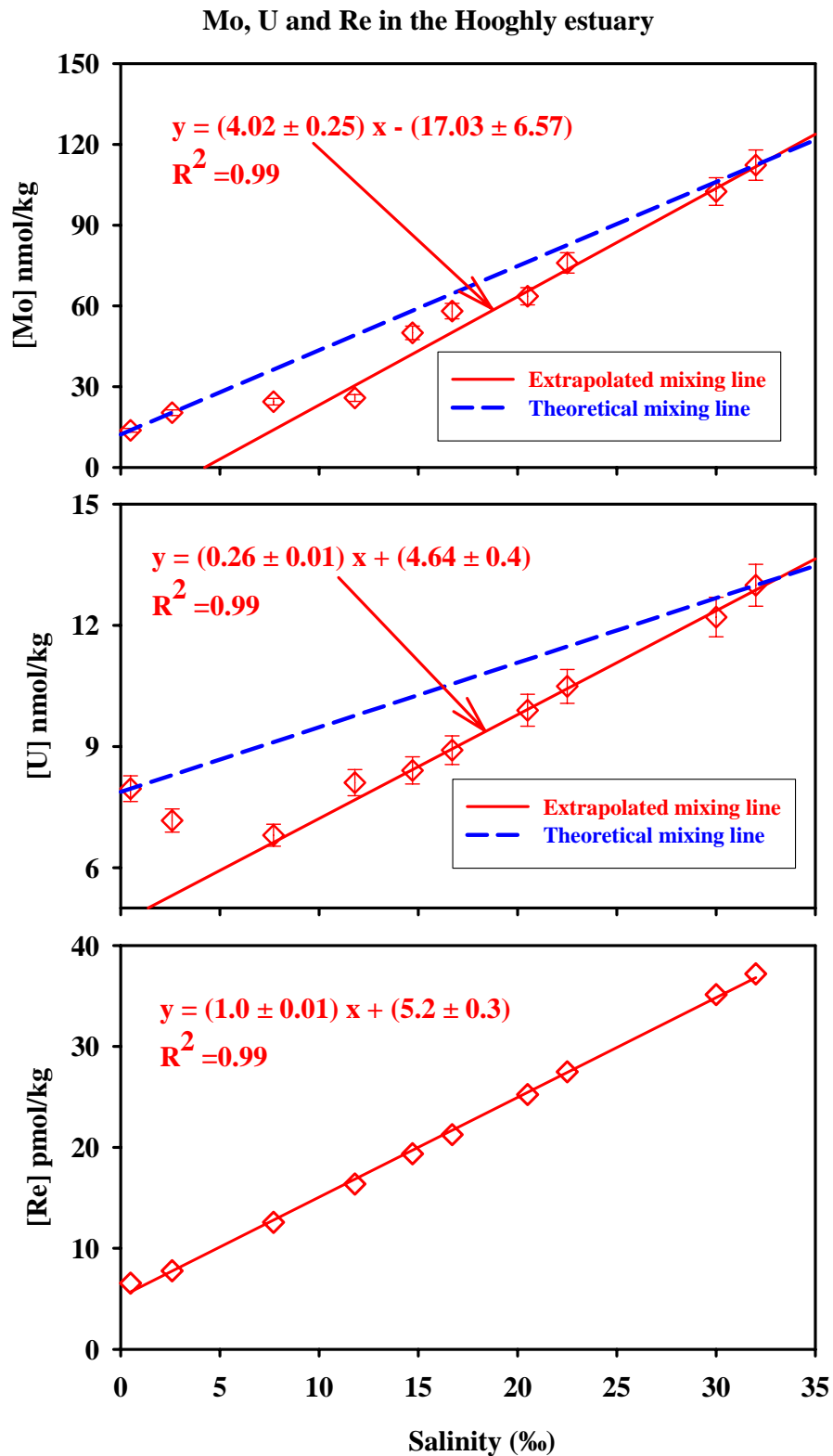


**Fig. 5.5 Mo, U and Re in the Hooghly estuary. Mo, U show removal in the low and mid salinity range, analogous to that in the Mandovi (Fig. 5). Mo loss is much higher compared to its riverine supply. The equation is based on four data points beyond 20‰ salinity. Re behaves conservatively.**

**Table 5.3: Properties of best fit lines and estimates of U, Mo and Re concentration at 0‰ and 35‰ salinity based on estuarine data**

| Estuary                                 | Riverine concentration | Re concentration from best fit lines*<br>at salinity                       |             | Equation for best fit lines*     | R <sup>2</sup> |
|---|------------------------|--|-------------|----------------------------------|----------------|
|   |                        | 0 (‰)  | 35 (‰)      |                                  |                |
| <b><u>Mo (nmol/kg) in estuaries</u></b> |                        |  |             |                                  |                |
| Narmada (Pre-monsoon)                   | 2.3-2.6                | 10.36±0.92   | 98.21±2.32  | y = (2.51±0.04) x + (10.36±0.92) | 0.99           |
| Narmada (Monsoon)                       | 2.9-4.3                | 6.39±1.07  | 109.29±4.92 | y = (2.94±0.11) x + (6.39±1.07)  | 0.98           |
| Tapi (Monsoon)                          | 3.6-6.1                | Non-conservative behaviour; gain of Mo in the lower salinity (3.9 - 11.5‰) |             |                                  |                |
| Mandovi(Post-monsoon)                   | 1                      | Non-conservative behaviour; removal of Mo in the lower salinity (~0-15‰)   |             |                                  |                |
| Hooghly ( Premonsoon)                   | ~13.8                  | Non-conservative behaviour; removal of Mo in the lower salinity (~3-12‰)   |             |                                  |                |
| <b><u>U (nmol/kg) in estuaries</u></b>  |                        |  |             |                                  |                |
| Narmada (Pre-monsoon)                   | 1.4                    | 2.46±0.11  | 13.31±1.86  | y = (0.31±0.05) x + (2.46±0.11)  | 0.99           |
| Narmada (Monsoon)                       | 1.2-1.5                | 1.62±0.08  | 12.82±0.43  | y = (0.32±0.01) x + (1.62±0.08)  | 0.99           |
| Tapi (Monsoon)                          | 1-1.4                  | 1.49±0.06  | 12.34±0.41  | y = (0.31±0.01) x + (1.49±0.06)  | 0.99           |
| Mandovi(Post-monsoon)                   | 0.02                   | Non-conservative behaviour; removal of Mo in the lower salinity (~0-15‰)   |             |                                  |                |
| Hooghly ( Premonsoon)                   | ~8.0                   | Non-conservative behaviour; removal of Mo in the lower salinity (~3-12‰)   |             |                                  |                |
| <b><u>Re(pmol/kg) in estuaries</u></b>  |                        |  |             |                                  |                |
| Narmada (Pre-monsoon)                   | 13.1                   | 14.5±0.8   | 113±4       | y = (2.8±0.10) x + (14.5±0.8)    | 0.99           |
| Narmada (Monsoon)                       | 8.5                    | 9.4±1.6  | 191±7       | y = (5.2±0.20) x + (9.4±1.6)     | 0.99           |
| Narmada (Monsoon)-<br>Second Channel    | -                      | 16.2±1.5   | 167±4       | y = (4.3±0.10) x + (16.2±1.5)    | 0.99           |
| Tapi (Monsoon)                          | 4.1                    | 5.1±0.4  | 85.5±3.5    | y = (2.3±0.10) x + (5.0±0.4)     | 0.99           |
| Mandovi(Post-monsoon)                   | 1.4                    | 1.0±0.2  | 39.5±0.4    | y = (1.1±0.01) x + (1.0±0.2)     | 1              |
| Hooghly ( Premonsoon)                   | -                      | 5.2±0.3  | 40.2±0.5    | y = (1.0±0.01) x + (5.2±0.3)     | 0.99           |

The bottom waters upwell to the surface causing an addition of Mo (Dalai et al., 2005). In this study, Mo distribution has been measured in four estuaries of India, these are discussed in detail in the following section.

The results of Mo distribution in the Narmada estuary during both pre-monsoon (March 2007) and monsoon (September 2007) are given in Table 5.1. Monsoon sampling could be done only upto salinity of  $\sim 17\text{‰}$  due to highly turbulent sea. Dissolved Mo distribution shows conservative mixing of sea water and river water end members ( $r^2 = 0.99$ ) during both these seasons. In monsoon season, two samples at salinities 12.1 and 14.1‰ lie above the mixing line (Table 5.1, Fig. 5.2). The sample with salinity 12.1‰ also has unusually high concentrations of Mo, U and Re. The Mo-salinity lines (Fig. 5.2, Table 5.3) provide Mo concentration of  $98 \pm 2$  and  $109 \pm 4$  nmol/kg for 35‰ salinity seawater endmember during pre-monsoon and monsoon respectively. These values are within the range measured for the Arabian Sea in this study  $101 \pm 1$  (Table 5.2) and reported for other ocean basins (Morris, 1975; Collier, 1985; Quiby-Hunt and Turekian, 1983). The conservative nature of Mo in the Narmada estuary is also consistent with distribution of Mo/Al in suspended phase with salinity as discussed later in section 5.3.

In the Tapi estuary, Mo increases with salinity (Table 5.1, Fig. 5.3) with a 'bulge' in 3.9 to 11.5‰ salinity range. This 'bulge' represents gain of Mo and suggests that it has an additional source in this salinity range. The gain ranges from 4 to 32% with respect to conservative mixing (Fig. 5.3). The additional source for Mo can be (i) its desorption from particles in the estuary as has been suggested for the Southampton river (Jones, 1974) (ii) supply of Mo from bottom sediments (Dalai et al. 2005; Morford et al. 2007). Development of seasonal oxygen minimum zone along the western Indian continental shelf (Naqvi et al, 2000) can sequester Mo into sediments which can be later released to bottom water as the sediments come in contact with oxic waters (Morford et al., 2007). Intense upwelling during the southwest monsoon in this region can bring high Mo from the bottom water to the surface causing the observed hump. However, this type of hump is not observed in other estuaries situated nearby, going against the above hypothesis. Further, the Mo bulge in the Tapi estuary coincides with an

increase in alkalinity. The likely cause for the increase in both Mo and alkalinity in this salinity range is their supply from a major steel plant along with a lime plant situated in the vicinity of this salinity range. Mo is used in steel manufacturing as a hardening agent. Discharge from these steel and lime plants can explain the increase in both Mo and alkalinity in the Tapi estuary.

Mo in the Hooghly and the Mandovi estuaries shows significant loss in the lower salinity range (Figs. 5.4, 5.5) in contrast to the Narmada and the Tapi estuaries data. A number of factors can contribute to the observed loss of Mo in these two estuaries. These include Mo complexation with organic matter, development of anoxic conditions within the particulate aggregates (Dellwig et al., 2007) and uptake of Mo from water by reducing sediments of salt marshes and mangrove forest. Such mechanisms have been reported for the loss of U in the estuaries of the lower Meghna (Ganga-Brahmaputra, Carroll and Moore, 1993), in the Delaware (Sarin and Church, 1994; Church et al. 1996) and in the Savannah (Windom et al., 2000). However, the observation that Re which is more susceptible to reducing condition (Colodner et al., 1993) behaves conservatively in the Hooghly and the Mandovi estuaries (as discussed later in this chapter and in Rahaman and Singh, 2010) challenges the importance of reductive removal of dissolved Mo. These results, therefore has to be explained by a mechanism that can preferentially remove U and Mo from solution without affecting the distribution of Re such as the selective incorporation of Mo and U to Fe-Mn hydroxides (Crusius et al., 1996; Morford and Emerson, 1999; Morford et al., 2005).

Isotope composition of dissolved Mo in the Hooghly and the Mandovi could provide additional clues to characterize the Mo removal processes in these estuaries. There is significant fractionation of Mo isotopes during its sequestration into Fe-Mn hydroxide,  $\delta^{98/95}\text{Mo}$  in the Fe-Mn hydroxide gets depleted by about 3‰ (Siebert et al., 2003) with respect to seawater leaving the later enriched. However, there is little or no fractionation of Mo isotopes during its sequestration to sediments in reducing condition (Siebert et al., 2003). It implies that if Mo in these estuaries are being lost with Fe-Mn hydroxide, corresponding seawater Mo will be enriched while there will be no impact on dissolved Mo in estuary if

reducing condition is responsible for its loss. Therefore isotope composition of dissolved Mo in the estuary holds potential to identify the process of Mo removal in them.

**(b) Uranium**

The distribution of U in estuaries has been extensively studied, the available data suggest its complex nature in the estuaries that is difficult to generalise (see Windom et al., 2000; Swarzenski et al., 2003; McKee et al., 2008 for reviews). The processes that regulate the temporal and spatial variations in the behaviour of uranium in estuaries are not well understood. Various mechanisms have been suggested for the removal or addition of uranium in estuaries. Adsorption by sediment plumes, precipitation with iron and manganese, flocculation with organic matter and reduction in organic matter rich sediments are some of the processes suggested for its removal whereas release from bottom sediments under oxic conditions and desorption from particulates are some of the processes proposed as additive processes of uranium.

U versus salinity plots for both the seasons in the Narmada estuary (Fig. 5.2) show conservative mixing ( $R^2=0.99$ ) with nearly identical slopes  $0.31 \pm 0.11$  and  $0.32 \pm 0.1$ . The conservative mixing of U in the Narmada estuary is consistent with the results of Borole et al. (1982). However, their study hinted at a slight removal of U in the lower salinity region of this estuary, which is not observed in this work. The conservative behaviour of U in the Narmada estuary is similar to that of other redox sensitive elements, Re and Mo measured in this estuary. Based on the best fit lines of Fig. 5.2, the extrapolated dissolved uranium concentration at 35‰ salinity corresponds to  $13.2 \pm 0.4$  and  $12.8 \pm 1.8$  nmol/kg (Table 5.3), for the two seasons and are within the range for average global sea water  $\sim 13.6$  nmol/kg (Ku et al., 1977), the Arabian seawater  $13.44 \pm 0.84$  nmol/kg (Rengarajan et al., 2003) and measured in this study offshore Goa  $12.8 \pm 0.2$  nmol/kg (Table 5.2).

Uranium in the Tapi estuary is also conservative as evident from the U-salinity plot (Fig. 5.3). The riverine and seawater uranium in the Tapi estuary estimated based on the Fig. 5.3 are  $1.5 \pm 0.1$  and  $12.3 \pm 0.4$  nmol/kg respectively. The marine U of the Tapi estimated from the mixing line is nearly same as that

measured directly in the seawater endmember and with that of the Arabian Sea water off Goa. In the Hooghly estuary, significant loss of U is observed (Fig. 5.5).

The overall trend of U distribution in the Narmada, Tapi and the Hooghly estuaries are similar to those reported earlier in them (Borole et al., 1982; Somayajulu et al., 1994). The Mandovi estuary is studied for the first time which shows U removal in low salinities (Fig. 5.4) similar to its behaviour in the Hooghly estuary (Fig. 5.5).

### **(c) Rhenium**

The dissolved Re concentration in the estuaries along with salinity are given in Table 5.1. In the Narmada estuary, Re ranges from 13.1 to 103 pmol/kg over the salinity range of ~0 to 31 ‰ during pre-monsoon and from 8.5 to 97 pmol/kg in the salinity range of ~0 to 17.2 ‰ during monsoon (Fig. 5.2). A similar distribution of Re with salinity is also seen in the second channel of the Narmada which was sampled during the monsoon of 2008 (Table 5.1, Fig. 5.2). Re concentrations in the Tapi estuary range from 4 to 51 pmol/kg corresponding to salinity 0 to 20.3 ‰ (Fig. 5.3). In the west coast, Mandovi estuary flowing through the Western Ghats of the Indian peninsula has the lowest range of Re concentration. In the estuary, it varies from 1.4 to 39.3 pmol/kg between salinities 0 to 33.6 ‰ (Table 5.1, Fig. 5.4). In the Hooghly estuary, Re varies from 6.6 to 37.2 pmol/kg between 0.5 and 32 ‰ salinity (Fig. 5.5).

Re distribution in the estuaries as a function of salinity are plotted in Figs. 5.2, 5.3, 5.4 and 5.5. The data show nearly perfect linear trends ( $R^2=0.99-1.0$ ). These results suggest that Re behaves conservatively in all the estuaries studied in this work. The equations for the best fit lines of the data along with their intercepts which represent Re concentration in '0' ‰ salinity water, are given in Table 5.3. Re in the seawater end members of these estuaries at 35 ‰ salinity, calculated using the best fit line, are also given in Table 5.3. The conservative behaviour of Re in the estuaries studied, differs from those reported for the Amazon (Colodner et al., 1993) and the Hudson estuaries (Walker and Peucker-Ehrenbrink, 2004), where a marginal addition of Re in the lower and middle salinity region is reported. Re measured in sediments of the Amazon river

and its shelf, however, do not confirm its loss from the shelf sediment to the water (Breckel et al., 2005). The difference in the behaviour of Re in different estuaries can result from a variety of reasons or their combinations that include the nature and composition of the particles in these estuaries, Eh-pH conditions, biological productivity and fate of organic matter and Fe-Mn oxide in sediments and submarine ground water discharge. This study along with those available in literatures on the Mandovi (Fig. 5.4), the Hooghly (Fig. 5.5; Somayajulu, 1994) and the Meghna estuaries (combined Ganga and the Brahmaputra rivers in Bangladesh, Carroll and Moore, 1993) show that U and Mo behave non-conservatively in them, unlike the conservative behaviour of Re observed for the Hooghly and the Mandovi in this work. Local anoxia resulting either from extensive mangrove forest cover in the mixing zone (Carroll and Moore, 1993) or due to pollution (Somayajulu et al., 2002) has been suggested as a potential cause for uranium loss in these estuaries. The contrasting behaviour of U, Mo and Re in the Hooghly estuary is puzzling, especially as Re is relatively more or equally redox sensitive, i.e. it gets incorporated in reducing sediments with more or equal efficiency, compared to U and Mo (Colodner et al., 1993, 1995; Crusius et al., 1996; Morford et al., 2007, 2009). The behaviour of both uranium (Borole et al., 1982) and rhenium in the Narmada and the Tapi estuary are conservative.

The correlation coefficients,  $R^2$  of the best fit lines of Re versus salinity plots for all the estuaries are  $>0.99$  suggestive of almost perfect conservative mixing lines. The slopes and intercept of these lines, however, vary significantly. Re concentrations of rivers based on the intercept of the best fit lines are quite similar to those measured in the rivers (Table 5.3). The surprising results, however, are that the Re concentration of seawater at 35‰ salinity in the Gulf of Cambay calculated based on the best fit lines of the Narmada and the Tapi estuarine data are much higher than those reported for global open ocean water and those observed for the Hooghly and the Mandovi estuaries. The seawater end members of Re concentration for the Hooghly and the Mandovi estuaries are  $40.2 \pm 0.5$  and  $39.5 \pm 0.4$  pmol/kg respectively, nearly the same within uncertainties as the values reported for open Pacific and Atlantic oceans (Anbar et al., 1992; Colodner et al., 1993) and to those measured in this study for the Arabian Sea off

the Goa coast (Table 5.2). These results suggest that the Bay of Bengal and the Arabian Sea have Re concentration similar to those reported for other oceanic regions (Anbar et al., 1992; Colodner et al., 1993) and confirms the suggestion that, in general, the global oceans are well mixed for Re. However, there are pockets of the global ocean, such as the Gulf of Cambay where dissolved Re concentration differs significantly from 'typical' oceanic values, due to regional processes.

### 5.3 Particulate Mo, U and Re in estuaries

Mo and U were measured only in the non-monsoon samples of suspended sediments from the Narmada estuary, whereas, Re was measured in both monsoon and pre-monsoon samples. Few samples of bank sediments from the Narmada and Tapi estuaries were measured for Re only. Mo concentrations in the suspended loads during pre-monsoon in the Narmada estuary range from 5.7 to 9.7 nmol/g with an average of  $8.1 \pm 1.1$  nmol/g, twice the average continental crustal abundance of 4.2 nmol/g (Manheim and Landergren, 1978). Average U in suspended load of pre-monsoon samples from the Narmada estuary is 6.9 nmol/g with a narrow range of 6.7 to 7.2 nmol/kg and similar to those reported earlier (Borole et al., 1982). The observation that Mo and U do not show any systematic trend with salinity seem to indicate that there are no loss or gain of Mo and U mediated by these particles (Fig. 5.6) in the salinity range (4.8 ‰ to 28.5‰).

The Re abundance in suspended particulate matter in the estuary mixing zone does not show any systematic trend with salinity in the Narmada estuary (Fig. 5.6). Re concentration in the suspended loads is generally uniform at  $\sim 1.3$  pmol/g with few of them having higher concentrations. The values are in general lower than that of the average continental crust. The variations in the Re contents of suspended matter are probably natural arising due to source variability. Re/Al versus salinity plot also does not show any discernible trend, ruling out any possibility of impact of size sorting on variation in Re content of suspended loads. The Re abundance in suspended matter does not show any systematic trend with salinity which independently rules out the possibility of any loss or gain of Re by or to these particles.

**Table 5.4: Re, Mo, U, organic carbon and Al in suspended and bed/bank sediments of the Narmada and Tapi estuaries**

| Sample   | Salinity<br>(‰) | [Al] | C <sub>Organic</sub><br>wt% | [Mo]   | [U]  | [Re]   |
|--|-----------------|------|-----------------------------|--------|------|--------|
|  |                 |      |                             | nmol/g |      | pmol/g |
| <b>Suspended sediments</b>                             |                 |      |                             |        |      |        |
| <b><u>Narmada Estuary(Pre-monsoon, March 2007)</u></b> |                 |      |                             |        |      |        |
| NESS-1   | 4.8             | 9.06 | 1.02                        | 9.7    | 6.83 | 1.54   |
| NESS-2   | 9.3             | 8.33 | 0.82                        | 5.7    | 6.69 | 1.87   |
| NESS-3   | 11.8            | 8.59 | 1.03                        | 8.8    | 6.89 | 1.33   |
| NESS-5   | 18.2            | 8.89 | 0.81                        | 8.0    | 6.87 | 1.17   |
| NESS-6   | 20              | 8.51 | 0.84                        | 7.3    | 7.05 | 1.2    |
| NESS-7   | 21.3            | 8.28 | 1.32                        | 7.9    | 7.06 | 1.26   |
| NESS-8   | 22.1            | 8.52 | 0.82                        | 7.6    | 6.98 | 1.24   |
| NESS-9   | 23.9            | 8.35 | 0.7                         | 9.4    | 6.73 | 1.48   |
| NESS-10  | 25.3            | 8.19 | 0.64                        | 7.7    | 6.89 | 1.16   |
| NESS-10R   | 25.3            | 8.21 | 0.64                        | 8.1    | 6.94 | 1.25   |
| NESS-11  | 25.5            | 9.04 | 0.63                        | 8.9    | 7.22 | 1.22   |
| <b><u>Narmada Estuary (Monsoon, July 2007)</u></b>     |                 |      |                             |        |      |        |
| NEMS-2   | 0               | -    | 0.13                        | -      | -    | 1.79   |
| NEMS-3   | 1.3             | -    | 0.84                        | -      | -    | 1.11   |
| NEMS-5   | 3.4             | -    | 0.77                        | -      | -    | 1.77   |
| NEMS-6   | 5.1             | -    | 0.87                        | -      | -    | 1.14   |
| NEMS-8   | 8               | -    | 0.97                        | -      | -    | 1.17   |
| NEMS-10  | 12.1            | -    | 1.1                         | -      | -    | 1.03   |
| NEMS-11  | 17.2            | -    | 0.94                        | -      | -    | 1.26   |
| NEMS-13  | 9.8             | -    | 0.89                        | -      | -    | 1.1    |
| NEMS-13R   | 9.8             | -    | -                           | -      | -    | 1.16   |
| <b><u>Tapi Estuary(Monsoon, July 2007)</u></b>         |                 |      |                             |        |      |        |
| TPMS-10  | 13.1            | -    | 0.99                        |        |      | 0.97   |
| <b><u>Bed sediments</u></b>                            |                 |      |                             |        |      |        |
| <b><u>Narmada</u></b>                                  |                 |      |                             |        |      |        |
| NE(BS)-1   | -               | -    | -                           | -      | -    | 2.29   |
| NE(BS)-8   | -               | -    | -                           | -      | -    | 2.59   |
| <b><u>Tapi</u></b>                                     |                 |      |                             |        |      |        |
| TP(BS)-1   | -               | -    | -                           | -      | -    | 2.85   |
| TP(BS)-4   | -               | -    | -                           | -      | -    | 3.51   |
| TP(BS)-12  | -               | -    | -                           | -      | -    | 15.42  |
| TP(BS)-12R   | -               | -    | -                           | -      | -    | 15.28  |

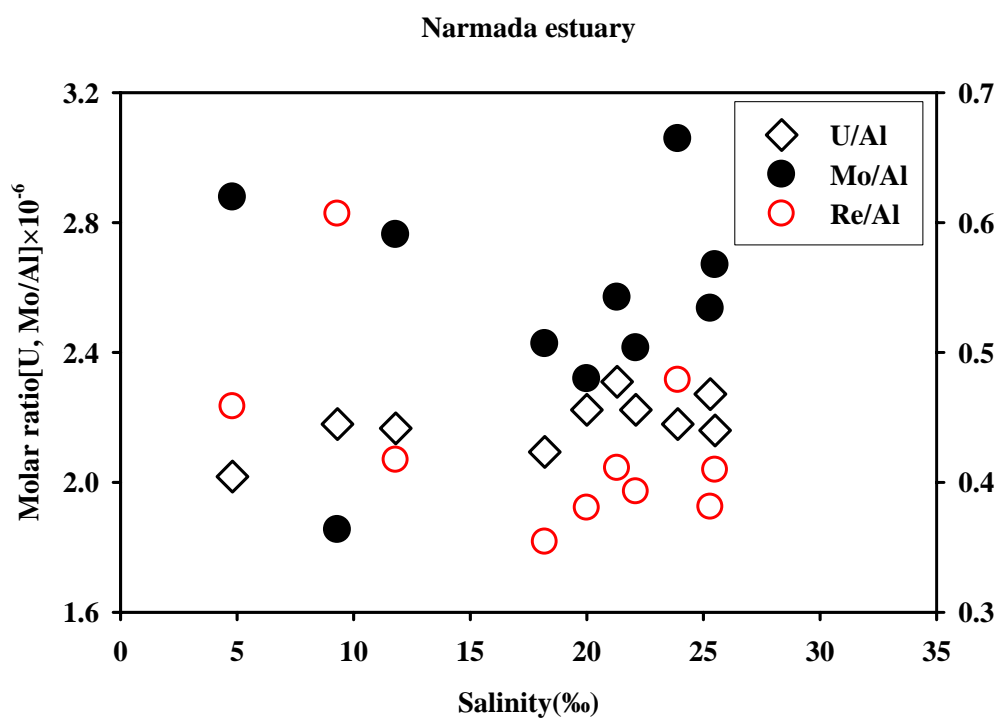


**Fig. 5.6 Mo/Al, U/Al of suspended load vs. salinity in the Narmada estuary. The U/Al varies within narrow range, whereas Mo/Al shows large scatter. The data however do not seem to show very systematic trend suggesting that both Mo and U are not being adsorbed on or being released from these particles in this estuary.**

Further, there is no relation between Mo, U and Re concentrations with the organic carbon content of the suspended load (Fig. 5.7) indicating their variabilities in these sediments related to their sources and not due to sequestration of Re in organic matter. Bank and bed sediments of the Narmada and the Tapi estuaries have higher concentration of Re compared to suspended loads. It could be due to loss of Re during weathering of suspended sediments or could be due to extensive evaporation of seawater in the bank and bed loads enhancing Re in them.

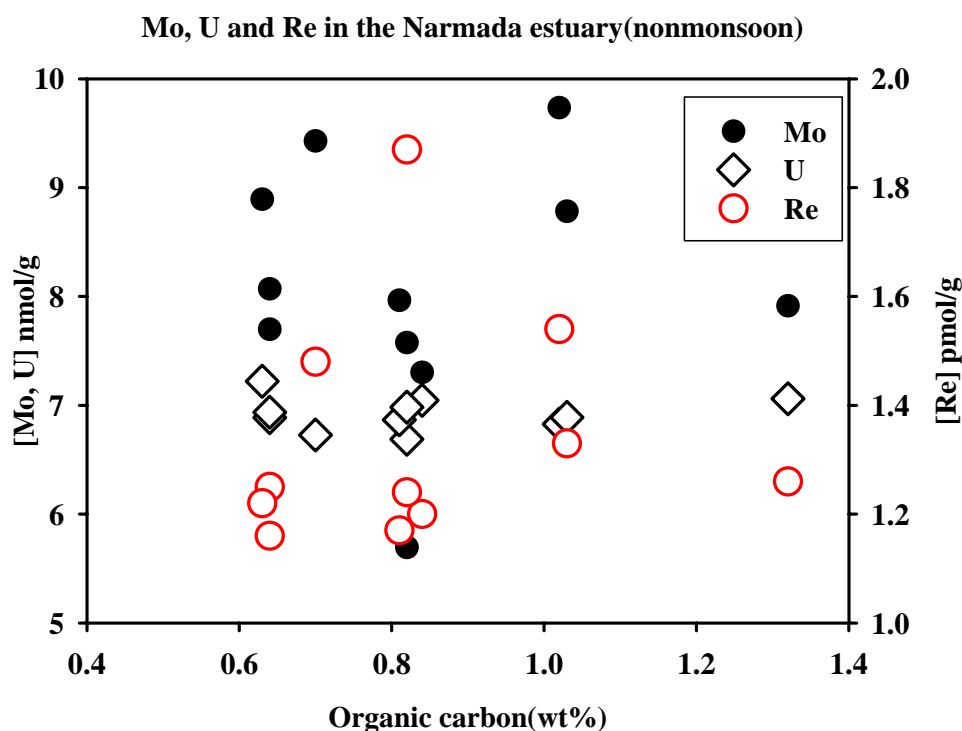


**Fig. 5.7 Scatter diagram of Mo, U and Re concentration in suspended matter of the Narmada versus their organic carbon abundance do not show any systematic trend during both monsoon and pre-monsoon seasons.**

#### **5.4 Comparative behaviour of U, Mo and Re in estuaries**

U, Mo and Re, all these three elements are sensitive to redox condition in the ocean with sediment deposition in reducing environment as one of their important sinks. However, affinity of all these three elements with prevailing reducing condition is not the same. Re has either higher or equal affinity compared to U to reducing condition whereas Mo is the least influenced by redox condition among them.

Current study indicate the loss of U and Mo in the Ganga and the Mandovi estuaries but Re is perfectly conservative in them (Rahaman and Singh, 2010). Mo/Re and U/Re in all the estuaries studied here are plotted with salinity in Figs. 5.8. In perfectly conservative environment in the estuary, both Mo/Re and U/Re should show an exponential mixing with salinity between river and seawater endmembers. Any deviation from the theoretical mixing lines could result from either addition or removal of these elements in the estuary.

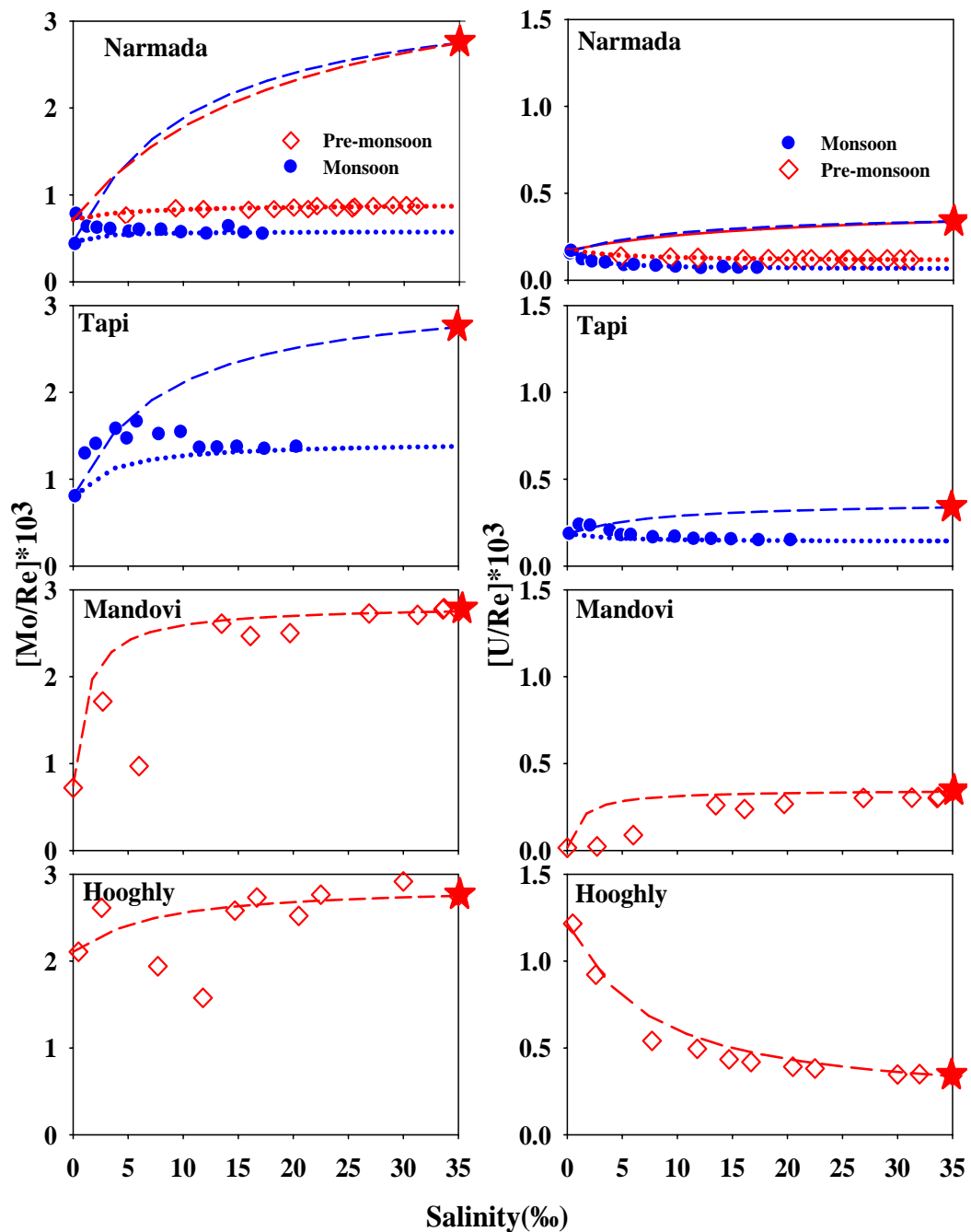


Fig. 5.8 Mo/Re and U/Re vs. salinity distribution. Seawater endmembers of U/Re and Mo/Re (★) is for the open ocean. Theoretical mixing lines (TML) between riverine and global ocean endmembers represent dashed lines. Dotted lines show the TML between riverine endmembers and the observed marine endmembers in the estuaries of the Narmada and the Tapi. The Hooghly and Mandovi show loss of both Mo and U as they fall below the mixing lines in lower salinity ranges.

Seawater endmembers of U/Re and Mo/Re (★) is estimated based on the U, Re and Mo concentrations available for the open ocean (Fig. 5.8). Theoretical mixing lines between riverine and global ocean endmembers are also shown (dashed lines, Fig 5.8). Nature of the exponential mixing line will depend on the difference between river and seawater endmembers. Mo, Re and U are conservative in the ocean with long residence times (Colodner et al., 1993, McManus et al., 2006), therefore the marine endmembers of U/Re and Mo/Re are expected to be the same in all the estuaries and equals to global open ocean values of  $0.34 \times 10^3$  and  $2.75 \times 10^3$  for U/Re and Mo/Re respectively (Colodner et al., 1993; McManus et al., 2006, Ku et al., 1977). This assumption, however, is not valid in the Gulf of Cambay and the open ocean end members of the Narmada and the Tapi estuaries are lower because of significant input of anthropogenic Re (Rahaman and Singh, 2010). In these estuaries, U/Re and Mo/Re are only  $0.12 \times 10^3$  and  $0.87 \times 10^3$  respectively, much lower than that expected for open ocean. Their riverine endmembers however can differ depending on their concentrations in different rivers. The nature of the Mo/Re and U/Re in all the estuaries follows the same trend as Mo, U versus salinity plots, as Re behaves quite conservatively in all the estuaries, albeit its major supply from anthropogenic sources in the Gulf of Cambay (Rahaman and Singh, 2010). Though, the Mo/Re in the Tapi has a hump in low salinity region due to addition of Mo from anthropogenic activity. In the Hooghly and the Mandovi, both Mo/Re and U/Re show dips in lower salinity ranges suggesting either removal of Mo and U or addition of Re, considering the conservative nature of Re in these estuaries (Rahaman and Singh, 2010). The dips in mixing lines can be interpreted in terms of the loss of Mo and U compared to Re, and thus bring out differences in the behaviour among these elements.

### **5.5 Removal of U and Mo in the Hooghly and the Mandovi estuaries**

U and Mo concentrations in the Hooghly and the Mandovi estuaries show non-conservative behaviour in the lower salinity zone; from fresh water to ~20‰ salinity indicating loss of both U and Mo in them. The loss of U and Mo in the Hooghly and the Mandovi estuaries are estimated following the approach of Li

and Chan (1979), Maeda and Windom et al., (1982) and Swarzenski et al., (1995) and using the U, Mo vs. salinity relationship (Figs. 4, 5). The relevant relation is

$$\text{Total Loss} = Q(I - R) \dots\dots\dots(i)$$

where, Q is the water discharge, I is the intercept on the U and Mo concentration axis of the conservative mixing lines of the samples with salinities more than 20‰ (Figs. 5.4 and 5.5) and R is the observed riverine U and Mo concentration.

For the Hooghly estuary, both the uranium and molybdenum mixing lines in the salinity ranges 20-35‰ indicate linear trend, the extrapolation of which yield intercepts of +4.64 and -17.03 nmol/kg on U and Mo axis respectively compared to the riverine U and Mo concentration of 8 and 14 nmol/kg respectively (sample close to the river endmember). Negative intercept denotes the removal of U and Mo “in excess” of their riverine supply indicating removal of entire riverine supply along with some component of seawater also. Using the relation (i) and the water flux of 52 km<sup>3</sup>/y, U loss in the Hooghly estuary is estimated to be  $\sim 1.7 \times 10^5$  moles/y and that of Mo to be  $\sim 1.6 \times 10^6$  moles/y. Similar calculations for the Mandovi estuary yield loss of  $\sim 3 \times 10^4$  and  $2 \times 10^5$  moles/y for U and Mo respectively. In case of Mandovi estuary, both U and Mo removal are larger than riverine supply whereas in the Hooghly only Mo removal is more than its riverine supply. These estimates indicate that loss of Mo is one order of magnitude higher compared to that of U in both the Hooghly and the Mandovi estuaries. In fact, both the Hooghly and the Mandovi estuaries act as net sinks of Mo in which its removal is much higher compared to its riverine supply. In the Hooghly, 40% of the uranium supplied by the river is sequestered in the estuary itself and only  $\sim 60\%$  of it is transported to the open ocean. However, Mo removal in the Hooghly estuary is  $\sim 1.6 \times 10^6$  moles/y compare to the riverine supply of  $\sim 7.2 \times 10^5$  moles/y. This study indicates that in addition to the riverine Mo, a significant fraction of marine Mo is also being lost in the river-ocean mixing zone. Estuaries also remove significant amount of riverine uranium and in some cases they remove marine U too.

It is important to estimate the loss of uranium and Mo in the estuary zone to estimate their oceanic budget. Such loss of U has been estimated and

considered to some extent in determining the oceanic uranium budget (e.g. Dunk et al., 2002). However, in case of Mo, its loss related to the estuaries needs to be estimated on global scale for proper determination of its sources and sinks pertaining to its oceanic budget. This will help in estimating the oceanic residence time of Mo for its appropriate usage as tracer of oceanographic processes.

### **5.6 Mo, U and Re in the Gulf of Cambay**

Three of the estuaries studied, the Narmada, the Tapi and the Mahi fall in the Gulf of Cambay, a semi enclosed basin at the northern end of the Arabian Sea. The estimated seawater concentrations at 35‰ in the Narmada and the Tapi estuaries are ~13 and 105 nmol/kg for uranium and molybdenum respectively. These estimates are similar to those observed for seawater of the Arabian Sea and average global seawater. However, the dissolved Re concentration in the Gulf of Cambay at 35‰ salinity ranges between ~85 and 200 pmol/kg, significantly higher than typical open ocean value of ~40 pmol/kg (Tables 5.2, 5.3).

The U concentrations of the two samples of the Mahi estuary, situated at the northern end of the Gulf are 12.2 and 15.2 nmol/kg at salinities 27 and 25.6‰ respectively, similar or slightly higher compared to average seawater, however Mo in the same samples are 118 and 132 nmol/kg and Re are 208 and 118 nmol/kg (Table 5.2). Mo contents of the seawater at Ghogha coast, along the western coast of the Gulf are ~110 and 111 nmol/kg at salinity 32.4 and 32.5‰ respectively, whereas, U contents for these samples are 12.5 and 12.7 nmol/kg. However, Re concentration in those samples are 171 and 129 pmol/kg which are 3-4 time higher than the average global ocean concentration ~40 pmol/kg. The measured concentrations of seawater Mo in northern Gulf of Cambay ranges from 111 to 132 nmol/kg at salinities 25.6 to 32.5 ‰ and the estimated Mo for the southern Gulf of Cambay based on estuarine data of the Narmada and the Tapi, ~105 nmol/kg indicate a north-south gradient for the dissolved Mo concentration in the Gulf of Cambay, with higher concentration of Mo in the northern side of the Gulf. Northern Gulf has ~35% higher Mo compared to that of the average seawater. Re in the Mahi estuary, extreme north in the Gulf of Cambay (Fig. 2.5) also shows high concentration, 208 pmol/kg and 118 pmol/kg at salinity of 27‰

and 25.6 % respectively. These results unequivocally show that dissolved Re and Mo concentrations in the Gulf of Cambay seawater is much higher than global sea water with significant spatial and temporal variations. Re seems to be higher during monsoon and in the northern part of the Gulf (Table 5.2) with a north-south gradient similar to the observation of Mo with lowest values off the Tapi estuary and the highest off the Mahi estuary. The north-south gradient in Mo and Re concentrations in the Gulf could be understood in terms of increasing residence time of water parcels northward in the Gulf.

Higher concentration of Mo and Re in the Gulf compared to that of the Arabian seawater and average global seawater is intriguing considering its very high residence time (700 ka, 750 ka Colodner et al., 1995). To determine the sources of high Mo and Re in the northern Gulf, some of the river waters falling in the Gulf and few industrial effluent waste waters were analysed for U, Mo and Re. Though the U contents of the Mahi river (7.9 nmol/kg) and of the effluent waste waters (1.4 and 2.8 nmol/kg) are in the range of other rivers of this region, their Mo and Re concentrations are extremely high. Mahi river has Mo and Re concentrations of 90 nmol/kg and 41 pmol/kg respectively, whereas the effluent waste waters have 569 and 828 nmol/kg of Mo and Re concentrations of 178 and 175 pmol/kg (Table 5.2).

### **5.6.1 Sources of high Mo and Re to Gulf of Cambay**

Both natural and anthropogenic sources can contribute to the high Mo and Re concentrations in the Gulf of Cambay. Average riverine flux of Mo and Re to the Gulf of Cambay, estimated based on their riverine concentrations (Table 5.2 and 5.6), are  $1.6 \times 10^6$  and  $\sim 1400$  moles per year respectively. However, many of these rivers are heavily polluted and receive Mo and Re from anthropogenic sources such as industries situated on their banks.

#### **(a) Natural supply of Mo and Re**

Natural sources of Mo and Re can be desorption from fluvial particulate matter. It has been shown that redox sensitive trace elements are carried by suspended particulates in rivers and released upon contact with sea water. For

example, in the Amazon estuary Mo and Re behaves non-conservatively in the low salinity region (Colodner et al., 1993) and the inner shelf of the estuary acts as their sources, though not confirmed by their study in shelf sediments (Breckel et al., 2005). However, the results of the present study on the estuaries of the Gulf of Cambay do not support gain of Mo and Re through desorption from the particulate matter.

Formation and intensification of seasonal oxygen minimum zone has been reported along the western Indian continental shelf during late summer and autumn (Naqvi et al., 2000). The highest accumulation of H<sub>2</sub>S is observed in these areas during these seasons. This hypoxic- anoxic condition starts developing in June, reaches peak intensity by September - October and dissipates by December. During the upwelling period, H<sub>2</sub>S concentration becomes very high, reaching upto 19 μM over the inner shelf north of ~12 °N latitude and also often along the Goa coast. The seasonal anoxia could sequester Re from seawater to sediments and its subsequent release from sediments could be a potential source of Re in the oxic waters of the Gulf. Post-depositional migration of Re from the reducing sediment has also been reported in various studies (Colodner et al., 1992; Crusius and Thomson, 2000; Morford et al., 2009). Sequestered Re could be remobilized from sediment to water during exposure to oxygen (Morford et al., 2009). However, the observation that Re in the Mandovi estuary shows conservative mixing and the mixing line extrapolated to 35 ‰ salinity yields to ~40 pmol/kg Re similar to the average concentration of the open ocean, despite the fact that seasonal anoxia also develops in the coastal regions of Goa, rules against the above hypothesis.

#### **(b) Anthropogenic supply of Mo and Re**

Mo and Re can be contributed to the environment by anthropogenic activities (Colodner et al., 1995; Peucker-Ehrenbrink et al., 2006, Chappaz et al., 2008). The coastal area of the Gulf of Cambay is heavily industrialized and the industrial effluents are continuously discharged directly to the open sea. An important and definite source of anthropogenic Re to the Gulf of Cambay is the industrial waste waters discharged directly through pipe-lines to the open ocean. The Gulf of Cambay receives  $\sim 5000 \times 10^6$  m<sup>3</sup> of industrial waste water (GoI

Report, 2002). Two samples of effluent water from the industrial waste collected from the pipe-line have high Mo and Re concentrations, 569 and 828 nmol/kg Mo, 175 and 178 pmol/kg Re (Table 5.2). Estimated annual fluxes of Mo and Re from the industrial waste water, based on the above measured concentrations, are  $\sim 3.5 \times 10^6$  and  $\sim 900$  moles respectively which are being discharged directly into the open Gulf of Cambay. In addition to the waste waters, the waters of the Sabarmati, Mahi and the Vishwamitri are also heavily contaminated with anthropogenic Mo and Re and together they deliver  $1.6 \times 10^6$  moles of Mo and  $\sim 1400$  moles of Re annually to the Gulf. These estimates indicate that anthropogenic sources contribute  $\sim 5 \times 10^6$  moles of Mo and  $\sim 2300$  moles of Re to the Gulf annually. The concentration of the pollutants in the Gulf of Cambay exhibits temporal and spatial variation and could be due to spatial variability in the residence time of water parcels in the Gulf. This study indicates that industrial effluents either directly or through the rivers are the common source of Re and Mo to the Gulf of Cambay; however, U seems to be decoupled from the anthropogenic sources. Re could come to the industrial waste waters from the petroleum industries situated along the coast of the Gulf which use Re as anti-knocking agent. Mo could come to these waters from pharmaceutical industries abundant in the localities which use Mo as a catalyst. In addition to the anthropogenic Mo, Gulf of Cambay may get excess Mo from the nearby salt marsh too as discussed in the earlier section

In addition to direct input of anthropogenic Re to the Gulf of Cambay, there are other potential pathways of Re to the adjoining rivers and to the Gulf. Petroleum industries situated along the Gulf of Cambay can contribute Re to the Gulf via waste waters or through atmospheric deposition as the petroleum has high concentration of Re  $\sim 2$ -200 ppb (Creaser et al., 2002). Re is used in high-temperature superalloys to make jet engine parts and in platinum-rhenium catalysts which in turn are primarily used for manufacturing lead-free, high-octane gasoline. Re is volatile at high temperature and combustion, at  $270^\circ\text{C}$  as  $\text{Re}_2\text{O}_7$  (Colodner et al., 1995), thereby burning of petroleum can add Re to the atmosphere and finally to the hydrosphere.

Alang – Sosia (Fig. 2.5) is one of the largest ship breaking yard in the world situated on the Gulf of Cambay. Every year about 365 ships get dismantled in this facility (Reddy et al., 2005). Various kinds of wastes in the form of solids, liquids and gasses are discharged into the sea while dismantling the ships. The pollutants mainly constitute heavy metals, petroleum hydrocarbons and bacterial contaminants and are dumped along the coast without proper treatment. This waste is carried by tides into intertidal zone and finally to the open ocean. High concentrations of petroleum hydrocarbons, polycyclic aromatic hydrocarbons and heavy metals along the coastal area of Alang-Sosia are observed (Reddy et al., 2005). The coal combustion and fossil fuel burning which are mainly used in thermal power plants, smelters and many other industries can be another source of Re to the Gulf of Cambay. Coal, lignite and diesel are being used in the thermal power stations and other industries situated along the Gulf of Cambay. They can add Re via atmospheric deposition (Chappaz et al., 2008).

### 5.7 Riverine fluxes of Mo and Re

Major source of Mo to the global ocean is its riverine input which supplies  $1.8-2.3 \times 10^8$  mol/y (Morford and Emerson, 1999; McManus et al., 2006 and references therein). Table 5.5 is a compilation of Mo concentration reported in global rivers (Martin and Meybeck, 1978; Colodner et al., 1993; Walker and Peucker-Ehrenbrink, 2004; Archer and Vance, 2008 and this study). The average global riverine concentration of dissolved Mo based on the data in Table 5.5 representing ~28% the fresh water discharge is ~6.2 nmol/kg (Archer and Vance, 2008). This increases marginally to 6.4 nmol/kg based on Mo data of this study (Table 5.5, Fig. 5.9) and those reported in Walker and Peucker-Ehrenbrink (2004) and Archer and Vance (2008). This corresponds to a global riverine Mo flux of  $\sim 2.4 \times 10^8$  mol/y.

The earlier estimate of the riverine flux to the ocean was based on Re content of four major rivers, the Amazon, Orinoco and the Ganga-Brahmaputra. The Amazon river contributes 17.8 % of the total riverine flux which has lower Re concentration (~1 pmol/kg) as compared to the other world rivers. Therefore, the estimate of average Re concentration of river was biased towards lower value of

the Amazon. It has been shown in this study along with the data available in literature that Re concentration of various global rivers is highly variable and in general much higher than that reported for the Amazon (Table 5.6).

**Table 5.5: Compilation of Mo in global rivers along with this study**

| <b>River</b>                                      | <b>[Mo]<br/>nmol/kg</b> | <b>Ref.</b> | <b>River</b>                | <b>[Mo]<br/>nmol/kg</b> | <b>Ref.</b> |
|---|-------------------------|-------------|-----------------------------|-------------------------|-------------|
| Mississippi                                       | 10.3                    | 1           | Brahmaputra                 | 9.0                     | 2           |
| Susquehanna River                                 | 3.0                     | 1           | Amazon                      | 4.3                     | 2           |
| Mad river   | 3.0                     | 1           | Chang Jiang<br>River, China | 16.7                    | 2           |
| Klamath River                                     | 14.8                    | 1           | Dnepr Kherson               | 18.0                    | 3           |
| Russian River                                     | 3.6                     | 1           | Prut @reni                  | 29.0                    | 3           |
| Eel River   | 3.5                     | 1           | Danube @ Reni               | 19.0                    | 3           |
| Wateree River                                     | 2.6                     | 1           | Danube @<br>Vilkovo         | 20.0                    | 3           |
| Lake superior                                     | 4.3                     | 1           | Dnestr @ Majaki             | 29.0                    | 3           |
| Brazos River                                      | 2.9                     | 1           | Bug @ Novaja<br>Odessa      | 30.0                    | 3           |
| Colorado River                                    | 1.1                     | 1           | Kuban @ Temruk              | 22.0                    | 3           |
| Rio Maipo   | 1.8                     | 1           | Hudson                      | 4.6                     | 4           |
| Po River  | 5.0                     | 1           | Houstonic                   | 5.5                     | 4           |
| Congo River                                       | 1.8                     | 1           | Connecticut                 | 7.8                     | 4           |
| Rhone river                                       | 21.1                    | 1           | Hooghly                     | 13.8                    | 5           |
| Red River   | 4.9                     | 1           | Narmada                     | 4.3                     | 5           |
| Itchen River, SE<br>England                       | 4.8                     | 2           | Tapi                        | 6.1                     | 5           |
| Kalix River,<br>Sweden                            | 4.9                     | 2           | Mahi                        | 90.0                    | 5           |
| Nile River, Sudan<br>and Egypt                    | 7.1                     | 2           | Sabarmati                   | 48.0                    | 5           |
| Volga River,<br>Russia                            | 6.7                     | 2           | Mandovi                     | 1.0                     | 5           |
| Ottawa River,<br>Canada                           | 2.2                     | 2           | Vishwamitri                 | 23.0                    | 5           |
| <b><i>Global Average (Discharge weighted)</i></b> |                         |             |                             | <b>6.4</b>              | <b>5</b>    |

**1: Burtine and Turekian, 1972, 2: Archer and Vance, 2008, 3: Colodner et al., 1995, 4 :Walker and Peucker-Ehrenbrink, 2004, 5: This study.**

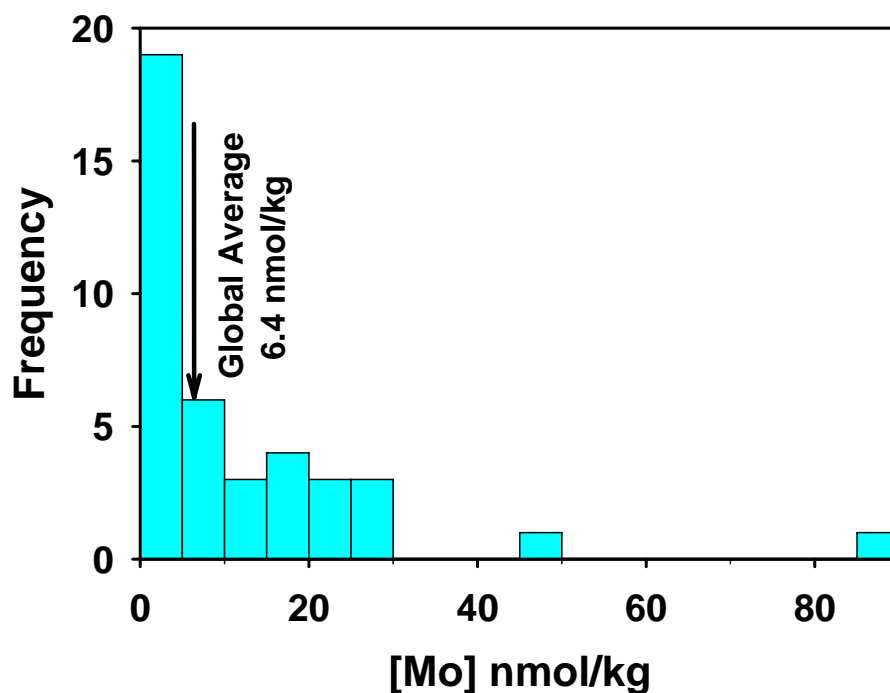


**Fig. 5.9** Histogram of dissolved Mo concentration of the global rivers based on reported data and from this study. Discharge weighted global average riverine Mo concentration is 6.4 nmol/kg.

Currently the Re concentrations are available for ~26.5% of global riverine discharge which yields a contemporary global average concentration of ~9.2 pmol/kg Re, ~4 times higher compared to the earlier reported value. Assuming that this Re concentration is typical of global rivers, an annual global Re flux from river to the ocean is estimated to be  $\sim 350 \times 10^3$  moles.

**Table 5.6: Dissolved Re in global rivers measured in this study and available in the literature**

| River       | Water Flux<br>km <sup>3</sup> /y | [Re]<br>pmol/kg | Reference |
|-------------|----------------------------------|-----------------|-----------|
| Amazon      | 6590                             | 1.1             | 1         |
| Orrinco     | 1135                             | 4.4             | 1         |
| Mississippi | 580                              | 90              | 2         |
| Brahmaputra | 603                              | 5.6             | 1         |
| Ganga       | 450                              | 9               | 1         |
| Yamuna      | -                                | 14              | 3         |

|   |       |            |            |
|---|-------|------------|------------|
| Danube  | 210   | 73         | 4          |
| Tibetan Rivers (Mekong, Huang He, Chang Jiang, Salween, Hong) and Eastern Siberian Rivers (Lena, Yana, Indigirka, Kolyma, Anadyr) | ~2400 | 0.5 to 240 | 5          |
| Hudson  | 12    | 38         | 2          |
| Houstonic   | 2     | 6.6        | 2          |
| Connecticut   | 12    | 14         | 2          |
| Hooghly   | 52    | 5.2        | This study |
| Narmada   | 47    | 14         | This study |
| Tapi  | 19    | 4          | This study |
| Mahi  | 12    | 41         | This study |
| Sabarmati   | 4     | 37         | This study |
| Vishwamitri   | 1     | 18         | This study |
| Mandovi   | 16    | 1.4        | This study |
| <b>Global Average (Discharge weighted)</b>  |       | <b>9.2</b> |            |

**1: Colodner et al., 1993; 2: Walker and Peucker-Ehrenbrink, 2004; 3: Dalai et al., 2002; 4: Colodner et al., 1995; 5: Huh et al., 2007.**

### 5.8 Global oceanic budget of Mo and Re

Major source of both Mo and Re to the global oceans is continental weathering through rivers. These riverine fluxes have been modified significantly as has been discussed in the preceding section. New estimates of their fluxes will have considerable impact on their global oceanic budgets. Further, the known sinks of Mo in the oceans are lower than its known sources and require knowledge of additional sinks. Loss of Mo in estuaries could be an important sink. These issues are discussed in the following sections.

As discussed earlier, rivers supply  $\sim 2.4 \times 10^8$  mol of Mo annually to the oceans. Mo input flux increases to  $\sim 2.6 \times 10^8$  mol/y (McManus et al., 2006 and references therein) if Mo flux from low temperature hydrothermal weathering ( $0.2 \times 10^8$  mol/y) is added. The primary sinks of Mo are the oxic ( $0.9 \times 10^8$  mol/y) and anoxic ( $0.2$  to  $0.8 \times 10^8$  mol/y) sediments. McManus et al. (2006) estimated, based on available Mo isotope composition of the various reservoirs, sinks of  $0.1 \times 10^8$  mol Mo/y in anoxic sediments and  $\sim 0.4 \times 10^8$  mol Mo/y in the continental margins. These estimates clearly indicate a significant deficit in the oceanic Mo sink (missing sink), if it is in steady state with respect to input/output. Present day mismatch between the input and output of Mo budget of seawater could be due to

increase in its riverine supply during the Holocene as has been suggested in case of Sr and other elements (Vance et al., 2009) resulting from enhanced chemical weathering of fresh sediments exposed by the glaciers during the Last Glacial Maxima. The role of such a process in contributing to Mo flux is unclear; if this is significant it can contribute to the imbalance. However, if the current riverine input of Mo is not affected by glacial hangover (Vance et al., 2009) and represents its long term average, its removal is certainly lower than its supply.

This study has demonstrated that Mo can be removed in the estuaries such as in the Hooghly and the Mandovi. These estuaries are associated with mangroves (Carroll and Moore, 1993; Singh et al., 2004). If Mo is being sequestered with similar efficiency in the estuaries containing the mangrove swamps in other parts of the coastal ocean, this could be an important sink for Mo. The Hooghly and the Meghna (combined Ganga and the Brahmaputra in Bangladesh) are part of the same mangrove swamp system and hence the Mo loss of Hooghly can be extended to this entire system. Similar loss of U (~40%) in both the Hooghly (this study) and the Meghna (Carroll and Moore, 1993) estuaries attest to this contention. Following the approach of Windom et al. (2000) and Dunk et al. (2002) and the annual water discharge of  $1000 \text{ km}^3$ , the Mo loss of the entire Ganga-Brahmaputra estuary can be estimated to be  $\sim 31 \times 10^6 \text{ mol/y}$ . If Mo loss in the estuary occurs only during lean flow period as has been suggested for U (Carroll and Moore, 1993), Mo loss, based on the water discharge of  $140 \text{ km}^3/\text{y}$ , could be  $\sim 4 \times 10^6 \text{ mol/y}$ . Considering the mangrove swamp area of the Ganga-Brahmaputra system  $\sim 1.8 \times 10^{10} \text{ m}^2$  (Carroll and Moore, 1993), the Mo sequestration rate in these estuaries show a range of 0.2 to  $1.7 \text{ mmol/m}^2/\text{y}$  depending on Mo loss occurring during the lean flow only or during the entire year. If this rate is applicable to mangroves globally, the global Mo removal rate based on mangrove swamp area of  $\sim 1.8 \times 10^{11} \text{ m}^2$  (Spalding, 1997) is in the range of  $0.4 \times 10^8$  to  $3.1 \times 10^8 \text{ mol/y}$ . This range corresponds to 15%-120% of Mo supply and underscores the important role of mangroves in determining the oceanic budget of Mo. This study indicates that the estuaries associated with mangrove swamps are an important sink of Mo which could serve as the reported missing sink of Mo (McManus et al., 2006).

The residence time of Re in the ocean was estimated to be  $\sim 0.75$  Ma (Colodner et al., 1993) based on its average global riverine concentration of  $\sim 2.1$  pmol/kg. The new estimate of global riverine flux of Re,  $\sim 350 \times 10^3$  moles/y, decreases its residence time in the ocean to  $\sim 175,000$  years as has been observed earlier by Peucker-Ehrenbrink et al. (2006). As discussed earlier, the estimates of riverine Re flux can be subject to significant uncertainty due to paucity of Re data in majority of the rivers and its temporal variation. In addition, the role of anthropogenic sources in contributing to Re in rivers needs to be assessed. If this is a significant source, it would imply that riverine Re flux have increased during the anthropocene and hence it will not be in steady state in the ocean with respect to its contemporary supply.

Several studies have attempted to constrain the sinks of Re in the ocean (Ravizza, 1992; Colodner et al., 1993; Crusius et al., 1996; Morford and Emerson, 1999). Anoxic sediments were previously thought to be the largest sink in the global Re mass balance (Ravizza, 1992; Colodner et al., 1993). Ravizza (1992) estimated that sequestration in anoxic sediments removes  $\sim 44 \times 10^3$  moles/y of Re. Suboxic sediments having larger areal extent than the anoxic sediments in the ocean and were later found to be another major sink of Re (Crusius et al., 1996 and references there in). Morford and Emerson (1999) demonstrated that suboxic sediments, where oxygen penetrates  $\leq 1$  cm, are the primary sink for Re which sequester  $60 \times 10^3$  to  $110 \times 10^3$  moles annually. A total Re sink of  $95 \times 10^3$  to  $154 \times 10^3$  moles annually through anoxic and sub-oxic sediments was estimated (Morford and Emerson, 1999). The riverine flux of Re ( $350 \times 10^3$  moles/y) estimated in this study is significantly higher ( $\sim 2-4$  times) compared to its sink in anoxic/suboxic sediments  $\sim (95-154) \times 10^3$  moles/y (Morford and Emerson, 1999). This imbalance, with Re supply far exceeding its known sinks, hints at the possibility of non steady state condition of Re in ocean. Therefore, estimates of Re residence time assuming steady state and its contemporary riverine flux may require reassessment, especially to evaluate the roles of natural versus anthropogenic sources in contributing to its riverine flux. Further, the observation that Re concentration in the Gulf of Cambay is  $\sim 5$  times higher compared to the open ocean brings out the need to trace such “Re hotspots” in other coastal

regions or semi enclosed basins of the world and the impact they may have on Re inventory of the oceans and on the estimate of residence time of Re in seawater. Hence, to exploit the use of Re as a geochemical tracer to study the oceanic processes, a detailed study of riverine Re flux and its total inventory in the ocean considering the Gulf of Cambay type coastal areas is needed.

## 5.9 Conclusions

Mo, U and Re concentration in the estuaries of the Hooghly in the Bay of Bengal and the Mahi, Narmada, Tapi and the Mandovi estuaries in the Arabian Sea are analysed in this study. River waters, seawaters and salt marsh samples along the Gulf of Cambay are also analysed for their U, Mo and Re concentrations. Mo and Re were analysed for the first time in the Indian estuaries. Dissolved Mo, U and Re show highly variable concentrations in the rivers, vary from 1 to 90 nmol/kg for Mo, 0.02 to 19.0 nmol/kg for U and 1.4 to 41 pmol/kg for Re. The highest concentration of U is found in the Sabarmati river whereas the Mahi river has the highest Mo and Re concentration, most probably sourced from anthropogenic sources such as industrial activities in the region. The lowest U, Mo and Re are measured in the Mandovi river resulting due to lateritic lithology, higher runoff and lower water-rock interaction in its drainage. Mo, U and Re measured in the Arabian Sea water are similar to their average global values.

Behaviour of Mo, U and Re in the four estuaries analysed in this study are highly variable. In the Narmada estuary, Mo, U and Re show conservative mixing between riverine and seawater endmembers during pre-monsoon and monsoon. U and Re are conservative in the Tapi estuary but Mo shows non-conservative behaviour (gain) in the mid salinity ranges resulting from anthropogenic activity. Both Mo and U show non-conservative behaviour (removal) in the Hooghly and the Mandovi estuaries. They get removed in the lower salinity ranges in these estuaries. This observation is inconsistent with Re in these estuaries showing perfectly conservative behaviour. The loss of U and Mo could be either due to reducing condition prevailing in the Hooghly and the Mandovi estuaries caused by mangrove forest or could result from its association with Fe-Mn precipitates in the estuaries. About 40% of riverine uranium is being

lost in the Hooghly estuary. Mo in the Hooghly and the Mandovi and U in the Mandovi estuary indicate their net sink. Annually  $\sim 1.6 \times 10^6$  moles of Mo is being lost in the Hooghly estuary, which is more than double of its riverine supply. Mandovi estuary loses  $\sim 2 \times 10^5$  moles of Mo annually. Uranium removal in both the Hooghly and the Mandovi estuaries are one order of magnitude lower compared to that of Mo. Such processes in the estuaries not only prevent the riverine supply of elements to enter the open ocean but also remove part of marine component and could be an important sink of such elements influencing their oceanic budget. Such removal on global scale has been estimated earlier for U. This study estimates Mo loss in the range of  $0.4 \times 10^8$  to  $3.1 \times 10^8$  mol/y in the global estuaries associated with mangrove swamp. This could be the missing sink of global Mo budget (McManus et al., 2006).

Though dissolved Re behaves conservatively in all the estuaries, the slopes and intercepts of the mixing lines between Re concentrations and salinity, however, differ among these estuaries suggestive of variations in riverine and seawater end members of Re concentrations. Dissolved Re concentration in most of the rivers analysed in this study is higher than the earlier estimate of global average riverine Re concentration,  $\sim 2.1$  pmol/kg. Based on this study and the available data, the contemporary annual riverine Re flux is estimated to be  $\sim 350 \times 10^3$  moles to the ocean with a global average riverine Re concentration of 9.2 pmol/kg, a factor of four higher compared to earlier estimate. Using this data and assuming that the oceans are in steady state with respect to this riverine flux yields a residence time of  $\sim 175,000$  years, for Re in ocean which is  $\sim 4$  times lower compared to its earlier estimate. The role of anthropogenic input of Re to rivers in contributing to this lower estimate of residence time needs further scrutiny.

Mo and Re concentration in the Gulf of Cambay is much higher compared to that of the Arabian Sea and that of global average seawater value. Higher value of Mo and Re in the Gulf is attributed to its supply from anthropogenic sources. Polluted rivers and industrial effluent waste waters supply  $\sim 5 \times 10^6$  moles of Mo annually to the Gulf of Cambay. The seawater Re estimated based on the Hooghly and the Mandovi estuaries are similar to that reported for

the open oceans,  $\sim 40$  pmol/kg. In contrast, the Re concentration in the Gulf of Cambay is 2 to 5 times higher compared to open ocean value reported for other global oceans and measured in this study off the Goa coast. High Re in the Gulf of Cambay is attributed to wastes discharged from various industries. Polluted rivers and the industrial waste waters deliver  $\sim 2300$  moles of Re every year directly to the Gulf of Cambay and seems to be mainly derived from various industries situated along the coast of the Gulf.

Numerous petrochemicals and pharmaceutical industries situated along the coast of the Gulf of Cambay are probably supplying Mo and Re to the effluent waters and finally to the Gulf, however these anthropogenic sources do not contain U in them and that may be the reason for normal U content in the Gulf of Cambay. Further, this study indicates that salt marshes act as a sink of oceanic U and probably a source of Mo to the seawater. This study underscores the importance of both natural and anthropogenic inputs of Mo and Re to the ocean budgets and its impact on the estimates of residence time in the ocean.

## **CHAPTER-6**

**Ba and Sr in Indian rivers and estuaries: Implications to  
geochemistry of alkaline earth metals and submarine  
groundwater discharge**

### 6.1 Introduction:

Estuary is the major pathway through which dissolved elements carried by rivers are transferred to the oceans. Estuaries play a key role in the geochemical cycling of many elements as they determine the fate of the elements before entering the ocean. This is because estuaries are a transition zone where major changes in chemistry, Eh-pH and environmental conditions occur that can substantially modify the fluxes of elements to the oceans. Steep gradients in the ionic strength and composition, Eh-pH, and suspended particulate matter (SPM) concentration in estuaries can cause elements/ions to change from dissolved to particulate phase or vice versa and alter their dissolved fluxes to the ocean. This makes the study of the behaviour of various elements in estuaries important to evaluate their fluxes to the oceans; such studies are being carried out in different types of estuaries to characterize the various factors controlling their behaviour and determine representative fluxes.

This study focuses on alkaline earth metals, particularly Sr and Ba to learn about their abundances, distribution, behaviour and transport in Indian estuaries linked to the Arabian Sea and the Bay of Bengal. Dissolved Sr and its isotope composition ( $^{87}\text{Sr}/^{86}\text{Sr}$ ) is uniform in contemporary global ocean because of its long residence time  $\sim 2.5$  to 5 Ma, orders of magnitude larger compared to ocean mixing time  $\sim 1000$  yrs. Biogenic and authigenic marine shells/precipitates that form in the ocean incorporate Sr in them with the same isotopic signature as dissolved Sr as there is no measurable isotope fractionation during phase separation, chemical speciation, evaporation and biological activity. Sr isotope ratio of these precipitates reveal past ocean Sr isotope variability, an important tool for correlating and/or dating marine sequences (Burke and Denison, 1982; McKenzie et al., 1988; McArthur, 1994; Patterson et al., 1995; Veizer et al., 1997; Vaiani, 2000). Any changes in the Sr isotope composition of the ocean through time are caused by changes in the relative contributions of two major sources of Sr to the oceans; hydrothermal input and weathering of rocks on the continents (Brass, 1976; Palmer and Edmond, 1989; Edmond, 1992). Hence, the study of Sr isotope evolution of the ocean can yield important information on global tectonic and/or climate change events (Burke and

Denison, 1982, Raymo, 1991; Andersson et al., 1994; Derry and France-Lanord, 1996; Harris et al., 1998; Huh and Edmond, 1998).

Recent studies (Andersson et al., 1994; Xu and Marcantano, 2004), however have shown that the geochemistry and isotope composition of Sr can deviate from that of contemporaneous seawater in shallow marine environments, because of riverine influence on Sr isotope systematics (Vaiani, 2000). This property of Sr isotopes in estuaries has found applications to investigate paleosalinity variations with river discharge (Ingram and Sloan, 1992; Ingram and DePaolo, 1993; Bryant et al., 1995; Cochran et al., 2003; Charette and Sholkovitz, 2006; Huang and You, 2007; Peros et al., 2007). Studies on the behaviour of Sr in estuarine region can therefore constrain paleo-salinity and continental weathering fluxes of Sr and  $^{87}\text{Sr}/^{86}\text{Sr}$  to the sea. Available studies (Ingram and Sloan., 1992; Depalo et al., 1993; Andersson et al, 1994; Wang et al., 2001; Xu and Marcantano, 2004) indicate both conservative and non-conservative behaviour of Sr in different estuaries. For example, nonconservative behavior of Sr has been observed in the transition of fresh and brackish water of Mississippi estuary and the Baltic Sea (Andersson et al., 1994). The strong interaction between sediment and water during high energy condition in the Changjiang estuary releases Sr to water (Wang et al., 2001), resulting in its non-conservative behaviour. Chemical speciation and biogenic processes have been reported to play important roles in determining the behaviour of Sr in the estuaries (Andersson et al, 1994; Xu et all, 2004). Submarine groundwater discharge (SGD) has been suggested as a significant supplier of dissolved elements including Sr to coastal oceans (Basu et al., 2001; Hwang et al., 2005; Paytan et al., 2006; Charrette et al., 2008; Moore, 2009). It has been suggested that SGD could be an important source of Sr to the global ocean and therefore could influence its marine budget significantly (Basu et al., 2001), however, its impact on oceanic Sr budget is yet to be assessed. Estuaries are suitable locations to study the impact of SGD on dissolved Sr. The estimate of continental flux of Sr to ocean requires knowledge of its inputs from both surficial and subsurface runoff and the role of estuaries in modifying its flux either by addition or sequestration.

Ba is another alkaline earth metal which has wide applications as a proxy for both modern and paleo-ceanographic processes (Schmitz, 1987; Bishop, 1988; Lea and Boyle, 1989; Elderfield, 1990; Dehairs et al., 1991, 1992; Dymond et al., 1992; Francois et al., 1995). The processes which control the marine geochemical cycle of Ba are drawing more attention due to the application as a tracer for paleo-productivity and paleo-ocean circulation (Bishop, 1988; Lea and Boyle, 1989, 1990; Dymond et al., 1992). Further, it has been shown that Ba together with Ra can be very useful proxy to determine SGD into the sea (Moore, 2010). The interaction of riverine particulates with saline waters results in desorption of Ba, contributing to its dissolved input. These observations have established that Ba shows non-conservative behaviour in estuary (Hanor and Chan, 1977; Edmond et al., 1978; Li and Chan, 1979; Carroll et al., 1993; Coffey et al., 1997), although only a few of the world's large estuaries have been studied for Ba.

One of the goals of this study is to investigate the Sr and Ba distribution and behaviour in tropical estuaries. Four estuaries were selected toward this based on the properties of rivers particularly those flowing through different geologic terrains. The Narmada and the Tapi are two medium river systems among the Indian peninsular rivers, flowing mainly through the Deccan basalt. The third river, the Mandovi drains through lateritic terrain and the Archean Dhrawar craton. All these estuaries are linked to the Arabian Sea. In addition to the Narmada, Tapi and the Mandovi which drain into the Arabian Sea, the behaviour of Ba has also been studied in the Hooghly estuary, flowing into the Bay of Bengal. The Hooghly is one of the distributaries of the Ganga. The geohydrology and coastal aquifer systems in the estuaries in the Bay of Bengal and in the Arabian Sea are different. The comparative studies of Ba and Sr would provide information about the processes i.e. adsorption-desorption and supply of dissolved material from the coastal aquifer through SGD.

## **6.2 Results and Discussion**

The concentration of dissolved Sr and its  $^{87}\text{Sr}/^{86}\text{Sr}$  were measured in three estuaries, the Narmada, Tapi and the Mandovi and that of Ba in four including the Hooghly are

presented in Table 6.1. In addition to measurements in these estuaries, two groundwater samples collected from the vicinity of the Narmada river were also analysed for Sr and Ba contents and Sr isotope composition (Table 6.1).

**Table 6.1: Dissolved Ba and Sr concentrations and  $^{87}\text{Sr}/^{86}\text{Sr}$  in the Narmada, Tapi, Mandovi and the Hooghly Estuaries**

| Sample  | Latitude  | Longitude | Salinity | Ba      | Sr      | $^{87}\text{Sr}/^{86}\text{Sr}$ |
|---|-----------|-----------|----------|---------|---------|---------------------------------|
|   |           |           | (‰)      | nmol/kg | μmol/kg |                                 |
| <b><u>Narmada (Pre-monsoon, March 2007)</u></b> |           |           |          |         |         |                                 |
| NE07-20   | 21°49.49' | 73°11.57' | 0        | 207     | 1.7     | 0.71064                         |
| NE07-21   | 21°50.02' | 73°45.34' | 0        | 143     | 1.4     | 0.71079                         |
| NE07-22   | 21°51.81' | 73°41.75' | 0        | 89      | 1.4     | 0.71076                         |
| NE07-18   | 21°40.51' | 72°57.00' | 0.2      | -       | 1.9     | 0.71006                         |
| NE07-19   | 21°40.63' | 72°57.54' | 0.2      | 30      | 2.1     | 0.71001                         |
| NE07-1  | 21°40.81' | 72°54.57' | 4.8      | 298     | 12.4    | 0.70939                         |
| NE07-2  | 21°41.26' | 72°52.60' | 9.3      | 508     | 27.3    | 0.70927                         |
| NE07-3  | 21°40.58' | 72°50.39' | 11.8     | 510     | 31.1    | 0.70933                         |
| NE07-4  | 21°39.20' | 72°47.42' | 15.9     | 546     | 41.5    | 0.70922                         |
| NE07-5  | 21°38.80' | 72°45.34' | 18.2     | 538     | 46.3    | 0.70919                         |
| NE07-6  | 21°40.75' | 72°42.05' | 20       | 507     | 51.3    | 0.70921                         |
| NE07-7  | 21°40.71' | 72°49.83' | 21.3     | 479     | 53.8    | 0.70918                         |
| NE07-8  | 21°39.46' | 72°35.89' | 22.1     | 427     | 55.9    | 0.70920                         |
| NE07-9  | 21°39.36' | 72°34.51' | 23.9     | 403     | 59.8    | 0.70920                         |
| NE07-10   | 21°39.62' | 72°33.28' | 25.3     | 356     | 65.1    | 0.70915                         |
| NE07-11   | 21°38.73' | 72°33.02' | 25.5     | 370     | 65.2    | 0.70919                         |
| NE07-12   | 21°38.04' | 72°32.70' | 27.2     | 341     | 68.0    | 0.70917                         |
| NE07-13   | 21°38.0'  | 72°32.7'  | 29       | 333     | 72.7    | 0.70920                         |
| NE07-15   | 21°37.94' | 72°32.05' | 31.1     | 191     | 77.1    | 0.70915                         |
| <b><u>Narmada ( Monsoon, July 2007)</u></b>     |           |           |          |         |         |                                 |
| NEM07-14  | -         | -         | 0        | 52      | 1.3     | 0.70994                         |
| NEM07-1   | 21°40.59' | 72°55.58' | 0        | 85      | 1.6     | 0.71053                         |
| NEM07-2   | 21°39.08' | 72°46.64' | 0.1      | 34      | 1.7     | 0.71026                         |
| NEM07-3   | 21°40.07' | 72°37.12' | 1.3      | 36      | 4.4     | 0.70942                         |
| NEM07-4   | 21°39.58' | 72°36.34' | 2.2      | 59      | 8.2     | 0.70937                         |
| NEM07-5   | 21°39.42' | 72°35.49' | 3.4      | 81      | -       | -                               |
| NEM07-6   | 21°39.15' | 72°34.28' | 5.1      | 113     | 13.4    | 0.70927                         |

|          |           |           |      |     |      |         |
|----------|-----------|-----------|------|-----|------|---------|
| NEM07-7  | 21°38.55' | 72°33.18' | 6.0  | 129 | 15.2 | 0.70926 |
| NEM07-8  | 21°38.39' | 72°33.26' | 8.0  | 147 | 18.6 | 0.70921 |
| NEM07-9  | 21°39.27' | 72°35.26' | 9.8  | 200 | 24.4 | 0.70921 |
| NEM07-10 | 21°38.52' | 72°33.2'  | 12.1 | 199 | 37.4 | 0.70918 |
| NEM07-11 | 21°38.81' | 72°33.94' | 14.1 | 198 | 34.2 | 0.70917 |
| NEM07-12 | 21°38.05' | 72°33.19' | 15.5 | 202 | 37.9 | 0.70918 |
| NEM07-13 | 21°38.55' | 72°32.93' | 17.2 | -   | 42.4 | 0.70918 |

**Groundwater upstream Narmada estuary**

|        |           |           |     |     |      |         |
|--------|-----------|-----------|-----|-----|------|---------|
| GW08-4 | 22°02.02' | 72°50.31' | 0.6 | 251 | 9.6  | 0.70951 |
| GW08-6 | 22°03.01' | 72°47.81' | 1.9 | 997 | 57.4 | 0.70941 |

**Tapi (Monsoon, July2007)**

|          |           |           |       |     |      |         |
|----------|-----------|-----------|-------|-----|------|---------|
| TPM07-14 | -         | -         | 0     | 49  | 1.3  | 0.70875 |
| TPM07-1  | 21°10.56' | 72°46.74' | 0-0.2 | 59  | 2.5  | 0.70894 |
| TPM07-2  | 21°8.9'   | 72°45.8'  | 1.1   | 79  | 5.0  | 0.70903 |
| TPM07-3  | 21°8.52'  | 72°43.61' | 2.1   | 101 | 7.3  | 0.70906 |
| TPM07-4  | 21°8.86'  | 72°42.26' | 3.9   | 147 | 11.2 | 0.70909 |
| TPM07-5  | 21°9.15'  | 72°4.73'  | 4.9   | 172 | 14.3 | 0.70911 |
| TPM07-6  | 21°9.3'   | 72°40.19' | 5.8   | 203 | 16.3 | 0.70911 |
| TPM07-7  | 21°7.97'  | 72°39.58' | 7.8   | 225 | 21.2 | 0.7091  |
| TPM07-8  | 21°7.05'  | 72°39.74' | 9.8   | 261 | 25.6 | 0.70913 |
| TPM07-9  | 21°5.79'  | 72°39.98' | 11.5  | 225 | 29.9 | 0.70912 |
| TPM07-10 | 21°4.97'  | 72°40.64' | 13.1  | 207 | 33.4 | 0.70915 |
| TPM07-11 | 21°4.41'  | 72°40.71' | 14.9  | 213 | 38.4 | 0.70915 |
| TPM07-12 | 21°3.6'   | 72°40.68' | 17.4  | 203 | 44.6 | 0.70915 |
| TPM07-13 | 21°3.16'  | 72°40.35' | 20.3  | 197 | 51.2 | 0.70915 |

**Mandovi (Post-Monsoon, October 2007)**

|         |           |           |       |     |      |         |
|---------|-----------|-----------|-------|-----|------|---------|
| MD07-1  | 15°32.56' | 73°57.69' | 0-0.1 | 27  | 0.7  | 0.71062 |
| MD07-2  | 15°32.39' | 73°55.95' | 2.7   | 65  | 6.9  | 0.70928 |
| MD07-3  | 15°31.55' | 73°55.60' | 6.0   | 49  | 14.3 | 0.70924 |
| MD07-4  | 15°31.33' | 73°55.38' | 13.5  | 102 | 32.9 | 0.70916 |
| MD07-5  | 15°30.33' | 73°54.82' | 16.1  | 99  | 39.8 | 0.70916 |
| MD07-6  | 15°30.27' | 73°54.16' | 19.7  | 94  | 48.1 | 0.70917 |
| MD07-7  | 15°30.11' | 73°52.88' | 26.9  | 78  | 65.7 | 0.70914 |
| MD07-8  | 15°30.34' | 73°50.63' | 31.3  | 59  | 77.7 | 0.70917 |
| MD07-9  | 15°29.29' | 73°48.40' | 33.7  | 50  | 81.9 | 0.70915 |
| MD07-10 | 15°29.07' | 73°41.09' | 33.6  | 27  | 82.8 | 0.70912 |

**Open Ocean off Goa coast**

|        |                    |   |    |   |   |
|--------|--------------------|---|----|---|---|
| GA07-1 | Open Ocean off Goa | - | 39 | - | - |
| GA07-2 | Open Ocean off Goa | - | 35 | - | - |

|   |                    |        |      |     |   |
|---|--------------------|--------|------|-----|---|
| GA07-3  | Open Ocean off Goa | -      | 32   | -   | - |
| GA07-4  | Open Ocean off Goa | -      | 37   | -   | - |
| GA07-5  | Open Ocean off Goa | -      | 31   | -   | - |
| <b><u>Hooghly (Post-monsoon, December 2006)</u></b> |                    |        |      |     |   |
| W-1   | 22.01°             | 88.19° | 0.5  | 266 | - |
| W-2   | 21.9°              | 88.09° | 2.6  | 381 | - |
| W-3   | 21.77°             | 88.02° | 7.7  | 391 | - |
| W-4   | 21.65°             | 88.02° | 11.8 | 343 | - |
| W-5   | 21.58°             | 88.08° | 14.7 | 274 | - |
| W-6   | 21.49°             | 88.13° | 16.7 | 232 | - |
| W-7   | 21.33°             | 88.19° | 20.5 | 163 | - |
| W-8   | 21.06°             | 88.2°  | 22.5 | 134 | - |
| W-9   | 20.69°             | 88.21° | 30.0 | 60  | - |
| W-10  | 20.0°              | 88.2°  | 32.0 | 59  | - |

In the Narmada estuary, the pH remains nearly constant at ~8 from fresh water to sea water, unlike the Tapi and the Mandovi estuaries which show variations between 7.5 to 8.0 and 6.6 to 8.2 respectively. Alkalinity varies between 2000 and 3000  $\mu\text{eq/l}$  in all the estuaries except in the Mandovi where it ranges from 384 to 2236  $\mu\text{eq/l}$  (Table 2.3). Lower pH and alkalinity in the Mandovi river is due to limited water-rock interaction, particularly carbonate dissolution. Alkalinity shows an increase in the 4-12 ‰ salinity range in the Tapi estuary.

### 6.2.1 Dissolved Sr

Dissolved Sr in the Narmada river (salinity  $\leq 0.2\text{‰}$ ) displays a range of 1.4 to 2.1  $\mu\text{mol/kg}$  and 1.3 to 1.7  $\mu\text{mol/kg}$  during pre-monsoon and monsoon respectively. Some of the river samples (NE07-20, 21, 22, NEM07-14; Table 6.1) were collected ~170 km upstream of the estuary region, near the Sardar Sarovar Dam.  $^{87}\text{Sr}/^{86}\text{Sr}$  of the river water varies from 0.71001 to 0.71079 and 0.70994 to 0.71053 during pre-monsoon and monsoon respectively. Sr content and its isotope composition of the Narmada river measured in this study (Table 6.1) fall within the range of those reported by Trivedi et al. (1995) and Dessert et al. (2001). Sr isotope composition of the Narmada bears the signatures of the Deccan basalts and the Vindhyan sediments

through which it flows. Two groundwaters collected from the depth of ~18 and ~24 m and ~40 km upstream of the estuary display narrow range in Sr isotope composition, 0.70941 - 0.70951 though their Sr concentration show wide range 9.6-57.4  $\mu\text{mol/kg}$  (Table 6.1).

The Tapi estuary was studied only during monsoon. It is less radiogenic in dissolved Sr compared to the Narmada. Two river water samples from the Tapi have  $^{87}\text{Sr}/^{86}\text{Sr}$  of 0.70875 and 0.70894 with Sr concentration of 1.3 and 2.5  $\mu\text{mol/kg}$  respectively. These values are similar to those reported earlier from the Tapi river (Trivedi et al., 1995; Dessert et al., 2001). Analogous to the Narmada, the Sr isotope composition of the Tapi also seems to be controlled predominantly by Sr supply from the Deccan basalts which are quite unradiogenic (Das et al., 2005) and lower compared to contemporary seawater. The Mandovi river and estuary was also sampled during post-monsoon. A sample of the Mandovi river analysed for Sr has  $^{87}\text{Sr}/^{86}\text{Sr}$  of 0.71062 with Sr concentration of 0.7  $\mu\text{mol/kg}$ . Among the three rivers, the lowest Sr is observed in the Mandovi, consistent with the lateritic lithology exposed in its drainage basin, higher runoff and lower water rock interaction. This observation is also supported by the lowest alkalinity and other trace metals U, Mo and Re data measured in the Mandovi river water (Rahaman and Singh, 2010; Table 2.2; Chapter 5).

Dissolved Sr in the Narmada estuary ranges from 1.4 to 77.1  $\mu\text{mol/kg}$  during pre-monsoon in the salinity range 0 to 31‰ whereas during monsoon, it ranges from 1.6 to 42.4  $\mu\text{mol/kg}$  in the salinity range 0 to 17‰. This estuary could not be sampled beyond 17 ‰ salinity during monsoon because of inadequate facilities for sample collection in highly turbulent conditions. During both seasons dissolved Sr-salinity plots for the Narmada estuary show conservative mixing with correlation coefficient,  $R^2 \geq 0.99$  (Fig. 6.1 a & b). The sample NEM07-10 collected during monsoon for salinity 12.1‰ deviated from the trend set by other data with low Sr. This data has not been included in the plot. This sample shows anomalous behaviour for all elements analysed Sr, Re, Mo and U; reason for which is unclear. The intercepts on Sr-axis at zero salinity based on conservative mixing lines are  $1.02 \pm 0.63$  and

1.54±0.40 (Fig. 6.1 a & b) which lie within the range of measured riverine Sr concentration, ~1.5 nmol/kg. The extrapolated seawater Sr endmember at 35 ‰ salinity using Sr-salinity plot is estimated to be 88±1.2 and 83.4±1.5 nmol/kg for pre-monsoon and monsoon sampling respectively (Figs. 6.1 a & b), comparable to those reported for open ocean, 90 nmol/kg (Palmer and Edmond, 1989; de Villiers, 1999). The slope of both pre-monsoon and monsoon lines are close to each other and are very similar to (Sr/salinity) ratio of seawater.

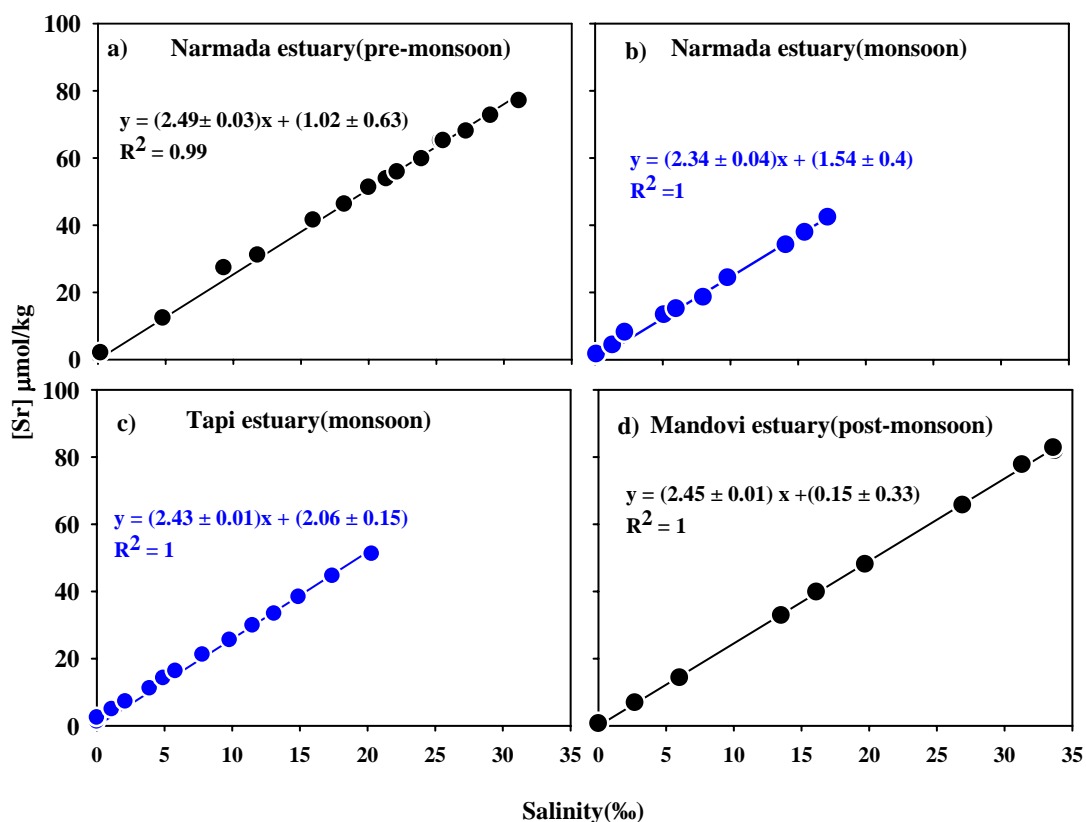


**Fig. 6.1** Dissolved Sr vs. salinity plots in the Narmada, Tapi and Mandovi estuaries from Arabian Sea. Sr exhibits conservative behaviour in all these three estuaries.

Sr concentration in the Tapi estuary ranges from 2.5 to 51.2  $\mu\text{mol/kg}$  within salinity ranges of 0.2 to 20.3‰. Sr versus salinity in Tapi estuary also shows strong conservative mixing between river water and seawater endmembers with correlation coefficient,  $R^2 \sim 1$ . Estimated Sr concentration at 35‰ salinity in Fig. 6.1c is 87.1±0.4

$\mu\text{mol/kg}$  which is close to the average seawater concentration  $\sim 90 \mu\text{mol/kg}$ . Dissolved Sr in the Mandovi river is half of those measured in the Narmada and the Tapi. Sr concentration vs. salinity plot for the Mandovi estuary also shows a very good conservative mixing between river and seawater endmembers. The intercept on Sr axis of Sr – salinity mixing line is  $0.15 \pm 0.33$  (Fig. 6.1d). The Sr concentration at 35‰ salinity corresponds to  $85.9 \pm 0.5 \mu\text{mol/kg}$  based on the extrapolated conservative mixing line (Fig. 6.1d). Sr measured in the Narmada, Tapi and the Mandovi estuaries in this study shows its conservative behaviour in all of them. There seems to be no measurable loss or gain of Sr in these estuaries during their sampling periods and the Sr concentration with salinity is defined by the mixing between river and seawater endmembers only.

### 6.2.2 Dissolved Ba

Dissolved Ba has been measured in four rivers, the Narmada, Tapi, Mandovi and the Hooghly and in their estuaries. Ba concentration shows significant variability within a river and also among the various rivers. Ba concentrations in the Narmada river near the Sardar Sarovar dam are 89 - 207 nmol/kg whereas at its mouth in the estuary, it is only 30 nmol/kg. The decrease along the river is likely due to mixing of tributaries. The Tapi has Ba concentration of 49 and 59 nmol/kg within the range reported for rivers draining the Deccan basalts such as the Godavari and the Krishna rivers, 8-105 nM (Das and Krishnaswami, 2005). The Mandovi has relatively lower Ba, 27 nmol/kg, consistent with the low concentration of other major and trace elements (Rahaman and Singh, 2010). Riverine Ba for the Hooghly is not measured in this study. One sample collected in the estuary with salinity 0.5 ‰ has Ba concentration 266 nmol/kg, significantly higher than Ba concentration in the Ganga water at Risikesh  $\sim 72$ -78 nM (Dalai et al., 2002), in the Ganges-Brahmaputra mixing zone, 147-167 nM (Carroll et al., 1993) and the Ganga before its confluence with

Brahmaputra in Bangladesh, 110-130 nM Ba (Moore, 1997).

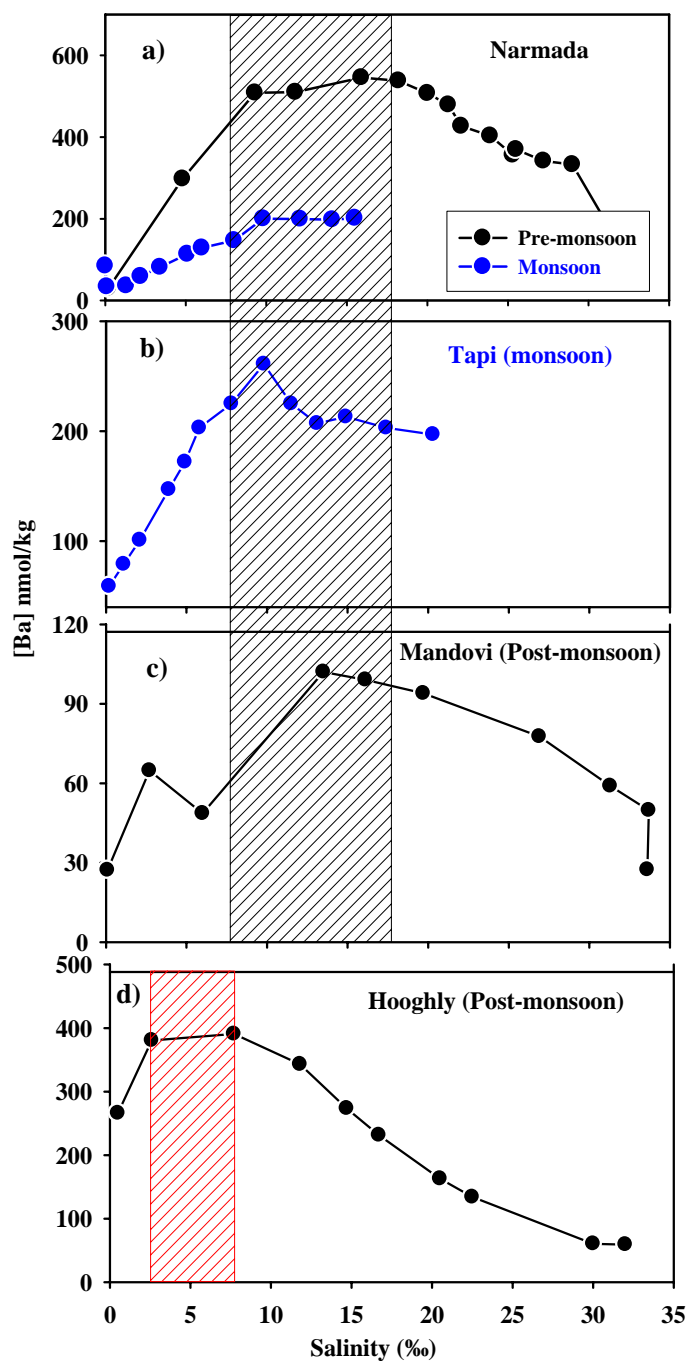


**Fig. 6.2** Dissolved Ba-salinity profile in four estuaries. All the profiles show non-conservative behaviour of Ba with its gain in the low to mid salinity regions.

The distribution of dissolved Ba as a function of salinity in the estuaries analysed are presented in Fig. 6.2 (a, b, c & d). All these profiles show upward curvature, i.e. gain of Ba at lower to mid salinity regions demonstrating its non-conservative behaviour. This is unlike that observed for dissolved Sr in these estuaries, underscoring the distinct differences in the behaviour of the two alkaline earths in the estuaries. The gain of Ba at low to mid salinity ranges is similar to that reported for the behaviour of Ba in a few global estuaries (Moore, 1997, Shaw et al., 1998). This gain has been attributed either to the desorption of Ba from particles (Coffey et al., 1997) or its supply from submarine groundwater discharge (Moore, 1997). Ba concentration in the Narmada estuary ranges from 30 (at salinity 0.2‰) to 546 nmol/kg and 34 (at salinity 0.1‰) to 202 nmol/kg during pre-monsoon and monsoon respectively (Table 6.1, Fig. 6.2a). Among the four estuaries analysed in this study, the highest Ba concentration was observed in the Narmada estuary during pre-monsoon. The mixing profile of Ba with salinity in the Narmada shows maxima at mid salinity of the profile. In both pre-monsoon and monsoon seasons, the humps in the Ba concentration in this estuary are observed in the salinity range of 10 to 16 ‰, however the magnitude of the hump in the monsoon is only about one third of that observed during the pre-monsoon. Ba concentration in the Tapi estuary during monsoon ranges from 49 to 261 nmol/kg. The Ba-salinity profile in this estuary also shows non-conservative behaviour with the highest abundance, 261 nmol/kg at ~10‰ salinity (Fig. 6.2b). The hump in the Ba-salinity profile in the Tapi estuary is similar to that in the Narmada.

Dissolved Ba in the Mandovi estuary ranges from 27 to 102 nmol/kg. Mid-salinity enrichment in Ba concentration is also observed in the Mandovi estuary. The peak of Ba concentration in this estuary is 102 nmol/kg at salinity 13.5 ‰. Ba in the Hooghly estuary ranges from 59 to 391 nmol/kg (Table 6.1, Fig. 6.2d). The characteristics of Ba concentration in the Hooghly estuary are different compared to the other three estuaries in that the Ba concentration peaks at a lower salinity, ~2.5-7‰ unlike the others where the maxima is in the mid-salinity range. The highest concentration of Ba in the Hooghly estuary is 391 nmol/kg, similar to what has been

observed in river dominated channels of the Ganga-Brahmaputra estuary during February, 1987 sampling (Carroll et al., 1993). The location (~2.6 ‰ salinity) of the peak Ba concentration in the Hooghly estuary is also similar to that reported for Ganga-Brahmaputra estuary (Carroll et al., 1993). Ba concentration measured in sea water samples collected from the Arabian Sea off Goa coast is  $\sim 35 \pm 3$  nmol/kg.

### 6.2.3 Particulate Ba, Sr and major elements in the Narmada estuary

Particulate Ba and Sr concentrations along with major element composition were analysed only for monsoon samples from the Narmada estuary (Table 6.2). Ba and Sr concentrations in the suspended load of the Narmada estuary vary from 207 to 233 and 178 to 284  $\mu\text{g/g}$  with average values of  $219 \pm 8$  and  $239 \pm 31$   $\mu\text{g/g}$  respectively. Ba and Sr abundances in sediments of rivers draining the Deccan basalts range from 79 to 273  $\mu\text{g/g}$  and 40 to 340  $\mu\text{g/g}$  with average of  $189 \pm 43$  and  $228 \pm 32$   $\mu\text{g/g}$  respectively (Das and Krishnaswami, 2005, Das et al., 2006) which are lower than the average continental crust value of Ba and Sr 500  $\mu\text{g/g}$  and 384  $\mu\text{g/g}$  respectively (Bowen, 1979).

**Table 6.2: Ba, Sr and major element abundances in particulate matter from the Narmada estuary during monsoon**

| <u>Sample Id</u> | <u>Salinity</u> | <u>Al</u>  | <u>Fe</u>  | <u>Ca</u>  | <u>Mg</u>  | <u>Na</u>  | <u>K</u>   | <u>Ba</u>       | <u>Sr</u>  |
|------------------|-----------------|------------|------------|------------|------------|------------|------------|-----------------|------------|
|                  | (‰)             | %          |            |            |            |            |            | $\mu\text{g/g}$ |            |
| NE-SS-1          | 4.8             | 9.1        | 8.8        | 2.7        | 2.5        | 0.5        | 1.1        | 213             | 178        |
| NE-SS-2          | 9.3             | 8.3        | 8.3        | 3.2        | 2.4        | 0.5        | 1.2        | 207             | 207        |
| NE-SS-3          | 11.8            | 8.6        | 8.1        | 3.1        | 2.3        | 0.5        | 1.2        | 207             | 207        |
| NE-SS-5          | 18.2            | 8.9        | 8.4        | 3.4        | 2.5        | 0.7        | 1.3        | 223             | 236        |
| NE-SS-6          | 20              | 8.5        | 8.3        | 3.4        | 2.4        | 0.8        | 1.4        | 214             | 243        |
| NE-SS-7          | 21.3            | 8.3        | 8.2        | 3.5        | 2.4        | 0.9        | 1.3        | 225             | 250        |
| NE-SS-8          | 22.1            | 8.5        | 8.5        | 3.5        | 2.4        | 0.6        | 1.9        | 219             | 259        |
| NE-SS-9          | 23.9            | 8.4        | 8.2        | 3.5        | 2.4        | 0.6        | 1.3        | 230             | 276        |
| NE-SS-10         | 25.3            | 8.2        | 8.0        | 3.8        | 2.3        | 1.0        | 1.3        | 233             | 284        |
| NE-SS-11         | 25.5            | 9.0        | 8.8        | 3.9        | 2.6        | 0.9        | 1.4        | 219             | 253        |
| <b>Average</b>   |                 | <b>8.6</b> | <b>8.4</b> | <b>3.4</b> | <b>2.4</b> | <b>0.7</b> | <b>1.3</b> | <b>219</b>      | <b>239</b> |

The abundances of Al and Fe in the particulates are almost uniform from fresh water to seawater along salinity gradient with average concentration of  $(8.6 \pm 0.3)$  wt% and  $(8.4 \pm 0.3)$  wt% respectively. Other major elements Na, K, Ca and Mg show minor variability. The distributions of Ca/Al and Sr/Al show increase with salinity most likely a result of increase in biogenic material in the particulates towards seaside (Fig. 6.3). The Al normalized Ba abundances do not show any clearly discernable variation with salinity.

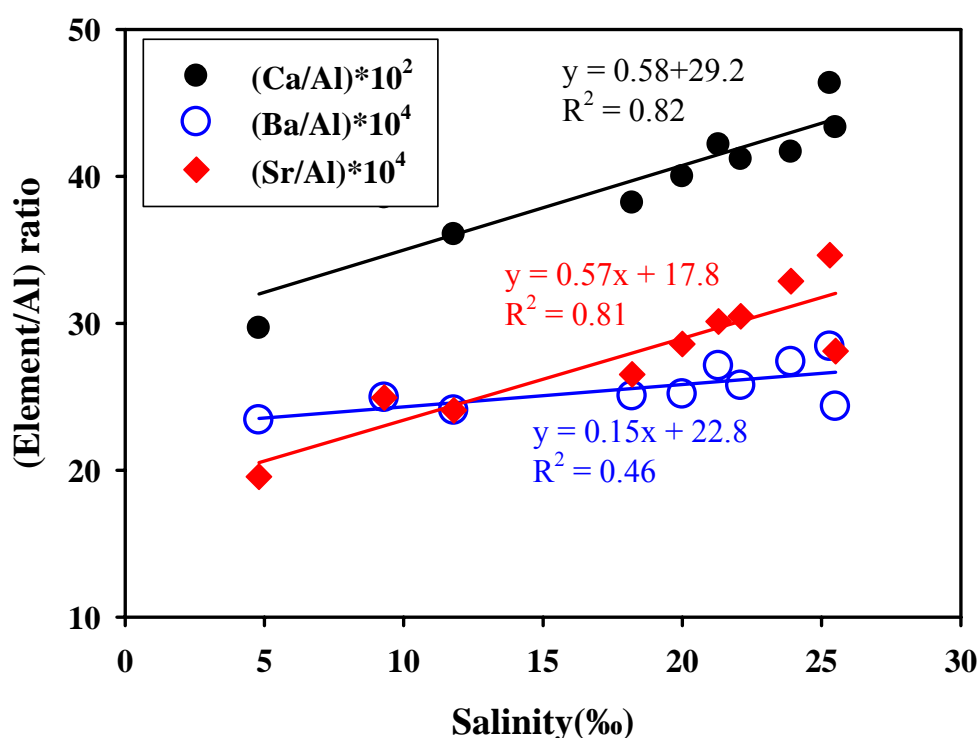


**Fig. 6.3** Scatter plots of Ca/Al, Sr/Al and Ba/Al of suspended particulate matter with salinity in the Narmada estuary. Ca/Al and Sr/Al show increase with salinity whereas Ba/Al is almost uniform along the salinity gradient. Element/Al ratios are in (wt%/wt%) for Ca and ( $\mu\text{g/g}$ )/(wt %) Sr and Ba.

#### 6.2.4 Behaviour of dissolved $^{87}\text{Sr}/^{86}\text{Sr}$ in estuaries

Sr versus salinity plots (Figs. 6.1) in all the estuaries indicates conservative mixing. There is no gain or loss of Sr within the experimental uncertainties of Sr and salinity measurements in these estuaries as all the data points fall on the mixing lines defined

by the sea and river endmembers (Figs. 6.1 a, b, c and d). Precision of Sr concentration measurement based on replicate analysis of estuarine water is in general, ~1% whereas in case of its isotope composition ( $^{87}\text{Sr}/^{86}\text{Sr}$ ), it is better than ~9 ppm (Table 2.5). This suggests that  $^{87}\text{Sr}/^{86}\text{Sr}$  variations in excess of 30 ppm can be reliably measured and therefore is a more sensitive tracer to investigate the mixing behaviour of dissolved Sr in estuaries. Thus, minor inputs from additional sources (e.g. SGD) that can cause deviations >30 ppm from the theoretical mixing lines can be identified using two end members in the  $1/\text{Sr}-^{87}\text{Sr}/^{86}\text{Sr}$  plots. In a two endmember system (seawater and river water) all the data should fall on the mixing line defined by Sr concentration and isotope ratio of the endmembers. If there are additional sources with distinctly different  $^{87}\text{Sr}/^{86}\text{Sr}$  compared to sea and river water, then the points will plot outside the theoretical mixing line. Thus, the scatter of the  $^{87}\text{Sr}/^{86}\text{Sr}$  data along with theoretical mixing lines can point to additional endmember supply of Sr to the estuary.

The Sr isotope mixing plots for the estuaries studied are presented in Figs. 6.4 a, b, c and d, along with theoretical mixing line between seawater and river waters. Samples with salinity (<0.2‰) in a given estuary are considered as riverine endmembers. Both Sr concentrations and its isotope composition of the riverine endmembers of the estuaries vary significantly. Further, even for a given estuary, these parameters show seasonal variations. As discussed in section 6.2.1, Sr concentration of rivers and their  $^{87}\text{Sr}/^{86}\text{Sr}$  depends on the lithology, flow regime and weathering intensity. Sr isotope composition of the Narmada, the Tapi and the Mandovi show significant variation with Tapi having the lowest radiogenic Sr as it drains mainly through the Deccan basalts which are quite unradiogenic in Sr. As all the estuaries considered in this study for Sr are linked to the Arabian Sea, the seawater endmember is taken to be the  $^{87}\text{Sr}/^{86}\text{Sr}$  measured in the Arabian Seawater  $0.709149 \pm 0.000016$ ,  $n=5$  (Rai, 2008, Ph.D. Thesis). Sr concentration for seawater is taken to be  $90 \mu\text{mol}/\text{kg}$  (Palmer and Edmond, 1989; de Villiers, 1999). The seawater Sr concentrations extrapolated from Sr – salinity relation (Figs. 6.4a–d) are close to this reported concentration. The Sr mixing diagrams (Figs. 6.4 a–d) show that in all

the estuaries, majority of the data points fall away from the theoretical mixing lines defined by the seawater and river water endmembers. This indicates supply of Sr to these estuaries from sources in addition to river and seawater. In this context, some of the earlier studies based on Sr and  $^{87}\text{Sr}/^{86}\text{Sr}$  have reported non-conservative behaviour of Sr in estuaries (Wang et al., 2001; Xu and Marcantano, 2004; Xu et al., 2007) which were attributed to environmental changes (Eh, pH, salinity, temperature) and other factors such as anoxia, large storms in the coastal areas which have the potential to release labile Sr from particulate to dissolve phase. The  $^{87}\text{Sr}/^{86}\text{Sr}$  mixing lines (Fig. 6.4) indicate non-conservative behaviour of  $^{87}\text{Sr}/^{86}\text{Sr}$  along almost the entire stretch of the estuary particularly at higher salinity ranges.

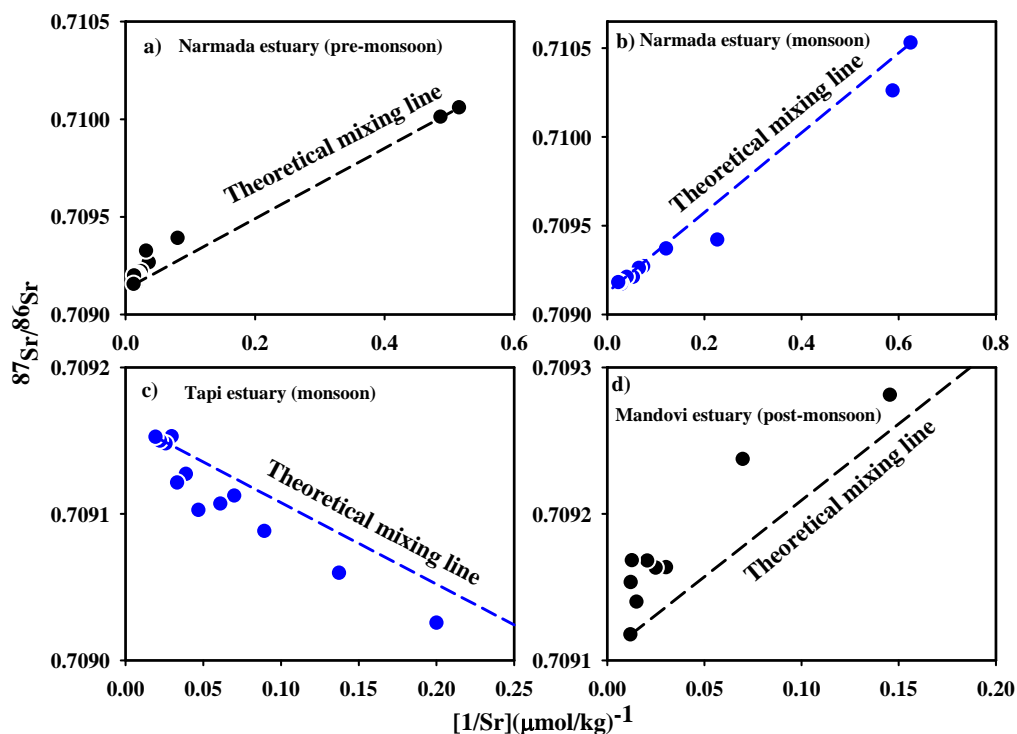


**Fig. 6.4** Plots of dissolved  $^{87}\text{Sr}/^{86}\text{Sr}$  vs.  $1/\text{Sr}$  concentration in estuaries. The dashed line is the theoretical mixing line for two end member mixing. Most of the data points plot away from the theoretical mixing line suggesting non-conservative behaviour of  $^{87}\text{Sr}/^{86}\text{Sr}$ .

Further, deviation from the theoretical mixing line (TML) in the Narmada estuary is observed during both pre-monsoon and monsoon seasons. There are two processes by which the  $^{87}\text{Sr}/^{86}\text{Sr}$  distribution with  $1/\text{Sr}$  can be explained (i) desorption of Sr from particles in the estuaries, (ii) supply of Sr by SGD. The SGD may be a combination of groundwater and/or re-circulated seawater (Moore, 2009), the composition of which is controlled by the hydraulic gradient in adjacent aquifers and varying tidal conditions in coastal waters (Fig.6.5). Earlier studies on the behaviour of Ba in estuaries had attributed its non-conservative behaviour to desorption from particles (Li and Chan, 1979; Carroll et al., 1993; Coffey et al., 1997). Similarly, Wang et al. (2001), Xu and Marcantano (2004) explained the non-conservative behaviour of Sr in the Changjiang and the Mississippi estuaries respectively due to desorption from particle during estuarine mixing. The role of this process in contributing to  $^{87}\text{Sr}/^{86}\text{Sr}$  in the estuaries investigated remains to be ascertained. Efforts to assess the variations in Sr/Al in particles in estuary as a function of salinity were unsuccessful because of Sr associated with carbonates. However, the observation that deviation in  $^{87}\text{Sr}/^{86}\text{Sr}$  is observed along the entire stretch of the estuary particularly at higher salinities and that it deviates even during non-monsoon season where particulate transport from the rivers are low rule out the possibility of desorption from particles as a source of  $^{87}\text{Sr}/^{86}\text{Sr}$  in the estuaries, however the role of re-suspended sediments in contributing to it needs to be assessed. Alternatively, SGD may be a possible source of additional Sr in the estuary. The SGD can have the  $^{87}\text{Sr}/^{86}\text{Sr}$  of continental signature or a mixture of seawater and continental signature depending on regional aquifer characteristics (Harvey et al., 2002). Large influx of submarine groundwater has been reported in the Meghna estuary (Ganga-Brahmaputra mixing zone) based on the study of Ba and  $^{226}\text{Ra}$  (Moore, 1997). Basu et al. (2001) based on detailed study of Sr and  $^{87}\text{Sr}/^{86}\text{Sr}$  in groundwater of the Bengal delta has suggested that Bay of Bengal receives significant input of Sr via SGD, in magnitude comparable to the combined fluxes of the Ganga-Brahmaputra rivers. Thus there are hints that submarine ground water discharge can be a potential source of Sr which can significantly contribute to its global oceanic budget. In this study attempts have been made based on Sr isotopes

to estimate SGD contribution to the estuaries relying on the hypothesis that deviations in  $^{87}\text{Sr}/^{86}\text{Sr}$  from the TML in the estuaries is only due to contributions from SGD.

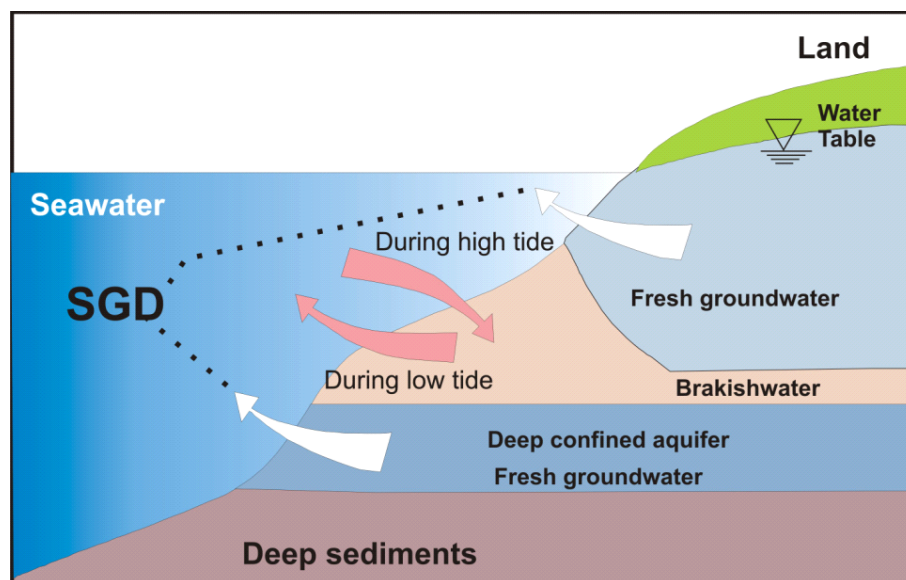


**Fig. 6.5 Schematic of submarine groundwater discharge in to coastal regions. Figure modified from Burnett et al. (2006)**

In the Narmada estuary, deviation of  $^{87}\text{Sr}/^{86}\text{Sr}$  data points from TML during the two seasons is opposite; they plot above the TML during pre-monsoon whereas they lie below the TML during monsoon.  $^{87}\text{Sr}/^{86}\text{Sr}$  and Sr concentrations have been measured in two groundwater samples collected from the vicinity of the Narmada River. The  $^{87}\text{Sr}/^{86}\text{Sr}$  of these two samples is within a narrow range, 0.70941-0.70951 whereas their Sr concentrations vary significantly, 9.6 and 57.4  $\mu\text{mol}/\text{kg}$ . During pre-monsoon, the majority of the data points on the  $1/\text{Sr}$  vs.  $^{87}\text{Sr}/^{86}\text{Sr}$  plot in the Narmada estuary fall above the TML defined between river and seawater (Fig. 6.6). In fact except the two river water samples, all other data points plot close to the mixing line defined by the seawater endmember and one of the groundwaters sampled (Sr: 7.9  $\mu\text{mol}/\text{kg}$ ,  $^{87}\text{Sr}/^{86}\text{Sr}$ : 0.70951) indicating that role of river in determining of  $^{87}\text{Sr}/^{86}\text{Sr}$  distribution in the estuary is only minor. This is likely as Narmada is dammed about

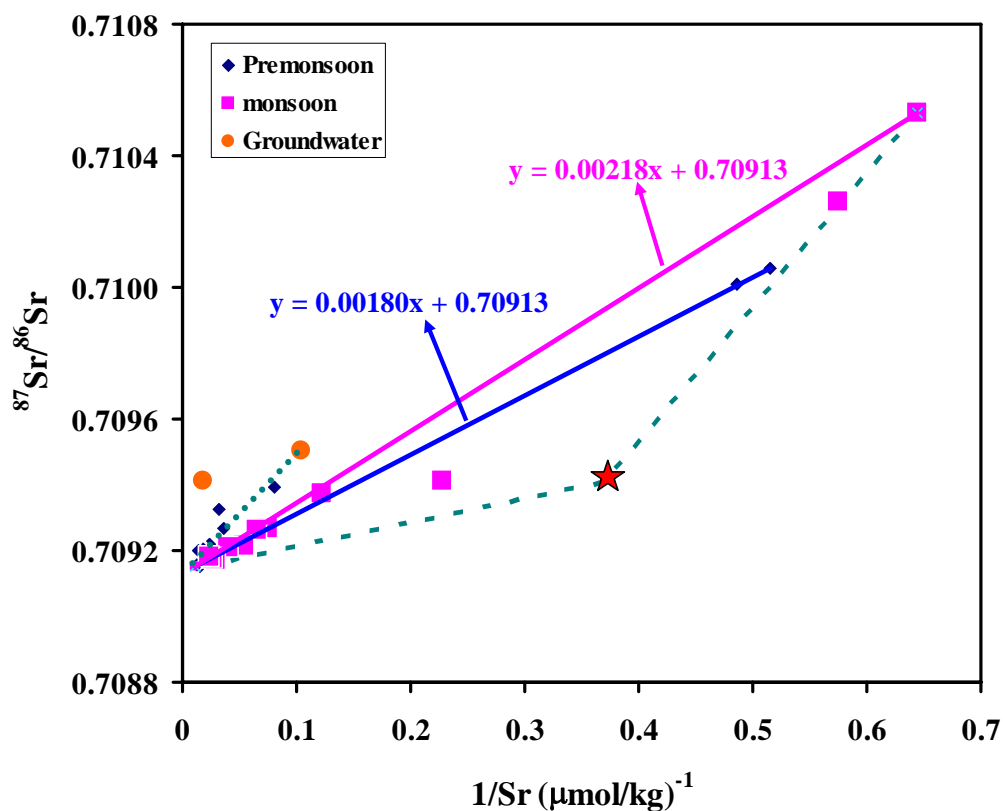


Fig. 6.6 Plot of  $^{87}\text{Sr}/^{86}\text{Sr}$  vs.  $1/\text{Sr}$  in the Narmada estuary. The data points plot below the TML during monsoon and above the TML during pre-monsoon. The deviation of the data points from the TML are explained in terms of three endmembers mixing, riverwater, seawater and sub-marine groundwater. During pre-monsoon, all the data points, except two river water samples, plot close to the mixing line (dotted line) defined by seawater and groundwater (Sr:  $7.9 \mu\text{mol}/\text{kg}$ ,  $^{87}\text{Sr}/^{86}\text{Sr}$ : 0.70951). Red star (★) represents the SGD endmember during monsoon with  $^{87}\text{Sr}/^{86}\text{Sr}$  of 0.70941 same as that measured in one of the samples this study but its Sr concentration is derived to explain the Sr content and  $^{87}\text{Sr}/^{76}\text{Sr}$  of the sample NEM08-2 by mixing of riverwater and the proposed groundwater. The estimated Sr concentration of the proposed groundwater is  $\sim 2.7 \mu\text{mol}/\text{kg}$ .

170 km upstream of the estuary and during pre-monsoon not much water reach to the river downstream of the dam. Further, during lean flow period the groundwater contribution to river could be significant and hence  $^{87}\text{Sr}/^{86}\text{Sr}$  of the estuary may be defined between groundwater and seawater. The impact of groundwater discharge into the river would be born out in Sr concentration and isotopic composition of the river at its mouth considering that the river and seawater mixing does not follow the TML. The deviation from the TML in the Fig. 6.6 may have to be explained into three endmember mixing e.g. the riverwater, seawater and groundwater. In this model the deviation in the  $^{87}\text{Sr}/^{86}\text{Sr}$  from the TML in the Narmada estuary is explained in terms of Sr supply from SGD. Interestingly, the two groundwater samples have salinity significantly higher than river water. The result during monsoon (Fig. 6.6), however, show that the data points fall close to the TML opposed to that observed during the pre-monsoon period. Such variations can result from groundwater contribution from different sources with different  $^{87}\text{Sr}/^{86}\text{Sr}$  discharging into the estuary during different seasons. For example, the data and Fig. 6.6 can also be explained in terms of three endmembers mixing with SGD having isotopic composition 0.70941. It is important to understand here that Sr isotope composition of SGD needs to be constrained far more precisely to evaluate its fluxes to the oceans more reliably.

To fit the monsoon data in terms of these end members, it can be estimated that a Sr concentration of  $\sim 2.7 \mu\text{mol}/\text{kg}$  for the groundwater is required (Fig. 6.6). Considering the three endmember mixing (Fig. 6.6), Sr concentration and  $^{87}\text{Sr}/^{86}\text{Sr}$  values of  $\sim 2.7 \mu\text{mol}/\text{kg}$  and 0.70941 respectively are assigned. The groundwater contribution for the sample NEM07-3 is estimated to be  $\sim 60\%$  with seawater contribution  $\sim 2\%$  and remaining is river water. To estimate the contribution from the groundwater, river water and seawater, two endmember mixing at a time has been considered. This estimate based on the simple model if valid, shows that during monsoon, the groundwater contribution seems to be double that of the river water. A major concern in the estimate of groundwater contribution to the estuary is the variability in their Sr concentration and  $^{87}\text{Sr}/^{86}\text{Sr}$ . A better estimate of Sr contribution

from groundwater can be made as more data on groundwater Sr composition becomes available.

During monsoon, water discharge from the river increases and hence the salinity front goes downstream in the estuary. Location of the sample NEM07-3 with salinity 1.3 ‰ collected during monsoon season, coincide with the samples collected around salinity 21-22 ‰ during pre-monsoon (Table 6.1). The flow and the location at which the SGD is interacting with the estuary water depends on the morphology of the river mouth, hydraulic gradient of the coastal aquifer and relationship between water table and local topography. In both the seasons, the impact of groundwater is observed in the Narmada estuary upstream of location 21°39' N and 72°34' E.

The plot of  $^{87}\text{Sr}/^{86}\text{Sr}$  and  $1/\text{Sr}$  in the Tapi estuary shows negative slope (Fig. 6.4c). As discussed earlier, the Tapi river water is less radiogenic compared to seawater defining mixing trend with a negative slope. Majority of the data points in the Tapi estuary plot below the TML (Fig. 6.4 c). This could also be explained by addition of Sr in the estuary through sub-marine groundwater. The major lithology through which the Tapi river drains is Deccan basalts with  $^{87}\text{Sr}/^{86}\text{Sr}$  lower than that of seawater. Hence, the  $^{87}\text{Sr}/^{86}\text{Sr}$  of groundwater in the vicinity of the Tapi river is expected to be lower than that of seawater. Influx of submarine groundwater to the estuary with  $^{87}\text{Sr}/^{86}\text{Sr}$  lower than river water would pull down the Sr isotope composition of the estuary water below the TML defined by the river and seawater. Sr isotope composition of the Tapi estuary also indicate significant contribution from the submarine groundwater discharge, however, in absence of Sr concentration and  $^{87}\text{Sr}/^{86}\text{Sr}$  data for groundwaters around the region, quantification of the contribution from this source to the estuary is difficult. In this context it is pertinent to mention here that this study is corroborated with flux of groundwater reported in the Tapi estuary receiving  $18,000 \times 10^6 \text{ m}^3/\text{y}$  of groundwater, much higher compared to the surface flow of the Tapi river  $7,686 \times 10^6 \text{ m}^3/\text{y}$  (Krupadam et al., 2006).

River endmember of the Mandovi estuary has lower Sr concentration with more radiogenic Sr than those of the Narmada and the Tapi. Similar to the Narmada and the Tapi estuaries the two end members mixing plot of  $1/\text{Sr}$  versus  $^{87}\text{Sr}/^{86}\text{Sr}$  in the

Mandovi estuary also shows non-conservative behaviour. In this estuary, significant deviation from the TML defined by the river and seawater endmembers has been observed for samples from higher salinity. There is no data for Sr concentration and  $^{87}\text{Sr}/^{86}\text{Sr}$  in groundwaters from catchments of the Mandovi; hence the quantification of its contribution to the estuary is difficult. As the lithology of the drainage basin of the Mandovi river is more radiogenic in Sr as is reflected in the riverine  $^{87}\text{Sr}/^{86}\text{Sr}$ , the groundwater is also expected to have more radiogenic Sr than that of seawater. If groundwaters are discharged into estuarine region, it would increase the  $^{87}\text{Sr}/^{86}\text{Sr}$  of the estuary water compared to that defined by the TML (Fig. 6.4d). Jacob et al. (2009) has reported the existence of submarine groundwater discharge (SGD) in the west coast of India; and made a semi-quantitative estimate of its rate in coastal area of Vizhinjam, Thiruvananthapuram, Kerala. This inferences based on Sr isotope data of this study is consistent with the conclusion of Jacob et al. (2009) from the west coast of India.

### **6.2.5 Implication of quasi-conservative behaviour of Sr in estuaries**

This Sr and  $^{87}\text{Sr}/^{86}\text{Sr}$  study of estuaries have yielded very interesting results; it shows that Sr behave conservatively in all the estuaries investigated whereas  $^{87}\text{Sr}/^{86}\text{Sr}$  data suggests a three end member mixing in the estuaries, the third end member can either by desorption from particles or SGD. The presently available data, it is difficult to choose between two sources, though SGD seems to be more favorable. If this is indeed valid then rough estimates of Sr budget in these estuaries show that SGD can have significant role in determining the  $^{87}\text{Sr}/^{86}\text{Sr}$  distribution in these estuaries.

### **6.2.6 Dissolved Ba in estuaries**

The distribution of Ba in estuaries shows considerable mid salinity increase in its concentration in all the estuaries studied, similar to those of the global estuaries (Hanor & Chan, 1977; Edmond et al., 1978; Li & Chan, 1979). The degree of enrichment in Ba and its salinity profile vary among the estuaries (This study, Coffey et al., 1995). The hump in the Ba distribution in estuaries often occurs in the low to

intermediate salinity (1-20‰). This hump has been explained in terms of desorption of Ba from suspended particles (Shaw et al., 1998). In river water and fresh ground water Ba gets strongly adsorbed to the particulate matter and when these particles come in contact with sea water in estuaries differences in chemical properties such as ionic strength, composition, Eh-pH condition can alter adsorption coefficient of Ba, causing its release to solution. Hanor and Chan (1977) modeled that barium release from clay particles, assuming a rapid ion exchange with  $Mg^{2+}$  as a representative seawater ion. Moore (1997) hypothesized that the high Ba flux observed in the Ganges-Brahmaputra delta during lean flow condition can only be sustained by large groundwater influx within the estuary which contains high Ba. Coastal aquifers get recharged with fresh water during high river discharge. Under these conditions the distribution coefficient ( $K_d$ ) for Ba on aquifer solids is high and Ba is adsorbed to solids. During low river discharge, the penetration of salt water into the coastal aquifer causes  $K_d$  to decrease and facilitates the desorption of Ba from particles in the aquifer. Salty groundwater transports the dissolved Ba to the sea. These processes are modulated by the tidal cycle.

In the following section an effort has been made to assess the sources of higher Ba concentration in the estuaries investigated in this study. Table 6.3 represents Ba concentration of dissolved and particulate phases of the rivers. Based on the particulate load and its Ba concentration, total Ba available for desorption is computed (Table 6.3). Ba concentrations in the particulate matter of the Narmada and the Tapi are considered to be same as that reported for sediments of the Krishna, and other rivers flowing through the Deccan (Das et al. 2006) whereas for the Hooghly, Ba concentration of Yamuna sediment (Dalai et al., 2002) is taken as representative. Ba concentration in the particulates of the Mandovi is taken to be same as average crustal value (Bowen, 1979).

Table 6.3: Dissolved and particulate Ba characteristics in estuaries

| River   | Annual water Discharge   | SPM  | Season*      | Ba peak at salinity | Ba Peak | Ba in sediment   | Ba available for desorption | Riverine Ba | EZSEMC of Ba | Excess Ba |
|---------|--------------------------|------|--------------|---------------------|---------|------------------|-----------------------------|-------------|--------------|-----------|
|         | 10 <sup>12</sup> liter/y | mg/l |              | (‰)                 | nmol/kg | µg/g             | nmol/kg                     | nmol/kg     | nmol/kg      | nmol/kg   |
| Narmada | 47                       | 3    | Pre-monsoon  | 15.9                | 546     | 189 <sup>1</sup> | 4                           | 30          | 981          | 951       |
|         |                          | 384  | Monsoon      | 15.5                | 202     | 189 <sup>1</sup> | 530                         | 34          | -            | -         |
| Tapi    | 19                       | 1600 | Monsoon      | 9.8                 | 261     | 189 <sup>1</sup> | 2207                        | 59          | 290          | 231       |
| Mandovi | 16                       | 5    | Post-monsoon | 13.5                | 102     | 500 <sup>2</sup> | 18                          | 27          | 151          | 124       |
|         |                          | 20   | Monsoon      |                     |         | 500 <sup>2</sup> | 72                          | -           | -            | -         |
| Hooghly | 52                       | 282  | Monsoon      | -                   | -       | 370 <sup>3</sup> | 773                         | -           | -            | -         |
|         |                          | 64   | Post-monsoon | 2.6                 | 391     | 370 <sup>3</sup> | 175                         | 266         | 486          | 220       |

<sup>1</sup> Das and Krishnaswami (2006)

<sup>2</sup> average crustal Ba (Bowen, 1979)

<sup>3</sup> Dalai et al. (2002)

\* The season is specified for suspended load concentration

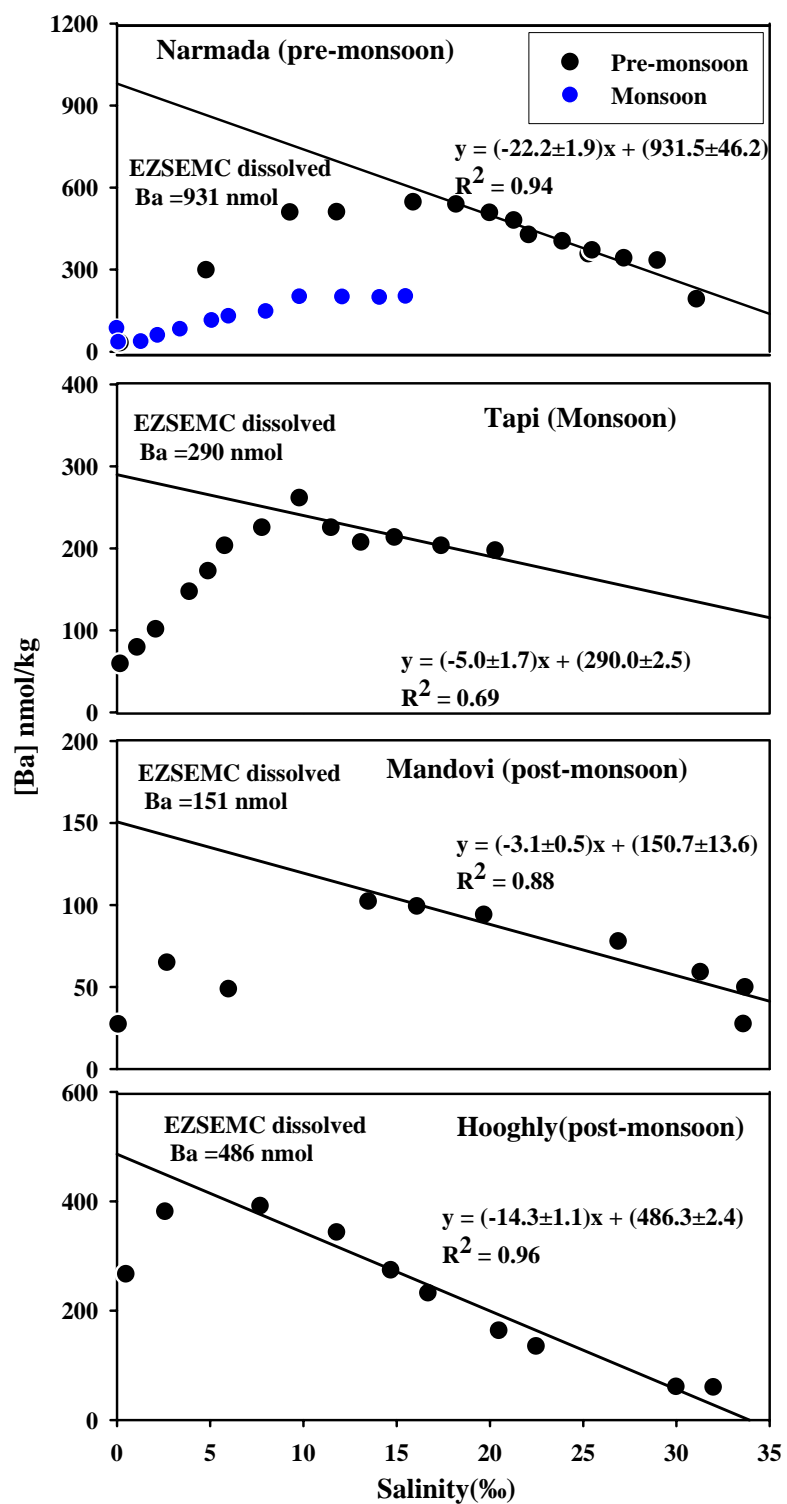


**Fig. 6.7** Effective zero salinity end member concentration of Ba in different estuaries.

While making this estimate, it is assumed that entire Ba of the suspended load is available for desorption, as a result, the estimate would be upper limit as significant part of Ba in the suspended load is associated with lattice sites and is likely to be unavailable for desorption (Coffey et al., 1997). Based on the hump in the Ba profile in the estuary, the effective zero salinity end member concentration (EZSEMC) is estimated by linear extrapolation of the Ba vs. salinity plot considering the points beyond the maximum concentration in the estuary (Fig. 6.7). EZSEMC of Ba in various estuaries vary considerably, from 151 to 981 nmol/kg. It is highest for the Narmada during pre-monsoon and lowest for the Mandovi during post-monsoon. The Hooghly has intermediate EZSEMC, 486 nmol/kg similar to that reported by Coffey et al. (1997) for the Ganga-Brahmaputra estuary. Excess Ba in the estuary is estimated by subtracting riverine Ba from EZSEMC of Ba (Table 6.3). In all the estuaries except the Tapi, excess Ba is much higher compared to Ba available for desorption from sediment. This is despite the fact that the estimate of desorbable Ba given in Table 6.3 is an upper limit. The peak Ba in the Narmada during pre-monsoon is three times higher compared to that during monsoon. Riverine sediment supply during pre-monsoon is very low compared to that during monsoon. More than 90% of the sediments are being transported to the Arabian Sea during monsoon period hence the much higher Ba during pre-monsoon is difficult to be explained in terms of desorption of Ba from suspended sediments. It is interesting to note that the peak Ba concentrations in the Narmada and the Tapi during monsoon are similar despite the fact that sediment concentrations in them are different. Further, Ba/Al in sediments of the Narmada estuary does not show measurable variation with salinity. All these observations seem to suggest that desorption of Ba from riverine sediments may not be an important cause for Ba hump in the estuaries, particularly during non-monsoon season. This conclusion critically depends upon the particulate matter abundance in the rivers; if they are much more than that is used in calculation then the conclusion will have to be reevaluated. A related issue is the resuspension of sediments and desorption from them. If, however, these above inferences are valid, then an additional source is required to explain the excess Ba in these estuaries. Submarine

groundwater discharge seems to be the possible source as has been suggested by Moore (1997) for the Ganga-Brahmaputra estuary. The Sr isotope study, as discussed in section 6.2.4, also hints at the significant contribution of SGD may have in this region. Two groundwater samples analysed in the vicinity of the Narmada estuary have Ba concentrations of 251 and 997 nmol/kg significantly higher than river water concentration. Groundwaters with such high Ba can be important source to the estuary. More groundwaters collected from the vicinity of various estuaries need to be analysed for Ba to quantify the SGD contribution through them.

The humps in Ba concentration of estuaries suggest that their input flux to ocean is significantly higher than that estimated using its river water concentration. While estimating their input fluxes to the ocean, the addition of Ba into the estuarine region from particulate and SGD in the estuary need to be considered. In view of large input of Ba in the estuary, the Ba fluxes need to be estimated using the river discharge and the EZSEMC of Ba for monsoon and non-monsoon seasons (Table 6.3). These fluxes would be significantly higher compared to the only riverine supply as significant Ba is being added in the estuary.

### 6.3 Conclusions

Dissolved Sr and  $^{87}\text{Sr}/^{86}\text{Sr}$  were measured in three estuaries, the Narmada, Tapi and the Mandovi whereas Ba was measured in four including the Hooghly estuary. Dissolved Sr,  $^{87}\text{Sr}/^{86}\text{Sr}$  and Ba show significant variability in rivers waters which depend on the lithologies of the basin. Dissolved Sr versus salinity plot in these estuaries show conservative mixing however, the mixing plots between  $^{87}\text{Sr}/^{86}\text{Sr}$  versus  $1/\text{Sr}$  clearly show deviation from the theoretical mixing line between seawater and riverwater endmembers, indicating non-conservative behaviour of Sr in the estuary. This observation is found in all the estuaries of this study. The extent of deviation from the expected mixing line is variable in different estuaries. Deviation from the theoretical mixing line is explained by the impact of submarine ground water discharge. This study suggests significant contribution of groundwater in all the estuaries. Further, this study highlights that Sr concentration and its isotope

composition in the estuary can be used as a tool to estimate submarine groundwater discharge.

Dissolved Ba/salinity profile in the estuary plots often exhibit upward curve indicating input in the mixing zone either from its release from suspended particulates or input from groundwater discharge. The upward curvature of Ba profile indicates gaining of Ba at low to mid salinity region of the estuaries. The highest Ba peak ~550 nmol/kg was observed in Narmada estuary during pre-monsoon whereas the lowest Ba peak ~100 nmol/kg observed in case of the Mandovi estuary. Excess Ba estimated for the Narmada, Tapi, Mandovi and the Hooghly estuaries is much higher compared to their riverine inputs. The excess Ba in these estuaries, in general, can not be supported by Ba desorption from particulate matter. Therefore, excess Ba can be explained by the significant amount of Ba contribution by the submarine groundwater discharge as has been suggested for Sr.

## **CHAPTER-7**

**Synthesis and future perspective**

This thesis deals with tracking the paleo-weathering intensity and the distribution of paleo-erosion over the Himalaya during past ~100 ka and the study of redox sensitive elements (Re, Mo and U) and alkaline earth metal Ba, Sr and  $^{87}\text{Sr}/^{86}\text{Sr}$  in the Indian estuaries, the Narmada, the Tapi, the Mandovi in the Arabian Sea and the Hooghly in the Bay of Bengal with the emphasis on their geochemistry and implications to their oceanic budgets. In this thesis, attempts have been made to understand distribution of erosion pattern over the central Himalaya during past ~100 ka using major element and Sr, Nd, O and C isotope compositions of the sediments from two sediment cores collected from the Ganga plain with an emphasis on climate-erosion coupling. Further, this thesis focuses on the study of sources, transport and behaviour of Re, Mo, U, Ba, Sr and  $^{87}\text{Sr}/^{86}\text{Sr}$  in river, estuary and ocean which highlights their natural and anthropogenic sources, distribution and fate of these elements and their final input to the oceans. Results of this study help to constrain riverine fluxes of these elements, their sources and sinks. The important results and findings of this study are summarized in the following sections.

### **7.1 Paleo-erosion over the Himalaya**

Major element compositions of the sediments of the 50-m long core from the Ganga plain show significant temporal variations. Major elements indicate their substantial depletion or enrichment with respect to the source rock compositions depending on the refractory or mobile nature of the elements. The chemical indices representing the intensity of chemical weathering such as modified chemical index of alteration, CIA\*,  $\text{Na}_2\text{O}/\text{Al}_2\text{O}_3$  and  $\text{Na}_2\text{O}/\text{TiO}_2$  of these sediments show considerable temporal variations. These indices indicate lower intensity of weathering of the sediments deposited during ~90, ~70, ~40 and ~20 ka compared to other sediments. These four excursions of lower intensity of weathering coincide with the precipitation minima during ~90, ~70, ~40 and ~20 ka and glacial maxima during ~70 and ~20 ka. These overlaps of timings of lower intensity in the chemical weathering and the climatic events suggest a strong coupling between climate and chemical weathering. The lower weathering over the Himalaya during ~90, ~70, ~40 and ~20 ka is result of

combined impact of lower rainfall and lower temperature. This study highlights the variation in intensity of chemical weathering with time indicating modulated fluxes of various elements from the Himalaya to ocean over glacial/interglacial time periods. Sr and Nd isotope compositions of these sediments exhibit significant temporal variations which are correlated with available paleo-climatic records i.e. solar insolation, precipitation and glaciations. Reduced monsoon intensity coupled with higher glacial cover over HH during ~90, ~70, ~40 and ~20 ka reduced erosion over HH which in turn enhanced the relative proportion of LH sediment to the Ganga plain causing higher  $^{87}\text{Sr}/^{86}\text{Sr}$  and depleted  $\epsilon_{\text{Nd}}$  in the Ganga plain sediments. This study underscores the significant influence of climate, particularly precipitation and glacial cover over the Himalaya, on the Himalayan erosion over millennium time scale and thereby highlights the climatic control on the regional tectonics by isostatic rebound. This study also illustrates that there is almost no time lag between the transfers of signal from source to sink.

## **7.2 Reconstruction of dissolved $^{87}\text{Sr}/^{86}\text{Sr}$ of the paleo-Ganga and paleoclimate of the Ganga plain**

$^{87}\text{Sr}/^{86}\text{Sr}$ ,  $\delta^{18}\text{O}$  and  $\delta^{13}\text{C}$  of the carbonate nodules analysed from sediment cores of the Ganga plain show significant temporal variations. Chemical compositions coupled with petrography of these carbonates indicate minor extent of later diagenesis and thereby indicating the preservation of their pristine chemical and isotopic signature. It is clearly observed that  $\delta^{18}\text{O}$  and  $\delta^{13}\text{C}$  show significant co-variations which could indicate climatic variation as a decrease in temperature and humidity (for example, during glacial periods) enhances evaporation causing enrichment in  $\delta^{18}\text{O}$  and will also be associated with increase of the proportion of  $\text{C}_4$  plants increasing the  $\delta^{13}\text{C}$ . However, this interpretation needs more work as significant positive correlation between  $\delta^{18}\text{O}$  and  $\delta^{13}\text{C}$  is generally considered to be the result of kinetic fractionation. It seems that carbonate precipitation has taken place out of equilibrium and hence they can not be used as a proxy for paleoclimatic reconstruction in the Ganga plain.

The  $^{87}\text{Sr}/^{86}\text{Sr}$  of the carbonate nodules of the Ganga plain is primarily controlled by  $^{87}\text{Sr}/^{86}\text{Sr}$  of ground waters from which they generally precipitates. Groundwater in the Ganga plain is in equilibrium with river water and hence  $^{87}\text{Sr}/^{86}\text{Sr}$  of the carbonate nodules represents  $^{87}\text{Sr}/^{86}\text{Sr}$  of the river water during the time of their precipitation. This study shows that the Sr isotope composition of the Ganga water was less radiogenic during last  $\sim 100$  ka compared to contemporary water. Ganga water became more radiogenic in recent past, exact timing of which is yet to be known. This abrupt increase in  $^{87}\text{Sr}/^{86}\text{Sr}$  of the Ganga water could result from enhanced silicate weathering of the Himalaya with more radiogenic Sr such as those present in the Lesser Himalaya. Recent increase in weathering of the LH could result from human occupation and associated activities over the mountains. In view of the recent increase observed in  $^{87}\text{Sr}/^{86}\text{Sr}$  of water of the Ganga at Kanpur, this study suggest the need of constructing temporal variations in  $^{87}\text{Sr}/^{86}\text{Sr}$  of the paleo Ganga at its out flow to assess its impact on oceanic  $^{87}\text{Sr}/^{86}\text{Sr}$  evolution.

### **7.3 Study of redox sensitive trace elements (Re, Mo and U) in estuary**

Mo, U and Re concentration in the Hooghly estuary in the Bay of Bengal and the Mahi, Narmada, Tapi and the Mandovi estuaries in the Arabian Sea are analysed in this study. River waters, seawaters and salt marsh samples along the Gulf of Cambay are also analysed for their U, Mo and Re concentrations. Mo and Re were analysed for the first time in any Indian estuaries. Dissolved Mo, U and Re show highly variable concentrations in the rivers, varying from 1 to 90 nmol/kg for Mo, 0.02 to 19.0 nmol/kg for U and 1.4 to 41 pmol/kg for Re. The highest concentration of U is observed in the Sabarmati river, probably contributed by the groundwater reported to have high U concentration where as the Mahi river has the highest Mo and Re concentrations, most probably sourced from anthropogenic sources such as industrial activities in the region. The lowest U, Mo and Re are measured in the Mandovi river resulting due to lateritic lithology, higher runoff and lower water-rock interaction in its drainage. U and Mo measured in the Arabian Sea water are similar to their average global values.

Behaviour of Mo, U and Re in the four estuaries analysed in this study are highly variable. In the Narmada estuary, Mo, U and Re show conservative mixing between riverine and seawater endmembers during both pre-monsoon and monsoon seasons. U and Re are conservative in the Tapi estuary, despite the fact that Mo shows non-conservative behaviour (gain) in the mid-salinity ranges resulting from anthropogenic activity. Re is conservative in the Hooghly and the Mandovi estuaries also. Both Mo and U show non-conservative behaviour (removal) in the Hooghly and the Mandovi estuaries. They get removed in the lower salinity regions of these estuaries. The loss of U and Mo could be either due to reducing condition prevailing in the Hooghly and the Mandovi estuaries caused by mangrove forest or resulting from their association with Fe-Mn precipitates in the estuaries. Mo and U in the Hooghly and the Mandovi estuary indicate their net sink. Annually  $\sim 1.6 \times 10^6$  moles of Mo is being lost in the Hooghly estuary, which is more than double of its riverine supply. The Mandovi estuary loses  $\sim 2 \times 10^5$  moles of Mo annually. About 40% of riverine uranium is being lost in the Hooghly estuary. Uranium removal in both the Hooghly and the Mandovi estuaries are one order of magnitude lower compared to that of Mo. Such processes in the estuaries not only prevent the riverine supply of elements to enter the open ocean but also remove part of marine component and could be an important sink of such elements influencing their oceanic budgets. This study estimates Mo loss in the range of  $0.4 \times 10^8$  to  $3.1 \times 10^8$  mol/y in the global estuaries associated with mangrove swamp. This could be one of the missing sinks of global Mo budget.

Though dissolved Re behaves conservatively in all the estuaries, the slopes and intercepts of the mixing lines between Re concentrations and salinity, however, differ among these estuaries suggestive of variations in riverine and seawater end members of Re concentrations. Dissolved Re concentration in most of the rivers analysed in this study is higher than the earlier estimate of global average riverine Re concentration,  $\sim 2.1$  pmol/kg. Based on this study and the available data, the contemporary annual riverine Re flux is estimated to be  $\sim 350 \times 10^3$  moles to the ocean with a global average riverine Re concentration of 9.2 pmol/kg, a factor of four

higher compared to earlier estimate. This data along with the assumption that the oceans are in steady state with respect to this riverine flux yields a residence time of  $\sim 175000$  years for Re in ocean which is  $\sim 4$  times lower compared to its earlier estimate. The role of anthropogenic input of Re to rivers in contributing to this lower estimate of residence time needs further scrutiny.

Mo and Re concentrations in the Gulf of Cambay are much higher compared to that of the Arabian Sea and global average seawater value. Higher value of Mo and Re in the Gulf is attributed to its supply from anthropogenic sources. Re concentration in the Gulf of Cambay is 2 to 5 times higher compared to open ocean value reported for other global oceans and measured in this study off the Goa coast. High Re in the Gulf of Cambay is attributed to waste waters discharged from various industries. Polluted rivers and the industrial waste waters deliver  $\sim 5 \times 10^6$  moles of Mo and  $\sim 2300$  moles of Re every year directly to the Gulf of Cambay and seems to be mainly derived from various industries situated along the coast of the Gulf.

Numerous petrochemicals and pharmaceutical industries situated along the coast of the Gulf of Cambay are probably supplying Mo and Re to the effluent waters and finally to the Gulf, however these anthropogenic sources do not contain U in them and that may be the reason for normal U content in the Gulf of Cambay. Further, this study indicates that salt marshes act as a sink of oceanic U and probably a source of Mo to the seawater. This study underscores the importance of both natural and anthropogenic inputs of Mo and Re to the ocean budgets and its impact on the estimates of residence time in the ocean.

#### **7.4 Studies on alkaline earth metals Ba, Sr and $^{87}\text{Sr}/^{86}\text{Sr}$ in estuary**

Dissolved Sr and  $^{87}\text{Sr}/^{86}\text{Sr}$  were measured in the Narmada, Tapi and the Mandovi estuaries for the first time. Ba was measured in the Hooghly in addition to the above estuaries. Riverine endmembers of Ba, Sr and  $^{87}\text{Sr}/^{86}\text{Sr}$  show significant variability depending on the lithologies of the basins. Mixing plot between dissolved Sr versus salinity in all the estuaries show conservative behaviour of Sr.  $^{87}\text{Sr}/^{86}\text{Sr}$  a more precisely measured parameter in the estuary compared to Sr concentration, however,

deviates significantly from the theoretical mixing line of  $^{87}\text{Sr}/^{86}\text{Sr}$  versus  $1/\text{Sr}$  of seawater and riverwater endmembers, clearly indicating non-conservative behaviour of Sr in the estuary. Deviation in  $^{87}\text{Sr}/^{86}\text{Sr}$  from the theoretical mixing line is explained by the impact of submarine ground water discharge in estuaries suggesting significant contribution of groundwater in all the estuaries. Further, this study highlights that Sr concentration and its isotope composition in the estuary can be used as a tool to estimate submarine groundwater discharge.

Dissolved Ba profile in the estuary often exhibit high concentration at low to mid-salinity region and could result from its additional supply either from Ba release from riverine particulates or input from groundwater discharge. Excess Ba estimated for the Narmada, Tapi, Mandovi and the Hooghly estuaries is much higher compared to its riverine input. The excess Ba in these estuaries, in general, can not be supported by Ba desorption from riverine particulate matter. Therefore, the submarine groundwater discharge has been suggested as an important contributor to dissolved Ba in the estuaries.

### **7.5 Scope of future research**

This study tracks the distribution of the paleo-erosion during past  $\sim 100$  ka over the central Himalaya, to be more precise, the drainage basins of the river Alaknanda and the Bhagirathi constituting Himalayan area of about  $19.6 \times 10^3$  km<sup>2</sup>. Further this represent only  $\sim 5\%$  of total water discharge of the Ganga. This study provides erosion distribution only over an small segment of the Himalaya. Therefore study of distribution of the paleo-erosion over the entire Himalaya is needed to understand the coupling between erosion and climate. For which elemental and isotopic studies of the sediments deposited at the outflow of the Ganga after joining all its major tributaries would be required. The proposed study would also provide the variation in the Sr isotope composition of the paleo-Ganga, if any, which has been considered as constant in the models evaluating the influence of the Himalaya over oceanic Sr isotope evolution.

Similar study needs to be extended to eastern Himalaya by studying the Brahmaputra system as contemporary erosion rate in the eastern Himalaya is estimated to be ~1.5 times higher than the central and western Himalaya. Catchment of the Brahmaputra is affected by both southwest and northeast monsoon. Pale-erosion studies over the eastern Himalaya would provide the relation between erosion and northeast/southwest monsoons. Further, a large part of the Brahmaputra drains through the Tibetan catchment and any variation in the erosion pattern, such as change in the course of the river over Tibet can be tracked.

Extensive studies of redox sensitive trace elements (Re, U and Mo) have been carried out in the estuaries. However, exact mechanism of removal of Mo and U in the estuaries is not yet known. Studies comprising dissolved and particulate matters and sediments in these estuaries and mangrove forests needs to be done which could help understand the process leading to the removal of Mo and U. In this regard, isotopic study of Mo in these estuaries could provide some clue regarding its removal from estuary.

U, Mo and Re were analysed in water samples collected from a salt marsh on the western coast of the Gulf of Cambay near Bhavnagar. Mo/salinity ratio in salt marsh samples have shown that the Mo in the salt marsh is “in excess” of what would be expected from evaporite enrichment of seawater for the region. The presence of “excess” Mo in the salt marsh indicates that it can act as a source of Mo to adjoining sea water. However, in contrast to Mo, Re behaves conservatively and U gets removed in the Bhavnagar salt marsh. This observation is based on only limited sampling. Behaviour of Mo and U needs to be studied in the salt marshes with their detail sampling.

## **REFERENCES**

- Agarwal, A.K., 1992. Carbonate deposits in the Ganga plain. In Singh, I.B. (Ed.), Gangetic plain. Terra Incognita. Geology Department, Lucknow University, 35-43.
- Ahmad, S. M., Babu, G. A., Padmakumari, V. M., Dayal, A. M., Sukhija, B. S., Nagabhushanam, P., 2005. Sr, Nd isotopic evidence of terrigenous flux variations in the Bay of Bengal: Implications of monsoons during the last ~34,000 years. *Geophys. Res. Lett.* 32, L 22711.
- Alagarsamy, R., Zhang, J., 2005. Comparative studies on trace metal geochemistry in Indian and Chinese rivers. *Curr. Sci.* 89, 299-309.
- Alagarsamy, R., 2006. Distribution and seasonal variation of trace metals in surface sediments of the Mandovi estuary, west coast of India. *Estuar. Coast. Shelf Sci.* 67, 333-339.
- Alam, M.S., Keppens, E., Paepe, R., 1997. The use of oxygen and carbon isotope composition of pedogenic carbonates from Pleistocene palaeosols in NW Bangladesh, as palaeoclimatic indicators. *Quat. Sci. Rev.* 16, 161-168.
- Alibert, C., Michard A., Albarede F., 1983. The transition from alkali basalts to kimberlites: Isotope and trace element evidence from melilitites. *Contrib. Mineral. Petrol.*, 82, 176–186.
- Allegre, C.J., Birck, J.L., Capmas, F., Courtillot, V., 1999. Age of the Deccan traps using  $^{187}\text{Re}$ - $^{187}\text{Os}$  systematics. *Earth Planet. Sci. Lett.* 170, 197-204.
- Anbar, A.D., Creaser, R.A., Papanastassiou, D.A., Wasserburg, G.J., 1992. Rhenium in seawater: Confirmation of generally conservative behavior. *Geochim. Cosmochim. Acta.* 56, 4099-4103.
- Andersson, P.S., Wasserburg, G.J., Ingri, J., 1992. The sources and transport of Sr and Nd isotopes in the Baltic Sea. *Earth Planet. Sci. Lett.* 113, 459-472.
- Andersson, P.S., Wasserburg, G.J., Ingri, J., Stordal, M.C., 1994. Strontium, dissolved and particulate loads in fresh and brackish waters: The Baltic Sea and Mississippi Delta. *Earth Planet. Sci. Lett.* 124(1-4), 195-210.
- Andrews J.E., Singhvi A.K., Kailath A. J., Kuhn R., Dennis P.F., Tandon S.K., Dhir R.P. 1998. Do Stable Isotope Data from Calcrete Record Late Pleistocene

- Monsoonal Climate Variation in the Thar Desert of India? *Quat. Res.*, 50, 240-251.
- Archer, C., Vance, D., 2008. The isotopic signature of the global riverine molybdenum flux and anoxia in the ancient oceans. *Nature Geo.Sci.*1, 597-600.
- Asahara, Y., Tanaka, T., Kamioka, H., Nishimura, A., 1995. Asian continental nature of  $^{87}\text{Sr}/^{86}\text{Sr}$  ratios in north central Pacific sediments. *Earth Planet. Sci. Lett.* 133, 105-116.
- Audry, S., Blanc, G., Schafer, J., Robert, S., 2007. Effect of estuarine sediment resuspension on early diagenesis, sulfide oxidation and dissolved molybdenum and uranium distribution in the Gironde estuary, France. *Chem. Geol.* 238, 149-167.
- Banner, J.L., Hanson, G.N., 1990. Calculation of simultaneous isotopic and trace element variations during water-rock interaction with applications to carbonate diagenesis. *Geochim. Cosmochim. Acta.* 54, 3123-3137.
- Basu, A.R., Jacobsen, S.B., Poreda, R.J., Dowling, C.B., Aggarwal, P.K., 2001. Large Groundwater Strontium Flux to the Oceans from the Bengal Basin and the Marine Strontium Isotope Record. *Science* 293, 1470.
- Bertine, K., Turekian K.K., 1973. Molybdenum in marine deposits, *Geochim. Cosmochim. Acta* 37, 1415-1434.
- Bhushan, R., Dutta, K., Somayajulu, B.L.K., 2001. Concentrations and burial fluxes of organic and inorganic carbon on the eastern margins of the Arabian Sea. *Mar. Geol.* 178, 95-113.
- Bickle, M.J., Harris, N.B.W., Bunbury, J. M., Chapman, H. J., Fairchild, I. J., Ahmad, T., 2001. Controls on the  $^{87}\text{Sr}/^{86}\text{Sr}$  ratio of carbonates in the Garhwal Himalaya, Headwaters of the Ganges. *Jour. of Geology* 109, 737-753.
- Bickle, M.J., Bunbury, J., Chapman, H.J., Harris, N.B.W., Fairchild, I.J., Ahmad, T., 2003. Fluxes of Sr into the headwaters of the Ganges. *Geochim. Cosmochim. Acta.* 67, 2567-2584.

- Bishop, J. K. B., 1988. The barite-opal-organic carbon association in oceanic particulate matter. *Nature* 332, 341-343.
- Biswas, A.N., 2006. Geohydro-morphometry of Hooghly estuary.. *J. Inst. Eng. (India)* 66, 61-73.
- Blum, J. D., Erel, Y., 1995. A silicate weathering mechanism linking increases in marine  $^{87}\text{Sr}/^{86}\text{Sr}$  with global glaciation. *Nature* 373, 415-418.
- Blum J.D., Gazis C.A., Jacobson A.D., Chamberlin C.P., 1998. Carbonate versus silicate weathering in the Raikhot watershed within the High Himalayan Crystalline Series. *Geology* 26, 411–414.
- Bookhagen, B., Thiede, R.C., Strecker, M.R., 2005a. Late Quaternary intensified monsoon phases control landscape evolution in the northwest Himalaya. *Geology* 33, 149–152.
- Bookhagen, B., Thiede, R.C., Strecker, M.R., 2005b. Abnormal monsoon years and their control on erosion and sediment flux in the high, arid northwest Himalaya: *Earth Planet. Sci. Lett.* 231, 131-146.
- Bookhagen, B., Burbank, D.W., 2006. Topography, relief, and TRMM-derived rainfall variations along the Himalaya. *Geophysical Research Letters*. 33, doi:10.1029/2006GL026037.
- Borole, D. V., Krishnaswami, S., Somayajulu, B. L. K., 1977. Investigations of dissolved uranium, silicon, and particulate trace elements in estuaries. *Estuarine and Coast. Mar. Sci.* 5, 743–754.
- Borole, D. V., Gupta, S.K., Krishnaswami, S., Datta, P.S., Desai, B.I., 1979. Uranium isotopic investigations and radiocarbon measurements of river-groundwater systems, Sabarmati Basin, Gujarat, India. *Isotope Hydrology 1978*. Vol. I, IAEA, Vienna, 181-201.
- Borole, D. V., Krishnaswami, S., Somayajulu, B. L. K., 1982. Uranium isotopes in rivers, estuaries and adjacent coastal sediments of western India: their weathering, transport and oceanic budget. *Geochim. Cosmochim. Acta.* 46, 125-137.

- Bowen, H. J. M., 1979. *Environmental Chemistry of the Elements*. London: Academic Press Inc.
- Brass, G.W., 1976. The variation of the marine  $^{87}\text{Sr}/^{86}\text{Sr}$  ratio during Phanerozoic time: interpretation using a flux model. *Geochim. Cosmochim. Acta.* 40, 721–730.
- Breckel, E.J., Emerson, S., Balistrieri, L.S., 2005. Authigenesis of trace metals in energetic tropical shelf environments. *Continental Shelf Res.* 25, 1321–1337.
- Bryant, J.D., Jones, D.S., Mueller, P.A., 1995. Influence of freshwater flux on  $^{87}\text{Sr}/^{86}\text{Sr}$  chronostratigraphy in marginal marine environments and dating of vertebrate and invertebrate faunas. *J. Paleontol.*, 69, 1–6.
- Burbank, D.W., Blythe, A.E., Putkonen, J., Pratt-Sitaula, B., Gabet, E., Oskin, M., Barros, A., Ojha, T.P., 2003. Decoupling of erosion and precipitation in the Himalayas. *Nature* 426, 652-655.
- Burke, W.H., Denison, R. E., 1982. Variation of seawater  $^{87}\text{Sr}/^{86}\text{Sr}$  throughout Phanerozoic time. *Geology* 10, 516–519.
- Burnett, W.C., Aggarwal, P.K., Aureli, A., Bokuniewicz, H., Cable, J.E., Charette, M.A., Kontar, E., Krupa, S., Kulkarni, K.M., Loveless, A., Moore, W.S., Oberdorfer, J.A., Oliveira, J., Ozyurt, N., Povinec, P., Privitera, A.M.G., Rajar, R., Ramessur, R.T., Scholten, J., Stieglitz, T., 2006. Quantifying submarine groundwater discharge in the coastal zone via multiple methods. *Sci. Total Environ.* 367, 498-543.
- Campbell, I.H., Reiners, P.W., Allen, C.M., Nicolescu, S., Upadhyay, R., 2005. He-Pb double dating of detrital zircons from the Ganges and Indus Rivers: Implication for quantifying sediment recycling and provenance studies. *Earth Planet. Sci. Lett.* 237, 402-432.
- Canfield, D.E. 1997. The geochemistry of river particulates from the continental USA: Major elements. *Geochim. Cosmochim. Acta.* 61, 3349–3365.
- Carroll, J., Moore, W.S., 1993. Uranium removal during low discharge in the Ganges-Brahmaputra mixing zone. *Geochim. Cosmochim. Acta.* 58, 4987-4995.

- Carroll J., Falkner K., Brown E.T., Moore W.S., 1993. The role of the Ganges-Brahmaputra mixing zone in supplying barium and  $^{226}\text{Ra}$  to the Bay of Bengal. *Geochim. Cosmochim. Acta.* 57, 2981-2990.
- Cerling, T.E., 1984. The stable isotopic composition of modern soil carbonate and its relationship to climate. *Earth Planet. Sci. Lett.* 71, 29-240.
- Chappaz, A., Gobeil, C., Tessier, A., 2008. Sequestration mechanisms and anthropogenic inputs of rhenium in sediments from Eastern Canada lakes. *Geochim. Cosmochim. Acta.* 72, 6027-6036.
- Charette, M.A., Sholkovitz, E.R., 2006. Trace element cycling in a subterranean estuary part 2: geochemistry of the pore water. *Geochim. Cosmochim. Acta* 70, 811–826.
- Charette, M.A., Moore W.S., Burnett W.C., 2008. Uranium- and thorium-series nuclides as tracers of submarine groundwater discharge. *Radioactivity in the Environment*, ed. S. Krishnaswami, J.K. Cochran, vol: U-Th Series Nuclides in Aquatic Systems. 13, 155-191.
- Church, T. M., Sarin, M. M., Fleisher, M. Q., Ferdelman, T. G., 1996. Salt marshes: An important coastal sink for dissolved uranium. *Geochim. Cosmochim. Acta.* 60, 3879-3887.
- Clemens, S.C., Murray, D.W., Prell, W.L., 1996. Nonstationary phase of the Plio-Pleistocene Asian monsoon. *Science* 274, 943-94.
- Clemens, S.C., Prell, W.L., 2007. The timing of orbital-scale Indian monsoon changes. *Quat. Sci. Rev.* 26, 275-278.
- Clift, P.D., Giosan, L., Blusztajn, J., Campbell, I.H., Allen, C., Pringle, M., Tabrez, A.R., Danish, M., Rabbani, M.M., Alizai, A., Carter, A., Lückge, A., 2008. Holocene erosion of the Lesser Himalaya triggered by intensified summer monsoon. *Geology* 36, 79–82.
- Coffey, M., Dehairs, F., Collette, O., Luther, C., Church, T., Jickells, T., 1997. The behaviour of dissolved barium in estuaries. *Estuar. Coast. Shelf Sci.* 45, 113–121.

- Colin, C., Turpin, L., Bertaux, J., Desprairies, A., Kissel, C., 1999. Erosional history of the Himalayan and Burman ranges during the last two glacial–interglacial cycles. *Earth Planet.Sci. Lett.* 171, 647–660.
- Collier, R.W., 1985. Molybdenum in the Northeast Pacific Ocean. *Limnol. Oceanogr.* 30, 1351-1354.
- Colodner, D.C., Boyle, E.A., Edmond, J.M., Thomson, J., 1992. Post-depositional mobility of platinum, iridium and rhenium in marine sediments. *Nature* 358, 402-404.
- Colodner, D., Sachs, J., Ravizza, G., Turekian, K.K., Edmond, J., Boyle, E., 1993. The geochemical cycle of rhenium: a reconnaissance. *Earth Planet. Sci.Lett.* 117, 205-221.
- Colodner, D., Edmond, J., Boyle, E., 1995. Rhenium in the Black Sea: comparison with molybdenum and uranium. *Earth Planet. Sci.Lett.* 131, 1-15.
- Creaser, R.A., Sannigrahi, P., Chacko, T., Selby, D., 2002. Further evaluation of the Re-Os geochronometer in organic-rich sedimentary rocks: A test of hydrocarbon maturation effects in the Exshaw Formation, Western Canada Sedimentary Basin. *Geochim. Cosmochim. Acta.* 66, 3441-3452.
- Crusius, J., Calvert, S., Pedersen, T., Sage, D., 1996. Rhenium and molybdenum enrichments in sediments as indicators of oxic, suboxic and sulfidic conditions of deposition. *Earth Planet. Sci. Lett.* 145, 65–78.
- Crusius, J., Thomson, J., 2000. Comparative behavior of authigenic Re, U, and Mo during reoxidation and subsequent long-term burial in marine sediments. *Geochim. Cosmochim. Acta.* 64, 2233-2242.
- Dalai, T. K., 2001. Major ions, stable isotopes,  $^{87}\text{Sr}/^{86}\text{Sr}$  and Re in the headwaters of the Yamuna: Implications to chemical weathering in the Himalaya. Ph.D. thesis, M. S University, Baroda.
- Dalai, T. K., Singh, S. K., Trivedi, J. R., Krishnaswami, S., 2002. Dissolved rhenium in the Yamuna River System and the Ganga in the Himalaya: Role of black shale weathering on the budgets of Re, Os, and U in rivers and  $\text{CO}_2$  in the atmosphere. *Geochim. Cosmochim. Acta.* 66, 29-43.

- Dalai, T. K., Nishimura, K., Nozaki, Y., 2005. Geochemistry of molybdenum in the Chao Phraya River estuary, Thailand: Role of suboxic diagenesis and porewater transport. *Chem. Geol.* 218, 189-202.
- Das, A., Krishnaswami, S., Bhattacharya, S.K., 2005. Carbon isotope ratio of dissolved inorganic carbon (DIC) in rivers draining the Deccan Traps, India: Sources of DIC and their magnitudes. *Earth Planet. Sci. Lett.* 236, 419-429.
- Das, A., Krishnaswami, S., 2006. Barium in Deccan Trap Basalt Rivers: its abundance, relative mobility and flux. *Aquat. Geochem.* 12, 221–238.
- Das, A., Krishnaswami S., Kumar A., 2006. Sr and  $^{87}\text{Sr}/^{86}\text{Sr}$  in rivers draining the Deccan Traps (India): implications to weathering, Sr fluxes, and the Marine  $^{87}\text{Sr}/^{86}\text{Sr}$  record around K/T. *Geochem. Geophys. Geosyst.* 7 Q06014 10.1029/2005GC001081
- Das, A., Krishnaswami, S., 2007. Elemental geochemistry of river sediments from the Deccan Traps, India: Implications to sources of elements and their mobility during basalt–water interaction. *Chem. Geol.* 242, 232–254.
- Dehairs, F., Neybergh, H., Hoenig, M., 1989. Direct determination of dissolved barium in sea water by inductively coupled plasma/atomic emission spectrometry. *Anal. Chim. Acta.* 222, 55–61.
- Dellwig, O., Beck, M., Lemke, A., Lunau, M., Kolditz, K., Schnetger, B., Brumsack, H. J., 2007. Non-conservative behaviour of molybdenum in coastal waters: Coupling geochemical, biological, and sedimentological processes. *Geochim. Cosmochim. Acta.* 71, 2745-2761.
- Denison, R.E., Koepnick, R.B., Burke, W.H., Hetherington, E.A., Fletcher, A., 1994. Construction of the Mississippian, Pennsylvanian and Permian seawater curve  $^{87}\text{Sr}/^{86}\text{Sr}$ . *Chem. Geol.* 112, 145-167.
- Derry, L.A., France-Lanord, C., 1996. Neogene Himalayan weathering history and river  $^{87}\text{Sr}/^{86}\text{Sr}$ : Impact on the marine Sr record. *Earth Planet. Sci. Lett.* 142, 59-74.
- Dessert C., Dupre B., Francois L. M., Schott J., Gaillardet J., Chakrapani G., and Bajpai S. 2001. Erosion of Deccan Traps determined by river geochemistry:

- impact on the global climate and the  $^{87}\text{Sr}/^{86}\text{Sr}$  ratio of sea water. *Earth. Planet. Sci. Lett.* 188, 459–474.
- De Villiers, S., 1999. Seawater strontium and Sr/Ca variability in the Atlantic and Pacific oceans. *Earth Planet. Sci. Lett.* 171, 623–634.
- Dunk, R.M., Mills, R.A., Jenkins, W.J., 2002. A reevaluation of the oceanic uranium budget for the Holocene. *Chem. Geol.* 190, 45–67.
- Dymond J., Suess E. and Lyle M., 1992. Barium in deep-sea sediments: a geochemical proxy for paleoproductivity. *Paleoceanography* 7, 163–181.
- Edmond, J.M., Boyle, E.D., Drummond, D., Grant, B., Mislick, T., 1978. Desorption of barium in the plume of the Zaire (Congo) River. *Neth. J. Sea Res.* 12, 324–328.
- Edmond, J. M., 1992. Himalayan Tectonics, Weathering Processes, and the Strontium Isotope Record in Marine Limestones. *Science* 258, 1594-1597.
- Edmond, J.M., Huh, Y., 1997. Chemical weathering yields in hot and cold climates, in *Tectonic Uplift and Climate Change* (eds. W.F. Ruddiman and Prell), Plenum Press, New York, 329-351.
- Ehleringer, J.R., Osmond, C.B., 1989. Stable isotopes. In: *Pearcy RW, Ehleringer JR, Mooney HA, Rundel PW (eds) Plant physio-logical ecology. Field methods and instrumentation.* Chapman and Hall, London, pp 281-300.
- Elderfield, H., 1990. Tracers of ocean paleoproductivity and paleochemistry: An introduction. *Paleoceanogr.* 5, 711–717.
- Emerson, S., Huested, S., 1991. Ocean anoxia and the concentrations of molybdenum and vanadium in seawater. *Mar. Chem.* 34, 177– 196.
- English, N.B., Quade, J., DeCelles, P.G., Garziane, C.N., 2000. Geologic control of Sr and major element chemistry in Himalayan Rivers, Nepal. *Geochim. Cosmochim. Acta.* 64, 2549-2566.
- Esser, B.K., Turekian, K.K., 1993. The osmium isotopic composition of the continental crust. *Geochim. Cosmochim. Acta.* 57, 3093-3104.

- Fedo, C.M., Nesbitt, H.W., Young, G.M., 1995. Unraveling the effects of potassium metasomatism in sedimentary rocks and paleosols, with implications for paleoweathering conditions and provenance. *Geology* 23, 921–924.
- Flietmann, D., Burns, S.J., Mudelsee, M., Neff, U., Kramers, J., Mangini, A., Matter, A., 2003. Holocene Forcing of the Indian Monsoon Recorded in a Stalagmite from Southern Oman. *Science* 300, 1737-1739.
- Foster, G.L., Carter, A., 2007. Insights into the patterns and locations of erosion in the Himalaya - A combined fission-track and in situ Sm-Nd isotopic study of detrital apatite. *Earth Planet.Sci. Lett.* 257, 407-418.
- France-Lanord, C., Derry, L., Michard, A., 1993. Evolution of the Himalaya since Miocene time: Isotopic and sedimentologic evidence from the Bengal Fan, *in* Treloar, P.J., and Searle, M., eds., *Himalayan Tectonics: Geological Society [London] Special Publication 74*, 603–621.
- France-Lanord, C., Derry, L. A., 1997. Organic carbonburial forcing of the carbon cycle from Himalayan erosion. *Nature* 390, 65–67.
- Francois, R., Honjo, S., Manganini, S. J., Ravizza, G. E., 1995. Biogenic barium fluxes to the deep sea: Implications for paleoproductivity reconstruction. *Global Biogeochem. Cycles* 9, 289–303.
- Gaillardet, J., Dupre, B., Allegre, C.J. 1995. A global geochemical mass budget applied to the Congo basin rivers: Erosion rates and continental crust composition. *Geochim. Cosmochim. Acta.* 59, 3469–3485.
- Gaillardet, J., Dupré, B., Allégre, C. J., 1999 Geochemistry of large river suspended sediments: silicate weathering or recycling tracer? *Geochim. Cosmochim. Acta.* 63, 4037–4051.
- Gaillardet J., Galy A., 2008. Himalaya--Carbon Sink or Source? *Science* 320, 1727 – 1728.
- Gajurel, A.P., France-Lanord, C., Huyghe, P., Guilmette, C., Gurung, D., 2006. C and O isotope compositions of modern fresh-water mollusc shells and river waters from the Himalaya and Ganga plain. *Chem. Geol.* 233, 156–183.

- Galy, A., France-Lanord, C., Derry, L.A., 1999. The strontium isotopic budget of Himalayan rivers in Nepal and Bangladesh. *Geochim. Cosmochim. Acta.* 63, 1905-1925.
- Galy, A., France-Lanord, C., 2001. Higher erosion rates in the Himalaya: Geochemical constraints on riverine fluxes. *Geology* 29, 23–26.
- Galy, V., France-Lanord, C., Lartiges, B., 2008. Loading and fate of particulate organic carbon from the Himalaya to the Ganga-Brahmaputra delta. *Geochim. Cosmochim. Acta.* 72, 1767-1787.
- Gansser A. 1964. *Geology of the Himalayas*. Wiley Interscience publishers, London, 284.
- GoI Report. 2002. Critical habitat information system for Gulf of Khambat-Gujarat, Government of India, Department of Ocean Development Integrated coastal and marine area management, Project Directorate, Chennai.
- Goodbred, S.L., Kuehl, S.A., 2000. The significance of large sediment supply, active tectonism, and eustasy on margin sequence development: Late Quaternary stratigraphy and evolution of the Ganges-Brahmaputra delta. *Sediment. Geol.* 133, 227-248.
- Goodbred, S.L., 2003. Response of the Ganges dispersal system to climate change: a source-to-sink view since the last interstade. *Sediment. Geol.* 162, 83–104.
- Goodbred, Jr.S.L., Kuehl, S.A., Steckler, M.S., Sarker, M.H., 2003. Controls on facies distribution and stratigraphic preservation in the Ganges-Brahmaputra delta sequence. *Sediment. Geol.* 155, 301-316.
- Granet, M., Chabaux, F., Stille, P., France-Lanord, C., Pelt, E., 2007. Time-scales of sedimentary transfer and weathering processes from U-series nuclides: Clues from the Himalayan rivers. *Earth Planet. Sci. Lett.* 261, 389-406.
- GSEAP. 2003. Gujarat State Environment Action Programme, the Gujarat Ecology Commission (GEC), Government of Gujarat through the World Bank assisted “Environment Management Capacity Building – Technical Assistance Project”.

- Guay, C.K., Falkner, K.K., 1998. A survey of dissolved barium in the estuaries of major Arctic rivers and adjacent seas. *Cont. Shelf Res.* 18, 859–882.
- Gupta, H., Chakrapani, G.J., 2007. Temporal and spatial variations in water flow and sediment load in the Narmada river. *Curr. Sci.* 92, 689-684.
- Hanor, J.S., Chan, L.H., 1977. Non-conservative behavior of Barium during mixing of Mississippi River and Gulf of Mexico waters. *Earth Planet. Sci. Lett.* 37, 242–250.
- Harris, N., 1995. Significance of weathering Himalayan metasedimentary rocks and leucogranites for the Sr isotope evolution of seawater during the early Miocene. *Geology* 23, 795-798.
- Harris, N., Bickle, M., Chapman, H., Fairchild, I., Bunbury, J., 1998. The significance of Himalayan rivers for silicate weathering rates: evidence from the Bhote Kosi tributary. *Chem. Geol.* 144, 205–220.
- Harrison, S.P., Kohfeld, K.E., Roelandt, C., Claquin, T., 2001. The role of dust in climate changes today, at the last glacial maximum and in the future. *Earth. Sci. Rev.* 54, 43–80.
- Hart, W.S., Quade, J., Madsen, D.B., Kaufman, D.S., Oviatt, C.G., 2004. The  $^{87}\text{Sr}/^{86}\text{Sr}$  ratios of lacustrine carbonates and lake-level history of the Bonneville paleolake system. *Geol. Soc. Am. Bull.* 116, 1107-1119.
- Harvey, C.F., 2002. Groundwater flow in the Ganges delta. *Science* 296, 1563.
- Hay, W.W., 1998. Detrital sediment fluxes from continents to oceans. *Chem. Geol.* 145, 287-323.
- Head, P.C., Burton, J.D., 1970. Molybdenum in some ocean and estuarine waters. *J. Mar. Biol. Assoc. UK* 50, 439–448.
- Helz, G.R., Miller, C.V., Charnock, J. M., Mosselmans, J. F. W., Patrick, R. A. D., Garner, C. D., Vaughan, D. J., 1996. Mechanism of molybdenum removal from the sea and its concentration in black shales: EXAFS evidence. *Geochim. Cosmochim. Acta* 60, 3631–3642.
- Hendy, C.H., 1971. The isotopic geochemistry of speleothems-I. The calculation of the effects of different modes of formation on the isotopic composition of

- speleothems and their applicability as palaeoclimatic indicators. *Geochim. Cosmochim. Acta.* 35, 801-824.
- [http://ic.gujarat.gov.in/Ind\\_guj/natural\\_resources.html](http://ic.gujarat.gov.in/Ind_guj/natural_resources.html).
- Hodge, V.F., Johannesson, K.H., Stetzenbach, K.J., 1996. Rhenium, molybdenum, and uranium in groundwater from the southern Great Basin, USA: Evidence for conservative behavior. *Geochim. Cosmochim. Acta.* 60, 3197-3214.
- Horwitz, E.P., Chiarizia, R., Dietz, M.L., 1992. A novel strontium-selective extraction chromatographic resin. *Solv. Extract. Ion Exch.*, 10: 313-336.
- Hren, M.T., Chamberlain, P.C, Hilley, G.E., Blisniuk, P.M., Bookhagen, B., 2007. Major ion chemistry of the Yarlung Tsangpo–Brahmaputra river: Chemical weathering, erosion, and CO<sub>2</sub> consumption in the southern Tibetan plateau and eastern syntaxis of the Himalaya. *Geochim. Cosmochim. Acta.* 71, 2907–2935.
- Huang, C.Y., Lee, N.M., Lin, S.Y., Liu, C.Y., 2002. Determination of vanadium, molybdenum and tungsten in complex matrix samples by chelation ion chromatography and on-line detection with inductively coupled plasma mass spectrometry. *Anal. Chim. Acta.* 466, 161-174.
- Huh, Y., Edmond, J.M., 1998. On the interpretation of the oceanic variations in <sup>87</sup>Sr/<sup>86</sup>Sr as recorded in marine limestones. *Proceedings of the Indian Academy of Sciences. Earth. Planet. Sci.* 107 (4), 293–305.
- Huh, Y., Olliver, T., Humayun, M., 2007. Dissolved rhenium in the rivers of eastern Tibet: proxy for weathering of organic carbon? *Geophys. Res.* 9, Abstracts EGU2007-A-03139.
- Hussain, N., Krishnaswami, S., 1980. U-238 series radioactive disequilibrium in groundwaters: implications to the origin of excess U-234 and fate of reactive pollutants. *Geochim. Cosmochim. Acta.* 44, 1287-1291.
- Ingram, B. L., Sloan, D., 1992. Strontium isotopic composition of estuarine sediments as paleosalinity-paleoclimate indicator. *Science* 255, 68–72.

- Ingram, B.L., De Paolo, D.J., 1993. A 4300-year strontium isotope record of estuarine paleosalinity in San-Francisco Bay, California. *Earth Planet. Sci. Lett.* 119, 103–119.
- Jacob, N., Suresh, D.S., Babu, Shivanna, K., 2009. Radon as an indicator of submarine groundwater discharge in coastal regions. *Curr. Sci.* 97, 1313-1320.
- Jaffe, L.A., Peucker-Ehrenbrink, B., Petsch, S.T., 2002. Mobility of rhenium, platinum group elements and organic carbon during black shale weathering. *Earth Planet. Sci. Lett.* 198, 339-353.
- Jones, P.G., 1974. Molybdenum in a near-shore and estuarine environment. *Estuar. Coast. Mar. Sci.* 2, 185–189.
- Krishnamurthy, R.V., Bhattacharya, S.K., 1991. Stable oxygen and hydrogen isotope ratios in shallow ground waters from India and a study of role of evapotranspiration in the Indian Monsoon. In: Taylor Jr., H.P., O'Neil, J., Kaplan, I.R. (Eds.), *Stable Isotope Geochemistry: A Tribute to Samuel Epstein*. Special Publication-Geochem. Soc. 3, 187–193.
- Krishnan, M.S., (1982) *Geology of India and Burma*, 6th addition, CBS Publishers & distributors, New Delhi, pp 536.
- Krishnaswami, S., Trivedi, J.R., Sarin, M.M., Ramesh, R., Sharma, K.K., 1992. Strontium isotopes and rubidium in the Ganga-Brahmaputra river system: Weathering in the Himalaya, fluxes to the Bay of Bengal and contributions to the evolution of oceanic  $^{87}\text{Sr}/^{86}\text{Sr}$ . *Earth Planet. Sci. Lett.* 109, 243-253.
- Krishnaswami, S., Singh, S.K., Dalai, T., 1999. Silicate weathering in the Himalaya: Role in contributing to major ions and radiogenic Sr to the Bay of Bengal. In: B.L.K. Somalyajulu, Editor, *Ocean Science, Trends and Future Directions*, Indian National Science Academy and Akademia International, New Delhi, 23–51.
- Krom, M.D., Berner, R.A., 1983. A Rapid Method for the Determination of Organic and Carbonate Carbon in Geological Samples, *J. Sed. Petrol.* 53, 660-663.

- Krupadam, R.J., Smita, P., Wate, S.R., 2006. Geochemical fractionation of heavy metals in sediments of the Tapi estuary. *Geochemical Journal*, 40, 513 to 522.
- Ku, T.L., Knauss, K.G., Mathieu, G.G., 1977. Uranium in open ocean: concentration and isotopic composition, *Deep Sea Res.* 24, 1005-1017.
- Lave, J., Avouac, J.P., 2001. Fluvial incision and tectonic uplift across the Himalayas of central Nepal. *J. of Geophys. Res. B: Solid Earth*, 106, 26561-26591.
- Lea, D., Boyle, E., 1990. A 210,000-year record of barium variability in the deep northwest Atlantic Ocean. *Nature* 347, 269–272.
- Le Fort P. 1975. Himalayas: The collided range, present knowledge of the continental arc, *Am. J. Sci.*, 275, 1 –44.
- Leier, A., Quade, J., DeCelles, P., Kapp, P., 2009. Stable isotopic results from paleosol carbonate in South Asia: Paleoenvironmental reconstructions and selective alteration. *Earth Planet. Sci. Lett.* 279, 242–254.
- Li, Y. H., Chan, L. H., 1979. Desorption of Ba and <sup>226</sup>Ra from river-borne sediments in the Hudson estuary. *Earth Planet. Sci. Lett.* 43, 343–350.
- Liu, Z., Colin, C., Trentesaux, A., Siani, G., Frank, N., Blamart, D., Farid, S., 2005, Late Quaternary climatic control on erosion and weathering in the eastern Tibetan Plateau and the Mekong Basin. *Quat. Res.* 63, 316 – 328.
- Madhavan, N., Subramanian, V., 2001. Fluoride concentration in river waters of south Asia. *Curr. Sci.* 80, 1312.
- Maeda, M., Windom, H.L., 1982. Behaviour of uranium in two estuaries of the south eastern United States. *Mar. Chem.* 11, 427– 436.
- Manheim, F.T., Landergren, S., 1978. *Handbook of Geochemistry II*, Section 42. B-O. Springer-Verlag, Berlin.
- Martin, J.M., Meybeck, M., Pusset, M., 1978. Uranium behaviour in Zaire Estuary. *Neth. J. Sea Res.* 12, 338–344.
- Martin, J.M., Meybeck, M., 1979. Elemental mass-balance of material carried by major world rivers. *Mar. Chem.* 7, 173–206.
- McArthur, J.M., 1991. Stratigraphy with strontium isotopes. *Geol. Today.* 7, 5i–5iv.

- McArthur, J.M., 1994. Recent trends in strontium isotope stratigraphy. *Terra Nova* 6, 331–358.
- McKee, B.A., 2008. U and Th-Series Nuclides in Estuarine Environments. In: S. Krishnaswami and K. Cochran (Ed.), *Radioactivity in the environment*, Elsevier publishers. 6, 192-226.
- McKenzie, J.A., Hodell, D.A., Mueller, P.A., Muller, D.W., 1988. Application of strontium isotopes to late Miocene–early Pliocene stratigraphy. *Geology* 16, 1022–1025.
- McLennan S. M. 1993. Weathering and global denudation. *J. Geol.* 101, 295-303.
- McManus, J., Berelson, W.M., Severmann, S., Poulson, R.L., Hammond, D.E., Klinkhammer, G.P., Holm, C., 2006. Molybdenum and uranium geochemistry in continental margin sediments: Paleoproxy potential. *Geochim. Cosmochim. Acta.* 70, 4643–4662.
- Mickler P., Stern L., Banner J., 2006. Large kinetic isotope effects in modern speleotherms. *Geolog. Soc. Am.* 118, 65–81.
- Milliman, J.D., Syvitski, J.P.M., 1992. Geomorphic/tectonic control of sediment discharge to the ocean: the importance of small mountainous rivers. *J. Geol.* 100, 525-544.
- Minissale, A., Vaselli, O., Chandrasekharam, D., Magro, G., Tassi, F., Casiglia, A., 2000. Origin and evolution of intracratonic thermal fluids from central-western peninsular India. *Earth Planet. Sci. Lett.* 181, 377-394.
- Molnar, P., England, P., 1992. Climate and landscape response. *Nature* 355, 306.
- Moore, W.S., 1997. The effects of groundwater input at the mouth of the Ganges–Brahmaputra Rivers on barium fluxes to the Bay of Bengal. *Earth Planet. Sci. Lett.*, 150, 141–150.
- Moore, W.S., 2010. The Effect of Submarine Groundwater Discharge on the Ocean. *Annual Rev. Mar. Sci.* 2, 59-88.
- Morford, J.L., Emerson, S., 1999. The geochemistry of redox sensitive trace metals in sediments. *Geochim. Cosmochim. Acta.* 63, 1735–1750.

- Morford, J.L., Emerson, S.R., Breckel, E.J., Kim, S.H., 2005. Diagenesis of oxyanions (V, U, Re, and Mo) in pore waters and sediments from a continental margin. *Geochim. Cosmochim. Acta.* 69, 5021–5032.
- Morford, J.L., Martin, W.R., Kalnejais, L.H., Francois, R., Bothner, M., Karle, I.-M., 2007. Insights on geochemical cycling of U, Re and Mo from seasonal sampling in Boston Harbor, Massachusetts, USA. *Geochim. Cosmochim. Acta.* 71, 895-917.
- Morford, J.L., Martin, W.R., François, R., Carney, C.M., 2009. A model for uranium, rhenium, and molybdenum diagenesis in marine sediments based on results from coastal locations. *Geochim. Cosmochim. Acta.* 73, 2938-2960.
- Morris, A.W., 1975. Dissolved molybdenum and vanadium in Northeast Atlantic Ocean. *Deep-Sea Res.* 22, 49–54.
- Najman, Y., Bickle, M., Chapman, H., 2000. Early Himalayan Exhumation: Isotopic constrains from the Indian foreland basin: *Terra-Nova.* 12, 28-34.
- Naqvi, S.W.A., Jayakumar, D.A., Narvekar, P.V., Naik, H., Sarma, V.V.S.S., D'Souza, W., Joseph, S., George, M.D., 2000. Increased marine production of N<sub>2</sub>O due to intensifying anoxia on the Indian continental shelf. *Nature* 408, 346-349.
- Nesbitt, H.W., Young, G.M., 1982. Early Proterozoic climates and plate motions inferred from major element chemistry of lutites. *Nature* 299, 715–717.
- Nesbitt, H.W., Young, G.M., McLennan, S.M., Keays, R.R., 1996. Effects of chemical weathering and sorting on the petrogenesis of siliclastic sediments, with implications for provenance studies. *Geology* 104, 525–542.
- Oliver, L., Harris, N., Bickle, M., Chapman, H., Dise, N., Horstwood, M., 2003. Silicate weathering rates decoupled from the <sup>87</sup>Sr/<sup>86</sup>Sr ratio of the dissolved load during Himalayan erosion. *Chem. Geol.* 201, 119-139.
- Owen, L.A., Finkel, R.C., Caffee, M.W., 2002. A note on the extent of glaciation throughout the Himalaya during the global Last Glacial Maximum: *Quat. Sci. Rev.* 21, 147-157.

- Oxburgh, R., 1998. Variations in the osmium isotope composition of sea water over the past 200,000 years. *Earth Planet. Sci. Lett.* 159, 183-191.
- Oxburgh, R., Pierson-Wickmann, A., Reisberg, L., Hemming, S., 2007. Climate-correlated variations in seawater  $^{187}\text{Os}/^{188}\text{Os}$  over the past 200,000 yr: Evidence from the Cariaco Basin, Venezuela. *Earth Planet. Sci. Lett.* 263, 246-258.
- Pal, D.K., Srivastava, P., Bhattacharyya, T., 2003. Clay illuviation in calcareous soils of the semiarid part of the Indo-Gangetic Plains, India. *Geoderma*. 115, 177-192.
- Palmer, M.R., Edmond, J.M., 1989. The strontium isotope budget of the modern ocean. *Earth Planet. Sci. Lett.* 92, 11–26.
- Palmer, M.R., Edmond, J.M., 1992. Controls over the strontium isotope composition of river water. *Geochim. Cosmochim. Acta.* 56, 2099-2111.
- Palmer, M.R., Edmond, J.M., 1993. Uranium in river water. *Geochim. Cosmochim. Acta.* 57, 4947–4955.
- Patterson, R.T., Blenkinsop, J., Cavazza, W., 1995. Planktic foraminiferal biostratigraphy and  $^{87}\text{Sr}/^{86}\text{Sr}$  isotopic stratigraphy of the Oligocene-to-Pleistocene sedimentary sequence in the Southeastern Calabrian microplate, Southern Italy. *J. Paleontol.* 69, 7–20.
- Paytan, A., Shellenbarger, G.G., Street, J.H., Gonnee, M.E., Davis, K., Young, M., B., Moore, W.S., 2006. Submarine Groundwater Discharge: An Important Source of New Inorganic Nitrogen to Coral Reef Ecosystems. *Limnol. Oceanogr.* 51, 343-348.
- Peros, M.C., Reinhardt, E.G., Schwarcz, H.P., Davis, A.M., 2007. High-resolution paleosalinity reconstruction from Laguna de la Leche, north coastal Cuba, using Sr, O, and C isotopes. *Palaeogeogr. Palaeocl.* 245, 535–550.
- Peucker-Ehrenbrink, B., Ravizza, G., Hofmann, A.W., 1995. The marine  $^{187}\text{Os}/^{186}\text{Os}$  record of the past 80 million years. *Earth Planet. Sci. Lett.* 130, 155-167.

- Peucker-Ehrenbrink, B., Walker, B.D., Martin, C.E., Marcantonio F., Raymond P.A., 2006. Reevaluating the aquatic rhenium cycle. *Eos Trans. AGU* 87, No. 36, Ocean Sci. Meet., Suppl., Abstract 1764 (oral OS43A-06).
- Pin, C., Bassin, C., 1992. Evaluation of a strontium-specific extraction chromatographic method for isotopic analysis in geological materials. *Anal. Chim. Acta*, 269, 249-255.
- Pin, C., Briot, D., Bassin, C., Poitrasson, F., 1994. Concomitant separation of strontium and samarium-neodymium for isotopic analysis in silicate samples, based on specific extraction chromatography. *Anal. Chim. Acta*, 298, 209-217.
- Prell, W.L., Kutzbach, J.E., 1987. Monsoon variability over the past 150 000 years. *J. Geophys. Res.* 92, 8411-8425.
- Quade, J., Roe L., DeCelles, P.G., Ojha, T.P., 1997. The late neogene  $^{87}\text{Sr}/^{86}\text{Sr}$  record of lowland Himalayan rivers. *Science* 276, 1828-1831.
- Quinby-Hunt, M.S., Turekian, K.K., 1983. Distribution of elements in sea water, *Eos, Trans. AGU*, 64, 130-131.
- Rahaman, W., Singh, S.K., Sinha, R., Tandon, S.K., 2009. Climate control on erosion distribution over the Himalaya during past ~100 ka. *Geology*. 37, 559-562.
- Rahaman, W., Singh S. K., 2010. Rhenium in rivers and estuaries of India: Sources, transport and behaviour. *Mar. Chem.* 118, 1-10.
- Rai, S.K., Singh, S.K., 2007. Temporal variation in Sr and  $^{87}\text{Sr}/^{86}\text{Sr}$  of the Brahmaputra: Implications for annual fluxes and tracking flash floods through chemical and isotope composition. *Geochem. Geophys. Geosyst.* 8, Q08008, doi: 10.1029/2007GC001610.
- Rai. S.K., 2008. Isotopic and geochemical studies of ancient and modern sediments. Ph.D Thesis, MS University Baroda.
- Rai, S.K., Singh, S.K., Krishnaswami, S., Ca and Sr budget of the Ganga, in Prep.
- Raj, R., Mulchandani, N., Bhandari, S., Maurya, D.M., Chamyal, L.S., 2004. Channel shifting of a highly sinuous meandering river in alluvial plain, Vishwamitri river, Mainland Gujarat. *Curr. Sci.* 86, 1648.

- Ravizza, G., Turekian, K.K., 1989. Application of the  $^{187}\text{Re}$ - $^{187}\text{Os}$  system to black shale geochronometry. *Geochim. Cosmochim. Acta.* 53, 3257-3262.
- Ravizza, G., Turekian, K.K., Hay, B.J., 1991. The geochemistry of rhenium and osmium in recent sediments from the Black Sea. *Geochim. Cosmochim. Acta.* 55, 3741-3752.
- Ravizza, G.E., 1992. Rhenium-osmium geochemistry of modern and ancient organic rich sediments. Ph.D. Thesis, Yale Univ., p. 245.
- Raymo, M.E., Ruddiman W.F., Froelich P.N., 1988. Influence of late Cenozoic mountain building on ocean geochemical cycles. *Geology* 16, 649-653.
- Raymo, M. E., 1991. Geochemical evidence supporting T.C. Chamberlin's theory of glaciation. *Geology* 19, 344-347.
- Raymo, M.E., Ruddiman, W.F., 1992. Tectonic forcing of late Cenozoic climate. *Nature.* 359, 117-122.
- Raymo, M.E., Oppo D.W., Curry W., 1997. The mid-Pleistocene climate transition: A deep sea carbon isotopic perspective. *Paleoceanography* 12, 546-559.
- Reddy, M.S., Basha, S., Joshi, H.V., Ramachandraiah, G., 2005. Seasonal distribution and contamination levels of total PHCs, PAHs and heavy metals in coastal waters of the Alang-Sosiya ship scrapping yard, Gulf of Cambay, India. *Chemosphere.* 61, 1587-1593.
- Reiners, P.W.T.A., Ehlers, S.G.M., Montgomery, D.R., 2003. Coupled spatial variations in precipitation and long-term erosion rates across the Washington Cascades. *Nature* 426, 645-647.
- Rengarajan, R., Sarin, M.M., Krishnaswami, S., 2003. Uranium in the Arabian Sea: role of denitrification in controlling its distribution. *Oceanologica Acta.* 26, 687-693.
- Richter, F.M., Rowley, D.B., DePaolo, D.J., 1992. Sr isotope evolution of seawaters the role of tectonics. *Earth Planet. Sci. Lett.* 170, 197-204.

- Rodushkin, I., Ruth, T., 1997. Determination of trace metals in estuarine and seawater reference materials by high-resolution inductively coupled plasma mass spectrometry. *J. Anal. At. Spect.* 12, 1181–1185.
- Roy, S., Gaillardet, J., Allègre, C. J., 1999. Geochemistry of dissolved and suspended loads of the Seine River, France: anthropogenic impact, carbonate and silicate weathering. *Geochim. Cosmochim. Acta*, 63, 1277-1292.
- Ruddiman, W.F., 1997. *Tectonic Uplift and Climate Change*, Plenum Publishing Corporation, New York, pp. 535.
- Sadhuram, Y., Sarma, V.V., Murty, T.V.R., Rao, B.P., 2005. Seasonal variability of physico-chemical characteristics of the Haldia channel of Hooghly estuary, India. *J. Earth Syst. Sci.* 114, 37-49.
- Salomons, W., Goudie, A., Mook, W.G., 1978. Isotopic composition of calcrete deposits from Europe, Africa and India. *Earth Surf. Processes Landforms*. 3, 43-57.
- Sanyal, P., 2004. Isotope geochemistry of Siwalik sediments and signature of past climate change. Ph.D Thesis, MS university, Baroda.
- Sarin, M.M., Krishnaswami, S., Dilli, K., Somayajulu, B.L.K., Moore, W.S., 1989. Major ion chemistry of the Ganga-Brahmaputra river system: Weathering processes and fluxes to the Bay of Bengal. *Geochim. Cosmochim. Acta*. 53, 997-1009.
- Sarin, M.M., Krishnaswami, S., Somayajulu, B.L.K., Moore, W.S., 1990. Chemistry of uranium, thorium, and radium isotopes in the Ganga - Brahmaputra river system—weathering processes and fluxes to the Bay of Bengal. *Geochim. Cosmochim. Acta*. 54, 1387– 1396.
- Sarin, M.M., Church, T.M., 1994. Behaviour of uranium during mixing in the Delaware and Chesapeake estuaries. *Estuar. Coast. and Shelf Sci.* 39, 619–631.
- Sarin M.M., Bhushan R., Dutta K., 1997. Determination of organic carbon and nitrogen in marine sediments using elemental analyzer, Abstract published in

- Proceedings of the conference on "Recent advances in elemental analysis" held at Homi Bhabha center for science education (TIFR), Mumbai India.
- Sastry, B.B.K., Gopinath, K., 1985. Bauxite resources of Goa, India. Earth Resources for Goa's Development. Geol. Surv.India; Calcutta, 62-70.
- Scheiderich, K., Helz, G.R., Walker, R.J., 2010. Century-long record of Mo isotopic composition in sediments of a seasonally anoxic estuary (Chesapeake Bay). Earth Planet. Sci. Lett. 289, 189-197.
- Sharma, S., Joachimski, M., Sharma, M., Tobschall, H.J., Singh, I.B., Sharma, C., Chauhan, M.S., Morgenroth, G., 2004. Lateglacial and Holocene environmental changes in Ganga plain, Northern India. Quat. Sci. Rev. 23, 145-159.
- Sharma, M., Balakrishna, K., Hofmann, A.W., Shankar, R., 2007. The transport of Osmium and Strontium isotopes through a tropical estuary. Geochim. Cosmochim. Acta. 71, 4856-4867.
- Sharma, S.K., Subramanian, V., 2008. Hydrochemistry of the Narmada and Tapi Rivers, India. Hydrol. Process. 22, 3444–3455.
- Shaw, T.M., Moore, W.S., Kloepfer, J., Sochaski, M., 1998. The flux of barium to the coastal waters of the southeastern USA: The importance of submarine groundwater discharge. Geochim. Cosmochim. Acta. 62, 3047 – 3054.
- Siebert, C., Nagler, T.F., Von Blanckenburg, F., Kramers, J.D., 2003. Molybdenum isotope records as a potential new proxy for paleoceanography. Earth Planet. Sci. Lett. 211, 159–171.
- Singh, I., Singh, S., Kushwaha, S., Ashutosh, S., Singh, R., 2004. Assessment and monitoring of estuarine mangrove forests of Goa using satellite remote sensing. Jour. Ind. Soc. Remote Sensing. 32, 167-174.
- Singh, I.B., 1992. Geological evolution of Gangetic plain: present status. In Singh, I.B. (Ed.), Gangetic plain. Terra Incognita. Geology Department, Lucknow University, 1-14.

- Singh, I.B., Ansari, A.A., Chandel, R.S., Misra, A., 1996. Neotectonic control on drainage system in gangetic plain, Uttar Pradesh. *J. Geol. Soc. India.* 47(5), 599-609.
- Singh, R.L., 1994. *India: A Regional Geography.* National Geographical Society of India, Varanasi.
- Singh, S.K., Trivedi, J.R., Pande, K., Ramesh, R., Krishnaswami, S., 1998. Chemical and strontium, oxygen, and carbon isotopic compositions of carbonates from the Lesser Himalaya: Implications to the strontium isotope composition of the source waters of the Ganga, Ghaghara, and the Indus rivers. *Geochim. Cosmochim. Acta.* 62, 743-755.
- Singh, S. K., 1999. *Isotopic and Geochemical Studies of the Lesser Himalayan Sedimentaries.* Ph. D. Dissertation, M. S. University, Baroda, pp. 160.
- Singh, S K., Trivedi, J.R., Krishnaswami, S., 1999. Re-Os isotope systematic in black shales from the Lesser Himalaya: Their chronology and role in the  $^{187}\text{Os}/^{188}\text{Os}$  evolution of seawater. *Geochim. Cosmochim. Acta.* 63, 2381-2392.
- Singh, S.K., France-Lanord, C., 2002. Tracing the distribution of erosion in the Brahmaputra watershed from isotopic compositions of stream sediments, *Earth Planet. Sci. Lett.*, 202, 645– 662.
- Singh, S.K., Reisberg, L., France-Lanord, C., 2003. Re-Os isotope systematics of sediments of the Brahmaputra River system. *Geochim. Cosmochim. Acta.* 67, 4101-4111.
- Singh, S.K., Sarin, M.M., France-Lanord, C., 2005. Chemical erosion in the eastern Himalaya: Major ion composition of the Brahmaputra and  $\delta^{13}\text{C}$  of dissolved inorganic carbon. *Geochim. Cosmochim. Acta.* 69, 3573-3588.
- Singh, S.K., Kumar, A., France-Lanord, C., 2006. Sr and  $^{87}\text{Sr}/^{86}\text{Sr}$  in waters and sediments of the Brahmaputra River System: Silicate weathering,  $\text{CO}_2$  consumption and Sr flux. *Chem. Geol.* 234, 308–320.
- Singh, S.K., Rai, S.K., Krishnaswami, S., 2008. Sr and Nd isotopes in river sediments from the Ganga Basin: Sediment Provenance and Hotspots of Physical Erosion. *J. Geophys. Res.* 113, F03006, doi:10.1029/2007JF000909.

- Sinha R., Friend P.F., 1994. River systems and their sediment flux, Indo-Gangetic Plains, Northern Bihar, India, *Sedimentology*, 41, 825–845.
- Sinha, R., Gibling, M.R., Tandon, S.K., Jain, V., Dasgupta, A.S., 2005. Quaternary stratigraphy and sedimentology of the Korea section on the Betwa River, southern Gangetic Plains, Uttar Pradesh. *J. Geol. Soc. India*. 65(4), 441-450.
- Sinha, R., Tandon, S.K., Sanyal, P., Gibling, M.R., Stuben, D., Berner, Z., Ghazanfari, P., 2006. Calcretes from a Late Quaternary interfluvium in the Ganga Plains, India: Carbonate types and isotopic systems in a monsoonal setting. *Palaeogeogr. Palaeoclimatol. Palaeoecol.* 242, 214-239.
- Sinha, R., Bhattacharjee, P.S., Sangode, S.J., Gibling, M.R., Tandon, S.K., Jain, M., Godfrey-Smith, D., 2007. Valley and interfluvium sediments in the Southern Ganga Plains, India: Exploring facies and magnetic signatures. *Sediment. Geol.* 201, 386–411.
- Sinha, R., Kettanah, Y., Gibling, M.R., Tandon, S.K., Jain, M., Bhattacharjee, P.S., Dasgupta, A.S., Ghazanfari, P., 2009. Craton-derived alluvium as a major sediment source in the Himalayan Foreland Basin of India. *Geol. Soc. Am. Bull.* 121, 1596-1610.
- Smith, B.N., Epstein, S., 1971. Two Categories of  $^{13}\text{C}/^{12}\text{C}$  Ratios for Higher Plants. *Plant Physiol.* 47, 380-384.
- Somayajulu, B.L.K., 1994. Uranium isotopes in the Hooghly estuary, India. *Mar. Chem.* 47, 291-296.
- Somayajulu, B.L.K., Rengarajan, R., Jani, R.A., 2002. Geochemical cycling in the Hooghly estuary, India. *Mar. Chem.* 79, 171-183.
- Spalding, R.F., 1997. The global distribution and status of mangrove ecosystems. *Intercoast Netw. Spec. Ed.* 1, 20– 21.
- Srivastava, P., 2001. Paleoclimatic implications of pedogenic carbonates in Holocene soils of the Gangetic Plains, India. *Palaeogeogr. Palaeoclimatol. Palaeoecol.* 172, 207-222.

- Srivastava, P., Tripathi, J.K., Islam, R., Jaiswal, M.K., 2008. Fashion and phases of late Pleistocene aggradation and incision in the Alaknanda River Valley, Western Himalaya, India. *Quat. Res.* 70, 68-80.
- Srivastava, P., Rajak, M.K., Sinha, R., Pal, D.K., Bhattacharyya, T., 2010. A high-resolution micromorphological record of the Late Quaternary paleosols from Ganga–Yamuna interfluvium: Stratigraphic and paleoclimatic implications. *Quat. Int.* In Press.
- Stallard, R.F., 1995. Tectonic, environmental and human aspects of weathering and climate: A global review using a steady-state perspective. *Ann. Rev. Earth Planet. Sci.* 23, 11–39.
- Swarzenski, P.W., McKee, B.A., Booth, J.G., 1995. Uranium geochemistry on the Amazon shelf: Chemical phase partitioning and cycling across a salinity gradient. *Geochim. Cosmochim. Acta* 59, 7–18.
- Swarzenski, P.W., Porcelli, D., Andersson, P.S., Smoak, J.M., 2003. The behavior of U- and Th-series nuclides in the estuarine environment. In: *Uranium-Series Geochemistry* (Eds B. Bourdon, G. M. Henderson, C. C. Lundstrom, and S. Turner), *Rev. in Min. and Geochem.* 52, Mineralogical Society of America, Chantilly, VA, 577–606. Scott, 1982.
- Taylor, R.S., McLennan, S.M., 1985. *The continental crust: its composition and evolution.* Blackwell, London, 312.
- Thompson, L.G., Yao, T., Davis, M.E., Henderson, K.A., Mosley-Thompson, E., Lin, P.-N., Beer, J., Synal, H.-A., Cole-Dai, J., Bolzan, J.F., 1997. Tropical climate instability: the last glacial cycle from a Qinghai–Tibetan ice core. *Science* 276, 1821– 1825.
- Tipper, E.T., Bickle, M.J., Galy, A., West, A.J., Pomies, C., Chapman, H.J., 2006. The short term climatic sensitivity of carbonate and silicate weathering fluxes: Insight from seasonal variations in river chemistry. *Geochim. Cosmochim. Acta.* 70, 2737-2754.

- Tripathi J.K., Bock B, Rajamani V., Eisenhauer A., 2004. Ca and Sr dynamics in the Indo-Gangetic plains: Different sources and mobilization processes in northwestern India, *Curr. Sci.*, 87, 1453-58.
- Tripathi, J.K., Bock, B., Rajamani, V., Eisenhauer, A., 2004. Is River Ghaggar, Saraswati? Geochemical constraints. *Curr.Sci.* 87, 1141-1145.
- Tripathi, J.K., Ghazanfari, P., Rajamani, V., Tandon, S.K., 2007. Geochemistry of sediments of the Ganges alluvial plains: Evidence of large-scale sediment recycling. *Quat. Int.* 159(1), 119-130.
- Tripathy, G.R., Singh, S.K., 2010. Chemical erosion rates of river basins of the Ganga system in the Himalaya: Reanalysis based on inversion of dissolved major ions, Sr, and  $^{87}\text{Sr}/^{86}\text{Sr}$ . *Geochem. Geophys. Geosyst.* 11, Q03013, doi:10.1029/2009GC002862.
- Trivedi, J.R., Pande, K., Krishnaswami, S., Sarin, M.M., 1995. Sr isotopes in rivers of India and Pakistan: A reconnaissance study. *Curr. Sci.* 69, 171–178.
- Trivedi, J.R., Singh, S.K., Krishnaswami, S., 1999.  $^{187}\text{Re}$ - $^{187}\text{Os}$  in Lesser Himalayan sediments: Measurement techniques and preliminary results. *Proc. Ind. Acad. Sci. (Earth Planet. Sci. Lett.)* 108, 179-187.
- Turekian K.K., Chan L.H., 1971. The marine geochemistry of the uranium isotopes,  $^{230}\text{Th}$  and  $^{231}\text{Pa}$ , in: *Activation analysis in geochemistry and cosmochemistry*, A.O. Brunfelt and E. Steinnes, eds., 311-320, Universitetsforlaget.
- Upadhyay, S., Gupta, R.S., 1995. The behaviour of aluminium in waters of the Mandovi estuary, west coast of India. *Mar. Chem.* 51, 261-275.
- Vaiani, S.C., 2000. Testing the applicability of strontium isotope stratigraphy in marine to deltaic Pleistocene deposits: an example from the Lamone River Valley (Northern Italy). *J. Geol.* 108, 585.
- Valdiya, K.S., 1980. *Geology of Kumaun Lesser Himalaya*, Wadia Inst. Himalayan Geol., Dehradun, India. 291.
- Van Campo, E., Duplessy, J.C., Rossingol-Strick, M., 1982. Climatic conditions deduced from a 150 kyr oxygen isotope pollen record from the Arabian sea. *Nature* 296, 56-59.

- Vance, D., Teagle, D.A.H., Foster, G.L., 2009. Variable Quaternary chemical weathering fluxes and imbalances in marine geochemical budgets. *Nature* 458, 493-496.
- Veizer, J., 1983. Trace elements and isotopes in sedimentary carbonates. *Carbonates: Mineralogy and Chemistry*. 11, 265-299.
- Veizer, J., 1989. Strontium isotopes in seawater through time. *Annual Review of Earth and Planetary Sciences* 17, 141-167.
- Veizer, J., Buhl, D., Diener, A., Ebner, S., Podlaha, O.G., 1997. Strontium isotope stratigraphy: potential resolution and event correlation. *Palaeogeogr. Palaeoclimatol. Palaeoecol.* 132, 65-77.
- Walker, B.D., Peucker-Ehrenbrink, B., 2004. Rhenium and Molybdenum in Rivers and Estuaries. *Eos Trans. AGU*, 85(47): Fall Meet. Suppl., Abstract H43C-0390.
- Wang, Z., Liu, C., Han, G., Xu, Z., 2001. Strontium isotopic geochemistry of the Changjiang estuarine waters: Implications for water-sediment interaction. *Sci. China, Ser. E Eng. Mater. Sci.* 44, 129-133.
- Willenbring, J., Von Blanckenburg, F., 2010. Long-term stability of global erosion rates and weathering during late-Cenozoic cooling. *Nature*. 465, 211-214.
- Wimpenny, J., Gannoun, A., Burton, K.W., Widdowson, M., James, R.H., Gislason, S.R., 2007. Rhenium and osmium isotope and elemental behaviour accompanying laterite formation in the Deccan region of India. *Earth Planet. Sci. Lett.* 261, 239-258.
- Windom, H., Alexander, C., Smith, R., Niencheski, F., 2000. Uranium in rivers and estuaries of globally diverse, smaller watersheds. *Mar. Chem.* 68, 307-321.
- Wobus, C., Heimsath, A., Whipple, K., Hodges, K., 2005. Active out-of-sequence thrust faulting in the central Nepalese Himalaya. *Nature* 434, 1008-1011.
- Wright, V.P., Tucker, M.E., 1991. Calcretes: an introduction. In: Wright, V.P., Tucker, M.E. (Eds.), *Calcretes. Repr. Ser. Intern. Assoc. Sediment* 2, 1-22.

- Xiong, Y., 2003. Solubility and speciation of rhenium in anoxic environments at ambient temperature and applications to the Black Sea. *Deep Sea Res. Part I.* 50, 681-690.
- Xu, Y., Marcantonio, F., 2004. Speciation of strontium in particulates and sediments from the Mississippi River mixing zone, *Geochim. Cosmochim. Acta*, 68, 2649–2657.
- Xu Y., Marcantonio, F., 2007. Strontium isotope variations in the lower Mississippi River and its estuarine mixing zone. *Mar Chem.*105, 118-128.
- Yadav, S., Rajamani, V., 2004. Geochemistry of aerosols of northwestern part of India adjoining the Thar desert *Geochim. Cosmochim. Acta* , 68, 1975-1988.
- Yamaguchi, K., 2002. “Geochemistry of Archean-Paleoproterozoic black shales: the early evolution of the atmosphere, oceans, and biosphere”. Thesis. The Pennsylvania State University, the Graduate School, Department of Geosciences.
- Yang, J., Chen, J., An, Z., Shields, G., Tao, X., Zhu, H., Ji, J., Chen, Y., 2000. Variations in  $^{87}\text{Sr}/^{86}\text{Sr}$  ratios of calcites in Chinese loess: a proxy for chemical weathering associated with the East Asian summer monsoon. *Palaeogeogr. Palaeoclimatol. Palaeoecol.* 157, 151-159.
- Zhang, W., Yu, L., Lu, M., Zheng, X., Shi, Y., 2007. Magnetic properties and geochemistry of the Xiashu Loess in the present subtropical area of China, and their implications for pedogenic activity. *Earth Planet. Sci. Lett.* 260, 86-97.

## List of Publications

### **(i) Peer Reviewed Journals:**

1. **Waliur Rahaman**, Sunil Kumar Singh, Rajiv Sinha, S K Tandon “Climate control on erosion distribution over the Himalaya during past ~100 ka” **Geology**, 2009, **37**, 559-562, doi: 10.1130/G25425A.1
2. **Waliur Rahaman** and Sunil Kumar Singh “Characterization of sources, transport and behaviour of Rhenium in rivers and estuaries of India” **Marine Chemistry** (Vol.118, Issues 1-2, 2010; doi:10.1016/j.marchem.2009.09.008).
3. **Waliur Rahaman**, Sunil Kumar Singh, Rajiv Sinha, S K Tandon “Climate control on erosion distribution over the Himalaya during past ~100 ka” **REPLY**, **Geology**, August 2010, v. 38, p. e217, doi:10.1130/G31119Y.1
4. **Waliur Rahaman**, Sunil Kumar Singh, Rajiv Sinha, S K Tandon “Sr, C and O isotopes in carbonate nodules from the Ganga Plain: Evidence for recent abrupt rise in dissolved  $^{87}\text{Sr}/^{86}\text{Sr}$  of the Ganga” **Chemical Geology (Under Review)**.
5. **Waliur Rahaman**, Sunil K Singh, Sanjeev Raghav “Dissolved Mo and U in rivers and estuaries of India: Implication to geochemistry of redox sensitive elements and their marine budgets” **Chemical Geology (Under Revision)**.

### **(ii) Manuscript under preparations:**

1. **Waliur Rahaman**, Sunil Kumar Singh and Anil Dut Shukla “Rhenium in Indian rivers: anthropogenic and natural sources”. (**Manuscript in preparation**).
2. **Waliur Rahaman** and Sunil Kumar Singh “Dissolved Sr and Ba in Indian estuaries: Implication to submarine groundwater discharge” (**Manuscript in preparation**).

**(iii) Abstract International Conference/ proceedings:**

1. **Waliur Rahaman, Sunil Kumar Singh, S K Tandon, Rajiv Sinha** “Tracing paleoerosion in the Ganga Basin” **International Conference on Terrestrial Planets: Evolution Through Time**, January 22-25, 2008 held at Physical Research Laboratory, Ahmedabad.
2. **Waliur Rahaman, Sunil Kumar Singh, S K Tandon, Rajiv Sinha** “Temporal variation in dissolved  $^{87}\text{Sr}/^{86}\text{Sr}$  of the Ganga River: Impact of climate” **International Conference on Terrestrial Planets: Evolution Through Time**, January 22-25, 2008 held at Physical Research Laboratory, Ahmedabad.
3. **Waliur Rahaman, Sunil Kumar Singh, A D Shukla** “Geochemical behavior of Rhenium in the Narmada estuary” **International Conference on Terrestrial Planets: Evolution Through Time**, January 22-25, 2008 held at Physical Research Laboratory, Ahmedabad.
4. **Waliur Rahaman, Sunil Kumar Singh, Rajiv Sinha, S K Tandon** “Tracing paleoerosion in the Ganga Basin” **International Symposium on Mountain Building and Climate-Tectonic Interaction (MBCT-2008)**, held at Wadia Institute of Himalayan Geology, Dehradun.
5. **Waliur Rahaman and Sunil Kumar Singh** “Geochemical behaviour of Rhenium in estuary.” **Goldschmidt™ conference**, "Challenges to Our Volatile Planet." June 21 – 26, 2009 in Davos, Switzerland.
6. **Waliur Rahaman, Sunil Kumar Singh, Rajiv Sinha, S. K. Tandon.** “Climate-erosion Coupling over the Himalaya during past ~100 ka” **Goldschmidt™ conference** "Challenges to Our Volatile Planet" June 21 – 26, 2009 in Davos, Switzerland.
7. **Waliur Rahaman and Sunil Kumar Singh** “Sr in estuaries: Impact of Submarine Ground Water Discharge.” **2009- American Geophysical Union (AGU) Fall Meeting**, December 14 – 18, San Francisco, California, USA.
8. **Waliur Rahaman and Sunil Kumar Singh** “Mo in estuaries: Impact on global oceanic budget of Mo” July, 2010, **AOGS**, Hyderabad, India.